



This is to certify that the

dissertation entitled

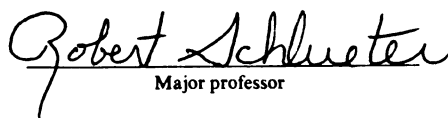
BIFURCATION SUBSYSTEM METHOD AND ITS APPLICATION
TO DIAGNOSIS OF POWER SYSTEM BIFURCATIONS
PRODUCED BY DISCONTINUITIES

presented by

Khadija Ben-Kilani

has been accepted towards fulfillment
of the requirements for

Ph.D degree in Electrical Eng


Major professor

Date 6/20/97

PLACE IN
TO AVOID

DAT

LIBRARY

Michigan State University

PLACE IN RETURN BOX to remove this checkout from your record.
TO AVOID FINES return on or before date due.

DATE DUE	DATE DUE	DATE DUE
_____	_____	_____
_____	_____	_____
_____	_____	_____
_____	_____	_____
_____	_____	_____
_____	_____	_____
_____	_____	_____

BEFORE
DIAG

**BIFURCATION SUBSYSTEM METHOD AND ITS APPLICATION TO
DIAGNOSIS OF POWER SYSTEM BIFURCATIONS PRODUCED
BY DISCONTINUITIES**

by

Khadija Ben-Kilani

A DISSERTATION

**Submitted to
Michigan State University
in partial fulfillment of the requirements
for the degree of**

DOCTOR OF PHILOSOPHY

Department of Electrical Engineering

1997

BIFURC
F

Re

power s

and the

outage-l

assessment

their eff

specific

Fi

complex

behaviour

Se

at assess

presente

limit by

the entire

Th

of the fu

The bid

ABSTRACT

BIFURCATION SUBSYSTEM METHOD AND ITS APPLICATION TO DIAGNOSIS OF POWER SYSTEM BIFURCATIONS PRODUCED BY DISCONTINUITIES

by

Khadija Ben-Kilani

Recurrent problems in diagnosing the cause and location of a stability problem in a power system are that of (a) the size and complexity of the model, (b) the various *kinds* and *classes* of bifurcations, and (c) the effects of discontinuous hard limit or equipment outage-induced transitions. Problem diagnosis in power systems is in need of stability assessment methods that (i) take into account both the existence of discontinuities and their effect, and (ii) identifies which physical elements or subsystems are associated with a specific bifurcation observed on the full model.

First, diagnosis is initiated by performing a classification of the modeling complexity and of the various bifurcations, based on their kinds and classes. The dynamic behavior of a simulated stability problem depends on the modeling complexity used.

Second, an Epoch-Based Trajectory Stability Assessment Methodology that is aimed at assessing asymptotic stability within time intervals free of hard limits discontinuities is presented. In this method, the stability assessment requires testing of quasi equilibria, limit cycles and trajectories within each epoch, rather than attempting to study stability of the entire trajectory.

The third major step is to identify the smallest subsystem, a subset of the equations of the full system model that experiences the same bifurcation in the full system model. The bifurcation subsystem must satisfy both the linear and the transversality conditions

of the

full system

of the

dependent

with the

of the

of the

of the

using the

presented

of the

of the

The

can identify

the future

including

for the bifurcation that is being experienced in the full system model. The portion of the full system external to this bifurcation subsystem has no effect on the linear conditions for bifurcation to be satisfied in the full system model, and yet the equilibrium point is dependent on the variations in the full system equations which results in bifurcation in both the full system and the bifurcation subsystem. The bifurcation subsystem method utilizes the geometry associated with the various submatrices of the differential-algebraic Jacobian J and with the eigenvectors associated with the bifurcating eigenvalue to establish conditions for existence of such subsystems. Two examples for validating and using the bifurcation subsystem method to identify bifurcation subsystems in a model are presented, and the results are compared with right eigenvector and participation information. The bifurcation subsystem method can be in disagreement with both eigenvector and participation information.

The bifurcation subsystem and the model dependency of test matrices T , K_S and K_D can identify the subsystem that experiences the bifurcation, the subsystem that produces the bifurcation, as well as possibly the location, cause and cure for the bifurcation, including loading changes or hard limit discontinuities.

Copyright by
Khadija Ben Kilani
1997

To my mother and father Fatma and Azzouz Ben Kilani

de

re

Se

La

Jer

Te

ACKNOWLEDGMENTS

I thank Allah the most powerful for giving me the power and the patience to accomplish this dissertation. I am in debt to my parents who although far away, were with me all steps of the way in every way possible.

I would like to express my sincere gratitude to my dissertation advisor Dr. Robert Schlueter for his continued academic advising, moral support, and constructive guidance. I' am also grateful to my committee members, Dr. Gerald Park, Dr. Hassan Khalil, and Dr. Jerry Schuur for giving me of their encouragements and their professional opinions.

The financial support from the Detroit Edison company and the MSU Computing and Technology, as well the Graduate School made this work possible.

CH
CH
CH

CH

CH

TABLE OF CONTENT

LIST OF TABLES.....	xii
LIST OF FIGURES.....	xiii
LIST OF SYMBOLS.....	xvii
CHAPTER 1 INTRODUCTION.....	1
1.0 Introduction to and Justification for Bifurcation Subsystems.....	1
1.1 Description of the Static Bifurcation Phenomena.....	9
1.2 Dynamic Bifurcation on Power Systems: A Brief Review.....	10
1.3 Objective.....	13
CHAPTER 2 POWER SYSTEM MODELING EFFECTS ON STABILITY PROBLEMS.....	19
2.1 Description of a Power System	20
2.1.1 Synchronous Generator	20
2.1.2 Electric Load	22
2.2 General Power System Model.....	24
2.2.1 Model Equations.....	25
2.3 Modeling Complexity	26
2.3.1 Type 1 Model.....	27
2.3.2 Type 2 Model.....	27
2.3.3 Type 3 Model.....	28
2.3.4 Type 4 Model.....	29
2.4 Classes and Kinds of Bifurcations in a Type 2 Model	31
2.4.1 Kinds of Bifurcation.....	34
2.4.2 Classes of Bifurcation	38
2.4.2.1 Classes of Loss of Causality.....	39
2.4.2.2 Classes of Static Bifurcation.....	40
2.4.2.3 Classes of Hopf Bifurcation.....	41

CHAPTER 3	POWER SYSTEM STABILITY ASSESSMENT A TAXONOMICAL APPROACH.....	42
3.1	Introduction.....	42
3.2	A Taxonomy of Stability Assessment in Power Systems.....	45
3.3	Development of a Taxonomy for Power System Models with Hard Limits.....	48
3.4	Stability Security Assessment for Models with Hard Limits.....	51
3.4.1	Epoch-Based Trajectory Stability Assessment.....	55
3.4.2	Bounded Stable Trajectory Feasibility Method.....	62
CHAPTER 4	BIFURCATION SUBSYSTEMS IN A POWER SYSTEM DIFFERENTIAL-ALGEBRAIC MODEL.....	65
4.0	Introduction.....	65
4.0.1	Bifurcation Subsystems for Epochs.....	69
4.0.2	Existence of Bifurcation Subsystems.....	70
4.0.3	Introduction to Bifurcation Subsystem Theory.....	73
4.0.4	Chapter Objective and Outline.....	75
4.1	Differential-algebraic Power System Model.....	78
4.2	Conditions for Bifurcation Subsystems Experiencing SN and LF Bifurcations.....	82
4.2.1	Equivalent System Models.....	82
4.2.1.1	Equivalent Algebraic System Model.....	84
4.2.1.2	Equivalent Dynamic System Model.....	85
4.2.2	Definition of Bifurcation Subsystems.....	87
4.2.3	Decoupling Conditions for Algebraic Bifurcation Subsystem and Differential Bifurcation Subsystems.....	94
4.2.4	Geometric Conditions.....	97
4.2.5	Algebraic Bifurcation Subsystem Experiencing LF Bifurcation.....	105
4.3	Bifurcation Subsystems Experiencing SN and LF Bifurcation.....	106
4.3.1	Differential Bifurcation Subsystems for SN Bifurcation.....	107
4.3.2	Algebraic Bifurcation Sub-subsystem for LF Bifurcation.....	109
4.3.3	Differential-Algebraic Sub-subsystems.....	110
4.4	Differential Bifurcation Sub-systems for Hopf Bifurcation.....	112

4.4.1	Differential Bifurcation Sub-subsystems for Hopf Bifurcation.....	114
4.5	Application of Algebraic Bifurcation Subsystem Experiencing LF Bifurcation in Power System Stability Assessment.....	115
4.5.1	Description of a Load Flow Model.....	117
4.5.2	Structural Conditions for Utilizing J_y	119
4.5.3	Comparison of Algebraic Equivalent Model, Algebraic Bifurcation Subsystem, and Load Flow Model.....	120
4.5.4	Bifurcation in LF or in Generator Dynamics.....	126
4.5.5	Conclusion.....	127
CHAPTER 5	Effect of Hard Limit Discontinuities on Stability Analysis	129
5.0	Introduction	129
5.1	Linearized Multi-machine Power System Model.....	132
5.2	Single Machine Infinite Bus Model with Local Load.....	134
5.2.1	Model Representation.....	134
5.2.2	Model Implications.....	136
5.2.3	Model Equations.....	139
5.2.4	Simplified Linear SMIB Model	140
5.2.4.1	The E'_q Equation.....	140
5.2.4.2	The electrical torque Equation.....	142
5.2.4.3	Terminal Voltage Equation.....	143
5.3	Application Examples of the Bifurcation Subsystem Method on a SMIB model.....	146
5.3.1	Differential Bifurcation Subsystem for SN (Unregulated Model).....	146
5.3.2	Differential Bifurcation Subsystem for Hopf (Regulated Model).....	154
5.4	Effect of Hard Limit Discontinuities on Stability Analysis	158
5.4.1	Synchronizing and damping torques.....	159
5.4.1.1	Unregulated System ($G_e(s)=0$).....	160
5.4.1.2	Thyristor-Type Excitation System.....	161
5.4.1.3	IEEE dc Type 1 Excitation System.....	164
5.4.2	Bifurcation Tests for the SMIB	167
5.4.3	Conclusions.....	170
CHAPTER 6	A Diagnosis for SN and Hopf Bifurcations in a SMIB Model.....	173
6.0	Introduction	173

6
CHAPTE
-

APPENDI

APPENDI

APPENDIX

APPENDIX

APPENDIX

APPENDIX

6.1	Diagnostic Models Formulation.....	174
6.1.1	Power Transfer Model ($R_{sh} = X_{sh} = \text{infinity}$).....	174
6.1.2	Local Load Model.....	175
6.1.3	Combination Model.....	176
6.2	Diagnostic Study.....	176
6.2.1	Power Transfer Model.....	179
6.2.1.1	Effect of P_{inf} and Q_{inf}	179
6.2.1.2	Effect of Transmission Network Inductance....	181
6.2.2	Power Local Loading Model.....	183
6.2.2.1	Effect of real-inductive local loading.....	183
6.2.2.2	Effect of real-capacitive local loading.....	184
6.2.2.3	Effect of the transmission network.....	184
6.2.3	Conclusion of the Power Transfer and Local Load Models.....	185
6.2.4	Combination Local Load-Power Transfer Model.....	187
6.2.4.1	Effect of Power Transfer.....	187
6.2.4.2	Effect of Local Loading.....	188
6.2.4.3	Effect of the Transmission Network.....	189
6.2.5	Discussion of the Combination Model Results.....	192
6.3	Diagnostic Summary.....	194
6.3.1	Classes of Hopf Bifurcation in a SMIB Model.....	194
6.3.2	Classes of Static Bifurcation in a SMIB Model.....	195
CHAPTER 7	SUMMARY AND FUTURE RESEARCH	197
7.1	Thesis Summary.....	197
7.2	Future Research.....	202
APPENDIX A	POWER SYSTEM DYNAMIC MODEL.....	205
APPENDIX B	COMMON DEFINITIONS IN POWER SYSTEM STABILITY.....	217
APPENDIX C	DEFINITION OF HOPF AND SADDLE NODE BIFURCATIONS WITH TRANSVERSALITY CONDITIONS.....	221
APPENDIX D	INPUT DATA FILES FOR THE BIFURCATION SUBSYSTEM EXAMPLES.....	223
APPENDIX E1	FIGURES FOR DIAGNOSTIC ANALYSIS POWER TRANSFER MODEL.....	227
APPENDIX E2	FIGURES FOR DIAGNOSTIC ANALYSIS LOCAL LOADING MODEL.....	231

APPENDIX

REFEREN

APPENDIX E3 FIGURES FOR DIAGNOSTIC ANALYSIS
COMBINATION MODEL..... 235

REFERENCES..... 249

LIST OF TABLES

Table 5.1	Computational results for identifying the bifurcation subsystem for SN bifurcation in the SMIB model	149
Table 5.2	Participation factor results for the SN bifurcation in the SMIB model.....	153
Table 5.3	Computational results for identifying the bifurcation subsystem for Hopf bifurcation in the SMIB model: Inertial mode.....	157
Table 5.4	Participation factor results for the inertial Hopf bifurcation in the SMIB model.....	158
Table 6.1 (a)	Results on the power transfer model bifurcation diagnosis.....	181
Table 6.1(b)	Power transfer model non-bifurcation results	182
Table 6.2(a)	Results on the local loading model bifurcation diagnosis.....	185
Table 6.2(b)	Non-Bifurcation Results on the local loading model Diagnosis.....	185
Table 6.3 (a)	Results on the combination model bifurcation diagnosis.....	190
Table 6.3 (b)	Combination model: Effect of Local loading	190
Table 6.3 (c)	Combination model: Non-bifurcation cases	191

LIST OF FIGURES

Figure 1.1	Identification of the Critical Area in 230 kV buses under area System Stress.....	5
Figure 2.1	Functional Block Diagram of a synchronous generator excitation control system.....	23
Figure 2.2	IEEE Type 1 Excitation System.....	23
Figure 3.1	2-D Example portraying the effects of the i 'th discontinuous control action. (x_i, y_i) is the i 'th quasi equilibria	45
Figure 3.2	Response of a system after a severe disturbance: EHV Line fault & line trip which resulted in a large generator off-line	61
Figure 3.3	Active power flow between central and south-east regions of the Swedish test system after the tripping of a line and generator in the North.....	61
Figure 5.1	Block Diagram of a Power System Model	134
Figure 5.2a	General Configuration of a single machine connected to a large system transmission line.....	137
Figure 5.2b	Equivalent system where the transmission network is reduced to its Thevenin's equivalent.....	137
Figure 5.2c	Circuit Model of (b) where R_E is neglected.....	137
Figure 5.3	Simplified single-machine infinite bus mode. (a) Equivalent Thevenin model where r_e , x_e and V_∞^e are given by equations (5.1), (5.2) and (5.3) respectively. (b) Phasor diagram for the synchronous machine connected to an infinite bus shown in (a).....	138
Figure 5.4	Block diagram of a simplified linear model of a synchronous machine connected to an infinite	

599

11

- 87 -

62.

11

1.

61

18

427

5.

2.

	synchronous machine connected to an infinite bus through an external impedance.....	145
Figure 5.5	Block Diagram of a linearized machine model showing Bifurcation Subsystems and the test matrix T	153
Figure A1	Power system stabilizer model.....	214
Figure A2	Speed-governing-turbine system model.....	215
Figure A3	Speed-governing-turbine system model.....	216
Figure B1a	Response of a four-machine System during a Transient-, stable System.....	219
Figure B1b	Response of a four-machine System during a Transient-unstable System.....	219
Figure E1.1	Power Transfer Model: Effect of real and reactive power transfer to the infinite bus on the parameter K_5 . (a) Real and reactive power flow in the same direction, (b) Real and reactive power flow in opposite directions.....	227
Figure E1.2	Power Transfer Model: Effect of real and reactive power transfer to the infinite bus on the parameter K_4 . (a) Real and reactive power flow in the same direction, (b) Real and reactive power flow in opposite directions.....	228
Figure E1.3	Power Transfer Model: Effect of real and reactive power transfer to the infinite bus on the parameter $K_1 - K_2 K_5 / K_6$. (a) Real and reactive power flow in the same direction, (b) Real and reactive power flow in opposite directions.....	229
Figure E1.4	Power Transfer Model: Effect of real and reactive power transfer to the infinite bus on the parameter $K_1 - K_2 K_3 K_4$. (a) Real and reactive power flow in the same direction, (b) Real and reactive power flow in opposite directions.....	230
Figure E2.1	Local Loading Model: Effect of the shunt local load on the parameters K_4 . (a) Inductive loading, (b) Capacitive loading.....	231
Figure E2.2	Local Loading Model: Effect of the shunt local load on the parameter K_5 . (a) Inductive loading, (b) Capacitive loading	232
Figure E2.3	Local Loading Model: Effect of the local load on the parameters	

Figure 1

Figure 1

Figure 1

Figure 1

Figure 1

Figure 1

Figure 1

Figure 1

Figure 1

Figure 1

Figure 1

	$K_1 - K_2 K_3 K_4$, (a) Inductive loading, (b) Capacitive loading.....	233
Figure E2.4	Local Loading Model: Effect of the local load on the parameters $K_1 - K_2 K_5 / K_6$, (a) Inductive loading, (b) Capacitive loading.....	234
Figure E3.1	Combination Model: Effect of power transfer on the parameter K_5 when the local load is real-inductive. (a) Power flow in the same direction, (b) Real and reactive power flow in opposite directions.....	235
Figure E3.2	Combination Model: Effect of power transfer on the parameter K_5 when the local load is real-capacitive. (a) Power flow in the same direction, (b) Real and reactive power flow in opposite directions.....	236
Figure E3.3	Combination Model: Effect of power transfer on the parameter K_4 when the local load is real-inductive. (a) Power flow in the same direction, (b) Real and reactive power flow in opposite directions.....	237
Figure E3.4	Combination Model: Effect of power transfer on the parameter K_4 when the local load is real-capacitive. (a) Power flow in the same direction, (b) Real and reactive power flow in opposite directions.....	238
Figure E3.5	Combination Model: Effect of power transfers to the infinite bus on the synchronizing term $K_1 - K_2 K_5 / K_6$ (regulated) when the local load is real-inductive. (a) Real and reactive power flow in the same direction, (b) Real and reactive power flow in opposite directions	239
Figure E3.6	Combination Model: Effect of power transfers to the infinite bus on the synchronizing term $K_1 - K_2 K_5 / K_6$ (regulated) when the local load is real-capacitive. (a) Real and reactive power flow in the same direction, (b) Real and reactive power flow in opposite directions.	240
Figure E3.7	Combination Model: Effect of power transfers to the infinite bus on the synchronizing term $K_1 - K_2 K_3 K_4$ (unregulated) when the local load is real-inductive. (a) Real and reactive power flow in the same direction, (b) Real and reactive power flow in opposite directions	241
Figure E3.8	Combination Model: Effect of power transfers to the infinite bus on the synchronizing term $K_1 - K_2 K_3 K_4$ (unregulated) when the local load is real-capacitive. (a) Real and reactive power flow in the same direction, (b) Real and reactive power flow in opposite directions.....	242
Figure E3.9	Combination Model: Effect of local loading on the parameter K_5 (regulated) when the transfer to the infinite bus is at $P_{inf}=0.8$, $Q_{inf}=0.5$. (a) real-inductive loading; (b) real-capacitive loading.....	243
Figure E3.10	Combination Model: Effect of local loading on the parameter	

Figure E3.11

Figure E3.12

Figure E3.13

Figure E3.14

	K_4 (unregulated) when the transfer to the infinite bus is at $P_{inf}=0.8$, $Q_{inf}=0.5$. (a) real-inductive loading; (b) real-capacitive loading.	244
Figure E3.11	Combination Model: Effect of local loading on the parameter $K_1 - K_2 K_3 K_4$ (unregulated) when the transfer to the infinite bus is at $P_{inf}=0.8$, $Q_{inf}=0.5$. (a) real-inductive loading; (b) real-capacitive loading.....	245
Figure E3.12	Combination Model: Effect of local loading on the parameter $K_1 - K_2 K_5 / K_6$ (regulated) when the transfer to the infinite bus is at $P_{inf}=0.8$, $Q_{inf}=0.5$. (a) real-inductive loading; (b) real-capacitive loading	246
Figure E3.13	Combination Model: Effect inductive-real local load on the system synchronizing and damping torque coefficients when $P_{inf}=0.8$, $Q_{inf}=0.5$ (a) synchronizing torque coefficient K_S , (b) damping torque coefficient K_D	247
Figure E3.14	Combination Model: Damping torque coefficient K_d and parameter K_5 for different levels of real local loading	248

LIST OF SYMBOLS

Synchronous machine

- E'_q : internal bus voltage proportional to d-axis flux linkage of field current
- D : damping constant due to damper winding effects (pu / (rad/sec))
- ω : angular speed of the machine (rad/sec)
- ω_s : nominal angular speed (rad/sec)
- V_t : terminal bus voltage
- P_m : mechanical power input to the rotor (pu)
- I_d : direct-axis (d-axis) current
- I_q : quadrature-axis (q-axis) current
- I_t : $I_d + j I_q$
- $\delta-\theta$: angle difference between internal bus (rotor) and terminal bus
- X_q : q-axis synchronous reactance
- X_d : d-axis synchronous reactance
- X'_d : d-axis transient reactance
- T'_{do} : d-axis open-circuit transient time constant (sec)
- R_s : resistance of the stator

Excitation system

- V_c : output of load (or line drop) compensator

V_s	:	output of power system stabilizer (PSS)
V_{REF}	:	reference voltage
V_A	:	output of automatic voltage regulator (AVR)
V_R	:	amplifier output voltage
V_1	:	measured voltage
V_3	:	stabilizer output voltage
K_A	:	dc gain of AVR
T_A	:	Time constant of AVR (sec)
$1/K_E$:	dc gain of exciter
T_E/K_E	:	time constant of exciter
K_F	:	washout gain of stabilizing feedback of excitation system
T_F	:	washout time constant of stabilizing feedback of excitation system
E_{fd}	:	output of the exciter (field voltage of synchronous machine)
X_c	:	compensator adjustable inductive reactance

v
s
c
m
in
th
di
Tr
co
470
par
qu
fig

I

Introduction

1.0 Introduction to and Justification for Bifurcation Subsystems

An important aspect of stability analysis of a power system is to determine which physical elements or subsystems are associated with a specific instability phenomena observed on the full system. The recurrent problem in diagnosing a specific power system stability problem is that of size and complexity of the model since a power system may be composed of 10,000 interconnected buses and 1000 generators. However, although the models required to study the dynamic effects of interest in a power system seem to initially involve a large set of variables associated with the many different components of the system, only a subset of these state variables may actually be critical to problem diagnosis for a specific stability problem associated with a specific eigenvalue or mode. The challenge is then not to obtain a reduced-order model that incorporates all of the components in the system, but to obtain a subsystem of the full model which experiences and causes the same bifurcation (a discontinuous change in system response as a parameter changes slowly) as the full model, i.e. the smallest subsystem that preserves the qualitative information of the system instability involving the specific bifurcating eigenvalue.

System modal reduction methods on a power system have mainly been based on modal analysis (or eigenanalysis) of the linearized power system model, a technique that has been found to be promising and of fruitful applications [1,2]. Sparsity, singular perturbation theory, coherency reduction as well as Kalman minimal realization theory [3] have also been applied in an attempt to simplify the large and complex dynamical system models that arise in various power system problems. These traditional methods for identifying subsystems are generally based on apriori knowledge of (a) the system or its control design; (b) time scale information on what system state variables are fast and which are slow variables; (c) eigenvectors and participation factor information from eigenvectors; or (d) decoupling within the state space model. While such methods are often useful, they are not always effective in identifying the smallest subsystem or subsystems that experience and cause the bifurcation in the full system because the criterion for deciding their effectiveness is their usefulness in model stabilization, designing controls, and developing operation schedules for a system. Obtaining a bifurcation subsystem model that experiences and causes the bifurcation in the full model requires a quite different set of methods.

The singular perturbation approach for problem diagnosis in power system [4] can not generally be applied for problem diagnosis of a particular stability problem that occurs after a power system disturbance since the states most involved in an unstable mode in a power system cannot generally be classified into either the slow or the fast dynamics groups. When a power system is subject to undamped inter-area oscillations or local generator oscillations, this technique seems to be inadequate to establish the bifurcation subsystem for a single mode since the frequency of all inter-area oscillation modes lie in a

2

3

4

5

6

7

8

9

10

11

12

13

14

15

16

17

18

19

20

21

22

23

24

narrow band and the frequency of all local generator oscillation modes also lie in a narrow band. A singular perturbation based subsystem model contains all the modes in the narrow band and not just the bifurcating mode.

In modal analysis theory, the location and involvement of specific components of the system in the system instability may be obtained from the right and left eigenvectors associated with the bifurcating eigenvalue. While the magnitude of the eigenvalue of the normalized modal-transformed system is only a relative measure to proximity to bifurcation (collapse) [2], the components of the left eigenvector can be interpreted as indicating a direction normal to the operational boundary of the system [5-6], and right eigenvectors indicate the degree to which given variables are involved in a given mode. The dimensionless participation matrix, obtained from right and left eigenvector information associated with the bifurcating eigenvalue, has widely been used as an indicator to the relative involvement of system components in the unstable system mode or as a tool for identifying the collapse regions in the system. Although Eigenvalue/modal analysis has provided promising results, it seems to be insufficient to locate the voltage collapse regions or system components causing the collapse as can be demonstrated by the following example.

Example

Modal analysis has been used in [7] on the 1993 B.C. Hydro system model to find the suitable locations where reinforcement and remedial actions ought to be taken. The relevant portion of the system in question as well as the three critical regions are shown in Figure 1.1. The system participation factor matrix for the critical mode of the normalized

system

the loc

uniform

particip

that the

having

Western

ineffect

A

Univers

SVC).

Method

imbalan

excitation

causes a

about vo

because

the site s

system has been computed when the entire B.C. Hydro system was stressed to determine the location where reactive power injection would benefit the system the most. With a uniform MVA load increase, modal analysis near the point of collapse has resulted in the participation factor plot shown in Figure 1.2. The modal information in the plot indicates that the British Columbia Lower Mainland was the critical area, with North Vancouver having the next larger participation factor elements. The Vancouver Island region in Western British Columbia had relatively small participation and thus was rated relatively ineffective for reactive compensation [7].

A study on the same B.C. Hydro system has been conducted by Michigan State University where the reactive compensation device was a synchronous var compensator (SVC). The study based on MSU Voltage Stability Security Assessment and Planning Methodology Programs [8] concluded that the collapse region was caused by reactive imbalance in the Vancouver Island region. It has been found [9] that in this system, loss of excitation voltage control on generators in one generating station on Vancouver Island causes a voltage collapse in Vancouver Island which uncontrollably spreads and brings about voltage collapse in the entire B.C. Hydro system. This result was later confirmed because ABB [10] installed one SVC and it was located in the Vancouver Island region at the site suggested by [9].

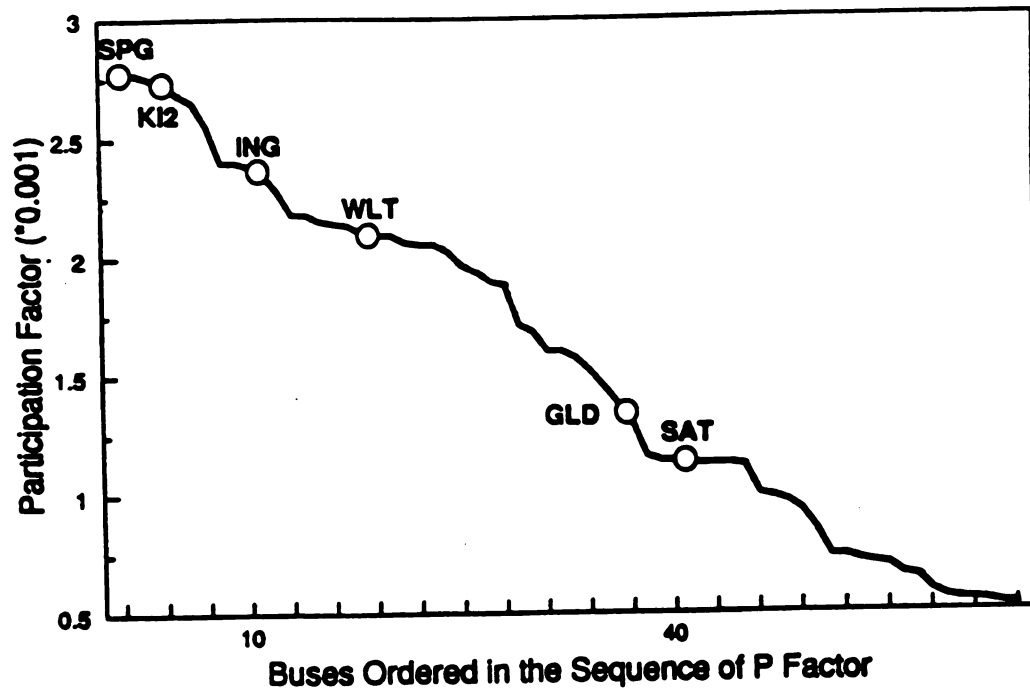


Figure 1.1 Identification of the critical areas in 230 kV buses under area system-stress

The ab
not sufficien
full system.
states have c
states with
may not be
very sparse
other buses
submodel a
weak coupl
reactive pow
the power sy
sequence of
chargers re
susceptance
groups resu
constraints.
differential-a
demonstrates
differential-a
Selectiv
participation
the qualitative

The above example demonstrates that the participation matrix can be misleading or not sufficient for indicating the portion of the system that is causing the instability in the full system, since (i) the voltage collapse can occur due to discontinuities in regions where states have quite small participation for the mode closest to bifurcation or (ii) out of many states with “high” participation, only few may be crucial for remedial actions. This result may not be surprising since for most realistic power systems (a) the Jacobian matrix is very sparse where a node in a 10,000 bus network may be connected to only three to five other buses in the system; (b) weak coupling exists between the real power-angle submodel and the reactive power-voltage submodel in the algebraic network model; (c) weak coupling of coherent bus groups exists in both the real power-angle and in the reactive power-voltage network submodels; (d) decoupling in the different dynamics of the power system model exists and (e) most bifurcations in a power system occur due to a sequence of discontinuities such as generators reaching field current limits, under load tap changers reaching tap position limits, and switchable shunt capacitors reaching susceptance limits. All of these factors suggest that loss of control in some coherent bus groups results in decoupling between some generator dynamics and system algebraic constraints, and thus will produce a bifurcation for the algebraic, differential, or differential-algebraic model associated with that coherent group. This has been demonstrated in [11] for a classical load flow model and is expected to be true in a differential-algebraic model.

Selective Modal Analysis is a model reduction approach that recognized that the participation matrix is not sufficient for obtaining the smallest subsystem that preserves the qualitative information of the system near collapse. In the modal analysis algorithm

(12) The

cases with

of the le

cases and

approach

factors in

Ca

and cau

are obta

center m

it manife

(a) a b

phy

dyn

by the

imp

will

(c) the n

the c

rd, a bif

analy

A bif

experiences

[12], state variables with high participation are divided into “relevant” and “less relevant” states where the relevant states are preserved in the reduced order model, while the effect of the less relevant states is incorporated in the final reduced model [12]. The relevant states are obtained either by intuition or from participation factor information. This approach demonstrates that only a few out of the many states with high participation factors in a model may be of crucial importance in a particular unstable mode.

Center manifold dynamics may be a subsystem of the actual system that produces and causes the bifurcation experienced in the full model. The center manifold dynamics are obtained through a nonlinear transformation of the original state space model. The center manifold dynamics are not considered a bifurcation subsystem despite the fact that it manifests the bifurcation similar to a bifurcation subsystem, because

- (a) a bifurcation subsystem is a subsystem of the state space model written in terms of physically meaningful variables and not a nonlinear transformation of these dynamics;
- (b) the nonlinear transformation on very large power system models generally makes it impossible to analyze how operating condition changes or model parameter changes will cause the bifurcation;
- (c) the needed nonlinear transformation is not quickly and easily computed, which is not the case for finding a bifurcation subsystem.
- (d) a bifurcation subsystem is not a reduced model that can necessarily be simulated or analyzed apart from the full system model.

A bifurcation subsystem is a subset of the equations of the full system model that experiences, produces and causes the full system bifurcation by satisfying the same

con

exp

the

bet

the

rect

bifur

struc

prod

expe

than

still

and

param

dis

shunt

that

under

system

conditions for bifurcation as satisfied by the full system model. The subsystem that experiences bifurcation may or may not produce the bifurcation in the full system since the structure or parameters external to the subsystem may help produce the bifurcation in both the full system and the subsystem. This is certainly true when geometric coupling of the bifurcation subsystem and external system approaches zero as bifurcation occurs rather than being zero. If the geometric coupling between the subsystem experiencing bifurcation and the external system is zero as bifurcation occurs, which is called a structural geometric decoupling, then the bifurcation subsystem both experiences and produces the full system bifurcation. Thus the subsystem that produces the bifurcation experienced by the bifurcation subsystem and the full system may be of larger dimension than the subsystem experiencing bifurcation. The subsystem causing bifurcation may be still larger than the subsystem experiencing or producing the bifurcation in the full system and the bifurcation subsystem. The system that causes bifurcation must include all model parameters, controls, and discontinuous changes that cause the bifurcation to develop. The discontinuous changes include under load tap changer tap position changes, switchable shunt capacitor switching changes, equipment outages, over-excitation limit relays, etc. that cause instability to occur. The controls include maximum excitation limiter controls, under load tap changer controls, switchable shunt capacitor controls, and excitation system controls.

1.1 Desc

In a p

character

more det

changes.

take vari

been dev

system

power s

limit cy

has nev

S

operat

B) ha

to be c

loss o

can o

of the

gene

Class

Jac

now

or

1.1 Description of the Static Bifurcation Phenomena

In a power system, the parameter space breaks up into open connected regions, each characterized by a particular behavior of the system in the state space. As parameters move across the boundary from one open region to another, the topology of the state space changes. This corresponds to the bifurcation phenomena. Although the bifurcation can take various forms, a great concentration of the study of bifurcation in power systems has been devoted to the study of saddle node bifurcation. It is only recently that the power system researchers have recognized the significance of other forms of bifurcations in power system stability analysis above and beyond the static bifurcations. The creation of limit cycles in the state space through Hopf bifurcation, although not fully investigated, has nevertheless been a familiar although undesirable phenomena in power systems.

Saddle node bifurcation is a kind of static bifurcation that occurs at the steady state operating point of a dynamic system. Significant research on static voltage stability [App. B] has resulted in (a) establishing the modeling requirements for static voltage stability, (b) classification of the various kinds of voltage instability such as algebraic bifurcation, loss of causality, and saddle node bifurcation. Each of these different kinds of bifurcations can affect different algebraic and/or differential states of a model and each is called a class of that particular kind of bifurcation. For example, a saddle node bifurcation can occur in generator flux decay dynamics or generator inertial dynamics. Each of these is a different class of saddle node bifurcation. A loss of causality is associated with singularity of the Jacobian of the algebraic equations at an equilibrium. The Jacobian can be singular due to row dependence of the real power balance equations and is referred to as angle instability, or due to row dependence of the reactive power balance equations and is termed a voltage

instabil

Aid

there is

for each

subsystem

subsystem

the class

onboard

bidirectional

cases in

discontin

method

literature

power sys

1.2 Dyn

As a

in a power

periodic se

frequency

variables. Th

modern in

identified f

instability; both are classes of loss of causality.

Although there is a theory for establishing which kind of these bifurcations occurs, there is no general method for defining subsystems associated with classes of bifurcation for each of these kinds of bifurcation. There is no actual test that identifies whether a subsystem actually causes the bifurcation. A method will be developed that (i) identifies subsystems that experience and cause saddle node, load flow, and Hopf bifurcations and the classes of each; (ii) provides tests for whether that specific subsystem causes the static bifurcation observed in the system, which in turn may identify the kind and class of static bifurcation which occurs; and (iii) establishes a diagnostic procedure for determining the causes in terms of the specific parameters in parameter space and the model structure discontinuities that produce this subsystem bifurcations. The bifurcation subsystem method will also be developed for Hopf bifurcations in power systems where less literature exists. A brief review of the literature on dynamic bifurcation in differential power system models is now given.

1.2 Dynamic Bifurcation on Power Systems: A Brief Review

As a continuing effort to the understanding of voltage stability [App B] mechanism in a power system, recent attention has been focused on dynamic bifurcation where periodic solutions suddenly appear. It is now evident that poorly damped or unstable low frequency oscillations are a major threat to the security of power systems for many utilities. The modes of oscillations observed are becoming more numerous and complex in modern interconnected systems. Three specific classes of Hopf bifurcation have been identified [25]: The local plant mode is associated with the mechanical dynamics of units



at a generating station swinging with respect to the mechanical generator dynamics of the rest of the system and the frequency of such modes is typically in the range of 0.8 to 2.0 Hz. The inter-area mode is associated with the swing of the mechanical dynamics of one group of machines in one part of the system against the mechanical dynamics of groups of machines in other parts of the system. The frequency of the inter-area mode is typically in the range 0.2 to 0.8 Hz [13]. The voltage mode appears in any machine's flux decay dynamics and exciter dynamics. Its frequency is higher than the local plant and inter-area modes.

In 1984, Abed and Varayia investigated generating units dynamics including both generator electro-mechanical and flux dynamics [14]. Their investigation revealed for the first time that generating unit dynamics may experience Hopf bifurcation. In 1989, Sauer and Pai [15] investigated the stability of a two-axis generator model connected to an infinite bus as load level at the generator terminals increased. The study showed that near the critical or maximum possible load level, a pair of complex eigenvalues associated with the excitation system experienced Hopf bifurcation, and that the onset periodic solutions were locally unstable. From 1990-1992, similar investigations have been carried on by others [16-19], where system stability was based on eigenvalue analysis at different loading conditions: The oscillatory instability in all of this literature was due to an apparent subcritical Hopf bifurcation in the generator flux decay and exciter dynamics. During 1992-1993, Ajarapu, Abed and Varayia [20-23] conducted a thorough testing on a similar single machine-infinite bus voltage collapse model developed by Dobson et al [24] in 1990. The results revealed that Hopf bifurcation and saddle node bifurcation occur on this model at different system loading levels. The oscillatory instability was characterized

by

can

ma

ma

can

syst

the

bifu

bifur

Engl

bifur

possi

deve

bifur

of th

the f

society

meth

suby

differ

suby

by the interaction of the generator angle dynamics and the induction motor dynamics.

A recent study on bifurcations on system models of increasing complexity has been completed by Ajjarapu [49]. Two models were of interest: one model included a detailed machine model with IEEE type DC-1 exciter, and network with a constant power load model, and a more complex model where a generic dynamic load model has replaced the constant power load model. Eigenvalue analysis on both models revealed that before the system collapses due to saddle node bifurcation (which occurs at the tip of the PV curve), the system experienced Hopf bifurcation, node focus bifurcation and singularity induced bifurcation. The sequence of Hopf, node focus, singularity induced and finally saddle node bifurcations occurred on both a 3-generator 9-bus system and a 10-generator 39-bus New England system model.

Issues that need additional research include (1) identification of generic sequences of bifurcations in a power system; (2) identification of a bifurcation subsystem for each possible class of saddle node, Hopf, node focus, or load flow bifurcation in the system; (3) development of tests for establishing whether a specific subsystem causes a specific bifurcation observed in the system; and (4) a diagnostic for establishing the specific cause of that subsystem bifurcation. Such a subsystem whose bifurcation causes bifurcation in the full system is called a bifurcation subsystem, and may be composed of a subset of solely differential, algebraic, or a combination of differential and algebraic equations. The method presented in this thesis establishes conditions for which a specific bifurcation subsystem exists. This subsystem method is first developed in Chapter 4 for (1) a general differential-algebraic model for identifying both differential and algebraic bifurcation subsystems; then (2) for an algebraic model for identifying algebraic bifurcation sub-

2. E
e
to
eq

subsystems; (3) to a differential model for identifying differential bifurcation subsystems; and (4) to a differential-algebraic model for identifying differential-algebraic bifurcation subsystems.

1.3 Objectives

1. Initiate a diagnostic classification of power system stability problems that is based on bifurcation kinds and classes for the different model types that have been used for bifurcation studies. The necessity for simplifying assumptions used in power system stability analysis has resulted in four types of power system models of increasing complexity [25], and which are commonly used to study the different forms of power system instabilities. Kinds of bifurcation refer to saddle node, Hopf, LF bifurcation, etc., thus refers to the bifurcation behavior observed, while a class of bifurcation refers to the specific dynamical or algebraic states experiencing the bifurcation. It has been shown in [25] that the type of model used for assessing stability has an effect on the kind and class of bifurcation observed. This classification based on model types as well as kinds and classes of power system stability problems seem to be necessary to diagnose the problem and to obtain information on how system stability can be improved most effectively. This diagnostic classification together with a description of a power system differential-algebraic model is given in Chapter 2.
2. Briefly review in Chapter 3 the recent development on power system stability which extends the classical theory of power systems as dynamical smooth nonlinear systems, to the ongoing development of a method that includes the effects of hard limits and equipment outages which discontinuously modify the model order and system

behavior. The theoretical framework for study of stability of a power system model, called a “taxonomy”, has been developed for smooth systems by Zaborsky [26]. The taxonomy addressed three regions that lie in state and parameter space: (i) stability region composed of the region of attraction defined for every parameter vector in parameter space; (ii) a feasibility region in state and parameter space composed of all connected stable equilibria and the parameter vectors that produce them; and (iii) a viability region composed of a subset of the equilibria and associated parameter vectors belonging to the feasibility region that lie within the acceptable range for each current, voltage, real power and reactive power variables.

Since hard limits associated with equipment outages, actions of operator control, protective devices such as relays and field current limit controllers, actions of under load tap changers and actions of switchable shunt capacitors cause most of the bifurcations experienced in a power system, the taxonomy is being extended to include such models. The taxonomy that includes the effects of hard limits [27] defines and describes similar stability, feasibility and viability regions as the taxonomy for smooth systems. However, the taxonomic assessment is only valid if one can predict and compute the sequence of quasi equilibria or limit cycles as well as the sequence of hard limits encountered along every system trajectory without simulation. This requirement and the assumptions made in [27] are not true in a power system with hard limits, where there is different time delay between the time that a specified hard limit surface is encountered and when the action associated with the hard limit is implemented.

A different approach to stability assessment methodology for systems with hard

1

C
P
C
W
T
C

limit discontinuities is then proposed in Chapter 3. This approach considers an episodal trajectory stability assessment rather than attempting to study the stability of all trajectories and stability of all quasi equilibria and limit cycles encountered in some subregion of state and parameter space. This new approach is aimed at assessing asymptotic stability of the transient during (t_i^-, t_i^+) and the stability of quasi equilibria or limit cycles in each epoch, where an epoch is a period of time (t_i^+, t_{i+1}^-) where no hard limit transitions occur. This procedure can be applied to a broader class of models with hard limits that need not obey the assumptions made in [27]. The Epoch Based Trajectory Stability Assessment Method is based on a stability simulation method implemented by Van Cutsem in 1992 [28] which does not require time simulation in (t_i^+, t_{i+1}^-) , but only computes the quasi equilibria (\bar{x}_i, \bar{y}_i) for $i = 1, \dots, N$ in a manner similar to how a classical load flow simulates the effects of hard limits. Specific rules and guidelines decide the sequence of discontinuities that occur using a procedure that avoids full time simulation that in turn determines the sequence of quasi equilibria (\bar{x}_i, \bar{y}_i) for $i = 1, \dots, N$ which can then be used to test for stability, feasibility and viability via trajectory segments in epochs (t_i^+, t_{i+1}^-) , $i = 1, \dots, N$.

A Bounded Trajectory Feasibility Region is then defined in Chapter 3, which classifies trajectories produced by continuous parameter changes or by discontinuous parameter or model structure changes that are induced by continuous operating condition or parameter changes. The classification of trajectories is based on (i) whether each quasi equilibria (\bar{x}_i, \bar{y}_i) or encircling orbit is stable and (ii) whether each trajectory segment in (t_i^+, t_{i+1}^-) belongs to the Region of Stability of the associated quasi stable equilibrium point or limit cycle. The subset of trajectories, where (a) all

equilibria or encircling orbits are stable and (b) all trajectory segments (or only the last trajectory segment) lie in the region of stability of a stable orbit or equilibrium, belongs to a Bounded Trajectory Feasibility Region.

Since the episodal stability assessment method is applied after each hard limit is encountered, the power system model in each interval may be different and yet analytic so that existing dynamical system theory can be applied. A natural desire is to find a reduced-order model or the smallest subsystem within each epoch that experiences the same bifurcation as the full model, which motivates the bifurcation subsystem method investigated in the rest of the thesis. If the bifurcation subsystem is identical in each epoch as discontinuities bring on the bifurcation, it is a bifurcation subsystem for the bifurcation that ultimately occurs and changes the system dynamical behavior.

3. A power system differential-algebraic model is investigated for the purpose of identifying the possible bifurcation subsystems for each kind of bifurcation (SN, Hopf, LF bifurcation) that may occur on a Type 2 power system model where load dynamics and controls are ignored. A Type 2 model with a constant power load model, tap changers, switchable shunt capacitors in the transmission, subtransmission and higher voltage distribution system will be assumed in this thesis because it generally contains the dynamics that experience bifurcation and cause voltage collapse in a large region [25]. The bifurcation subsystem method allows one to find a specific subsystem that experiences, produces and causes the same bifurcation that occurs in the full model. The bifurcation subsystem always experiences the bifurcation that occurs in the full system model. The geometric coupling of the bifurcation subsystem may not be null

a

b

v

f

b

s

t

n

in

cl

bi

gi

an

bif

bif

bif

on b

may

epoch

bifur

mode

a netw

and may produce the bifurcation in the full system and the bifurcation subsystem as it becomes zero. The system that causes the bifurcation in the bifurcation subsystem contains all the discontinuities, operating changes, equipment outages and model parameter changes that cause the bifurcation to develop in both the full system and the bifurcation subsystem. Thus, this subsystem may be larger than the bifurcation subsystem that experiences the bifurcation of the full system model, or the subsystem that includes the effects of coupling to the external system when this coupling is not null but approaches zero as bifurcation occurs.

The bifurcation subsystem method is an extension of the diagnostics employed in producing the taxonomy for feasibility, stability and viability for an equilibrium or closed orbit developed in Chapter 3, the classification of kinds and classes of bifurcation given in Chapter 2, and the episodal epoch by epoch stability assessment given in Chapter 3, because it finds the smallest subsystem that experienced, produced and caused the loss of stability, feasibility and viability for that equilibrium for bifurcations produced by encountering hard limit induced discontinuities. The bifurcation subsystem method allows one to better diagnose the causes of a subsystem bifurcation and separate causes and effects of this bifurcation for bifurcations brought on by hard limit induced discontinuities. Since the sequence of discontinuities are the major cause for many bifurcations, a bifurcation subsystem method based on epoch by epoch diagnosis appears to be the only way to understand the causes and the bifurcation subsystem that produced the bifurcation. This is needed in a power system model when there are hundreds of generators, tens of thousands of dynamic loads, and a network that couples the load and generator dynamics. The bifurcation subsystem

method should identify bifurcations that occur in

- (a) algebraic subsystems composed of generator bus groups, groups of load buses, and groups of generators and load buses;
- (b) differential subsystem dynamics in one or more groups of generators;
- (c) differential-algebraic subsystems in one or more groups of generator and in one or more groups of generator and load buses.

The bifurcation subsystem method, developed in Chapter 4 would allow a very complex behavior to be seen as being very simple so that one can potentially explain virtually everything about feasibility, viability and stability for each and every subsystem that can produce loss of feasibility, loss of viability or loss of stability. The bifurcation subsystem model is produced to study the causes of a specific bifurcation and may have no value except for studying that bifurcation. It may not be useful for control design or even simulating the contingencies which produce that bifurcation, because the subsystem that produces the bifurcation may be quite small compared to the subsystem needed to simulate a specific contingency or design a control system to prevent that bifurcation.

In chapter 5, two examples for validating and using the bifurcation subsystem method in a model are presented, and the results are compared with the participation factor information. In Chapter 6 a diagnostic study for the occurrence of SN and Hopf bifurcations in a single-machine-infinite bus model is performed based on test matrices derived in Chapter 5. Chapter 7 summarizes the dissertation and suggests topics of future investigation.

II

Power System Modeling Effects on Stability Problems

In this chapter, a diagnostic classification of power system stability problems that is based on bifurcation kinds and classes is developed, and a description of the model types that have been used for bifurcation study is initiated. A specific model type (Type 2) is selected for further study in this thesis. A further classification of kinds and classes of bifurcations for this Type 2 model is then given. Kinds of bifurcations include saddle node, Hopf, load flow bifurcation, thus refer to the kind of qualitative change in dynamical or algebraic network behavior encountered at the point of bifurcation. Classes of bifurcations are the specific subsystem dynamics or algebraic network variables that experience a particular kind of bifurcation for a given model type. For the model Type to be used (Type 2 model), there are two classes of saddle node bifurcation, three classes of Hopf bifurcation, and three classes of loss of causality bifurcation.

The effort to classify model types as well as kinds and classes of bifurcation is necessary since later, a bifurcation subsystem method will be developed and applied to saddle node, load flow and Hopf bifurcations and the classes for each. This bifurcation subsystem method will attempt to diagnose the geometric subsystem structure that bifurcates, what locations in a system are vulnerable to this particular kind and class of



(

S

2

to

to

to

an

tra

2.

to

get

not

get

bifurcation, what causes it in terms of model parameter changes, equipment outages, or operating condition changes. This systematic diagnosis needs a classification of kinds and classes of bifurcation in a given model type. Details of the classification to be given in this Chapter comes from a paper published by the author [25] in 1994.

As a natural start to this diagnostic classification, a general power system model description including models for generators, transmission network and loads are given in Sections 2.1 and 2.2. Section 2.3 presents the four model types suggested by the author in [25], and finally kinds and classes of bifurcations in a Type 2 model are presented in Sections 2.4.

2.1 Description of a Power System

Electric power systems are comprised of generation, transmission and distribution/load. Electric power is produced at generating stations and transmitted to consumers through a complex network of individual components including transmission lines, transformers, and switching devices. Power systems models, although they vary in size and complexity, all have three basic structural components: synchronous generators, a transmission network, and electric load.

2.1.1 Synchronous generator

Prime movers convert the primary sources of energy (fossil, nuclear and hydraulic) to mechanical energy that is in turn converted to electrical energy by synchronous generators. The synchronous generator output voltage is usually regulated to maintain a constant value using an excitation system. A functional diagram of a synchronous generator with an excitation control system is shown in Figure 2.1 [29]. The subsystems

inside the dashed-line box in Figure 2.1 constitute the excitation system, of which a typical model widely used in literature is the IEEE Type DC1 excitation system model shown in Figure 2.2. For consistency and task simplification, this specific model will be used in this work. First, a brief description of the indicated functional blocks is given.

- (a) *Exciter*. provides dc voltage to the synchronous machine field winding based on input from the regulator control;
- (b) *Regulator*. Processes and amplifies input control signals (as shown in Figure 2.1) to a level and form appropriate for the control of the exciter. This includes both regulating and stabilizing functions (rate feedback or lead-lag compensation);
- (c) *Terminal voltage transducer and load compensator*. senses generator terminal voltage, rectifies and filters it to dc quantity, and compares it to a reference which represents the desired terminal voltage. In addition, load compensation may be provided if it is desired to hold constant voltage at some point electrically close to or distant from the generator terminal bus;
- (d) *Power system stabilizer*. provides an additional input signal to the regulator to damp oscillations in generator mechanical dynamics. Some common input signals are rotor speed deviation, accelerating power, and frequency deviation;
- (e) *Limiters and protective circuits*. They include a wide array of control and protective functions whose role is to insure that the capability limits of the exciter and synchronous generator are not exceeded. A recent textbook [29] provides a detailed description of the various limiters and protective devices commonly used on power systems.

١٢٤

wh
is
para
curr
most
conse
requir
therm

2.1.2 Electric load

The diversity of electric loads present on a power system, makes it virtually impossible to represent every individual component in a power system model. The common practice is to make considerable simplifications of the composite load characteristics as seen from bulk power delivery points. Load models have been broadly classified into two categories, static loads and dynamic loads. The static load model expresses the load as algebraic equations, classically in the exponential form

$$P = P_o(\bar{V})^b$$

$$Q = Q_o(\bar{V})^b$$

where P and Q are active and reactive components of the load and the voltage magnitude is \bar{V} . The subscript “o” refers to the values at the initial operating condition. If the parameters a and b are 0, 1 and 2, the models are respectively constant power, constant current and constant impedance load. The dynamic attributes to motors are usually the most significant aspects of dynamic characteristics of system loads. Typically motors consume 60-70% of the total energy produced by a power system. Other devices that require dynamic consideration are load shedding, operation of protective relays, thermostatic control of loads, response of under load tap changers (ULTC), etc...

R.



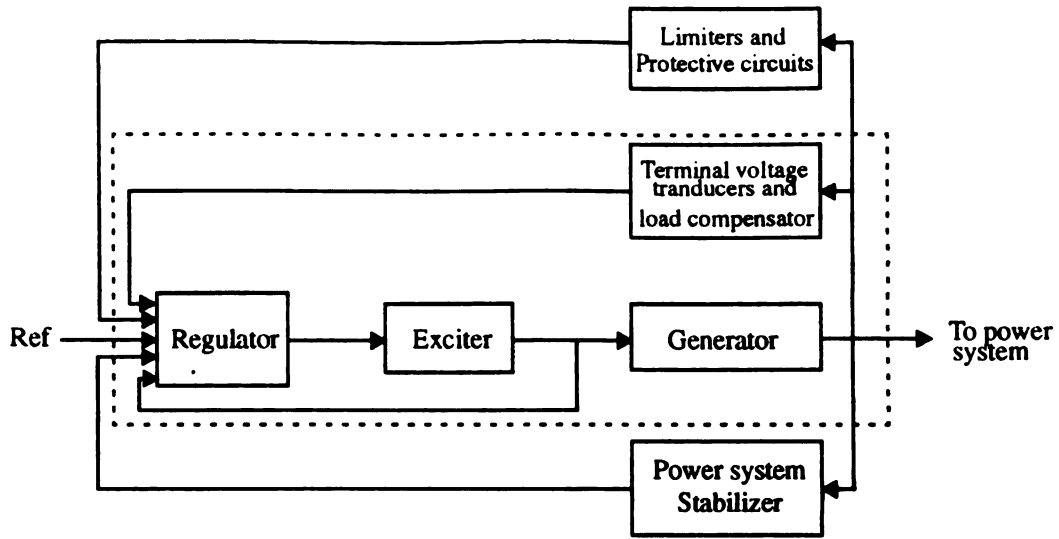


Figure 2.1 Functional block diagram of a synchronous generator excitation control system

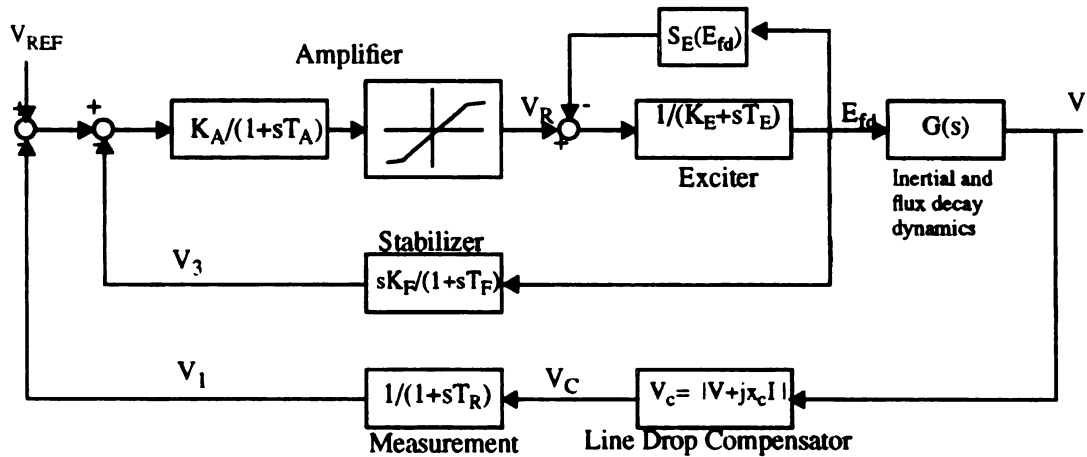


Figure 2.2 IEEE Type DC 1 Excitation system model

2.2 Gene

The g
subject to
dynamics, f
the algebra
bus in the
generators
differential

where

$$f : R^{n \times n}$$

$$g : R^{n \times n}$$

$$x(t) : \in \mathbb{R}^n$$

$$y(t) : \in \mathbb{R}^m$$

$$u(t) : \in \mathbb{R}^p$$

$$v(t) : \in \mathbb{R}^q$$

$$w(t) : \in \mathbb{R}^r$$

$$z(t) : \in \mathbb{R}^s$$

$$a(t) : \in \mathbb{R}^t$$

$$b(t) : \in \mathbb{R}^u$$

$$c(t) : \in \mathbb{R}^v$$

$$d(t) : \in \mathbb{R}^w$$

$$e(t) : \in \mathbb{R}^x$$

$$f(t) : \in \mathbb{R}^y$$

2.2 General Power System Model

The general power system model consists of a set of first order differential equations, subject to algebraic constraints. The differential equations represent the mechanical dynamics, flux decay dynamics, and excitation system dynamics of a generator whereas the algebraic equations represent the real and reactive power balance equations for each bus in the network. A multi-machine system consisting of m network buses and n generators with voltage regulation can therefore be written in the parameter dependent differential-algebraic model

$$\dot{x} = f(x(t), y(t), \mu(t)) \quad \mu(t) \in P \quad 2.1(a)$$

$$0 = g(x(t), y(t), \mu(t)) \quad 2.1(b)$$

where

$f : R^{n+m+p} \rightarrow R^n$, an n -vector of real smooth nonlinear functions.

$g : R^{n+m+p} \rightarrow R^m$, an m -vector of real smooth nonlinear functions.

$x(t) : \in X \subset R^n$, a state vector of dynamic state variables, typically time dependent values of generator voltages, rotor phases and induction motor variables.

$y(t) : \in Y \subset R^m$, a state vector of instantaneous variables, typically time dependent values of voltage and angle of terminal buses, high side transformer buses and load buses.

$\mu(t) : \in P \subset R^p$, a vector of slow varying operating parameters. It can represent structural parameters like system components, reactances, under-load tap changers and switchable shunt capacitors, or operational parameters like reactive power load or generation, voltage set points on voltage control devices, as well as generation dispatch. As μ varies over the parameter space P , it is assumed that there must be at least one solution to the above differential-algebraic system of equations.

$X \times Y$: state space

for the

list of

that date

P : parameter space.

2.2.1 Model Equations

The differential-algebraic model consists of

a) Differential equations

$$\begin{aligned}
 \frac{d\delta_i}{dt} &= \omega_i - \omega_s & i = 1, \dots, n \\
 M_i \frac{d\omega_i}{dt} &= P_{mi} - D_i(\omega_i - \omega_s) - P_{ei} & i = 1, \dots, n \\
 T_{doi} \frac{dE'_{qi}}{dt} &= -E'_{qi} - (X_{di} - X'_{di})I_{di} + E_{fdi} & i = 1, \dots, n \\
 T_{Ei} \frac{dE_{fdi}}{dt} &= -(K_{Ei} + S_{Ei}(E_{fdi}))E_{fdi} + V_{Ri} & i = 1, \dots, n \\
 T_{Ri} \frac{dV_{1i}}{dt} &= -V_{1i} + |V_{Ti} + j(I_{Ti}x_{ci})| & i = 1, \dots, n \\
 T_{Fi} \frac{dV_{3i}}{dt} &= -V_{3i} + \frac{K_{Fi}V_{Ri}}{T_{Ei}} - \frac{K_{Fi}E_{fdi}(S_{Ei}(E_{fdi}) + K_{Ei})}{T_{Ei}} & i = 1, \dots, n \\
 T_{Ai} \frac{dV_{Ri}}{dt} &= -V_{Ri} + K_{Ai}(V_{REFi} - V_{1i} - V_{3i}) & i = 1, \dots, n
 \end{aligned}$$

for the generator and exciter dynamics where the variables and constants are defined in the list of symbols.

b) Stator algebraic equations

$$\begin{aligned}
 &V_i \cos \theta_i + R_{si}(I_{di} \sin \delta_i + I_{qi} \cos \delta_i) - X'_{di}(I_{qi} \sin \delta_i - I_{di} \cos \delta_i) \\
 &- [E'_{di} \sin \delta_i + (X'_{qi} - X'_{di})I_{qi} \sin \delta_i + E'_{qi} \cos \delta_i] = 0 \\
 &V_i \sin \theta_i + R_{si}(I_{qi} \sin \delta_i + I_{di} \cos \delta_i) - X'_{di}(I_{di} \sin \delta_i - I_{qi} \cos \delta_i) \\
 &- [E'_{qi} \sin \delta_i - (X'_{qi} - X'_{di})I_{qi} \cos \delta_i + E'_{di} \cos \delta_i] = 0 & i = 1, \dots, n
 \end{aligned}$$

that define the I_{qi} and I_{di} at the generator terminal buses.

c) \mathbf{M}

that de

the loc

can be

where

suscep

2.3

dimen

enviro

using

model

simul

been

c) Network (Power Balance) Equations

Terminal bus equations

$$\begin{aligned} P_i &= V_i [I_{di} \sin(\delta_i - \theta_i) + I_{qi} \cos(\delta_i - \theta_i)] + P_{Li}(V_i) & i = 1, \dots, n \\ Q_i &= V_i [I_{di} \cos(\delta_i - \theta_i) + I_{qi} \sin(\delta_i - \theta_i)] + Q_{Li}(V_i) & i = 1, \dots, n \end{aligned}$$

that define voltage and angle at generator terminal buses where $P_{Li}(V_i)$ and $Q_{Li}(V_i)$ are the loads at the terminal buses.

Load and high side transformer bus equations

The net real and reactive powers at each of the network load and transformer buses can be expressed in terms of the voltage magnitudes, conductances and susceptance as,

$$P_i = -P_{Li}(V_i) = \sum_{k=1}^n V_i V_k (G_{ik} \cos \theta_{ik} + B_{ik} \sin \theta_{ik}) \quad i=n+1, \dots, n+m$$

$$Q_i = -Q_{Li}(V_i) = \sum_{k=1}^n V_i V_k (G_{ik} \sin \theta_{ik} - B_{ik} \cos \theta_{ik}) \quad i=n+1, \dots, n+m$$

where $P_{Li}(V_i)$ and $Q_{Li}(V_i)$ are the loads at bus i and G_{ik} and B_{ik} are the conductance and susceptance of the ik 'th element of the Y-bus.

2.3 Modeling Complexity

In dynamical system theory, the power system is generally a very high-order, high dimensional multi-variable process, that is operating in a constantly changing environment. Simplifying assumptions are therefore a virtual necessity for developing and using power system analytical methods. A classification of four types of power system models of increasing complexity, that are used in the existing literature to study or simulate the various forms of power system instability is presented. A model type has been defined in [25] by the author as the simplest model that captures observability,

6
2
s

2.

me
lea
into
and
exci
1 me
actio
contr
devel
action

2.3.2

7
simula
power
exclud
dynami

controllability, feasibility region, region of attraction and modal behavior associated with at least one class of stability problem. This paper [25] discusses the known classes of stability problems for each model type.

2.3.1 Type 1 model

Type 1 model reduces a complex differential-algebraic model that includes dynamic models of both generator and loads, to an algebraic model of the generator, network and load, because the dynamic states are assumed at equilibrium. However this model takes into account the time sequence of tap changing transformer, switchable shunt capacitor and low voltage relaying actions as well as secondary voltage control, AGC and over-excitation limiter (OEL) control actions. A classical load flow model approximates a Type 1 model at steady state ($t=\infty$) and often incorrectly estimates the sequence of control actions of under load tap changers, switchable shunt capacitors, and field current limit controllers after a contingency or due to slow operating condition changes. The recently developed simulation tool of Van Cutsem [28] is an example of a Type 1 model if relaying actions are represented.

2.3.2 Type 2 model

Type 2 model is perhaps the most common power system dynamic model used to simulate and study instability. It currently includes generator inertial, flux decay, exciter, power system stabilizer, and boiler turbine governor dynamics. However this model excludes all load dynamics, for they are assumed to be decoupled from the generator dynamics, and thus do not contribute to the stability problems observed on this model. The

gen

when

P_L

2.3.

the l

contr

therm

voluta

deco

dynam

equat

dynam

model

order

althou

general form of the Type 2 model is:

$$\dot{x} = f(x, I_d, I_q, V, \theta) \quad 2.2(a)$$

$$0 = I_d - g_d(x, V, \theta) \quad 2.2(b)$$

$$0 = I_q - g_q(x, V, \theta) \quad 2.2(c)$$

$$0 = P_L - g_P(x, V, \theta) \quad 2.2(d)$$

$$0 = Q_L - g_Q(x, V, \theta) \quad 2.2(e)$$

where

x : generator dynamics

P_L, Q_L : real and reactive power load

v, θ : voltage and angle of generator terminal, high side transformers and load buses.

2.3.3 Type 3 model

In this model, the generator dynamics are modeled by constant power sources, while the load modeling includes all of induction motor and under load tap changers (ULTCs) controller dynamics, as well as dynamic models of switchable shunt capacitors, and thermostatically controlled loads. An extensive use of this model is for studying radial voltage instability, since by definition, this instability problem occurs at points electrically decoupled from the generator dynamics [30]. The vector x representing the generator dynamical states is either a constant vector or not included in the state space model equations. Therefore the complexity of this model depends on the complexity of the dynamic model used to represent the induction motor dynamics. A Type 3 power system model has the following form (2.3a-e), where the induction motor model used is a 3rd order model recently derived by Sauer and Pai [31] as an implicit load dynamic model, although other dynamic load models may alternatively be used.

where

study s

brough

2.3.4

T

load m

decay,

the loa

compos

a-c) an

equatio

Ty

power s

in Chap

models

A

experien

$$0 = P_L - g_p(x, V, \theta) \quad 2.3(a)$$

$$0 = Q_L - g_q(x, V, \theta) \quad 2.3(b)$$

$$0 = h_v\left(P_L, Q_L, V, \omega, \frac{dV}{dt}, \frac{dP_L}{dt}, \frac{dQ_L}{dt}\right) \quad 2.3(c)$$

$$0 = h_\theta\left(\omega, \frac{d\theta}{dt}\right) \quad 2.3(d)$$

$$0 = h_\omega\left(P_L, Q_L, V, \omega, \frac{dV}{dt}, \frac{d\omega}{dt}, \frac{dP_L}{dt}, \frac{dQ_L}{dt}\right) \quad 2.3(e)$$

where V , q and ω are N dimensional state variables. A type 3 model ought to be used to study saddle node bifurcation in load dynamics and saddle node and Hopf bifurcations brought on by under load tap changers and switchable shunt capacitors.

2.3.4 Type 4 model

This model combines the complexity in generator modeling of a type 2 model and in load modeling of a type 3 model. The generator model includes generator inertial, flux decay, exciter, power system stabilizer, and boiler-turbine-generator dynamics, whereas the load model may be a separate dynamic model for real and reactive power, or a composite model of real and reactive power dynamics. A Type 4 model has the form 2.2(a-c) and 2.3(a-e) if a nonlinear implicit load model is used, although the load model equations 2.3(c-e) may differ.

Type 1-3 models will later be viewed as specific subsystem models for the Type 4 power system model. This will be made clear when differential subsystems are discussed in Chapter 6. Thus it will be clear that a Type 4 model is quite general and that Type 1-3 models are only used when specific types and classes of bifurcations are to be studied.

A Type 2 model may be able to capture the generator dynamics that ultimately experience saddle node bifurcation, Hopf, or node focus bifurcation, and which may be

in

to

the

the

exp

con

over

load

event

dynam

couple

stable

approa

orbit si

under le

to take

tolerabl

dynamic

they hav

being dev

Since

tap chang

affected by load flow bifurcation, algebraic bifurcation and singularity induced bifurcation. A Type 2 model with a constant power load model, tap changers, switchable shunt capacitors in the transmission, subtransmission and higher voltage distribution system will be assumed in this thesis because it generally contains the dynamics that experience bifurcation and cause voltage collapse in a large region, a utility, or even a county. However, a Type 2 model can not accurately capture the load buildup and overshoot but just approximates the peak load produced by action of distribution system load control dynamics and the voltage control dynamics.

A Type 4 model is the only model that can hopefully simulate actual voltage collapse events. For Hopf bifurcation studies, a Type 4 model must be used because both the load dynamics and generator dynamics must be considered. Load dynamics may strongly couple to generator dynamics when subcritical (unstable), or low frequency supercritical (stable) Hopf bifurcations occur. In fact, when a pair of stable conjugate eigenvalues approaches the $j\omega$ -axis, the real part of the eigenvalues also decreases, which causes the orbit size of the associated limit cycles to increase. This causes more control actions of under load tap changers, switchable shunt capacitors and thermostatically controlled loads to take place to prevent the system equipment from operating beyond the maximum tolerable range. The impact of the load dynamics is therefore present and a full Type 4 dynamic load model is necessary to represent them. Although Type 4 models are needed, they have generally been developed only for small regions within a utility or are only being developed at the present time for larger regions.

Since a Type 2 model with voltage dependent algebraic load model, with under load tap changers, switchable shunt capacitors, control in the transmission, subtransmission,

and

voltage

1.

2.

3.

determ

capac

that is

assum

recent

perturb

Taylor

2.4 C

A

power s

Kind

and higher voltage rating distribution system is the best model available at present to study voltage collapse, they will be used in this thesis with the following assumptions

1. The load dynamics are electrically far from the generator such that they are decoupled from the generator dynamics;
2. There is reasonably good voltage control at the load buses in the system so that the load variation with voltage is small;
3. If the magnitude of stable orbits associated with generator dynamics remains large enough and if the frequency of the associated oscillations remains small enough, then significant control actions of tap changers, switchable shunt capacitors and thermostatically controlled loads should take place in response to these oscillations.

These assumptions indicate a constant power load model would be satisfactory to determine the equilibrium point set by the actions of tap changers, switchable shunt capacitor and thermostatically controlled loads, and that a perturbation load component that is voltage dependent and responsive to orbital dynamics need not exist using this assumption. Indeed, a perturbation load component model has been validated and used in recently developed simplified dynamic load models, that include both steady state and perturbation components. The perturbation load component model can be viewed as the Taylor series approximation of the system load model around equilibrium [31].

2.4 Classes and Kinds of Bifurcations in a Type 2 Model

A classification of stability problems that are observed and/or may occur on a Type 2 power system model is established in terms of kind and class:

Kind - Kind (SN, Hopf, Load Flow bifurcation...) of local bifurcations that may

occur on the specific model type.

Class - The subset of generators, controls, and/or load dynamics which exhibits the specific kind of bifurcation in this model type.

The bifurcation phenomena in the nonlinear power system model (2.1) refers to characterizing the qualitative change of the fixed points of the differential-algebraic model in (2.2) for a smooth continuous change in parameter value μ over a specified range. Although all system bifurcations usually result in a qualitative change in system behavior, they however have different effects on the dynamics of the system. Kinds of bifurcation simply refers to saddle node, Hopf etc., while a class is a further division of each bifurcation kind into the specific system dynamics experiencing the bifurcation. Kinds of bifurcations observed in a Type 2 power system model have been reported in [25] and include saddle-node, Hopf, load flow bifurcation and period doubling bifurcations. Loss of causality bifurcation may be split into a voltage, angle, or both voltage and angle bifurcation classes. Similar classes may be found for the other kinds of bifurcations. A class of bifurcation is necessary to (a) identify the subsystem dynamics and specific parameter μ or parameters μ_i of a power system model, that cause a specific kind and class of bifurcation to occur in the full dynamic model; (b) to develop methods that can identify all potential bifurcations that exist in a particular model; and (c) to find the underlying continuous or discontinuous parametric, operating schedule, or structural model control changes that produce such bifurcations.

In order to present the kinds and classes observed on a Type 2 power system model, rewrite the differential-algebraic model (2.1) as

$$\dot{x} = f(x, \theta_T, V_T, \mu) \quad 2.4(a)$$

$$0 = G_P(x, \theta_T, V_T, \mu) \quad 2.4(b)$$

$$0 = G_Q(x, \theta_T, V_T, \mu) \quad 2.4(c)$$

where

$x = [\delta, E'_q, y]$: generator dynamic state variables: δ is the angle at synchronous machine internal bus excluding swing bus, E'_q is the voltage behind transient reactance at generator internal bus and y presents the states of exciter dynamics of synchronous generator.

V_T, θ_T : voltage and angle at generator terminal, generator high side transformer and load buses, not including synchronous machine internal buses and the swing bus.

μ : parameter of interest that has an impact on the stability property of the equilibrium points of (2.4), such as real and reactive loads and generator real generation.

Local stability of a steady state equilibrium point of interest for some $\mu \in R$

$$\bar{X}_o = (x_o(\mu), \theta_{T_o}(\mu), V_{T_o}(\mu))$$

may be investigated using a linearized version of (2.4) evaluated at the equilibrium, obtained by solving the system of equations

$$0 = f(x, \theta_T, V_T, \mu) \quad 2.5(a)$$

$$0 = G_P(x, \theta_T, V_T, \mu) \quad 2.5(b)$$

$$0 = G_Q(x, \theta_T, V_T, \mu) \quad 2.5(c)$$

The Jacobian matrix of (2.4) at the equilibrium point $\bar{X}_o = (x_o(\mu), \theta_{T_o}(\mu), V_{T_o}(\mu))$ may be obtained by linearizing the differential and algebraic equations and then combining all the linearized components as shown below

$$\begin{bmatrix} \Delta \dot{x} \\ 0 \\ 0 \end{bmatrix} = J(\mu) \cdot \begin{bmatrix} \Delta x \\ \Delta \theta_T \\ \Delta V_T \end{bmatrix} \quad 2.6(a)$$

where

$$J(\mu) = \frac{\partial F(\bar{X}_o)}{\partial X} = \begin{bmatrix} \frac{\partial f}{\partial x} & \frac{\partial f}{\partial \theta_T} & \frac{\partial f}{\partial V_T} \\ \frac{\partial G_P}{\partial x} & \frac{\partial G_P}{\partial \theta_T} & \frac{\partial G_P}{\partial V_T} \\ \frac{\partial G_Q}{\partial x} & \frac{\partial G_Q}{\partial \theta_T} & \frac{\partial G_Q}{\partial V_T} \end{bmatrix}_{\bar{X}_o} \equiv \begin{bmatrix} A_1 & B_1 & C_1 \\ A_2 & B_2 & C_2 \\ A_3 & B_3 & C_3 \end{bmatrix} \quad 2.6(b)$$

$$X = (x(\mu), \theta_T(\mu), V_T(\mu))$$

$$F(X) = [f(X), G_P(X), G_Q(X)]$$

An equilibrium point $X^*_{o} = (x^*_{o}, \theta^*_{T_o}, V^*_{T_o})$ of (2.4) is called a bifurcation point and μ^* a bifurcation value if the complete Jacobian matrix $J(\mu^*)$ is singular, in which case existence or uniqueness of solutions is lost. Since the power system model as given in (2.4) is composed of both algebraic and differential equations, it is clear that an equivalent differential or equivalent algebraic equation model ought to be obtained to derive the kinds of bifurcation that may occur in the model, as will be shown in the following section.

2.4.1 Kinds of Bifurcation

From the implicit function theorem [33], a unique solution to 2.4(b) and 2.4(c) exists locally if and only if the matrix

$$J_c(\mu) = \begin{bmatrix} B_2 & C_2 \\ B_3 & C_3 \end{bmatrix} \equiv \begin{bmatrix} \partial G_P / \partial \theta_T & \partial G_P / \partial V_T \\ \partial G_Q / \partial \theta_T & \partial G_Q / \partial V_T \end{bmatrix}_{\bar{X}_o}$$

is nonsingular. If $J_c(\mu)$ is nonsingular for all x , θ_T , V_T and μ in a neighborhood of \bar{X}_o then 2.4(b-c) may be solved uniquely for $\theta_T(x(\mu)), V_T(x(\mu))$, which results in the equivalent differential equation model

$$\Delta \dot{x} = f(x, \theta_T(x(\mu)), V_T(x(\mu)))$$

which linearization gives the linear equivalent differential model

$$\dot{x} = J_x(\mu) \cdot \Delta x \quad 2.7(a)$$

$$J_x(\mu) = A_1 - \begin{bmatrix} B_1 & C_1 \end{bmatrix} \begin{bmatrix} B_2 & C_2 \\ B_3 & C_3 \end{bmatrix}^{-1} \begin{bmatrix} A_2 \\ A_3 \end{bmatrix} \quad 2.7(b)$$

Similarly, a unique solution to 2.5(a) exists locally if and only if the matrix $A_1(\mu) = \frac{\partial f}{\partial x} \Big|_{\bar{x}_o}$ is nonsingular. If $A_1(\mu)$ is nonsingular for all x , θ_T , V_T and μ in a neighborhood of \bar{x}_o then 2.5(a) may be solved uniquely for $x(\theta_T(\mu), V_T(\mu))$, which results in the equivalent algebraic equation model

$$0 = g(x(\theta_T(\mu), V_T(\mu)), \theta_T(\mu), V_T(\mu)) \quad 2.8(a)$$

or upon linearization gives the linear equivalent algebraic model

$$0 = J_y(\mu) \cdot \Delta y \quad 2.8(b)$$

$$J_y(\mu) = \begin{bmatrix} B_2 & C_2 \\ B_3 & C_3 \end{bmatrix} - \begin{bmatrix} A_1 \\ A_2 \end{bmatrix} [A_1]^{-1} \begin{bmatrix} B_1 & C_1 \end{bmatrix} \quad 2.8(c)$$

The power system defined by (2.4) with equivalent differential equation model 2.7(a) is said to be asymptotically stable iff all the eigenvalues of the equivalent differential system Jacobian matrix $J_x(\mu)$ have negative real parts. Hence a critical state is a state when one or a pair of eigenvalues become non-hyperbolic and have zero real part. Kinds of bifurcation on a Type 2 model are summarized in the following:

(i) **Saddle Node Bifurcation (SN)**

Occurs at $\mu = \mu^*$ when $J_c(\mu^*)$ is nonsingular and the system (2.7) has one real eigenvalue that crosses the imaginary axis of the complex plane and where certain transversality conditions hold [App C]. In this case the system trajectories are attracted by the center manifold, and the system behavior becomes monotonic and

may experience monotonic instability, i.e. collapse type of instability.

(ii) **Hopf Bifurcation (H)**

Occurs at $\mu = \mu^*$ when $J_c(\mu^*)$ is nonsingular and the equivalent differential Jacobian matrix $J_x(\mu^*)$ has one pair of imaginary eigenvalues with zero real parts. Additional transversality conditions must also be satisfied [App C]. In the neighborhood of this point, periodic solutions always exist and the stability of the system is determined by the stability of the periodic solutions (limit cycles). A Hopf bifurcation can be stable (supercritical) or unstable (subcritical). Both supercritical and subcritical Hopf bifurcations have been observed on a single-machine-infinite-bus model [25].

(iii) **Load Flow Bifurcation (LF)**

Occurs in the system equivalent algebraic model 2.8(a), at $\mu = \mu^*$ when $A_1(\mu^*)$ is nonsingular and the equivalent algebraic Jacobian $J_y(\mu^*)$ in 2.8(c) has one simple zero eigenvalue. This bifurcation is called Load Flow (LF) bifurcation because it indicates a system at equilibrium is unable to satisfy the system power flow requirements imposed by the given generation and demand requirements. The system in 2.8(a) is called the Exact Load Flow Model since these equations represent the power balance equations at all buses in the system, while the 'classical' load flow model will be shown in Chapter 4 to be an approximation of this model.

(iv) **Loss of Causality**

Occurs when $J_c(\mu)$ becomes singular as μ varies. Simulation cannot be performed on the system (2.4) since 2.4(b-c) have no solution or have multiple solutions

$$\begin{bmatrix} \theta_{T_i}(x(\mu)) \\ V_{T_i}(x(\mu)) \end{bmatrix} \quad i = 1, 2, \dots$$

in the neighborhood of an equilibrium $\bar{x}_o = (x_o, \theta_{T_o}, V_{T_o})$. If there is no solution, the system trajectory terminates abruptly. If multiple solutions exist, random discontinuous trajectories can occur as the solution $(\theta_{T_i}(x(\mu)), V_{T_i}(x(\mu)))$ changes rapidly from time point to time point. Two types of loss of causality may occur.

(a) Algebraic Bifurcation [35]

Occurs when the submatrix of $J(\mu)$,

$$J^*(\mu) = \begin{bmatrix} A_2 & B_2 & C_2 \\ A_3 & B_3 & C_3 \end{bmatrix} = \begin{bmatrix} J_{PL}^* \\ J_{QL}^* \end{bmatrix}$$

becomes row dependent at $\mu = \mu^*$. Hence it requires that the differential-algebraic bifurcation occurs in a subset of the equations. Note that algebraic bifurcation may suggest that there are no solutions of the form (x_T, θ_T, V_T) or multiple solutions $(x_i, \theta_{T_i}, V_{T_i})$, $i=1,2,\dots$

(b) Singularity Induced Bifurcation (SI)

Occurs when the full system Jacobian matrix $J_x(\mu)$ is nonsingular with eigenvalues crossing from the right half plane to the left half plane or vice versa by going through infinity, rather than across the imaginary axis ($j\omega$ -axis).

At this point, one real eigenvalue of the system is at infinity and the rest of them are bounded which makes simulations using the differential-algebraic model not possible.

(v) Node-Focus (NF)

Occurs in the case of multiple eigenvalues when a pair of complex conjugate

eigenvalues become two equal real eigenvalues. A node focus bifurcation (NF) may be stable or unstable depending on whether the real part of the eigenvalue pair is negative or positive, respectively.

- (vi) **1:1 Resonance**: Occurs in the case of multiple eigenvalues when two pairs of complex conjugate eigenvalues become two equal complex eigenvalues.

At (SN), (H) and (SI) bifurcation points, local system steady state stability around the equilibrium point changes. At 1:1 resonance point, the system may experience non-linear oscillatory behavior due to order 1 resonance. In this case, participation factors, eigenvectors and residues can be misleading because eigenvectors are not unique and they lose their physical meaning.

2.4.2 Classes of Bifurcation

For each kind of bifurcation, the bifurcation subsystem method will attempt to identify subsystems of smaller and smaller dimension to determine the smallest bifurcation subsystem that produces and causes the bifurcation. The bifurcation subsystem implies the class of bifurcation of the particular kind which will be investigated in Chapters 4-6. Classes of bifurcation in a Type 2 power system model may be

- (a) the power system differential equations;
- (b) the power balance equations at load buses;
- (c) a generator's inertial, flux and exciter dynamics;
- (d) a generator's electrical dynamics;
- (e) the control systems dynamics (PSS, Governor..) on a generator;
- (f) a combination of the above.

An investigation to find the smallest bifurcation subsystem that experiences and causes the bifurcation in the full system is initiated theoretically in Chapter 4 and continued to the end of the thesis.

2.4.2.1 Classes of Loss of Causality in a Type 2 Model

Although the two kinds of loss of causality system bifurcations (algebraic bifurcation, and SI bifurcation) all produce truncation of trajectory, they have quite different effects on generator dynamics. Loss of causality may occur in real power-angle variables, in reactive power-voltage variables, or in both angle and voltage variables.

(i) Angle Loss of Causality

Occurs when $\begin{bmatrix} B_2 & C_2 \end{bmatrix} = \begin{bmatrix} \partial G_P / \partial \theta_T & \partial G_P / \partial V_T \end{bmatrix}$ is row dependent, thus since $\begin{bmatrix} B_2 \end{bmatrix}$ is singular, this loss of causality is due to real power-angle instability.

(ii) Voltage Loss of Causality

Occurs when $\begin{bmatrix} B_3 & C_3 \end{bmatrix} = \begin{bmatrix} \partial G_Q / \partial \theta_T & \partial G_Q / \partial V_T \end{bmatrix}$ is row dependent, thus since the square matrix $\begin{bmatrix} C_3 \end{bmatrix}$ is singular, the loss of causality is due to reactive power-voltage instability.

(iii) Voltage and Angle Loss of Causality

Occurs when $J_c(\mu)$ is row dependent but neither $\begin{bmatrix} B_2 & C_2 \end{bmatrix}$ nor $\begin{bmatrix} B_3 & C_3 \end{bmatrix}$ is row dependent resulting in a voltage and angle loss of causality.

2.4.2.2 Classes of Static Bifurcation in a Type 2 Model

Static bifurcation in a Type 2 model occurs when the matrix $J_c(\mu)$ is nonsingular and

$$J_x(\mu) = A_1 - [B_1 \ C_1] \begin{bmatrix} B_2 & C_2 \\ B_3 & C_3 \end{bmatrix}^{-1} \begin{bmatrix} A_2 \\ A_3 \end{bmatrix}$$

is singular as m changes. Saddle node bifurcation is a special but generic case of static instability which occurs when a single eigenvalue of $J_x(\mu)$ is zero and certain transversality conditions hold [App C]. Two classes of static bifurcation may occur on a Type 2 power system model:

(i) Static Bifurcation in generator inertial dynamics

Static bifurcation in generator inertial dynamics may be associated with the loss of transient [App. B] stability [36] such as the voltage instability that occurred in the Czechoslovakian system after tripping lines in a major interface [30]. This class of static bifurcation is likely to occur when the disturbances are very large and the transmission interfaces or boundaries are weak, so that loss of stability occurs soon after the contingency before the field current level/duration limits are reached.

(ii) Static Bifurcation in generator flux decay dynamics

This bifurcation has been called classic voltage instability and is due to insufficient reactive supply in the EHV system, an example of which is the blackout that occurred in the French system [37]. This class of stability has been analyzed with the use of a sensitivity matrix between reactive generation and voltage at generator internal buses $S_{Q_{GE}}$. The matrix $S_{Q_{GE}}$ is diagonally dominant for inductive networks (networks that absorb reactive power), and not diagonally dominant for capacitive

network (network with long high voltage transmission lines). Classic voltage instability has been described as occurring when generators reach their field current limits and the field current limit controllers disable the exciters. An important implication to this result is that studying this saddle node bifurcation must include the field current limit controllers action in the model.

2.4.2.3 Classes of Dynamic Bifurcation in a Type 2 Model

Three classes of dynamic bifurcation may exist and have been observed in a Type 2 power system model

(i) **Hopf in generator inertial/flux decay/exciter dynamics:**

Hopf bifurcation in generator inertial, flux decay and exciter dynamics and is associated with low frequency inter-area oscillations in a power system. This mode of oscillation is usually referred to as a swing mode and appears as stable limit cycles (supercritical) [15].

(ii) **Hopf in generator flux decay/exciter dynamics:**

Hopf bifurcation in the flux decay/exciter control dynamics. This mode of oscillation is usually referred to as voltage swing modes and appear as unstable limit cycles (subcritical) in literature [15].

(iii) **Hopf in generator inertial/flux decay dynamics:**

Hopf bifurcation in generator inertial/flux decay dynamics and occurs only when the exciter is completely disabled. This mode of oscillation is called the voltage collapse mode and has been shown to occur in the single machine infinite bus model [15].

III

POWER SYSTEM STABILITY ASSESSMENT A TAXONOMICAL APPROACH

3.1 Introduction

Power system stability can be broadly defined as that property of a power system which enables it to remain in a state of operating equilibrium under normal operating conditions, and to regain, in a finite time, an acceptable state of equilibrium after being subject to a disturbance [29]. Stability analysis of post contingency equilibrium point or limit cycle using dynamical system theory for smooth nonlinear systems, although necessary, is not generally sufficient for assessing stability of equilibria or limit cycles of the power system dynamical model. Stability analysis for smooth nonlinear systems must also be performed for points in parameter space where parameter change is continuous. Assuring power system security based on describing local stability of an equilibrium, determining local connected regions in state and parameter space where local stability is retained (feasibility region) and region of stability for trajectories when parameters are fixed, has been investigated in [26]. This work is being extended [27] to include effects of hard limits and equipment outages which discontinuously modify the model order, the structure, equilibria and dynamic behaviors

A realistic power system model is characterized by nonsmooth elements, the most important of which are the hard limits encountered during system operation. In power system terminology, “saturation” is usually reserved for denoting smooth effects associated with saturation phenomena such as field saturation; and “hard limits” are usually associated with nonsmooth effects such as actuation limits, tap changer limits, relay effects, etc. From a conceptual point of view, there exists three types of hard limits: (a) windup limits or actuation limits [27]; (b) nonwindup limits or state limits [27]; and (c) relay type limits or switching limits [27]. Depending on how a system with saturation limits comes back to the limit, windup and non-windup limits are distinguished. Whereas windup limits can come off the constraint at any time, this is not possible for nonwindup limits before the windup variable has been released completely. Hard limits are generally associated with actions of operator control; actions of protective devices such as relays or field current limit controllers; actions of under load tap changers and actions of switchable shunt capacitors.

An example that qualitatively portrays the effect of consecutive discontinuities on a state trajectory is shown in Figure 3.1 as well as Figure 3.2 [40] and Figure 3.3 [41] for simulations on actual detailed power system models. The standard bifurcation theory for smooth systems [26], being based on the functions f and g in Equation (2.1) being smooth, is not applicable to assess the stability of the system experiencing such discontinuous transitions. Since voltage collapse time scenarios are characterized by all of the discontinuities described above, it is necessary to extend the stability analysis for models with discontinuities (hard limits and contingencies).

The stability analysis of a power system is complicated by the lack of smoothness

needed to characterize not only the bifurcations existing on smooth systems, but also because new bifurcations that are directly connected with the hard limits must be described. Such bifurcations include hard limit induced static bifurcations and hard limit induced dynamic bifurcations [27,42-43]. Although the purpose of this thesis is not to develop an extension of stability theory for hard limits, a brief description of the current development on this subject is necessary for consistency and a better understanding of the theoretical framework under which the bifurcation subsystem method is being developed.

In this chapter, a rather brief description of the recent development of the taxonomy of the large differential algebraic power system model is given. Zaborsky's taxonomical work of 1991 [26] which summarizes a method for applying dynamical system theory to a smooth power system model is reviewed in Section 3.2 and a discussion of the status of the theoretical development on the extensions of this taxonomy to include models with hard limits discontinuities [27] is briefly reviewed in Section 3.3. A parametric episodal approach to security assessment is then proposed that

- a. analyzes the stability region, feasibility region and viability region for the continuous analytical model in intervals (t_i^+, t_{i+1}^-) between instants t_i and t_{i+1} where discontinuities brought on by equipment outages or hard limit induced model changes occur; and uses this analysis to decide stability, feasibility and viability of the entire trajectory;
- b. enumerates all equipment outages and operating changes for which the trajectories and attracting equilibria and limit cycles of the system are expected to be stable and viable and then establishes for which contingencies and operating changes the trajectories are indeed unstable or nonviable. Viability for equilibria, limit cycles and

transients is defined to be those equilibria, limit cycles and transients which (i) do not cause equipment damage; (ii) do not cause relaying actions for protecting equipment of the system; and (iii) have voltage, current, frequency and power variations that are within acceptable design and operating ranges.

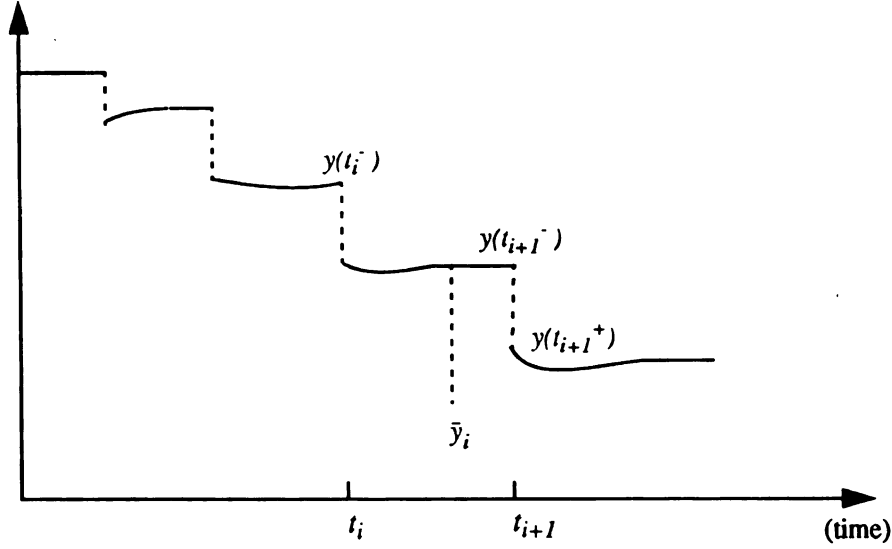


Figure 3.1 2-D example portraying the effects of the i th discontinuous control action. (y_i) is the i th quasi equilibria

3.2 A Taxonomy of Stability Assessment in Power System

A taxonomy theory refers to a general and structural theoretical analysis of the dynamic behavior of very large nonlinear systems. Assessing local and transient stability [App B] of a power system as well as maintaining its security for parameter changes in an operating range is certainly a taxonomical task. Security has been defined in Zaborszky [26] in parameter and state space as operating conditions which belong to the feasibility region, stability region (region of attraction) and viability region. The state space includes

both the dynamic state vector x and algebraic state vector y , whereas the parameter space includes structural parameters such as transmission network capacitances and topology, and operational parameters that could include

- a. the level and variation of real and reactive load as a function of voltage and frequency at each bus;
- b. the real generation at every generator and its change with frequency, load level, and area control error as well as its upper and lower limits;
- c. the voltage setpoints on generators exciters, or voltage setpoint upper and lower voltage limits on switchable shunt capacitors and the upper limit on their susceptance, and voltage limits and tap setting limits on under load tap changing transformers;
- d. the transfer or wheeling actions taken.

There are numerous parameters above and beyond those itemized above but these are certainly important parameters in deciding when voltage stability is retained or lost [11]. Assessing stability of the large power system for a specific equilibria or limit cycle requires the assessment of four regions: region of stability, feasibility region, viability region and security region, which definitions are based on Zaborszky [26], the Zaborszky's discussion [47] of a paper by Schlueter and Benkilani [25], and their reply [48]. The definitions are not new but generalize the definitions found in [26] as suggested by the discussion and reply.

3.2.1 Region of Attraction of a Specific Equilibrium or Limit Cycle

The region in state space where every trajectory originating inside, will finally converge to the specific attractor of a particular type (equilibrium point or closed orbit) for a

specific set of operating parameters $p = p_o$. The region of attraction in state space is different for each specific point p_o in parameter space that belongs to a feasibility region of that specific attractor of a particular type.

3.2.2 Feasibility Region of a Specific Equilibrium or Limit Cycle

The region in parameter and state space, within which a specific attractor of a particular type (operating equilibrium point or stable closed orbit) can be shifted smoothly from any point in the region to any other point by continuous parameter change while retaining local stability. Structural stability holds [34,50] within the feasibility region for each specific attractor of a particular type.

3.2.3 Viability Region of a Specific Equilibrium or Limit Cycle

The region in parameter and state space belonging to a feasibility region of a specific attractor of a particular type where the values of the state variables, i.e. voltages, current, frequency, active or reactive power for the specific attractor of a particular type remain within prescribed limits. The bounds can be based on physical device limitations on parameters or states; safe operating limits on parameters or states; hard limits based on device limitations or relay actions for protection of the device or system.

3.2.4 Viability of Transient Trajectory

A trajectory that is stable and belongs to a region of attraction of a specific simple attractor of a particular type that belongs to the feasibility region for that specific attractor of a particular type is viable if the current, voltage, frequency or other variable trajectory does not cause equipment damage, does not exceed design limits, and does not trigger relay actions that protect equipment or system operation.

3.3 Development of a Taxonomy for Power System Models with Hard Limits

The taxonomy developed in [26,27] is certainly the first rigorous effort to describe stability in a differential-algebraic power system model, and yet the taxonomy is still under development. One major area of development is the inclusion of hard limit-induced discontinuities, which occur during operation when

1. the generator field current reaches its magnitude and duration limits so the field current limit controller either causes a relay to disable the generator exciter or reduces the exciter voltage setpoint and thus field current down to a sustainable level that will not produce thermal damage to the generator rotor;
2. the controlled bus voltage remains outside the prescribed upper or lower voltage limits, and under load tap changers discontinuously and abruptly change the turns ratio on a transformer to bring the voltage within limits. The action is possible as long as the tap settings remain within tap position limits. If under load tap changers reach upper or lower tap position limits, a second hard limit induced discontinuity is encountered;
3. the voltage at the controlled bus exceeds lower or upper voltage limits, a switchable shunt capacitor switches one or more banks of capacitors in or out to bring the controlled voltage within limits.

Voltage collapse in the distribution system can be prevented by actions of under load tap changers and switchable shunt capacitors as long as the under load tap changers remain within the tap setting limits and switchable shunt capacitors remain within the capacitive susceptance limits. However when a sufficient number of generators reach field

current limits, tap changers reach tap position limits, and switchable shunt capacitors reach capacitive susceptance limits, voltage collapse will occur due to loss of voltage controllability [11].

The discontinuities associated with generator field current limit controllers, under load tap changer controllers, and switchable shunt capacitor controllers can be modeled using actuation (windup); state (nonwindup); and relay hard limits. Due to the discontinuous nature of the actuation, state and relay hard limit models [27], the taxonomy described for smooth dynamical systems can not be used to describe the feasibility region and stability region for voltage collapse which develop when generator field current limit controllers, under load tap changer controllers and switchable shunt capacitor controllers hit hard limits in response to equipment outages or continuous operating changes.

Zaborszky [27] has started the long process of extending the taxonomy so that it can include actuation, state and relay limits. The status of taxonomy development and its structure is now described.

- (1) The model used [27] is a differential equation model rather than the differential-algebraic model used in the taxonomy without hard limits [26]. When hard limits are ignored in the model, the boundary of the feasibility region has segments due to Hopf bifurcation, saddle node bifurcation and singularity induced bifurcation, whereas singularity induced bifurcation can not be part of a feasibility region boundary in the taxonomy being developed for a differential equation model with hard limits. In the taxonomy without hard limits [27], the boundary of the region of stability allows

- (i) stable manifolds of order 1 equilibria;

- (ii) stable manifold of periodic orbits;
 - (iii) stable manifolds of pseudo saddles, semi saddles and bad anchors;
 - (iv) singular boundary pieces;
- among others where the stable manifolds of pseudo saddles, semi saddles, bad saddles and singular pieces could not belong to the stability boundary for a taxonomy being developed for a differential equation model with hard limits [27];
- (2) the feasibility region for a differential equation model with actuation and state hard limits have been derived but not for relay limits. The feasibility boundary for actuation (state) limits is composed of segments due to saddle node bifurcation, Hopf bifurcation, actuation (state) induced dynamic bifurcation, and actuation (state) induced static bifurcation. The actuation induced static bifurcation and state induced static bifurcation behaviors near the feasibility boundary are similar to saddle node bifurcation except that the transversality and bifurcation conditions are somewhat different. The actuation induced dynamic bifurcation behavior is similar to Hopf bifurcation except that the transversality conditions at the bifurcation point are different;
- (3) When windup limits are modeled in the analysis, equilibria and their stability properties change and the system transient trajectories are characterized by nonsmoothness (“kinks”). The unstable equilibria which anchor the stability boundary may correspond to points where hard limits are encountered, hence results from these equilibria differ from those of the smooth systems. Although the boundary of the stability region is composed of stable manifolds of unstable equilibrium and periodic orbits, these manifolds have corners or kinks (actuation) or have different dimension

if state or relay limit are reached. The analysis of the region of stability and characterization of its boundary is only complete for actuation limits. This task is far more challenging for state and relay hard limits since the state space for state and relay limits consists of several smooth systems of varying dimensions.

The most important conclusion [27] is that there is indeed a stability region boundary when hard limits are included in the model and where one or more hard limits are reached either on the trajectories on the stability boundaries or on trajectories that are initiated at some point within the region of stability and converge to some equilibrium. Another conclusion is that within the epoch (t_i^*, t_{i+1}^*) , the trajectory is smooth and the feasibility and stability regions satisfy all the properties of a model where hard limits are ignored. A final conclusion is that the nonsmoothness of the stable manifolds means that the construction of Lyapunov functions or energy functions is more difficult and requires different techniques than the typical u.e.p based methods used in models without hard limits.

3.4 Stability Security Assessment for Model with Hard Limits

The desire in developing a taxonomy for studying stability in a power system model is to be able to assess retention or loss of stability without time simulation of the system, or quite possibly with almost no simulation of the contingency or operating change. The stability region, feasibility region, and viability region and their boundaries are known if such a taxonomy is complete. Even if the taxonomy were known, its success of avoiding time simulations appears questionable, since one is unable to predict apriori the post contingency or operating change steady state equilibrium point or limit cycle without time

simulation. This is because (1) the set of hard limits and the sequence through time at which they are encountered is impossible to predict apriori and (2) knowing the set of hard limits and their sequence over time is necessary to determine the final post contingency equilibrium point or limit cycle. The fact that the set and time sequence of hard limits encountered not only determine the equilibria or limit cycle trajectories converge to but whether they are stable or unstable, is documented in [41]. The reasons that it is impossible to predict the equilibria or limit cycles and their stability are (i) that the hard limit encountered in a power system model are never enabled instantaneously when the limit is encountered, (ii) the delay for each hard limit is different and can depend on the magnitude of the violation and duration of the hard limit, and (iii) the delay may be large compared to the transient response of the dynamics, (iv) the sequence of future hard limit control actions are dependent on previous ones, (v) the system is highly nonlinear so different sequence of hard limit control actions give different ultimate results.

An approach is now proposed that studies stability of the equilibrium or limit cycle as well as transient stability epoch by epoch where an epoch is a period of time $t_i^+ < t < t_{i+1}^-$ (see Figure 3.1) where no hard limit transitions occur. This method would utilize the taxonomy to study stability of equilibria, limit cycles and trajectories within epochs, rather than attempting to study stability of the entire trajectory as well as the steady state equilibrium or limit cycle without simulation. The justification for this approach is that the taxonomy being developed with hard limits [27] indicates that the taxonomy developed for models without hard limits [27] applies to time intervals (t_i^+, t_{i+1}^-) as well as for subintervals in state space where no hard limit transition surfaces are encountered. An Epoch Based Trajectory Stability Assessment Method is discussed in Section 3.4.1.

A second change in stability assessment methodology to be discussed is to consider an episodal trajectory stability assessment rather than attempting to use a taxonomy which might determine stability without time simulations for all trajectories resulting from (a) disturbance initiated changes in initial state but no change in model; (b) continuous slow operating changes in parameters of that model and (c) power system models with no delay hard limit so that the set and sequence of hard limits encountered can be known. Utilities currently utilize an episodal stability assessment rather than a taxonomy based method in dynamic security assessment and contingency selection for fault contingencies [52]. The motivation for this taxonomy is based upon the earlier work on fault contingencies. The use of an episodal rather than a taxonomic method is due to the fact that most realistic fault contingencies are followed by a number of discontinuities which could not be predicted to occur without time simulation. Thus taxonomy based methods and episodal methods are competing in an application where taxonomy based methods held dominance for years due to their promise in providing accurate stability assessment without the need for time simulation. An episodal trajectory stability assessment is thus proposed for the equipment outages and operating changes that cause voltage instability. Utilities currently specify the contingencies and the range of operating condition changes they expect to survive without loss of voltage stability. If one can quickly assess stability of trajectories produced by each of the set of contingencies for the ranges of operating conditions specified epoch by epoch to find those that are stable and those that are unstable, then a contingency selection or stability assessment procedure, in the language of power system engineering, could be produced. The set of trajectories that are viable and transient stable [App B] to attracting sets (equilibria and limit cycles) that are feasible and viable for every epoch are

said to belong to a Bounded Trajectory Feasibility Set. A discussion of the contingency selection and Bounded Stable Trajectory Feasibility Methodology is given in Section 3.4.2.

3.4.1 Epoch Based Trajectory Stability Assessment

The Epoch Based Trajectory Stability Assessment is proposed because each hard limit induced model change may produce

- (a) a model

$$\begin{aligned} \dot{x}_i &= f_i(x_i, y_i, \mu_i) & t_i^+ < t < t_{i+1}^- \\ 0 &= g_i(x_i, y_i, \mu_i) \end{aligned} \quad (3.1)$$

where an equilibrium (\bar{x}_i, \bar{y}_i) may or may not exist;

- (b) a stable or unstable equilibrium point;
(c) a stable limit cycle encircling the unstable equilibrium point;
(d) a region of attraction for that stable equilibrium point or limit cycle that is sufficiently large to include $(x(t_i^-), y(t_i^-))$.

All four questions (a-d) must and will be assessed for each time epoch (t_i^+, t_{i+1}^-) to be able to diagnose when and why the trajectory does not converge to a final attracting set as time progresses. The Epoch Based Trajectory Stability Assessment is based on a trajectory simulation method implemented by Van Cutsem in 1992 [28] that does not require time simulation in (t_i^+, t_{i+1}^-) , but only computes the quasi equilibria (\bar{x}_i, \bar{y}_i) for $i = 1, \dots, N$ since it has been found that

- (a) the transition to the quasi equilibria (\bar{x}_i, \bar{y}_i) is stable because the region of attraction is generally large;
(b) that $x_i(t_{i+1}^-) = \bar{x}_i$ and $y_i(t_{i+1}^-) = \bar{y}_i$ since the time $T = t_{i+1}^- - t_i^+$ between hard limit

model changes is large enough to cause the trajectory to reach steady state at each hard limit model change;

- (c) The lack of a stable equilibrium without existence of a stable limit cycle may be observed as a diverging set of quasi equilibria.

If one has an unstable sequence of quasi equilibria (\bar{x}_i, \bar{y}_i) but a stable encircling limit cycle around each quasi equilibria, this rapid simulation method [28] would not indicate retention or loss of stability. Furthermore it has been found that the short term dynamics and long term dynamics interact and thus such a rapid simulation method is not always adequate [41]. The Epoch Based Stability Assessment Method utilizes the rapid simulation method to evaluate quasi equilibria (\bar{x}_i, \bar{y}_i) but takes into account not only stability and feasibility of quasi equilibrium (\bar{x}_i, \bar{y}_i) but also stability of trajectory during each epoch.

In order to illustrate the argument that the rapid simulation method is needed to simulate the voltage stability trajectories with a large number of discontinuities but is inadequate to assess the interactions of short and long term dynamics that cause instability without Epoch Based Trajectory Stability Assessment, we bring out two examples from recent literature. Figure 3.2 shows the time simulation of the active power load of a large utility system after a severe fault where the over-excitation limiter controller (OEL) disabled the exciter on one machine but all other machine protection devices are enabled [41]. The disturbance was an EHV line fault and line trip which resulted in tripping a large generator unit off-line. The model includes excitation systems, turbine/governor systems, PSSs, generator protection functions, AGC...etc. The transition dynamics which occur due to the action of voltage protective devices (LTCs, switchable shunt caps..) clearly manifest a nonsmooth behavior. A number of discontinuities occurred before the system was driven

to voltage collapse and thus a rapid time simulation method [28] is needed. This example would not need to simulate the trajectories in epochs but only needs to determine quasi equilibria provided by the Epoch Based Trajectory Stability Assessment because the quasi equilibria capture the response of the system and no short term dynamic behavior is observed. Feasibility and viability of equilibria could be utilized to assess why the system experienced voltage collapse.

Figure 3.3 is intended to demonstrate interaction of short term and long term dynamic behavior via simulation of the active power flow between two regions following tripping of a line and a generator in a Swedish test system [41]. We notice that due to the severe fault, the dynamic behavior was initiated by large oscillations, which after the activation of the OEL and the tap changers reduced to smaller limit cycles. As the voltage keeps dropping, the system was finally driven to voltage collapse. Three crucial phenomena are demonstrated by this figure: (1) Viability of limit cycles is necessary in each epoch; (2) quasi stable/unstable limit cycles rather than quasi equilibria may exist; and (3) both long term and short term dynamics must be considered to assess stability and security of the entire trajectory. Viability, feasibility and region of stability of trajectory segments and the feasibility and viability of equilibria and limit cycles would be needed to assess why voltage collapse occurred in this system.

In order to address the stability of the full trajectory $(x(t), y(t))$ as well as the interaction of short term and long term dynamics, time simulation or taxonomy based stability assessment within epochs $t_i^+ < t < t_{i+1}^-$ is necessary. The Epoch Based Trajectory Stability Assessment that avoids complete time simulation within (t_i^+, t_{i+1}^-) that utilizes a taxonomy stability assessment in each epoch to computes

(1) $x(t_i^+) = \bar{x}_{i-1}$ and $y(t_i^+) = \bar{y}_{i-1}$ by solving for $(\bar{x}_{i-1}, \bar{y}_{i-1})$ from

$$f_{i-1}(x_{i-1}, y_{i-1}) = 0 \quad 3.2(a)$$

$$g_{i-1}(x_{i-1}, y_{i-1}) = 0 \quad 3.2(b)$$

(2) $y(t_i^+)$ by assuming $x(t_i^+) = x(t_i) = \bar{x}_{i-1}$ using

$$g_i(\bar{x}_{i-1}, y(t_i^+)) = 0 \quad (3.3)$$

This assumption is based on the fact that whereas the algebraic state vector $y(t)$ may change instantly, this is not possible for the dynamic state vector $x(t)$. Infinite power is needed to cause an instantaneous change in $x(t)$. The Epoch Based Trajectory Stability Assessment then checks

- (i) if solutions $(\bar{x}_{i-1}, \bar{y}_{i-1})$ and $(\bar{x}_{i-1}, y(t_i^+))$ exist;
- (ii) if $(\bar{x}_{i-1}, \bar{y}_{i-1})$ is stable and viable;
- (iii) if $(x(t_{i-1}^+), y(t_{i-1}^+))$ lies within the region of attraction of $(\bar{x}_{i-1}, \bar{y}_{i-1})$ if step (ii) is true;
- (iv) establishes if there are attracting sets (closed orbits) surrounding the unstable equilibrium and whether they are stable if step (ii) is not true;
- (v) establishes whether these attracting sets are stable and viable if step (iv) is true;
- (vi) establishes whether $(x(t_{i-1}^+), y(t_{i-1}^+))$ lies in the region of attraction of the attracting set if steps (iv) and (v) are true.

Stability and viability are assumed to be retained if the answer to step (i) and either steps (ii) and (iii) or steps (vi), (v), and (vi) are true. Such a procedure would eliminate the need to perform time simulation and would only require solving $y(t_i^+)$ using equation (3.3) and checking (i-vi)

A slight expansion of the above (i-v) rules for testing trajectories via trajectory seg-

ments in epochs (t_i^+, t_{i+1}^-) for the diagnostics of knowing feasibility, viability and stability is given below

- (a) Every post contingency steady state operating point or stable limit cycle, and every quasi equilibrium point (\bar{x}_i, \bar{y}_i) or limit cycle which occurs at the i 'th discontinuous control action, must exist, be stable and viable and thus reside in the (non-empty) intersection of its viability region and its feasibility region. (feasibility, viability)
- (b) Assuming $(x(t_i^+), y(t_i^+))$ accurately reflects the unmodeled transition from $(x(t_i^-), y(t_i^-))$ to $(x(t_i^+), y(t_i^+))$ for each i , the stability for the transition from $(x(t_i^-), y(t_i^-))$ to the stable steady state or quasi equilibrium point (\bar{x}_i, \bar{y}_i) or its stable encircling limit cycle can be decided by checking whether $(x(t_i^+), y(t_i^+))$ lies within its region of attraction for each $i = 1, 2, \dots, N$.
- (c) Shrinking unstable limit cycles around the stable steady state or quasi equilibrium point constrain the size of its region of attraction. A lower limit on the size of the unstable limit cycles should be prescribed. (viability of unstable limit cycles)
- (d) Every trajectory initiating in the region of attraction of each steady state or quasi stable equilibria does not stall or trip motors, does not cause equipment damage, relay action to protect equipment, and operator emergency action to trip generators off the system. (viability of transient trajectory)
- (e) Stable limit cycles around unstable steady state or quasi equilibrium points that are viable must also satisfy the additional condition to be small enough to prevent damage of equipment. An upper limit on the size of the limit cycles is prescribed so that (e) equipment damage could not occur or (b) so that the region of attraction could not disappear (as the limit cycles reach the boundary of the region of attraction).

(viability of stable limit cycles)

Performing steps (ii - vi) or (a-e) is computationally difficult if not impossible at present due to the very large dimension of models. Research is underway to make possible rapid evaluation of steps (ii - vi). This thesis on development of a bifurcation subsystem method would allow one to quickly assess whether the equilibrium is stable or unstable and whether the attracting set (if one exists) is stable or not with very little computation. The bifurcation subsystem method identifies the small dimension subsystem that experiences the same bifurcation as the entire system and for the same value of the bifurcation parameter. The natural sparse structure, weak coupling and geometric structure of the model cause bifurcation subsystems to exist. Furthermore, the bifurcation subsystem method would indicate not only which parameters of a linearized model cause a specific bifurcation to occur, but also what operating changes cause that bifurcation to occur.

The bifurcation subsystem method may also identify the subsystem dynamics that determine the stable manifold of a particular unstable equilibrium that belongs to the boundary of the region of attraction. Although investigation of how the dynamics of the bifurcation subsystem defines a stable manifold of an unstable equilibrium, is beyond the scope of this thesis, it is an important subject for the future.

Bifurcation subsystems appear to be omnipresent in a power system model. The bifurcation subsystem can not generally be identified using eigenvectors or participation factors because the eigenvectors indicate the states affected by the bifurcation eigenvalue and not the subsystem that specifically experiences the same bifurcation as that experienced in the full system. The bifurcation subsystem of a differential-algebraic model may be differential, algebraic, or differential-algebraic depending on the kind and class of

bifurcation experienced. Each bifurcation subsystem needs to be checked for structural stability and retention of stability at each quasi equilibrium (\bar{x}_i, \bar{y}_i) to assume stability during each epoch. If such assessments are rapid, the epoch based trajectory stability assessment is a natural procedure for performing a contingency selection and stability assessment that does not require time simulation in each epoch.

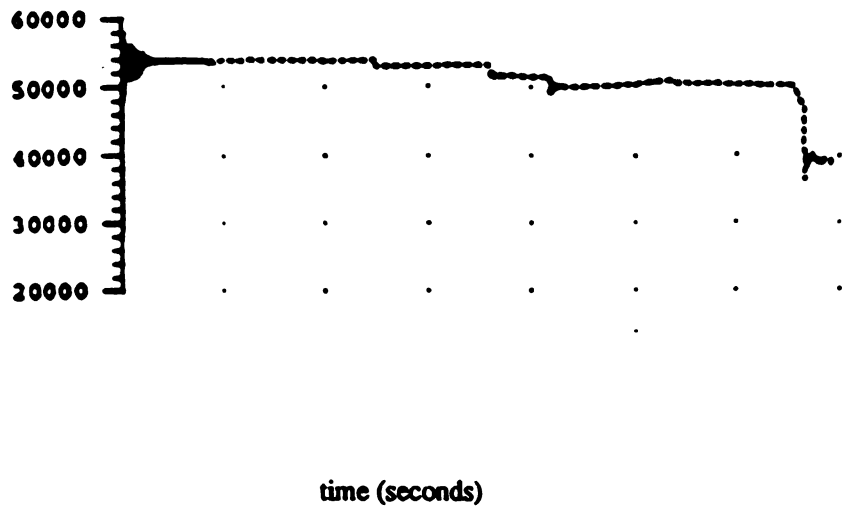


Figure 3.2 System active power load (MW) of a system [40] after a severe disturbance: EHV line Fault & line trip which resulted in a large generator off-line

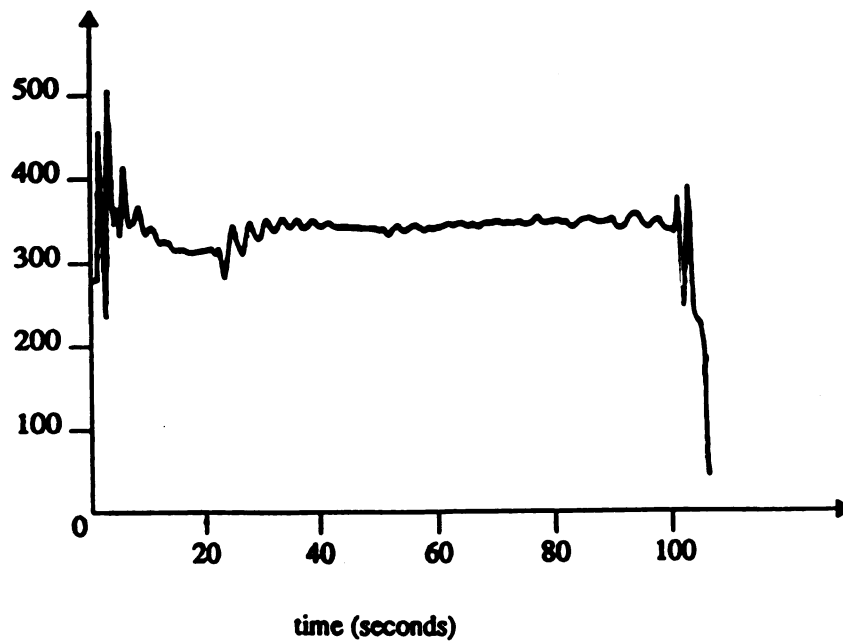


Figure 3.3 Active power flow between Central and Southwest regions of the Swedish test system [41] after the tripping of a line & generator in the North

3.4.2 Bounded Stable Trajectory Feasibility Method

A Bounded Stable Trajectory Feasibility Method is proposed because the trajectories initiated by contingencies or operating changes which experience voltage collapse or other types of instability are marked by a number of discontinuities such as the contingency itself or a hard limit-induced discontinuity such as described in Section 3.3. Since the number of such discontinuous control actions is typically large and quite different, an episodal classification based on trajectory segments and thus trajectories and their attracting sets being stable appeared to be logical and consistent with electric utility practice. Contingency selection methods have been widely used to

- a. determine contingencies where the currents on every branch (element) of the transmission network lie within thermal limits and those contingencies where the currents on one or more branches exceed thermal limits.
- b. determine contingencies where voltages at every bus (node) lie within a secure range ($0.95 pu \leq V_i \leq 1.05 pu$) and those trajectories where one or more bus voltages lie outside the range;
- c. determine contingencies where voltage collapse does not occur in any subregion and determine the contingencies that cause voltage collapse in some identified subregion. Each of these subregions can be proven to be a bifurcation subsystem where the saddle node bifurcation makes it impossible to obtain solutions or may cause multiple solutions to exist.

All of these contingency selection and security assessment procedures are based on load flow solution which attempts to find $\lim_{i \rightarrow N} (\bar{x}_i, \bar{y}_i)$ where N is the number of discontinuities experienced along the trajectory. A Bounded Trajectory Feasibility Method

appears far more reasonable because it uses the Epoch Based Trajectory Stability Assessment that actually simulates

- (i) the actual sequence of quasi equilibrium points (\bar{x}_i, \bar{y}_i) that would occur after each discontinuity;
- (ii) the transitions from $\bar{x}_i = x(t_i^-); \bar{y}_i = y(t_i^-)$ to $x(t_i^+) = x(t_i^-); y(t_i^+) = y(t_i^-)$;

also evaluates feasibility and viability of each equilibrium and limit cycle, and assess stability of trajectories $(x(t), y(t))$ over epochs (t_i^+, t_{i+1}^-) . The Bounded Trajectory Feasibility Method would utilize an Epoch Based Trajectory Stability Assessment rather than a load flow because the load flow often does not calculate a steady state equilibrium $\lim_{i \rightarrow N} (\bar{x}_i, \bar{y}_i)$ that actually occurs since it does not determine the correct set or sequence of discontinuities that occur, and thus the correct equilibrium as explained earlier. Therefore the conclusions concerning its stability, viability and whether the initial conditions after a contingency lie within its region of stability are irrelevant. Even if load flow calculated the correct steady state equilibrium $\lim_{i \rightarrow N} (\bar{x}_i, \bar{y}_i)$ the hard limit based taxonomy would be difficult to apply to assess stability and viability of trajectories within each epoch.

The set of equipment outage and operating condition combinations evaluated by the Bounded Trajectory Feasibility Method is clearly specified by a utility's planning criterion. For each such combination the Bounded Trajectory Feasibility Method would determine stability and viability based on

- (a) existence and uniqueness of a solution or equilibrium point (\bar{x}_i, \bar{y}_i) for each trajectory segment;
- (b) stability of the equilibrium point or stable closed orbit for each trajectory segment;
- (c) asymptotic stability of the trajectory segment towards a stable closed orbit or

equilibrium for the epoch (t_i^+, t_{i+1}^-) ;

- (d) viability of the equilibrium, stable closed orbit, and trajectory segment transient for each trajectory segment;
- (e) classification of the trajectory as being or not being stable, and bounded trajectory feasible based on (a-d) for each segment.

The Bounded Trajectory Feasibility Method would then attempt to assess why the bifurcation subsystem was affected by the equipment outage and operating change combination, why it was unstable or nonviable, and what could be done to prevent the problem, based on information that can be determined once the bifurcation subsystem is known. This diagnostic step of the Bounded Trajectory Feasibility Method is similar to the diagnostic that can be performed for the voltage stability security assessment procedure in [11].

IV

Bifurcations Subsystems in a Power System Differential-Algebraic Model

4.0 Introduction

The focus of this chapter is to initiate investigation on the bifurcation phenomena in a differential-algebraic power system model for the purpose of identifying the various bifurcation subsystems for each kind of bifurcation (saddle node, Hopf and load flow bifurcation) observed on a Type 2 power system model. The bifurcation subsystem method will attempt to identify subsystems of very small dimension, called bifurcation subsystems, that are associated with each kind and class of bifurcation.

Diagnostic classification of power system instability problems that is based on bifurcation kinds and classes, as well as model types used for bifurcation studies has been presented in Chapter 2. A Type 2 power system model was selected for further study in this thesis. The kinds of bifurcations that have been observed on this model include saddle node, Hopf, load flow, and each exhibits a different qualitative change in dynamical or algebraic network behavior encountered at the point of bifurcation. Classes of bifurcations are associated with the specific subsystem dynamics that experience a particular kind of bifurcation for a given model type. Possible bifurcation subsystems of a Type 2 power

system model are

- (a) the power system differential equations,
- (b) the power balance equations at load buses,
- (c) a generator's inertial, flux and exciter dynamics,
- (d) a generator's electrical dynamics,
- (e) the control systems dynamics (PSS, Governor..) on a generator,
- (f) a combination of the above

One known class of Hopf bifurcation occurs in generator flux decay and exciter dynamics and another occurs in generator flux decay and inertial dynamics. Two other classes of saddle node bifurcation are also known to exist; one in generator flux decay dynamics and the other in generator inertial dynamics. Similiar classes may be found for other kinds of bifurcations. Since a power system trajectory after a disturbance is generally characterized by a sequence of hard limit induced discontinuities, during each epoch (t_i^+, t_{i+1}^-) , the bifurcation subsystem method will be applied to a differential-algebraic Type 2 power system model to

- (i) determine the subsystems that experience the same bifurcation as that observed in the full power system model during each time epoch (t_i^+, t_{i+1}^-) . These bifurcations capture the effects of the previous discontinuous or continuous parameter changes that had occurred in the past time epochs (t_k^+, t_{k+1}^-) for $k = 1, \dots, i-1$. The subsystem that produces the bifurcation in the subsystem and in the full system may at times be larger than the subsystem experiencing the bifurcation of the full system.
- (ii) find the cause and the remedial action for preventing the bifurcation without actually finding the center manifold dynamics. The subsystem containing all the causes

including model parameters, controls, and model discontinuities may extend outside the subsystem that experiences or produces the bifurcation. Even though the research ultimate objective is to find the subsystem experiencing, producing, and experiencing bifurcation, the present work is solely aimed at finding the subsystem experiencing bifurcation as the full system experiences bifurcation. The diagnostics on the bifurcation subsystem may be more easily performed because retaining how specific continuous model parameter changes, how continuous operating, or scheduling changes affect the center manifold dynamics is not easily retained on very large power system models. The ability to analyze how the center manifold change along the whole trajectory when discontinuities are encountered has been investigated by Zaborszky [27] and is not an easy task.

The traditional methods for identifying subsystems are generally based on apriori knowledge of (a) the system or its control design, (b) time scale information on real eigenvalues or imaginary components of complex eigenvalues, (c) eigenvectors and participation factor information from eigenvectors, or (d) decoupling within the state space model. While such methods are often useful in model reduction that preserves time or modal behavior at one operating condition or developing and redesigning particular excitation systems, system stabilizers or FACTS controls, they are not always effective in identifying the smallest subsystem or subsystems that manifests the same bifurcation in the full system. These traditional methods (a-d) for determining subsystems are not effective because obtaining a bifurcation subsystem model which experiences the bifurcation in the full model has a different objective than preserving modal or coherent behavior, designing controls or developing operation schedules for a system. The objective

of a bifurcation subsystem is to capture the nonlinear behavior that produces and causes a bifurcation in a specific eigenvalue or a particular model or operating condition changes. Time scales are often not effective in defining a bifurcation subsystems for a specific bifurcating eigenvalue in a power system model, because the frequencies of all inter-area oscillations lie in a narrow band and because the frequencies of all local generator oscillations also lie in a narrow band. A singular perturbation method would preserve all the modes in a band and not just the bifurcating modes for a particular bifurcation parameter. Subsystems used for control design must be satisfactory nonlinear model representations of the full system and the associated linearized model must be a satisfactory representation for several eigenvalues of the specific device or process being controlled and for a range of operating conditions. Despite the fact that eigenvector methods indicate the system state variables most severely affected by each Hopf bifurcation or the controls that are controlling that mode, this information does not always describe the location or cause of the bifurcation as noted in the power system example presented in Chapter 1. In that case, the modal information (participation factor) showed a rather large region near the city of Vancouver was the most severely impacted, but did not capture the fact that the disabling of voltage control on generators on Vancouver Island could actually cause the voltage collapse. Decoupling of subsystem dynamics by inspection of the structure of the system Jacobian matrix could also be used for model reduction and for identification of system states with high participation in a particular bifurcation.

4.0.1 Bifurcation Subsystems for Epochs

The great majority of the literature on bifurcation in power systems assumes that the differential-algebraic power system model is continuous and differentiable. The discussion in Chapter 3 shows that virtually all bifurcations occur after (1) generators reach field current limits, (2) switchable shunt capacitors act, (3) tap changers reach upper or lower tap position limits, and (4) switchable shunt capacitors reach upper susceptance limits. All of these actions are discontinuous and violate the smoothness assumptions needed to apply bifurcation theory. Thus an extended bifurcation theory is being developed in [27] to properly describe the bifurcation that occurs in power system models that experience actuation, state, and relay hard limits [27]. Since inclusion of these discontinuities is absolutely essential for system stability analysis of power systems, the framework for the bifurcation subsystem method should accommodate and include the effects of such discontinuities. If the effects of discontinuities were neglected, then the bifurcation subsystem method would have limited and possibly little value, since there are relatively few if any bifurcations that occur in an actual power system without one and likely several discontinuities.

Therefore, in this chapter we adopt the Epoch Based Trajectory Stability Assessment method, where system stability analysis is performed epoch by epoch where an epoch is a period of time (t_i^+, t_{i+1}^-) free of hard limit discontinuous transitions. In this method presented in Chapter 3, stability analysis for smooth systems may be performed within epochs (t_i^+, t_{i+1}^-) for $i = 1, \dots, N$, where $t_{i+1}^- - t_i^+$ is very long compared to the time constants of the linearized dynamics, rather than attempting to study stability of the entire trajectory. In each time epoch (t_i^+, t_{i+1}^-) , bifurcation subsystems need to be determined and checked

for retention and structural stability at each quasi equilibrium (\bar{x}_i, \bar{y}_i) . Since the progress of discontinuities during system operation is accompanied by loss of control and loss of subsystem coupling, bifurcations may be of different kinds, and bifurcation subsystems may be different for each epoch. Consequently, the bifurcation subsystem method makes the Epoch Based Trajectory Stability Assessment Method a rapid and natural procedure for stability assessment and contingency selection in a power system.

4.0.2 Existence of Bifurcation Subsystems

Stability analysis and testing for bifurcations in a power system had always put special focus on its subsystem structure and on finding the critical subsystem dynamics or subsystems which exhibit the bifurcation. For example, it is quite clear that the generator flux decay dynamics and the generator excitation system are a subsystem based on the fact that the exciter controls both the flux and the voltage produced by a generator, and that a subcritical Hopf bifurcation is known to occur in these dynamics [25]. It is also known that a supercritical Hopf bifurcation can be observed in the generator mechanical, flux decay, and excitation system dynamics [25]. Since two Hopf bifurcations affect the exciter and flux decay dynamics, it might be difficult to define the proper subsystem for the subcritical and the supercritical Hopf bifurcations. These classes of bifurcation motivate the investigation of whether a subsystem composed of those dynamics produces and experiences the same bifurcation as the full system, what produces bifurcation in both and causes of the specific bifurcation, thus the name bifurcation subsystem.

A nonlinear transformation can reduce a very complex high dimensional nonlinear system into a simple subsystem that describes the system behavior along the center

manifold. If one is able to retain how the parameters and equilibrium state change with the changes in operating conditions in the system, one could fully diagnose causes of the bifurcation and how it might be effectively prevented through direct control actions or through better adjustment or scheduling of the operating conditions. Although the subsystem that describes behavior at or near the center manifold is typically of very low dimension, the dimension of the participation factor subvector (obtained from normalized right and left eigenvectors of a specific mode) with large (> 0.1) elements can be quite large. From the example shown in Chapter 1, the right and left eigenvectors do not necessarily indicate the cause or the geographical location of the bifurcation, nor the states in the model where the bifurcation has an effect. In this system, loss of excitation voltage control on generators in one generating station on Vancouver Island causes a voltage collapse on Vancouver Island that uncontrollably spreads and brings about voltage collapse in the entire B.C Hydro system. The Vancouver Island subsystem experiencing bifurcation may not be even retained based on the magnitude of the participation factor elements of the bifurcating eigenvalue before this loss of excitation control occurs which is shown in Figure 1.1. Once the loss of excitation occurs, there may be no load flow solution that can be used to calculate participation factor information, or eigenvectors.

This result indicates that when discontinuities in the model exist and cause the occurrence of bifurcation [11] in a power system, the magnitude of the eigenvectors and participation factors may be insufficient or may give misleading information on the location, cause, or remedial action needed to prevent bifurcation.

The result in [11] indicate that there are small coherent bus groups, called voltage control areas, with independent voltage collapse problems. Each of these coherent bus

groups in the electric transmission network is protected from experiencing a voltage collapse bifurcation by retaining reactive supply and thus voltage control on one or more of the generators in the unique subset of generators that protect that voltage control area from voltage collapse. This result indicates there are indeed small subsystems of a power system model, called bifurcation subsystems, that produce and cause the bifurcation that is experienced in the entire power system.

The reasons that bifurcation subsystems exist on a power system model are

- (1) Bifurcations in a power system algebraic network model are typically brought on by a series of hard limit or equipment outage induced discontinuities. While hard limit actions are result of disablement of system (voltage) protective devices and can result in loss of voltage control, equipment outages such as the trip of a tie line result in decoupling or separation of two regions in the system. Therefore in each time epoch (t_i^*, t_{i+1}^*) , the effect of the previous discontinuities which occurred at times t_k for $k=1, \dots, i-1$ may fully be captured through the disappearance of certain dynamics, isolation of some subset of dynamics, increase in matrix sparsity when dynamic equations are substituted by algebraic equations,.. etc. The resulting subsystems within each epoch (t_i^*, t_{i+1}^*) may experience different kinds of bifurcations. Bifurcation subsystems with different kinds of bifurcations seem to be a natural and essential way for tracking the subsystem experiencing, producing, and causing bifurcation, as well as the actual cause for the final system instability;
- (2) the extreme sparsity of the transmission network where every bus or node in a 10,000 bus network may only be connected to three to five other buses;
- (3) the weak coupling between real power and voltage magnitude as well as the weak

e

c

s

sy

4.

Th

sut

ass

bif

geo

in ic

prod

deco

ident

coupling of reactive power-voltage angle. This decoupling implies the existence of a real power-voltage angle subsystem and a reactive power-voltage magnitude subsystem. Both subsystems have the extreme sparsity discussed above;

- (4) effective decoupling of coherent bus groups within the real power-voltage angle subsystem and within the reactive power-voltage magnitude subsystem.

The decoupling of the two subsystems, the decoupling of coherent groups within each subsystem, and the extreme sparsity make a power system vulnerable to loss of control induced bifurcations;

The bifurcation subsystem model is just a truncated portion of the actual power system model where the impact of parameter and operating changes simulated on a full system model can be easily observed and analyzed on the subsystem model.

4.0.3 Introduction to the Bifurcation Subsystem Method

The bifurcation subsystem method utilizes the geometry associated with the various submatrices of the differential-algebraic Jacobian matrix J and with the eigenvectors associated with the bifurcating eigenvalue to establish conditions for existence of a bifurcation subsystem. Conditions for existence of a bifurcation subsystem require geometric decoupling that encompasses time scales, matrix decoupling and eigenanalysis in identifying the smallest subsystem that not only experiences the bifurcation but also produces and causes the same bifurcation observed in the full model. Geometric decoupling will be shown to be the most effective as well as a generalized method for identifying bifurcation subsystems.

A bifurcation subsystem can therefore be loosely defined as a truncated portion of

the a

sys

bifur

(1)

v

t

t

t

P

(2)

(3)

bre:

sys

these

However

diagnostic

the actual power system model that experiences and causes the same bifurcation in the full system model. Special characteristics of a bifurcation subsystem come from the fact that a bifurcation subsystem

- (1) is a reduced model developed for a specific kind of bifurcation since the geometric decoupling conditions for a bifurcation subsystem are only on the linearized model and only on the subspace associated with the left and right eigenvectors of the bifurcating eigenvalue as the bifurcation parameter μ approaches the bifurcation value μ^* . The bifurcation subsystem should not only experience the bifurcation of the full system model, but may also be useful in capturing what produces and causes the bifurcation in any epochs (t_i^*, t_{i+1}^*) at the quasi equilibrium (\bar{x}_i, \bar{y}_i) , but also in tracking the model transitions which uncover the persisting dynamics that finally produced the collapse.
- (2) is not necessarily an equivalent model to the full differential-algebraic model in the sense that it preserves all the characteristics of the full model, since it can not be used to observe and investigate all other bifurcations of the full model.
- (3) geometric decoupling can break down at the point of bifurcation so that the entire system produces the bifurcation rather than just the bifurcation subsystem.

The fact that the geometric decoupling at a quasi equilibrium for an epoch (t_i^*, t_{i+1}^*) breaks down before the actual bifurcation occurs and does not always solely produce the system bifurcation may discredit application of the bifurcation subsystem method for these cases if one views the bifurcation subsystem in the strict sense of its definition. However as an engineering tool, the bifurcation subsystem method still provides diagnostic information on how much the geometric decoupling and how much the full

system

from

future

bifurc

bifurc

since

Also, i

bifurca

no par

pattern

4.0.4

Th

identifi

an equiv

existence

bifurcation

examples

example i

bifurcation

These

this knowle

system behavior after the breakdown contribute to the bifurcation in the full system model.

It should be noted that geometric decoupling does not ever prevent the entire system from experiencing the bifurcation experienced in the subsystem, but hopefully can in the future help identify the subsystem that produces and causes the bifurcation. The fact that bifurcation subsystems experience and could produce most bifurcations even though the bifurcation affects all dynamic and algebraic states of the system should not be a surprise since almost all system bifurcations are understood in terms of affecting some subsystem. Also, it should be noted that one should not and can not assume all bifurcations develop in bifurcation subsystems, because the bifurcation could be produced by the full system, in no particular identifiable subsystem or subsystems, and in very strange unexplainable patterns of state variables.

4.0.4 Chapter Objective and Outline

The three main objectives of this investigation are therefore to (a) develop tests for identifying subsystem dynamics that produce and cause a specific bifurcation to occur in an equivalent dynamic or equivalent algebraic system model; (b) utilize the test for existence of bifurcation subsystems to develop methods that can help identify all potential bifurcations that may exist in a particular model; and (c) introduce several application examples of bifurcation subsystems in stability assessment of power systems. One such example in this thesis is the justification of the classical load flow model as an algebraic bifurcation subsystem for load flow bifurcation of the differential-algebraic model.

These objectives are quite ambitious since the study of bifurcations usually assumes this knowledge while it is often unknown and is rather essential for excitation system

red
kno
vol
ger
Ty
be
an
Th
me
tur
di
de
di
ec
ge
or
ec
w
st
ec
re

redesign and FACTS control that may prevent the bifurcation from occurring. This knowledge may also be useful in developing unit commitment, generation dispatch and voltage setpoint schedules that could prevent each specific kind and class of bifurcation.

The development of this bifurcation subsystem method will be first developed for a general differential-algebraic model and then applied to a Type 2 power system model. A Type 2 power system model is chosen rather than any other power system model type because (1) the bulk of bifurcation studies in power systems has been based on this model and (2) because the kinds and classes of bifurcations are best understood for this model. The differential equations in this Type 2 power system model represent generator mechanical and flux decay dynamics, generator excitation system dynamics, and governor turbine system dynamics. The algebraic equations represent the transmission and distribution networks as well as the load. The Type 2 power system model is described in details in Chapter 2 and structurally as a differential-algebraic model in Section 4.1.

The first step in this investigation is to assume that it is possible to obtain a differential (dynamic) system model and/or an algebraic system models, that are equivalent to the full differential-algebraic power system model. Such assumption is generally made because most bifurcations do not occur solely in the differential equations or solely in the algebraic equations of the differential-algebraic model. Formulation of equivalent differential and algebraic system models will be based on Schuur's theorem as will be shown in Section 4.3.1. The conditions for existence of an algebraic bifurcation subsystem and a differential bifurcation subsystem which experience bifurcation in the equivalent algebraic system model and the equivalent differential system model, respectively, are then derived in Section 4.3.2.

The conditions for a differential bifurcation subsystem to exist are further refined to provide conditions for a subsystem of the differential equations to produce bifurcation in the equivalent differential equation model. When the bifurcation is experienced solely in a subsystem of the differential equations, then a bifurcation sub-subsystem is said to exist. Conditions for a differential sub-subsystem are given in Section 4.4.1.

The conditions for an algebraic bifurcation subsystem to exist are further refined to provide conditions for a subsystem of the algebraic equations to experience bifurcation in the equivalent algebraic system model. When the bifurcation is experienced solely in a subset of the algebraic equations, then an algebraic bifurcation sub-subsystem is said to exist. Conditions for algebraic sub-subsystems to exist are given in Section 4.4.2.

The bifurcation produced in the full set of differential and algebraic equations can be experienced solely in a subsystem composed of a subset of the differential equations and a subset of the algebraic equations. When this occurs, a differential-algebraic sub-subsystem is said to exist. Conditions for a differential-algebraic subsystem to exist are given in section 4.4.3

Under normal conditions, a power system should never experience bifurcation solely in the differential equations, if the generators, governor and excitation system are properly designed. However, during voltage collapse, generator exciters cause the generator to reach field current limits in an effort to produce the reactive power needed by the network, and the exciter is completely disabled on excitation systems built prior to 1970 [51]. This can produce bifurcations that are solely in the generator dynamics. A condition for an algebraic bifurcation subsystem is also derived in section 4.3 where bifurcation in the equivalent algebraic system model is captured totally in the algebraic equations. Voltage

collapse is often studied using an algebraic model and thus its use is theoretically justified based on the conditions derived for an algebraic bifurcation subsystem to exist. This understanding motivates the development of Sections 4.3, 4.4 and 4.5.

Finally, an application example of bifurcation subsystems in stability assessment of power systems, is given in Section 4.6. A classical load flow model is justified for the first time in terms of being both a bifurcation subsystem for saddle node bifurcation in the differential-algebraic model or equivalent differential model and a bifurcation subsystem for algebraic bifurcation in the algebraic equations of the network far from generator terminal and internal buses. In Chapters 6 and 7, the concept of bifurcation subsystems will be used to study several different kinds and classes of bifurcations in a Type 2 power system model.

4.1 Differential-algebraic Power System Model

From power system stability assessment practice it is currently assumed that the underlying cause of voltage collapse is typically a bifurcation associated with the nonlinear power system dynamics, and can be invoked by a small change in system parameters. First, recall the nonlinear power system differential-algebraic model presented in Chapter 2, where the differential and algebraic nonlinear equations describe the generator and control dynamics, the network and load, respectively. The form of the nonlinear model in each time epoch (t_i^*, t_{i+1}^*) after the i 'th discontinuity occurs in the system, $1 \leq i \leq N-1$ is given by:

$$\text{Differential equations:} \quad \dot{x}_i = f_i(x_i(t), y_i(t), \mu_i(t)) \quad t \in (t_i^*, t_{i+1}^*) \quad 4.1(a)$$

$$\text{Algebraic equations:} \quad 0 = g_i(x_i(t), y_i(t), \mu_i(t)) \quad t \in (t_i^*, t_{i+1}^*) \quad 4.1(b)$$

wh

f_i

g_i

$x_i(t)$

y_i

μ

X

P

N

T

m

x_i

where

$f_i : R^{n+m+p} \rightarrow R^n$, an n-vector of real analytic nonlinear functions

$g_i : R^{n+m+p} \rightarrow R^m$, an m-vector of real analytic nonlinear functions

$x_i(t) : \in X \subset R^n$, a state vector of dynamic state variables, typically time dependent values of generator and excitation system voltages, rotor phases and induction motor variables for $t \in (t_i^+, t_{i+1}^-)$.

$y_i(t) : \in Y \subset R^m$, a state vector of instantaneous variables, typically time dependent values of voltage and angle at generator terminal buses, high side transformer buses and load buses for $t \in (t_i^+, t_{i+1}^-)$.

$\mu_i(t) : \in P \subset R^p$, a vector of slow varying operating parameters for the time epoch $t \in (t_i^+, t_{i+1}^-)$. It can represent a scaling of any of the parameters discussed in Chapter 3 as belonging to parameter space. The parameter $\mu_i(t)$ is likely to scale parameters like reactive power load or generation, generator exciter voltage set points, or active generation or load. As $\mu_i(t)$ varies over the parameter space P , there must be at least one solution to the above differential-algebraic system of equations.

$X \times Y$: state space

P : parameter space

Note (Notation):

The subscript 'i' used in the vectors $x_i(t)$, $y_i(t)$, $f_i(x_i(t), y_i(t), \mu_i(t))$,... indicates that the model is valid after the *i*'th discontinuity, during the epoch (t_i^+, t_{i+1}^-) . For example,

$x_i(t) = (x_{i_1}, x_{i_2}, \dots, x_{i_n}) \in R^n$ is the n-dimensional state vector during (t_i^+, t_{i+1}^-) .

$$\bar{X}_i = 1$$

equat

A line

be ob

series

The J

linear

comp

where

and

In the

$x_i(x_i, t)$

occur v

and the

stands f

A

For an arbitrary fixed parameter $\mu_i = \mu_e$, a steady state quasi equilibrium point $\bar{X}_i = (\bar{x}_i(\mu_e), \bar{y}_i(\mu_e))$, is a point of quasi equilibrium defined by locally solving the system of equations

$$0 = f_i(\bar{x}_i(\mu_e), \bar{y}_i(\mu_e), \mu_e) \quad (4.2a)$$

$$0 = g_i(\bar{x}_i(\mu_e), \bar{y}_i(\mu_e), \mu_e) \quad (4.2b)$$

A linearized model of (4.1) about an isolated equilibrium point of interest $(\bar{x}_i, \bar{y}_i, \mu_e)$ may be obtained using Taylor's theorem where every function is approximated by its Taylor series expansion of the first degree, in the neighborhood of the isolated equilibrium point. The Jacobian matrix of (4.1) at an equilibrium point $(\bar{x}_i, \bar{y}_i, \mu_e)$ may be obtained by linearizing the differential and algebraic equations and then combining all the linearized components, as shown below.

$$\begin{bmatrix} \Delta \dot{x}_i \\ 0 \end{bmatrix} = J_i \cdot \begin{bmatrix} \Delta x_i \\ \Delta y_i \end{bmatrix} \quad (4.3a)$$

where

$$J_i = \begin{bmatrix} \partial f_i / \partial x_i & \partial f_i / \partial y_i \\ \partial g_i / \partial x_i & \partial g_i / \partial y_i \end{bmatrix}_{(\bar{x}_i, \bar{y}_i, \mu_e)} \equiv \begin{bmatrix} f_{ix_i} & f_{iy_i} \\ g_{ix_i} & g_{iy_i} \end{bmatrix} \quad (4.3b)$$

and

$$\Delta x_i = x_i(t) - \bar{x}_i$$

$$\Delta y_i = y_i(t) - \bar{y}_i$$

In the rest of the thesis, sufficient smoothness of the functions $f_i(x_i(t)), y_i(t), \mu_i(t)$ and $g_i(x_i(t), y_i(t), \mu_i(t))$ is assumed to be preserved since no discontinuous system changes occur within the time epoch (t_i^+, t_{i+1}^-) . Therefore, for simplicity, we omit the subscript i and the argument ' t ' in the analysis within the epoch. That is, unless otherwise noted, g stands for $g_i(x_i(t), y_i(t), \mu_i(t))$, f_x stands for $f_i(x_i(t), y_i(t), \mu_i(t))$... etc.

A linearized differential-algebraic power system model has been derived in [52] for

a ge

sys

(Lin

Gov

When

.

.

S

Δ

Δ

T

T_E

T_{θ}

a general Type 2 power system model, where each synchronous machine and its control systems are described. The control systems include (a) Excitation control with Load (Line-Drop) Compensator, (b) Power System Stabilizer (PSS) [52], and (c) Speed-Governor-Turbine System. The full linearized system model [52] is given by:

$$\begin{bmatrix} T_{XX}\Delta\dot{X}_X \\ T_{EE}\Delta\dot{X}_E \\ T_{GG}\Delta\dot{X}_G \\ T_{SS}\Delta\dot{X}_S \\ -\Delta P_C \\ -\Delta Q_C \end{bmatrix} = \begin{bmatrix} A_{XX} & A_{XE} & A_{XG} & 0 & A_{X\theta} & A_{XV} \\ A_{EX} & A_{EE} & 0 & A_{ES} & A_{E\theta} & A_{EV} \\ A_{GX} & 0 & A_{GG} & 0 & 0 & 0 \\ A_{SX} & 0 & 0 & A_{SS} & 0 & 0 \\ A_{PX} & 0 & 0 & 0 & A_{P\theta} & A_{PV} \\ A_{QX} & 0 & 0 & 0 & A_{Q\theta} & A_{QV} \end{bmatrix} \begin{bmatrix} \Delta X_X \\ \Delta X_E \\ \Delta X_G \\ \Delta X_S \\ \Delta\theta \\ \Delta V \end{bmatrix} + B_o \Delta U_o \quad (4.4)$$

Where

ΔX_X : states of mechanical and flux decay dynamics;

ΔE_F : states of flux decay dynamics

ΔX_E : states of excitation system

ΔX_G : states of speed-governing-turbine systems;

ΔX_S : states of power system stabilizer;

$\Delta\theta$: angle variables at network buses;

ΔV : voltage variables at network buses;

ΔP_C : coefficients of non-voltage-dependent active power load demand model;

ΔQ_C : coefficients of non-voltage-dependent reactive power load demand model;

T_{XX} : diagonal matrix composed of inertia constants of synchronous machines;
identity matrix, and time constants of flux decay dynamics;

T_{EE} : time constants of the excitation systems dynamics;

T_{GG} : time constants of speed-governing-turbine systems;

T_{ss} : time constants of power system stabilizers;

4.2 Conditions for Bifurcation Subsystems Experiencing SN and LF Bifurcations

4.2.1 Equivalent System Models

Although testing for singularity of the full Jacobian matrix J in (4.3b) is a sufficient indication of a system bifurcation, this test is not sufficient to tell (a) whether either saddle node bifurcation (when g_y is nonsingular), load flow bifurcation (when f_x is nonsingular), or algebraic bifurcation ($[g_x \ g_y]$ is row dependent) occurred; (b) whether the bifurcation is associated with strictly an equivalent dynamic system model or an equivalent algebraic system model; or (c) what system dynamics were associated with the bifurcation. Schur's theorem [53] is used to establish conditions under which equivalent systems to (4.1) comprised solely of differential equations or solely of algebraic equations can be constructed with different eigenvalues than the differential equation model which better reflect the effects of the eigenvalue qualitative changes of the full system model.

Existence of equivalent differential or algebraic system models to (4.1) depends on the row dependence of the rows associated with the differential equations and/or the row dependence of the rows associated with the algebraic equations in the linearized full system (4.3). This will be clear from Schur's theorem which reduces the computation of a determinant of a matrix of order n to the computation of a determinant of a matrix of order $r < n$ [53].

Schur's Theorem

If a square matrix A of order n is represented in partitioned form as

$$A = \begin{bmatrix} A_{11} & A_{12} \\ A_{21} & A_{22} \end{bmatrix}_{n \times n}$$

where A_{11} is a square nonsingular matrix of order $r < n$, then

(a) If A_{22} is nonsingular, then $\text{Det}(A) = \text{Det}(A_{22}) \cdot \text{Det}(A_{11} - A_{12}A_{22}^{-1}A_{21})$

(b) If A_{11} is nonsingular, then $\text{Det}(A) = \text{Det}(A_{11}) \cdot \text{Det}(A_{22} - A_{21}A_{11}^{-1}A_{12})$

The reduced order matrices

$$A_{r1} = A_{11} - A_{12}A_{22}^{-1}A_{21}$$

$$A_{r2} = A_{22} - A_{21}A_{11}^{-1}A_{12}$$

are commonly called system reduced matrices, system modified matrices or system sensitivity matrices [38,51], since they preserve the singularity of A , a property that is very desirable for system reduction techniques and absolutely essential in bifurcation analysis. Indeed, intensive power system research has been performed using these low-order matrices to investigate system sensitivities and proximity to voltage instability bifurcation where A and A_{r1} , A and A_{r2} , or A , A_{r1} and A_{r2} approach singularity together. Eigenvalue analysis, singular value decomposition technique, and system sensitivity analysis to various operating parameter variations are examples of power system stability analytical methods that are based on formulating system submatrices in the form of A_{r1} and A_{r2} in a classical load flow model [38]. Letting $A_{22} = A_{QV}$, $A_{21} = A_{Q\theta}$, $A_{12} = A_{PV}$, and $A_{11} = A_{P\theta}$ submatrices of the load flow Jacobian A , test results in [38] show that the minimum singular value of A , A_{r2} , and A_{22} , are identical down to nearly the point of bifurcation. The changes in all the minimum singular values of all matrices occur at discontinuities

when generator buses become load buses and control of voltage is lost. This result establishes that A_{22} is a bifurcation subsystem of the load flow model with Jacobian A and motivates development of a general theory for describing when a bifurcation subsystem exists in the differential-algebraic model.

Since we are interested in reduced order equivalent system models that have the same dynamic and algebraic properties as the full model, we apply Schur's theorem to the matrix J in (4.3b), where we can see that two possible equivalent matrices may be used to obtain equivalent reduced order models, namely

$$\begin{aligned} J_x &= f_x - f_y g_y^{-1} g_x \\ J_y &= g_y - g_x f_x^{-1} f_y \end{aligned}$$

J_x and J_y are indeed two equivalent system Jacobian matrices associated with an equivalent dynamic model and an equivalent static/algebraic model respectively, as can be seen below.

4.2.1.1 Equivalent Algebraic System Model (Exact Load Flow model)

If f_x is nonsingular at steady state ($\Delta \dot{x} = 0$), the differential equations in (4.2a) model may be aggregated into the algebraic equations (4.2b) by setting $\dot{x} = 0$ and solving for $x(y)$ from $f(x, y, \mu) = 0$ by the Implicit Function Theorem [33], resulting in a model where no saddle node bifurcation in the differential equations occurs, i.e. the full system bifurcation may be determined from the equivalent reduced order algebraic equivalent model given in 4.5(a), or locally from the linearized model about $\bar{X} = (\bar{x}, \bar{y}, \mu)$ given in 4.5(b):

$$g(x(y), y, \mu) = 0 \tag{4.5(a)}$$

$$0 = J_y \cdot \Delta y = [g_y - g_x f_x^{-1} f_y] \cdot \Delta y \tag{4.5(b)}$$

This result suggests using an algebraic model $g(x(y), y, \mu) = 0$, called an Exact Load Flow

model is obtained. This Exact Load Flow model $g(x(y), y, \mu) = 0$ is implemented as a load flow where generator and exciter algebraic equations from $f(x, y, \mu) = 0$ are included in the model. The usual procedure of incorporating generator PV and PQ buses is an approximation of $g(x(y), y, \mu) = 0$ and is referred to as a *classical load flow model*. If the Exact Load Flow model $g(x(y), y, \mu) = 0$ is valid because there exists a unique solution $x(y)$ then test for bifurcation on the full model using (4.1) is equivalent (if and only if) to the test for bifurcation on the Exact Load Flow model $g(x(y), y, \mu) = 0$ using J_y .

4.2.1.2 Equivalent Dynamic System Model

From 4.3(a) and 4.3(b), we can see that if g_y is nonsingular, the algebraic equations may be aggregated into the set of differential equations by obtaining $y(x)$, resulting in an equivalent dynamic model $\dot{x} = f(x, y(x), \mu)$. This reduced order model consists only of differential equations, making this system suitable for assessing static and dynamic bifurcations associated with the full system using 4.6(a), or locally from the linearized model about $\bar{X} = (\bar{x}, \bar{y}, \mu)$ given in 4.5(b):

$$\dot{x} = f(x, y(x), \mu) \quad 4.6(a)$$

$$\Delta \dot{x} = J_x \cdot \Delta x = [f_x - f_y g_y^{-1} g_x] \cdot \Delta x \quad 4.6(b)$$

Based on these two equivalent models, we can see that a qualitative change in the full linearized system behavior, may be determined from the algebraic or the differential equivalent models depending on the singularity of the matrices f_x and g_y . An equilibrium point $\bar{X}^* = (x^*, y^*, \mu^*)$ of 4.3(a) can experience bifurcation at a bifurcation value of μ , μ^* when J is singular and either :

- (i) g_y is nonsingular, and $J_x = f_x - f_y g_y^{-1} g_x$ is singular. This bifurcation in the equivalent dynamic system model is called static bifurcation, which is generically a saddle node

bifurcation.

- (ii) f_x is nonsingular, and $J_y = g_y - g_x f_x^{-1} f_y$ is singular. This bifurcation in the equivalent algebraic system model called a load flow bifurcation since it occurs in the Exact Load Flow model $g(x(y), y, \mu) = 0$.
- (iii) Both f_x and g_y are singular. There is no known description of this case in dynamical system literature on systems composed of differential and algebraic equations, such as a power system.

There is no theory to establish that the dynamics experience, produce, or cause the bifurcation in (i) or that the load flow would experience, produce, or cause the bifurcation in (ii), but convention has assumed such is the case. This result suggests that the first step in the investigation of bifurcation subsystems is generally to determine (if possible) whether the bifurcation occurs in the equivalent differential or algebraic system model. It may be possible that f_x and g_y are both nonsingular when J is singular and one may study the bifurcation in both the equivalent differential model

$$\dot{x} = f(x, y(x), \mu)$$

and the equivalent algebraic model (Exact Load Flow model)

$$g(x(y), y, \mu) = 0$$

Our subsequent results will show that some of the kinds and classes of bifurcations being investigated in this research can be studied in both the equivalent dynamic and algebraic system models. Identification of such differential-algebraic bifurcation subsystems will be investigated in this thesis and will be shown to be quite useful in determining voltage instability/collapse regions in a power system.

Now, a conceptual and formal definitions of bifurcation subsystems are given, using the notation and definitions of systems (4.1) and (4.3).

4.2.2 Definitions of Bifurcation Subsystems

Definitions of Hopf and saddle node bifurcations with transversality and nondegeneracy conditions are given in Appendix C. For saddle node bifurcation, Hypotheses (SN2) and (SN3) given in [App C] are the transversality conditions which control the nondegeneracy of the behavior with respect to the parameter μ and the dominant effect of the quadratic nonlinear term. For Hopf bifurcation, hypothesis (H2) is the transversality condition. Although testing for SN and Hopf requires testing all hypothesis (SN1-3) and (H1-2) respectively, in practical investigations, only (SN1) and (H1) are tested since transversality conditions are generally satisfied [59]. Therefore, in the rest of the thesis and without loss of generality, we assume that as the system eigenvalues cross the imaginary axis, the transversality conditions are satisfied so that a Hopf or a saddle node bifurcation occurs.

An Exact Load Flow model is a model that describes an equilibrium situation $g(x(y), y, \mu) = 0$ that exists when $\dot{x} = 0$, and the dynamic model $f(x, y, \mu) = 0$ at equilibrium has a unique solution $x(y)$ for each y in some set. The bifurcations in the Exact Load Flow model are called load flow bifurcations and occur when J_y is singular.

(a) Conceptual Definition of a Bifurcation Subsystem

A bifurcation subsystem is any subsystem of the original power system model equations that experiences the same saddle node (Hopf, load flow bifurcation) that occurs in the full model. Therefore, the dynamic behavior in the full model is associated with the dynamic behavior in the subsystem and thus investigating the specific bifurcation occurring in the full model may be greatly simplified by investigating the lower order bifurcation subsystem.

Formal definitions of bifurcation subsystems for saddle node, Hopf, load flow bifurcation, differential sub-subsystems, algebraic sub-subsystems, and differential-algebraic bifurcation subsystems are now given. These definitions are based on the dynamic relation of the physically based subsystem of the full model, as the system approaches bifurcation. These definitions may be extended to other kinds of bifurcations.

(b) Formal Definition of a Bifurcation Subsystem

Consider the systems in (4.1) and (4.3) where we partition Δx , Δy , f , g , and the full system Jacobian matrix J as follows:

$$\begin{bmatrix} \dot{x}_1 \\ \dot{x}_2 \\ 0 \\ 0 \end{bmatrix} = \begin{bmatrix} f_1(x, y, \mu) \\ f_2(x, y, \mu) \\ g_1(x, y, \mu) \\ g_2(x, y, \mu) \end{bmatrix} \quad \text{I(a)}$$

$$\begin{bmatrix} \Delta x_1 \\ \Delta x_2 \\ 0 \\ 0 \end{bmatrix} = \begin{bmatrix} f_{x_{11}}(\mu) & f_{x_{12}}(\mu) & * & * \\ f_{x_{21}}(\mu) & f_{x_{22}}(\mu) & * & * \\ * & * & g_{y_{11}}(\mu) & g_{y_{12}}(\mu) \\ * & * & g_{y_{21}}(\mu) & g_{y_{22}}(\mu) \end{bmatrix} \cdot \begin{bmatrix} \Delta x_1 \\ \Delta x_2 \\ \Delta y_1 \\ \Delta y_2 \end{bmatrix} \quad \text{I(b)}$$

$$f_x(\mu) = \begin{bmatrix} f_{x_{11}}(\mu) & f_{x_{12}}(\mu) \\ f_{x_{21}}(\mu) & f_{x_{22}}(\mu) \end{bmatrix} \quad g_y(\mu) = \begin{bmatrix} g_{y_{11}}(\mu) & g_{y_{12}}(\mu) \\ g_{y_{21}}(\mu) & g_{y_{22}}(\mu) \end{bmatrix}$$

with equivalent differential model 4.6(a) when $g_y(\mu)$ is nonsingular and with equivalent algebraic model 4.5(a) when $f_x(\mu)$ is nonsingular, and assume that the full system experiences a bifurcation at a parameter value $\mu^* \in (\mu_1, \mu_2)$. Also assume that

$$\begin{aligned} x &= [x_1^T, x_2^T]^T, & x_1 &\in R^{n_1}, & x_2 &\in R^{n_2}, & y &= [y_1^T, y_2^T]^T \\ y_1 &\in R^{m_1}, & y_2 &\in R^{m_2}, & n_1 + n_2 &= n, & m_1 + m_2 &= m, \end{aligned}$$

$$f_{x_{ij}}(\mu) = \partial f_i / \partial x_j$$

and note that the “*” in the matrices indicate unspecified elements or submatrices. Then

(A) the subset of differential equations of I(a)

$$\dot{x} = f(x(t), y(\mu), \mu) \quad \text{II(a)}$$

with linearization

$$\begin{bmatrix} \Delta \dot{x}_1 \\ \Delta \dot{x}_2 \end{bmatrix} = f_x(\mu) \cdot \begin{bmatrix} \Delta x_1 \\ \Delta x_2 \end{bmatrix} \quad \text{II(b)}$$

where the algebraic state vector y is not a function of t , but only function of the parameter μ , is called a bifurcation subsystem of 4.6(a) if the dynamic and/or static behavior of 4.6(a) is related to the dynamic and/or static behavior of II(a) in one of the following ways:

(A1) If $f_x(\mu)$ in II(b) has an eigenvalue $\lambda(\mu)$ approaching $\lambda(\mu^*) = 0$ with eigenvector $u(\mu) \in R^n$, then the equivalent differential Jacobian matrix $J_x(\mu)$ has an eigenvalue $\tilde{\lambda}(\mu)$ approaching $\tilde{\lambda}(\mu^*) = 0$ with eigenvector $u(\mu) \in R^n$. At $\bar{X}^* = (x(\mu^*), y(\mu^*), \mu^*)$, transversality conditions for SN must hold [App C].

(A2) If $f_x(\mu)$ in II(b) has eigenvalues $\lambda_{1,2}(\mu)$ approaching $\lambda_{1,2}(\mu^*) = \pm j\omega$ for some $\omega \neq 0, \omega \in R$ with associated conjugate eigenvectors $u(\mu) \in C^n$, $u^*(\mu) \in C^n$, then the equivalent differential Jacobian matrix $J_x(\mu)$ has eigenvalues $\tilde{\lambda}_{1,2}(\mu)$ approaching $\tilde{\lambda}_{1,2}(\mu^*) = \pm j\tilde{\omega}$ and with conjugate eigenvectors $u(\mu) \in C^n$, $u^*(\mu) \in C^n$ and $\tilde{\omega} \neq 0, \tilde{\omega} \in R$. At $\bar{X}^* = (x(\mu^*), y(\mu^*), \mu^*)$, transversality conditions for Hopf must hold [App C]

(B) the subset of algebraic equations of I(a)

$$g(x(\mu), y(\mu), \mu) = 0 \quad \text{III(a)}$$

with linearization

$$\begin{bmatrix} 0 \\ 0 \end{bmatrix} = g_y(\mu) \cdot \begin{bmatrix} \Delta y_1 \\ \Delta y_2 \end{bmatrix} \quad \text{III(b)}$$

is called a bifurcation subsystem of 4.5(a) if the equilibrium behavior of (4.5) is related to the equilibrium behavior of (IIIa) in the following way:

If $g_y(\mu)$ in III(b) has an eigenvalue $\lambda(\mu)$ approaching $\lambda(\mu^*) = 0$ with eigenvector $u(\mu) \in R^m$, then $J_y(\mu)$ has an eigenvalue $\tilde{\lambda}(\mu)$ approaching $\tilde{\lambda}(\mu^*) = 0$, with eigenvector $u(\mu) \in R^m$

(C) the subset of differential equations of I(a)

$$\dot{x}_1 = f(x_1(t), x_2(\mu), y(\mu), \mu) \quad \text{IV(a)}$$

with linearization

$$\Delta \dot{x}_1 = f_{x_{11}}(\mu) \cdot \Delta x_1 \quad \text{IV(b)}$$

where the algebraic state vector y and the dynamic state subvector x_2 are not function of t but only function of the parameter μ , is called a bifurcation subsystem of 4.6(a) if (i) $\dot{x} = f(x(t), y(\mu), \mu)$ is a bifurcation subsystem of (4.5) when $g_y(\mu)$ is nonsingular, (ii) $f_{x_{22}}(\mu)$ is nonsingular, and (iii) the dynamic and/or static behavior of 4.6(a) is related to the dynamic and/or static behavior of IV(a) in one of the following ways:

(C1) If $f_{x_{11}}(\mu)$ in IV(b) has an eigenvalue $\lambda(\mu)$ approaching $\lambda(\mu^*) = 0$ with eigenvector $u(\mu) \in R^{n_1}$, then the equivalent differential Jacobian matrix $J_{xx}(\mu)$ given by

$$J_{xx}(\mu) = f_{x_{11}}(\mu) - f_{x_{12}}(\mu) f_{x_{22}}^{-1}(\mu) f_{x_{21}}(\mu)$$

has an eigenvalue $\tilde{\lambda}(\mu)$ approaching $\tilde{\lambda}(\mu^*) = 0$ with eigenvector

$u(\mu) \in R^{n_1}$. At $\bar{X}^* = (x(\mu^*), y(\mu^*), \mu^*)$, transversality conditions for SN must hold [App C]

- (C2) If $f_{x_{11}}(\mu)$ in IV(b) has eigenvalues $\lambda_{1,2}(\mu)$ approaching $\lambda_{1,2}(\mu^*) = \pm j\omega$ for some $\omega \neq 0, \omega \in R$ with associated conjugate eigenvectors $u(\mu) \in C^{n_1}$, $u^*(\mu) \in C^{n_1}$, then the equivalent differential Jacobian matrix $J_{xx}(\mu)$ has eigenvalues $\tilde{\lambda}_{1,2}(\mu)$ approaching $\tilde{\lambda}_{1,2}(\mu^*) = \pm j\tilde{\omega}$ and with conjugate eigenvectors $u(\mu) \in C^{n_1}$, $u^*(\mu) \in C^{n_1}$ and $\tilde{\omega} \neq 0, \tilde{\omega} \in R$. At $\bar{X}^* = (x(\mu^*), y(\mu^*), \mu^*)$, transversality conditions for Hopf must hold [App C]

- (D) the subset of algebraic equations of I(a)

$$g_1(x(\mu), y(\mu), \mu) = 0 \quad \text{V(a)}$$

with linearization

$$0 = g_{y_{11}}(\mu) \cdot \Delta y_1 \quad \text{V(b)}$$

is called a bifurcation sub-subsystem of (4.5a) if (i) $g(x(\mu), y(\mu), \mu) = 0$ is a bifurcation subsystem of (4.5) when $f_x(\mu)$ is nonsingular, (ii) $g_{y_{22}}(\mu)$ is nonsingular, and (iii) the equilibrium behavior of (4.5) is related to the static behavior of V(a) in the following way:

If $g_{y_{11}}(\mu)$ in V(b) has an eigenvalue $\lambda(\mu)$ approaching $\lambda(\mu^*) = 0$ with eigenvector $u(\mu) \in R^{m_1}$, then $J_{yy}(\mu)$ given by

$$J_{yy}(\mu) = g_{y_{11}}(\mu) - g_{y_{12}}(\mu)g_{y_{22}}^{-1}(\mu)g_{y_{21}}(\mu)$$

has an eigenvalue $\tilde{\lambda}(\mu)$ approaching $\tilde{\lambda}(\mu^*) = 0$, with eigenvector $u(\mu) \in R^{m_1}$

- (E) the subset of differential-algebraic equations of I(a)

$$\begin{bmatrix} \dot{x}_1 \\ 0 \end{bmatrix} = \begin{bmatrix} f_1(x_1(t), x_2(\mu), y(\mu), \mu) \\ g_1(x(\mu), y(\mu), \mu) \end{bmatrix} \quad \text{VI(a)}$$

with linearization

$$\begin{bmatrix} \Delta \dot{x}_1 \\ 0 \end{bmatrix} = \begin{bmatrix} f_{x_1}(\mu) & * \\ * & g_{y_1}(\mu) \end{bmatrix} \cdot \begin{bmatrix} \Delta x_1 \\ \Delta y_1 \end{bmatrix} \quad \text{VI(b)}$$

where the algebraic state vector y and dynamic state vector $x_2(\mu)$ are not function of t but only function of the parameter μ , is called a bifurcation subsystem of I(a) if the static behavior of (Ia) is related to the static behavior of VI(a) in the following way:

If the subsystem in VI(b) has an eigenvalue $\lambda(\mu)$ approaching $\lambda(\mu^*) = 0$ with eigenvector $u(\mu) \in R^{n_1+m_1}$, then $J(\mu)$ has an eigenvalue $\tilde{\lambda}(\mu)$ approaching $\tilde{\lambda}(\mu^*) = 0$ with eigenvector $v(\mu) \in R^{n+m}$

From the above definitions, possible bifurcation subsystems are:

(a) **Differential Bifurcation Subsystem Experiencing SN**

If (A1) holds, then II(a) is a differential bifurcation subsystem experiencing saddle node bifurcation that causes saddle node bifurcation in the equivalent differential system model (4.6)

(b) **Differential Bifurcation Subsystem Experiencing Hopf**

If (A2) holds, then II(a) is a differential bifurcation subsystem experiencing Hopf Bifurcation which causes Hopf bifurcation in the equivalent differential system model (4.6)

(c) **Algebraic Bifurcation Subsystem for LF**

If (B) holds, then III(a) is an algebraic bifurcation subsystem experiencing load flow bifurcation which causes bifurcation in the Exact Load Flow model (4.5).

(d) **Differential Bifurcation Sub-subsystem Experiencing SN**

If (C1) holds, then III(a) is a differential bifurcation sub-subsystem experiencing saddle node bifurcation that causes saddle node bifurcation in the equivalent differential system model (4.6)

(e) **Differential Bifurcation Sub-subsystem Experiencing Hopf**

If (C2) holds, then III(a) is a differential bifurcation sub-subsystem experiencing Hopf Bifurcation which causes Hopf bifurcation in the equivalent differential system model (4.6)

(f) **Algebraic Bifurcation Sub-subsystem for LF Bifurcation**

If (D) holds, then IV(a) is an algebraic bifurcation sub-subsystem for load flow (LF) bifurcation which causes load flow bifurcation in the Exact Load Flow model (4.5).

(g) **Differential-algebraic Bifurcation Subsystem**

If (E) holds then VI(a) is a differential-algebraic bifurcation subsystem which causes bifurcation in the full differential-algebraic model I(a).

Finally, it is important to note that in the case of differential-algebraic bifurcation subsystems, the kind of bifurcation could not be determined, unless an equivalent differential or algebraic model exists.

Note that as μ approaches μ^* , $x(\mu)$ and $y(\mu)$ approach $x(\mu^*)$ and $y(\mu^*)$ where bifurcation occurs. The algebraic bifurcation subsystem depends on both $x(\mu)$ and $y(\mu)$ determined from the full model even though the bifurcation subsystem equations may only define $y(\mu)$ or some subset. The remainder of the equations not in the bifurcation subsystem help define the approach to bifurcation but do not have effect when load flow bifurcation occurs in the bifurcation subsystem. Similarly, the saddle node or Hopf

bifurcations that occur in the bifurcation subsystem dynamics and simultaneously in the full system model due to satisfaction of hypotheses SN1 or H1 in the bifurcation subsystem model depends solely on the bifurcation subsystem differential and possibly algebraic equations, even though the differential and algebraic equations not in the bifurcation subsystem are used to determine $x(\mu)$ and $y(\mu)$ but not whether hypotheses SN1 and H1 are satisfied in the bifurcation subsystem model. The time behavior of the components of $x(t, \mu)$ and $y(t, \mu)$ not in the bifurcation subsystem model is ignored in testing for SN1 or H1 in the bifurcation subsystem model.

4.2.3 Decoupling Conditions for Algebraic Bifurcation Subsystems and Differential Bifurcation Subsystems

An equivalent differential subsystem model $\dot{x} = f(x, y(x), \mu)$ or an equivalent algebraic subsystem model $g(x(y), y, \mu) = 0$ exist if g_y or f_x are nonsingular respectively, and may be used to study static or dynamic bifurcations in the differential-algebraic model from Schur's Theorem. In fact, to understand the bifurcation physically, the use of equivalent models is imperative. The usefulness of the equivalent models is universally known in power systems and certainly not the subject of this thesis.

The bifurcation subsystem method to be developed states conditions where the subspace in which the bifurcation subsystem experiences bifurcation is totally independent and unaffected by coupling to the rest of the model. Thus geometric decoupling conditions which formally state this principle, is the core of the bifurcation subsystem method to be developed. This result does not solely attempt to show that $f_x \approx J_x$ for differential bifurcation subsystems or that $g_y \approx J_y$ for algebraic bifurcation subsystems,

but rather the far more feasible condition that near the bifurcation value $\mu = \mu^*$ and in some subspace of x , $J_x \cdot u = f_x \cdot u$ because $[f_y g_y^{-1} g_x] \cdot u = 0$ for some $u \in \text{Null}(f_x)$ and that in some subspace of y , $J_y \cdot v = g_y \cdot v$ since $[g_x f_x^{-1} f_y] \cdot v = 0$ for some $v \in \text{Null}(g_y)$. If these geometric decoupling conditions for a bifurcation subsystem hold, then in $\text{Null}(J_x)$ and $\text{Null}(f_x)$ the equivalent linearized dynamic model becomes

$$\Delta \dot{x} = J_x \cdot \Delta x = f_x \cdot \Delta x$$

and in $\text{Null}(J_y)$ and $\text{Null}(g_y)$ the equivalent linearized algebraic model becomes

$$0 = J_y \cdot \Delta y = g_y \cdot \Delta y$$

for the specific differential bifurcation subsystem or algebraic bifurcation subsystem respectively.

Consequently, it is clear that a trivial decoupling condition is the case when the generator and control dynamics are fully decoupled from the network equations, i.e. when the off-diagonal matrix f_y in 4.3(b) is null near the bifurcation value $\mu = \mu^*$. Similarly, when the off-diagonal matrix g_x in 4.3(b) is null near μ^* , the network equations are fully decoupled from the generator and controls dynamics equations. These two conditions can formally be stated as two corollaries to Schur's Theorem, Corollary 4.1 and Corollary 4.2.

Corollary 4.1

Given J, f_x, f_y, g_x and g_y as in 4.3(b) where g_y is nonsingular and near μ^ , f_y or g_x are null, then $\dot{x} = f(x(t), y(\mu), \mu)$ is a differential bifurcation subsystem experiencing SN bifurcation for the full model in (4.1).*

Proof:

It is clear that if f_x has an eigenvalue $\lambda(\mu)$ approaching $\lambda(\mu^) = 0$ with eigenvector*

$u(\mu^*) \in R^n$ then $J_x \cdot u(\mu) = [f_x - f_y g_y^{-1} g_x] \cdot u(\mu) = f_x \cdot u(\mu) = \lambda(\mu) \cdot u(\mu)$ approaches $\lambda(\mu^*) \cdot u(\mu^*) = 0$, which says that J_x has an eigenvalue $\tilde{\lambda}(\mu)$ approaching $\tilde{\lambda}(\mu^*) = 0$ with eigenvector $u(\mu^*) \in R^n$. Hence assuming that transversality conditions (for SN bifurcation) hold near $\lambda(\mu^*) = 0$, definition A1 imply that $\dot{x} = f(x(t), y(\mu), \mu)$ is a bifurcation subsystem for (4.1) experiencing SN bifurcation

The decoupling condition given by Corollary 4.1 implies that the system dynamic behavior is totally dictated by the machine and control dynamics. This type of modeling which appears to be inappropriate to real situations, is encountered in system modeling techniques where study of stability of a specific synchronous machine in the system is based on a single machine infinite bus model. The load bus and generator terminal bus are aggregated back to the generator terminal bus and the swing bus, so that the network seems to be virtually decoupled from the generator dynamics. If the shunt admittance at the load bus is zero, the single machine infinite bus model is a differential bifurcation subsystem since $f_x = J_x$.

Corollary 4.2

Given J, f_x, f_y, g_x , and g_y as in 4.3(b) where f_x is nonsingular and near μ^* , f_y or g_x are null, then $g(x(\mu), y(\mu), \mu) = 0$ is an algebraic bifurcation subsystem experiencing LF bifurcation for the full system in (4.1).

Corollaries 4.1 and 4.2 imply the equivalent differential and algebraic system models could be decoupled so that an algebraic bifurcation subsystem and a differential bifurcation subsystem exist. Total decoupling of the algebraic and differential subsystems

is of course never true for the differential-algebraic power system model and thus this thesis needs not pursue non-geometric decoupling. The more general geometric decoupling is now investigated

4.2.4 Geometric Conditions

Since the power system model is nonlinear, it is clear that a bifurcation subsystem of a real system should also be nonlinear, so that the effects of the nonlinearities would be captured. A bifurcation subsystem could but may not have to contain the exact center manifold dynamics as the full system model, but this is difficult to verify since computing the center manifold of the specific critical operating point, has been argued (in Section 4.0.2) to be impractical if not impossible to compute for the 10,000 state variable power system model. Whether center manifolds of the bifurcation subsystem and the full system are identical and whether the effects of the nonlinear terms of the normalized power system model on the system dynamics are identical is impossible to know without further research. Although the description of the center manifold is crucial for stability analysis near the nonhyperbolic equilibrium point, their study is beyond the scope of this work and are not of high concern to us for establishing a rather fast and practical method for identifying bifurcation subsystems of the full model.

The transversality conditions (H2) for Hopf bifurcation and (SN2) and (SN3) for saddle node are generally assumed to hold without testing so that only (SN1) is generally tested for saddle node bifurcation and (H1) is tested for Hopf bifurcation. Since the theoretical results that follow only relate to (SN1), (H1) tests on a linearized model and do

not attempt to prove that the transversality conditions that hold on the full system model are sufficient to assure that they hold in the bifurcation subsystem (which can be assumed due to genericity of these transversality conditions), the existence of a bifurcation subsystem of the system model are limited to a first order (linear) satisfaction and simultaneity of SN1 and H1 tests in the full model and the bifurcation subsystem model. If the transversality conditions (SN2) and (SN3) for saddle node and (H2) for Hopf bifurcation were checked for the bifurcation subsystem (second order conditions), then the bifurcation subsystem would be the nonlinear model found in the bifurcation subsystem definitions, rather than a bifurcation subsystem of first order (the linearized bifurcation subsystem model) found in the propositions which follow.

Proposition 4.1

Let $f_x(\mu^)$ in 4.3(b) be singular for some $\mu^* \in (\mu_1, \mu_2)$ where transversality conditions for SN hold at $\bar{X}^* = (x^*, y^*, \mu^*)$, $g_y(\mu)$ nonsingular near μ^* , and let $N_1 = \text{Null}(f_x(\mu^*))$ and $N_2 = \text{Null}(f_x^T(\mu^*))$. Then $\Delta \dot{x} = f_x(\mu) \cdot \Delta x$ is a differential bifurcation subsystem of first order for (4.1) experiencing SN bifurcation if and only if near μ^* , condition (i) or (ii) is satisfied*

$$(i) \quad [f_y g_y^{-1} g_x] \cdot u_1 = 0 \text{ for some } u_1 \in N_1$$

$$(ii) \quad v_1^T \cdot [f_y g_y^{-1} g_x] = 0 \text{ for some } v_1 \in N_2$$

Proof:

Necessity:

Given that $f_x(\mu^*)$ is singular, we need to show that if (i) or (ii) is satisfied, then the equivalent differential Jacobian matrix $J_x(\mu^*)$ is also singular with eigenvector u_1 .

- (i) Let $[f_y g_y^{-1} g_x] \cdot u_1 = 0$ for some $u_1 \in N_1$. Since $f_x(\mu^*) \cdot u_1 = 0$ by definition of u_1 and the assumption that $f_x(\mu^*)$ is singular, we have

$$J_x(\mu^*) \cdot u_1 = [f_x(\mu^*) - f_y g_y^{-1} g_x] \cdot u_1 = 0$$

by condition (i). Therefore $J_x(\mu^*)$ is singular with eigenvector u_1 as required by definition A1. Therefore, $\Delta \dot{x} = f_x(\mu) \cdot \Delta x$ is a bifurcation subsystem of (4.3) and a bifurcation subsystem of first order for (4.1) experiencing SN bifurcation.

- (ii) Let $v_1^T \cdot [f_y g_y^{-1} g_x] = 0$ for some $v_1 \in N_2$. Since $v_1^T \cdot f_x(\mu^*) = 0$ by definition of v_1 and the assumption that $f_x(\mu^*)$ is singular, we have

$$v_1^T \cdot J_x(\mu^*) = v_1^T \cdot [f_x(\mu^*) - f_y g_y^{-1} g_x] = 0$$

by condition (ii). Therefore $J_x(\mu^*)$ is singular with eigenvector u_1 as required by definition A1. Therefore, $\Delta \dot{x} = f_x(\mu) \cdot \Delta x$ is a bifurcation subsystem of (4.3) and a bifurcation subsystem of first order for (4.1) experiencing SN bifurcation.

Sufficiency:

Given that $\Delta \dot{x} = f_x(\mu) \cdot \Delta x$ is a bifurcation subsystem, we need to show if singularity of $f_x(\mu^*)$ is associated with singularity of $J_x(\mu^*)$ as in definition A1, then we must have condition (i) or (ii) satisfied. Suppose $J_x(\mu^*)$ is singular, and let N and N^T be the Null spaces of $J_x(\mu^*)$ and $J_x(\mu^*)^T$ respectively.

- (i) Suppose there exists $u_1 \in N_1$ such that

$$f_x(\mu^*) u_1 = 0 \tag{4.7(a)}$$

and

$$J_x(\mu^*) u_1 = [f_x(\mu^*) - f_y g_y^{-1} g_x] \cdot u_1 = 0 \tag{4.7(b)}$$

Which implies that the singularity of f_x is associated with the singularity of J_x , because the vector u_1 satisfying 4.7(a) also satisfies 4.7(b). From 4.7(a) and 4.7(b) we have

$$\begin{aligned} [f_x(\mu^*) - f_y g_y^{-1} g_x] \cdot u_1 &= f_x(\mu^*) \cdot u_1 - [f_y g_y^{-1} g_x] \cdot u_1 \\ &= -[f_y g_y^{-1} g_x] \cdot u_1 = 0 \end{aligned}$$

Therefore $u_1 \in N_1$, and $[f_y g_y^{-1} g_x] \cdot u_1 = 0$, as required.

(ii) Suppose there exists $v_1 \in N_2$ such that

$$v_1^T \cdot f_x(\mu^*) = 0 \quad 4.8(a)$$

and

$$v_1^T \cdot J_x(\mu^*) = v_1^T \cdot [f_x(\mu^*) - f_y g_y^{-1} g_x] = 0 \quad 4.8(b)$$

Which implies that the singularity of $f_x(\mu^*)$ is associated with the singularity of $J_x(\mu^*)$ as in definition A1, because the vector v_1 satisfying 4.7(a) also satisfies 4.7(b). From 4.8(a) and 4.8(b) we have

$$v_1^T \cdot [f_x(\mu^*) - f_y g_y^{-1} g_x] = v_1^T f_x(\mu^*) - v_1^T \cdot [f_y g_y^{-1} g_x] = -v_1^T \cdot [f_y g_y^{-1} g_x] = 0$$

Therefore $v_1 \in N_2$ and $v_1^T \cdot [f_y g_y^{-1} g_x] = 0$, as required.

Implication of Proposition 4.1

Proposition 4.1 implies that singularity of the matrix $f_x(\mu^*)$ is associated with the singularity of the equivalent differential system Jacobian matrix $J_x(\mu^*)$ if and only if the system submatrices f_y , g_x , and g_y satisfy at least one of the conditions (i) and (ii) as $\mu \rightarrow \mu^*$. Under these conditions, singularity of the reduced order matrix f_x becomes crucial for analyzing and studying the occurrence of saddle node bifurcation in the equivalent dynamic model of (4.3). The reduced order system is called a bifurcation subsystem of first order for (4.1), since its change in dynamic behavior experiences the change in dynamic behavior in the full system. Recall conditions (i) and (ii) of Proposition 4.1

$$v_1^T \cdot [f_y g_y^{-1} g_x] = 0 \quad [f_y g_y^{-1} g_x] \cdot u_1 = 0 \quad \text{as } \mu \rightarrow \mu^* \quad (4.9)$$

These equalities are seldom perfectly satisfied in a real power system Type 2 model. However taking into account the extreme sparsity, decoupling of reactive power and voltage from real power and angle, and the decoupling of coherent bus groups in both the

I

L

N

b

ne

Im

ln

mat

diag

real power and angle as well as reactive power and voltage model, (i) and (ii) are likely to be satisfied to an $O(\epsilon)$ as discontinuities occur that cause J to be singular when f_x is nearly singular. Hence, the subsystem $\Delta \dot{x} = f_x \cdot \Delta x$, may effectively be used to assess the causal factors of the bifurcation in the full model. Equations in (4.9) are approximately satisfied for the following five conditions:

- (a) $\|g_x\|$ is $O(\epsilon)$ and $\|g_y^{-1}\| \|f_y\| \cdot \|u_1\|$ is $O(1)$ near μ^*
- (b) $\|f_y\|$ is $O(\epsilon)$ and $\|g_y^{-1}\| \|g_x\| \cdot \|u_1\|$ is $O(1)$ near μ^*
- (c) $\|g_y^{-1}\|$ is $O(\epsilon)$ and $\|f_y\| \|g_x\| \cdot \|u_2\|$ is $O(1)$ near μ^*
- (d) None of the above but near μ^* , the vector v_1 satisfies $v_1^T \cdot [f_y g_y^{-1} g_x] \approx 0$
- (e) None of the above but near μ^* , a vector $u_1 \in N_1$ satisfies $[f_y g_y^{-1} g_x] \cdot u_1 \approx 0$

where $\|\cdot\|$ is any suitable matrix norm.

Proposition 4.2

Let $g_y(\mu^)$ in 4.3(b) be singular for some $\mu^* \in (\mu_1, \mu_2)$, f_x nonsingular near μ^* and let $N_1 = \text{Null}(g_y(\mu^*))$ and $N_2 = \text{Null}(g_y(\mu^*)^T)$. Then, $0 = g_y(\mu) \cdot \Delta y$ is an algebraic bifurcation subsystem of first order for (4.1) experiencing LF bifurcation if and only if near μ^* , condition (i) or (ii) is satisfied*

$$(i) \quad [g_x f_x^{-1} f_y] \cdot u_2 = 0 \text{ for some } u_2 \in N_1$$

$$(ii) \quad v_2^T \cdot [g_x f_x^{-1} f_y] = 0 \text{ for some } v_2 \in N_2$$

Implication of Proposition 4.2

In contrast to (4.9), conditions (i) and (ii) of Proposition 4.2 may be satisfied when the matrix f_x associated with the machine dynamics, exciter and governor controls is diagonally dominant, a condition which is generally satisfied in a real power system Type

2 model. It can be shown that conditions (i) and (ii) of Proposition 4.2 can be satisfied to an $O(\epsilon)$ only in Section 4.6.5 if the bifurcation occurs near or in the distribution system and electrically far from generator terminal and internal buses. The resulting bifurcating model $0 = g_y(\mu) \cdot \Delta y$ may then effectively be used to assess the causal factors of the bifurcation in the full model. Structural and operating conditions and constraints for the validity of using the algebraic bifurcation subsystem will be discussed in Section (4.3.5).

Discussion of Propositions 4.1 and 4.2

The geometric conditions that *near* μ^* , $[g_x f_x^{-1} f_y] \cdot u_2 = 0$, $v_2^T \cdot [g_x f_x^{-1} f_y] = 0$, $v_1^T \cdot [f_y g_y^{-1} g_x] = 0$, and $[f_y g_y^{-1} g_x] \cdot u_1 = 0$ generalize the case of full decoupling of the differential equations and the algebraic equations stated in Corollaries 4.1 and 4.2, while Corollaries 4.1 and 4.2 give conditions for the existence of equivalent reduced-order systems to the full differential-algebraic model and would never occur. The more general geometric conditions given in Propositions 4.1 and 4.2 are for the existence of bifurcation subsystems and can indeed occur.

(a) Sparsely connected subsystems

Although these conditions seem to be a strong requirement, they are indeed a quite easily satisfied requirement since the submatrices of J and especially g_y have few nonzero elements, so that there is a natural column or row dependence in the submatrices of J , because so many elements of each column and row are identical or are zero. In a 10,000 node network, each node may be connected to at most five other nodes making g_y virtually null except for five nonzero elements in the block

submatrices corresponding to the Jacobians $dP/d\theta$, dP/dV , $dQ/d\theta$ and dQ/dV . The submatrices of f_x in (4.4) are diagonal which makes f_x very sparse as well.

(b) Weakly connected subsystems

Weakly connected may be expressed by elements in off-diagonal matrices being multiples of a small scalar $\epsilon > 0$. If some of the few nonzero elements in different rows and columns are $O(\epsilon)$ and can be approximated by zero, then the combination of sparsity and weak coupling can produce row or column dependence. The natural decoupling of real power-angle submodel and reactive power-voltage submodel as well as the decoupling within bus groups of both these models satisfies the weak coupling assumptions.

(c) Discontinuous system changes

Time epochs (t_i^*, t_{i+1}^*) are defined in Chapter 3 as the time interval after the i 'th discontinuity and before the $i+1$ hard limit or equipment outage discontinuities. These nonsmooth system transitions described in Chapter 3 usually result in loss of voltage control of certain buses in the system and/or decoupling and islanding of certain areas or group of buses of the system. Loss of control implies that the generator dynamics and controls or other voltage protective devices of the system are disabled which results in a decoupling of the generator dynamics and the system algebraic operational constraints. Loss of control induced discontinuities occur when generators reach field current limits that cause the exciter to effectively lose control of voltage, tap position limits to cause tap changer controls to lose control of voltage

3

v

c

2

t

7

v

d

d

a

(r

0

w

re

th

pe

st

ar

re

vo

be

de

and switchable shunt capacitor susceptance limits that also cause loss of control of voltage discontinuously affect the structure and in some cases change the dimension of f_x and g_y . On the other hand an equipment outage such as the trip of a tie line, i.e. a line that connects two major areas in a power system results in decoupling between the two regions or even an isolation or islanding of a major part of a system. Therefore in each time epoch (t_i^+, t_{i+1}^-) , the effect of the previous discontinuities which occurred at times t_k for $k=1, \dots, i-1$ may fully be captured through the disappearance of certain dynamics, decoupling or isolation of some subset of dynamics, increase in matrix sparsity when dynamic equations are substituted by algebraic equations,.. etc. For example, the effects of the discontinuities in epoch (t_i^+, t_{i+1}^-) , in addition to the extreme sparsity in the network create the weak coupling of the reactive power and voltage and real power and angles as submodels in g_y , as well as the weak coupling of coherent bus groups in both models. Therefore, the resulting model within each epoch (t_i^+, t_{i+1}^-) may experience separate bifurcations in the real power inertial (angle) dynamics, flux decay, exciter, voltage and reactive power dynamics within coherent groups. The evolution of the bifurcation subsystems with different kinds of bifurcations for each discontinuity is a natural and essential way for tracking the actual cause for the final system instability. The relative isolation of the real power and angle coherent groups and reactive power and voltage coherent bus groups in submodels of g_y allows Proposition 4.1(i) and (ii) to be satisfied for eigenvalues associated with the inertial dynamics and for the flux decay exciter dynamics in coherent groups of buses.

(d) Geometric Structural Decoupling

The decoupling may only be geometric and thus occurring in the direction of the bifurcating eigenvalue. The geometric decoupling may occur as $\mu \rightarrow \mu^*$, or may be such that it holds for all μ as $\mu \rightarrow \mu^*$. This geometric decoupling, asymptotic as $\mu \rightarrow \mu^*$ or structural for all μ , is quite easy to achieve given factors (a-c).

It is often impossible to determine all of the bifurcation subsystems without comprehensive stress tests at every bus in the network and possibly every subsystem of the generator model since the coordination of controls in different bifurcation subsystems mask the existence of such subsystems. Comprehensive stress test cause the discontinuities that disable the controls to allow one to observe the subsystem or subsystem that experience bifurcation, which result when conditions of Proposition 4.1 and 4.2 are satisfied.

4.2.5 Algebraic Bifurcation Subsystem Experiencing LF Bifurcation

Until the last decade, the classical method for analyzing local power system stability has been limited to the use of a load flow model. This model commonly called classical or standard load flow model, will be shown in Section 4.5 to be an approximation of a linearization of the Exact Load Flow model

$$0 = g(x(y), y(\mu), \mu)$$

Under the Conditions of Proposition 4.2, the linearized Exact Load Flow model is shown to be a bifurcation subsystem of first order for the differential-algebraic model. The P-V or Q-V curves computed using the classical load flow model have been the principal methods used to study voltage stability [App B] and proximity to voltage collapse. Studies [54]

have shown that voltage collapse occurs at a bifurcation in the classical load flow model and results either in no solution or multiple solutions in the model equations. The results in [11] show that each coherent bus group where the Q-V curve have nearly identical minima have unique voltage collapse problems. These voltage collapse problems occur whenever the generators that exhaust reactive reserves and lose control of voltage in computing the Q-V curve minima for each coherent group exhaust reserves for equipment outages or operating changes. The fact the classical load flow is an approximation of an algebraic bifurcation subsystem of the differential-algebraic model supports the discussion of how bifurcations occur due to extreme sparsity, decoupling of real power-angle and reactive power-voltage submatrices, weak coupling of coherent groups in each submodel and loss of voltage control discontinuities actually cause bifurcation in the differential-algebraic model as claimed in Section 4.2.4.

4.3 Bifurcation Sub-subsystems Experiencing SN and LF Bifurcation

The results presented in 4.6.5 indicate the classical load flow model is a bifurcation subsystem when generator exciters have high gain and are not disabled and results presented in Chapter 5 indicate that the reduced differential equation model $\Delta \dot{x} = J_x \cdot \Delta x$ can be a bifurcation subsystem of first order when generator exciters are disabled. The fact that the classical load flow is a bifurcation subsystem that produces and cause bifurcation in the differential-algebraic model does not end the application or investigation of bifurcation subsystems. The bifurcation subsystem method will attempt to identify algebraic sub-subsystems of smaller and smaller dimension to determine the smallest

bifurcation sub-subsystem (a coherent bus group) that produces and causes the bifurcation in the complete system as will be shown in Chapter 5. Similarly, differential bifurcation sub-subsystems containing (a) generator mechanical dynamics, (b) electrical dynamics, (c) generator flux decay dynamics, (d) the power balance equations at terminal buses, (e) the control systems dynamics or (f) a combination of the above would be investigated to find the smallest bifurcation subsystem once it is confirmed that a differential subsystem bifurcation has occurred. If a differential or algebraic bifurcation subsystem does not exist when conditions of Propositions 4.1 and 4.2 do not hold, a differential-algebraic bifurcation subsystem containing both differential and algebraic equations may exist. For the following results on finding the smallest algebraic subsystem, the smallest differential bifurcation subsystem and the smallest differential-algebraic subsystems, the Jacobian matrix J must be partitioned as follows

$$J = \begin{bmatrix} f_{x_{11}} & f_{x_{12}} & f_{y_{11}} & f_{y_{12}} \\ f_{x_{21}} & f_{x_{22}} & f_{y_{21}} & f_{y_{22}} \\ g_{x_{11}} & g_{x_{12}} & g_{y_{11}} & g_{y_{12}} \\ g_{x_{21}} & g_{x_{22}} & g_{y_{21}} & g_{y_{22}} \end{bmatrix}$$

4.3.1 Differential Bifurcation Sub-subsystem for Saddle-Node Bifurcation

Not all system dynamical states are generally involved in a differential subsystem bifurcation. The differential subsystem Jacobian matrix f_x includes the machine electrical and flux decay dynamics, excitation system dynamics, governor control dynamics and power system stabilizer dynamics. The matrices associated with each set of dynamics are

shown in the partitioned f_x matrix. The matrix $f_{x_{11}}(\mu)$ in

$$\Delta \dot{x} = \begin{bmatrix} \Delta \dot{x}_1 \\ \Delta \dot{x}_2 \end{bmatrix} = f_x(\mu) \cdot \Delta x = \begin{bmatrix} f_{x_{11}}(\mu) & f_{x_{12}}(\mu) \\ f_{x_{21}}(\mu) & f_{x_{22}}(\mu) \end{bmatrix} \cdot \begin{bmatrix} \Delta x_1 \\ \Delta x_2 \end{bmatrix} \quad (4.12)$$

can represent any subsystem of the the differential equation in (4.12), and the conditions for differential bifurcation sub-subsystems of first order are given in the following two corollaries.

Corollary 4.3.1(a)

Given that (4.1) has a differential bifurcation subsystem for SN bifurcation because conditions of Proposition 4.1 hold. Let $f_{x_{11}}(\mu^)$ in (4.12) be singular for some $\mu^* \in (\mu_1, \mu_2)$ where transversality conditions for SN hold at \bar{X}^* , $f_{x_{22}}$ nonsingular near μ^* and let $N_1 = \text{Null}(f_{x_{11}}(\mu^*))$ and $N_2 = \text{Null}(f_{x_{11}}(\mu^*)^T)$. Then $\Delta \dot{x}_1 = f_{x_{11}}(\mu) \cdot \Delta x_1$ is a differential bifurcation sub-subsystem of first order for (4.1) experiencing SN bifurcation if and only if near μ^* , condition (i) or (ii) is satisfied*

- (i) $\begin{bmatrix} f_{x_{12}} & f_{x_{22}}^{-1} & f_{x_{21}} \end{bmatrix} \cdot u_1 = 0$ for some $u_1 \in N_1$
- (ii) $v_1^T \cdot \begin{bmatrix} f_{x_{12}} & f_{x_{22}}^{-1} & f_{x_{21}} \end{bmatrix} = 0$ for some $v_1 \in N_2$

Corollary 4.3.1(b)

Given that (4.3) has a differential bifurcation subsystem for SN bifurcation because conditions of Proposition 4.1 hold. Let $f_{x_{22}}(\mu^)$ in (4.12) be singular for some $\mu^* \in (\mu_1, \mu_2)$ where transversality conditions for SN hold at \bar{X}^* , $f_{x_{11}}$ nonsingular near μ^* and let $N_1 = \text{Null}(f(\mu^*))$ and $N_2 = \text{Null}(f(\mu^*)^T)$. Then $\Delta \dot{x}_2 = f_{x_{22}}(\mu) \cdot \Delta x_2$ is a differential bifurcation sub-subsystem of first order for (4.1) experiencing SN bifurcation if and only if*

near μ^* , condition (i) or (ii) is satisfied

- (i) $\begin{bmatrix} f_{x_{21}} & f_{x_{11}}^{-1} & f_{x_{12}} \end{bmatrix} \cdot u_1 = 0$ for some $u_1 \in N_1$
- (ii) $v_1^T \cdot \begin{bmatrix} f_{x_{21}} & f_{x_{11}}^{-1} & f_{x_{12}} \end{bmatrix} = 0$ for some $v_1 \in N_2$

4.3.2 Algebraic Bifurcation Sub-subsystem for Load-Flow Bifurcation

Let the algebraic bifurcation subsystem 4.3(b) be partitioned as

$$0 = g_y \cdot \Delta y = \begin{bmatrix} g_{y_{11}} & g_{y_{12}} \\ g_{y_{21}} & g_{y_{22}} \end{bmatrix} \cdot \begin{bmatrix} \Delta y_1 \\ \Delta y_2 \end{bmatrix} \quad (4.13)$$

where $g_{y_{11}}$, $g_{y_{12}}$, $g_{y_{21}}$, $g_{y_{22}}$ are arbitrary submatrices of g_y . Depending on the singularity of $g_{y_{11}}$ and $g_{y_{22}}$, algebraic bifurcation sub-subsystems experiencing LF bifurcation may be obtained by applying Propositions 4.1 and 4.2 to the system in (4.13) as given in the two corollaries below.

Corollary 4.3.2(a)

Given that (4.3) has an algebraic bifurcation subsystem for LF bifurcation because conditions of Proposition 4.2 hold. Let $g_{y_{11}}(\mu^)$ in (4.13) be singular for some $\mu^* \in (\mu_1, \mu_2)$, $g_{y_{22}}(\mu)$ in (4.13) nonsingular and let $N_1 = \text{Null}(g_{y_{11}}(\mu^*))$ and $N_2 = \text{Null}(g_{y_{11}}(\mu^*)^T)$. Then $0 = g_{y_{11}}(\mu) \cdot \Delta y_1$ is an algebraic bifurcation sub-subsystem of first order for (4.1) experiencing LF bifurcation if and only if condition (i) or (ii) is satisfied*

- (i) $\begin{bmatrix} g_{y_{12}} & g_{y_{22}}^{-1} & g_{y_{21}} \end{bmatrix} \cdot u_1 = 0$ for some $u_1 \in N_1$
- (ii) $v_1^T \cdot \begin{bmatrix} g_{y_{12}} & g_{y_{22}}^{-1} & g_{y_{21}} \end{bmatrix} = 0$ for some $v_1 \in N_2$

Corollary 4.3.2(b)

Given that (4.3) has an algebraic bifurcation subsystem for LF bifurcation because conditions of Proposition 4.2 hold. Let $g_{y_{22}}(\mu^)$ in (4.13) be singular for some $\mu^* \in (\mu_1, \mu_2)$, $g_{y_{11}}$ nonsingular near μ^* and let $N_1 = \text{Null}(g_{y_{22}}(\mu^*))$ and $N_2 = \text{Null}(g_{y_{22}}(\mu^*)^T)$. Then $0 = g_{y_{22}}(\mu) \cdot \Delta y_{22}$ is an algebraic bifurcation sub-subsystem of first order for (4.1) experiencing LF bifurcation if and only if, near μ^* , conditions (i) or (ii) is satisfied*

$$(i) \quad \begin{bmatrix} g_{y_{21}} & g_{y_{11}}^{-1} & g_{y_{12}} \end{bmatrix} \cdot u_1 = 0 \text{ for some } u_1 \in N_1$$

$$(ii) \quad v_1^T \cdot \begin{bmatrix} g_{y_{21}} & g_{y_{11}}^{-1} & g_{y_{12}} \end{bmatrix} = 0 \text{ for some } v_1 \in N_2$$

The thesis will show that the disablement of generator excitation control produces voltage collapse in a load flow model, which is an algebraic bifurcation subsystem and will also cause bifurcations in the differential subsystem composed of the generator inertial and flux decay dynamics. These bifurcations in this differential bifurcation subsystem can explain the dynamical behavior observed as a system experiences voltage collapse.

4.3.3 Differential-algebraic Bifurcation Sub-subsystem

Differential-algebraic subsystems may be the most common type of bifurcation subsystem that produces and causes bifurcation in the full differential algebraic model. It has been reported that the transfer of real power across long transmission network is the reason behind the low-frequency oscillations, which may affect one or many generators in the system, or may affect more than one coherent generator groups. Differential-algebraic subsystems may therefore exist to represent not only the generator and control dynamics involved in the bifurcation, but also the contribution of the power balance constraints in

causing the failure. These subsystems may be derived by first permuting the order of the state variables as for instance,

$$[x \ y]^T = [x_1 \ x_2 \ y_1 \ y_2]^T \rightarrow [x_1 \ y_1 \ x_2 \ y_2]^T$$

Then the full system (4.3) now has the form

$$\begin{bmatrix} \Delta \dot{x}_1 \\ 0 \\ \Delta \dot{x}_2 \\ 0 \end{bmatrix} = \begin{bmatrix} f_{x_{11}} & f_{y_{11}} & f_{x_{12}} & f_{y_{12}} \\ g_{x_{11}} & g_{y_{11}} & g_{x_{12}} & g_{y_{12}} \\ f_{x_{21}} & f_{y_{21}} & f_{x_{22}} & f_{y_{22}} \\ g_{x_{21}} & g_{y_{21}} & g_{x_{22}} & g_{y_{22}} \end{bmatrix} \cdot \begin{bmatrix} \Delta x_1 \\ \Delta y_1 \\ \Delta x_2 \\ \Delta y_2 \end{bmatrix} = \begin{bmatrix} f_x^* & f_y^* \\ g_x^* & g_y^* \end{bmatrix} \cdot \begin{bmatrix} \Delta x_1 \\ \Delta y_1 \\ \Delta x_2 \\ \Delta y_2 \end{bmatrix} \quad (4.14)$$

Differential-algebraic sub-subsystems may be obtained by applying Propositions 4.1 and 4.2 on the Jacobian matrix as partitioned in Equation (4.14), where f_x^* , f_y^* , g_x^* and g_y^* are given by:

$$g_x^* = \begin{bmatrix} f_{x_{21}} & f_{y_{21}} \\ g_{x_{21}} & g_{y_{21}} \end{bmatrix} \quad ; \quad g_y^* = \begin{bmatrix} f_{x_{22}} & f_{y_{22}} \\ g_{x_{22}} & g_{y_{22}} \end{bmatrix} \quad 4.15(a)$$

$$f_x^* = \begin{bmatrix} f_{x_{11}} & f_{y_{11}} \\ g_{x_{11}} & g_{y_{11}} \end{bmatrix} \quad ; \quad f_y^* = \begin{bmatrix} f_{x_{12}} & f_{y_{12}} \\ g_{x_{12}} & g_{y_{12}} \end{bmatrix} \quad 4.15(b)$$

Corollary 4.4.3(a)

Let $f_x^*(\mu^*)$ in (4.14) be singular for some $\mu^* \in (\mu_1, \mu_2)$, $g_y^*(\mu)$ in (4.15) nonsingular near μ^* and let $N_1 = \text{Null}(f_x^*(\mu^*))$ and $N_2 = \text{Null}(f_x^*(\mu^*)^T)$. Then

$$\begin{bmatrix} \Delta \dot{x}_1 \\ 0 \end{bmatrix} = f_x^*(\mu) \cdot \begin{bmatrix} \Delta x_1 \\ \Delta y_1 \end{bmatrix}$$

is a differential-algebraic bifurcation subsystem of first order for (4.1) if and only if near μ^* , condition (i) or (ii) is satisfied

$$(i) \quad [f_y^* g_y^{*-1} g_x^*] \cdot u_1 = 0 \text{ for some } u_1 \in N_1$$

$$(ii) \quad v_1^T \cdot [f_y^* g_y^{-1} g_x^*] = 0 \quad \text{for some } v_1 \in N_2$$

Corollary 4.4.3(b)

Let $g_y^*(\mu^*)$ in (4.14) be singular for some $\mu^* \in (\mu_1, \mu_2)$, $f_x^*(\mu)$ in (4.15) nonsingular near μ^* and let $N_1 = \text{Null}(g_y^*(\mu^*))$ and $N_2 = \text{Null}(g_y^*(\mu^*)^T)$. Then

$$\begin{bmatrix} \Delta \dot{x}_2 \\ 0 \end{bmatrix} = g_y^*(\mu) \cdot \begin{bmatrix} \Delta x_2 \\ \Delta y_2 \end{bmatrix}$$

is a differential-algebraic bifurcation subsystem of first order for (4.1) if and only if near μ^* , condition (i) or (ii) is satisfied

$$(i) \quad [g_x^* f_x^{*-1} f_y^*] \cdot u_1 = 0 \quad \text{for some } u_1 \in N_1$$

$$(ii) \quad v_1^T \cdot [g_x^* f_x^{*-1} f_y^*] = 0 \quad \text{for some } v_1 \in N_2$$

4.4 Differential Bifurcation Subsystems for Hopf Bifurcation

The analysis and results carried out so far in this chapter have been based on Propositions 4.1 and 4.2 which focused on the system's change in behavior when a simple real eigenvalue of the differential-algebraic Jacobian matrix crosses the $j\omega$ -axis. It has been shown that under certain system operating conditions, two bifurcation subsystems of 4.3(a) are of interest:

- (a) An algebraic bifurcation subsystem for studying load flow bifurcation (also called loss of causality) in the equivalent algebraic system model (4.5) is given by

$$0 = J_y \cdot \Delta y = [g_y - g_x f_x^{-1} f_y] \cdot \Delta y \approx g_y \cdot \Delta y$$

- (b) A differential bifurcation subsystem for studying saddle node (SN) bifurcation in the equivalent differential system model (4.6) is given by

$$\Delta \dot{x} = J_x \cdot \Delta x = [f_x - f_y g_y^{-1} g_x] \cdot \Delta x \approx f_x \cdot \Delta x$$

Such results are desired and may easily be extended to the case where the system behavior

is characterized by the onset of unstable (subcritical) or stable (supercritical) oscillations. With no further analysis Proposition 4.1, Corollaries 4.4.1(b) and 4.4.1(b) may be generalized to cover the case when the equivalent dynamic system Jacobian matrix J_x has a pair of pure imaginary eigenvalues $\lambda_{1,2} = \pm i\omega_o$. If $\omega_o=0$, the equivalent dynamic system model experiences SN bifurcation, otherwise the system experiences undamped oscillatory behavior whose frequency depends on ω_o . Also it is evident that if the system $\Delta\dot{x} = J_x(\mu^*) \cdot \Delta x$ has a pair of pure imaginary eigenvalues $\lambda_{1,2} = \pm i\omega_o$ with associated conjugate (complex) eigenvectors $u_{1,2} \in C^n$ then we have

$$\begin{aligned}\lambda_1 \cdot u_1 &= i\omega_o \cdot u_1 = J_x(\mu^*) \cdot u_1 \\ [J_x(\mu^*) - i\omega_o I_{n \times n}] \cdot u_1 &= 0\end{aligned}$$

which says that when the matrix J_x has a pair of pure imaginary eigenvalues $\lambda_{1,2} = \pm i\omega_o$, the matrix $[J_x(\mu^*) - i\omega_o I_{n \times n}]$ has a zero eigenvalue, i.e. singular. Therefore, with the following definitions,

$$f_x^{\omega_o}(\mu) = f_x(\mu) - i\omega_o I_{n_1 \times n_1} \quad 4.16(a)$$

$$\begin{aligned}J_x^{\omega_o}(\mu) &\equiv J_x(\mu) - i\omega_o I_{n_1 \times n_1} \quad 4.16(b) \\ &= f_x(\mu) - f_y g_y^{-1} g_x - i\omega_o I_{n_1 \times n_1} \\ &= f_x^{\omega_o}(\mu) - f_y g_y^{-1} g_x\end{aligned}$$

similar proposition and corollaries to Proposition 4.1 and Corollaries 4.4.1(a-b) may be stated for the existence of differential bifurcation subsystems of 4.3(a) for Hopf bifurcation.

Proposition 4.3

Let $f_x^{\omega_o}(\mu)$ in (4.16) be singular for some $\mu^ \in (\mu_1, \mu_2)$ where transversality conditions for Hopf hold at \bar{x}^* , $g_y(\mu)$ nonsingular near μ^* and let $N_1 = \text{Null}[f_x^{\omega_o}(\mu^*)] \subset C^n$ and $N_2 = \text{Null}[f_x^{\omega_o}(\mu^*)^T] \subset C^n$. Then, $\Delta\dot{x} = f_x(\mu) \cdot \Delta x$ is a differential bifurcation subsystem of*

first order for (4.1) experiencing Hopf if and only if near μ^* , condition (i) or (ii) is satisfied

$$(i) \quad [f_y g_y^{-1} g_x] \cdot u_1 = 0 \text{ for some } u_1 \in N_1$$

$$(ii) \quad v_1^T \cdot [f_y g_y^{-1} g_x] = 0 \text{ for some } v_1 \in N_2$$

4.4.1 Differential Bifurcation Sub-subsystems for Hopf Bifurcation

The Hopf bifurcation in a differential bifurcation model for Hopf, may exist in only a subset of the generator inertial dynamics, flux decay dynamics, exciter system control dynamics, governor control dynamics...etc. Condition for bifurcation of $\Delta \dot{x} = f_x(\mu) \cdot \Delta x$ or bifurcation sub-subsystems of (4.1) for Hopf are given below. Let the matrix $f_x^{\omega_o}(\mu)$ be partitioned as

$$f_x^{\omega_o}(\mu) \cdot \Delta x = \begin{bmatrix} f_{x_{11}}^{\omega_o}(\mu) & f_{x_{12}} \\ f_{x_{21}} & f_{x_{22}}^{\omega_o}(\mu) \end{bmatrix} \cdot \begin{bmatrix} \Delta x_1 \\ \Delta x_2 \end{bmatrix} \quad (4.18)$$

then conditions for differential bifurcation sub-subsystems for Hopf bifurcation are given in the following two corollaries.

Corollary 4.4.1(a)

Given that (4.3) has a differential bifurcation subsystem of first order for Hopf bifurcation exists because conditions of Proposition 4.3 hold. Let $f_{x_{11}}^{\omega_o}(\mu^*)$ in (4.18) be singular for some $\mu^* \in (\mu_1, \mu_2)$ where transversality conditions for Hopf hold at \bar{X}^* , $f_{x_{22}}^{\omega_o}(\mu)$ nonsingular near μ^* , and let $N_1 = \text{Null}[f_{x_{11}}^{\omega_o}(\mu^*)]$ and $N_2 = \text{Null}[(f_{x_{11}}^{\omega_o}(\mu^*))^T]$. Then $\Delta \dot{x}_1 = f_{x_{11}}(\mu) \cdot \Delta x_1$ is a differential bifurcation sub-subsystem of first order for (4.1) for Hopf if and only if near μ^* , condition (i) or (ii) is satisfied

- (i) $\left[f_{x_{12}} f_{x_{22}}^{\omega}(\mu)^{-1} f_{x_{21}} \right] \cdot u_1 = 0$ for some $u_1 \in N_1$
- (ii) $v_1^T \cdot \left[f_{x_{12}} f_{x_{22}}^{\omega}(\mu)^{-1} f_{x_{21}} \right] = 0$ for some $v_1 \in N_2$

Corollary 4.4.1(b)

Given that (4.3) has a differential bifurcation subsystem for Hopf bifurcation because conditions of Proposition 4.3 hold. Let $f_{x_{22}}^{\omega}(\mu^*)$ in (4.18) be singular for some $\mu^* \in (\mu_1, \mu_2)$ where transversality conditions for Hopf hold at \bar{x}^* , $f_{x_{11}}^{\omega}(\mu)$ nonsingular near μ^* and let $N_1 = \text{Null}\left[f_{x_{22}}^{\omega}(\mu^*)\right]$ and $N_2 = \text{Null}\left[\left(f_{x_{22}}^{\omega}(\mu^*)\right)^T\right]$. Then $\Delta \dot{x}_2 = f_{x_{22}}(\mu) \cdot \Delta x_{22}$ is a differential bifurcation sub-subsystem of first order for (4.1) for Hopf bifurcation if and only if near μ^* , condition (i) or (ii) is satisfied

- (i) $\left[f_{x_{21}} f_{x_{11}}^{\omega}(\mu)^{-1} f_{x_{12}} \right] \cdot u_1 = 0$ for some $u_1 \in N_1$
- (ii) $v_1^T \cdot \left[f_{x_{21}} f_{x_{11}}^{\omega}(\mu)^{-1} f_{x_{12}} \right] = 0$ for some $v_1 \in N_2$

4.5 Application of Algebraic Bifurcation Subsystem Experiencing LF Bifurcation in Power System Stability Assessment

When the linearized system model (4.4) satisfies conditions of Proposition 4.2, the algebraic bifurcation subsystem of first order $0 = g_y \cdot \Delta y$ or consisting only of the network equations $0 = g(x, y, \mu)$ is a bifurcation subsystem of the Exact Load Flow model $0 = g(x(y), y, \mu)$ that is used to study load flow bifurcation occurring in the full differential-algebraic model

$$\begin{bmatrix} \Delta \dot{x} \\ 0 \end{bmatrix} = J \cdot \begin{bmatrix} \Delta x \\ \Delta y \end{bmatrix}.$$

Considering the similarity between g_y and the classically used approximate load flow model with Jacobian matrix J_{LF} [52], such a result would justify why experience has shown that a classical load flow model is such a useful tool in assessing stability that

occurs in a differential-algebraic model. The classical load flow model was the first and for some time the only tool for studying voltage collapse or voltage stability [App B]. The P-V or Q-V curves computed using a classical load flow model have been the principal methods used to study voltage instability and proximity to voltage collapse. Studies [54] have shown that voltage collapse occurs as a bifurcation in the classical load flow model and results either in no solution or multiple solutions in the model equations. Over the past ten years far more accurate Type 2-4 differential-algebraic models have been developed. However the classical load flow model is still the model and computer program being used in power system voltage stability assessment programs despite the existence of far more accurate models and simulation tools. The objective is therefore to use the present knowledge of bifurcation subsystems, to assess when and why a classical load flow model is a bifurcation subsystem for the full differential-algebraic model. The discussion will start with a brief description of a classical load flow model, then take hierarchical steps by first looking into the preliminary system condition (f_x nonsingular) for utilizing J_y as a test matrix that is equivalent to J for testing when a static or algebraic bifurcation occurs in the differential-algebraic model. The second step is to compare the Exact Load Flow model $0 = J_y \cdot \Delta y$ ($0 = g(x(y), y(\mu), \mu)$) with the algebraic bifurcation subsystem $0 = g_y \cdot \Delta y$ ($0 = g(x(\mu), y(\mu), \mu)$), and the classical load flow model $0 = J_{LF} \cdot \Delta y$ ($0 = g^*(y, \mu)$). Finally, based on the bifurcation subsystem conditions, some operational and geometric grounds are established for the use of the classical load flow power system model when algebraic bifurcation subsystem experiences the same algebraic bifurcation as the Exact Load Flow model.

4.5.1 Description of a Classical Load Flow Model

The classical load flow model describes the power system steady state condition of the transmission network and is a set of algebraic equations composed of the active and reactive power balance equations of the transmission network at load buses and only the active power balance equations at generator terminal PV buses. The reactive power balance equations at generator buses are neglected since the excitation systems of these generators are assumed to have infinite gain and thus hold the generator terminal voltage to set point value. The classical load flow model can also be viewed as a simplified model of a power system differential-algebraic model under the following assumptions: (a) the generator armature resistance is zero; (b) f_x is invertible (c) the excitation gain of each generator is infinite; and (d) all time constants in the differential equations are set to zero since the time interval over which the model is to be valid is infinite.

Buses in a classical load flow model are conventionally divided into three types: (1) a swing bus is a generator bus with infinite active and reactive power reserves so that its voltage and angle are fixed while its active and reactive power generations are dependent variables that provide the power mismatch between generation and load plus losses in the rest of the system; (2) a generator PV-bus represents a generator bus operating under over-excitation limits (OEL), and thus its reactive power generation and angle are dependent variables while its voltage and real power generation are independent variables. (3) load PQ-bus is any bus with no reactive or real power generation, and thus instead active and reactive power injections are specified at this bus and are independent variables in the model. The voltage and angle at PQ buses are dependent variables that must be solved for using the model.

The classical load flow model consists of active power balance equations at all PV-buses and PQ-buses, and reactive power balance equations at all PQ-buses. The reactive power generation at each PV-bus and the active and reactive power generations at the swing bus are output variables (dependent variables) of the load flow model. In addition, if a generator PV-bus exciter is disabled by field current limit controllers, the generator PV-bus becomes a load PQ bus due to action of field current limit controller that disables the exciter and controls the reactive power to be the continuous rating limit. Thus, one more reactive power balance equation at that generator terminal bus needs to be added, since the voltage magnitude at its terminals is no longer held fixed. The general structure of the classical load flow Jacobian has been derived in [52] and presented in Appendix A as:

$$J_{LF} = \begin{bmatrix} \frac{\partial P}{\partial \theta} & \frac{\partial P}{\partial V} \\ \frac{\partial Q}{\partial \theta} & \frac{\partial Q}{\partial V} \end{bmatrix} = \begin{bmatrix} J^{PT} \\ J^{PH} \\ J^{PL} \\ J^{PQ} \\ J^{QH} \\ J^{QL} \end{bmatrix} = \begin{bmatrix} A_1 & B_{1H} & 0 & C_1^{PQ} & D_{1H} & 0 \\ A_{2H} & B_{2HH} & B_{2LH} & C_{2H}^{PQ} & D_{2HH} & D_{2HL} \\ 0 & B_{2LH} & B_{2LL} & 0 & D_{2LH} & D_{2LL} \\ A_3^{PQ} & B_{3H}^{PQ} & 0 & C_{3K}^{PQ} & D_{3H}^{PQ} & 0 \\ A_{4H} & B_{4HH} & B_{4LH} & C_{4H}^{PQ} & D_{4HH} & D_{4HL} \\ 0 & B_{4LH} & B_{4LL} & 0 & D_{4LH} & D_{4LL} \end{bmatrix} \quad (4.18)$$

Where

$$\begin{aligned} \theta &= [\theta_T' \ \theta_H' \ \theta_L']' & : & \text{angle variables at network buses;} \\ V &= [V_T^{PQ'} \ V_H' \ V_L']' & : & \text{voltage variables at network buses;} \\ P &= [P_T' \ P_H' \ P_L']' & : & \text{voltage-dependent active power load demand;} \\ Q &= [Q_T^{PQ'} \ Q_H' \ \Delta Q_L']' & : & \text{voltage-dependent reactive power load demand;} \end{aligned}$$

The real and reactive power balance equations in (4.18) have been arranged according to the types of bus variables in the transmission network, i.e generator terminal (T) buses, high side (H) transformer buses and load (L) buses. The matrices in the fourth row block and column blocks are solely associated with the generator PV buses which became PQ

buses, thus the superscript notation PQ.

4.5.2 Structural Conditions for Utilizing J_y

The structural condition (f_x nonsingular) imposed by Proposition 4.2 for formulating the algebraic bifurcation subsystem $0 = g_y \cdot \Delta y$ may be understood by observing the matrix f_x as presented in (4.4). The derivation of the model used is given in [52] and summarized in Appendix A. The matrices f_x and A_{CC} are given by

$$f_x = \left(\text{diag} \begin{bmatrix} T_{XX} & T_{EE} & T_{GG} & T_{SS} \end{bmatrix} \right)^{-1} \cdot \begin{bmatrix} A_{XX} & A_{XE} & A_{XG} & 0 \\ A_{EX} & A_{EE} & 0 & A_{ES} \\ A_{GX} & 0 & A_{GG} & 0 \\ A_{SX} & 0 & 0 & A_{SS} \end{bmatrix} \quad (4.19)$$

$$A_{CC} = \begin{bmatrix} A_{EE} & 0 & A_{ES} \\ 0 & A_{GG} & 0 \\ 0 & 0 & A_{SS} \end{bmatrix}$$

Matrix f_x is composed of diagonal block submatrices where each diagonal element is associated with one machine. The elements of each submatrix of f_x is defined based on the single machine infinite bus matrix, since it represents the operating condition when the terminal bus of each machine is assumed to be an infinite (swing) bus with constant terminal voltage. Note that each diagonal block submatrix of f_x can be viewed as an element of a single machine model, since the dynamics of each machine are uncoupled in f_x . The control systems form an upper triangular block matrix A_{CC} and its eigenvalues are those of each control system: A_{EE} , A_{GG} , and A_{SS} . Based on IEEE general models of speed-governing-turbine system and power system stabilizers [52], both A_{GG} and A_{SS} are lower triangular matrices with real and negative eigenvalues. Regarding the excitation

system matrix A_{EE} , when the excitation system is “properly tuned” and is able to be manually operated, all the eigenvalues of A_{EE} are nonzero negative real values. Moreover, under the assumption that each synchronous machine is operated below its steady state stability limit, the matrix f_x can be shown to be nonsingular, with stable eigenvalues. It will be shown in Chapter 6 that f_x can be singular if the mechanical dynamics or flux decay dynamics experience saddle node bifurcation. Operationally neither saddle bifurcations should occur if the machine is operated within its real power generation limits and the exciter is properly designed. Therefore, under the above assumptions, the equivalent algebraic Jacobian matrix $J_y = g_y - g_x f_x^{-1} f_y$ can be analytically defined.

4.5.3 Comparison of Exact Load Flow model, Algebraic Bifurcation Subsystem, and Classical Load Flow Model

The Exact Load Flow model $0 = g(x(y), y(\mu), \mu)$, algebraic bifurcation subsystem $0 = g(x(\mu), y(\mu), \mu)$, and the classical load flow model $0 = g^*(y, \mu)$ are all quite similar because they all have real and reactive power balance equations at generator high side transformer buses. The associated linearized models with Jacobians J_y , g_y and J_{LF} are also quite similar. The differences in J_y and g_y is investigated first to establish (i) when and if load flow bifurcation occurs due to loss of causality so that $0 = g(x(\mu), y(\mu), \mu)$ is an algebraic bifurcation subsystem of $0 = g(x(y), y(\mu), \mu)$, and (ii) when the classical load flow model is a bifurcation subsystem model of the Exact Load Flow model.

The geometric conditions of existence of an algebraic bifurcation subsystem of first order for LF bifurcation.

$$[g_x f_x^{-1} f_y] \cdot u_2 = 0 \quad \text{when} \quad g_y \cdot u_2 = J_y \cdot u_2 = 0$$

$$v_2^T \cdot [g_x f_x^{-1} f_y] = 0 \quad \text{when} \quad v_2^T \cdot g_y = v_2^T \cdot J_y = 0$$

where u_2 and v_2 are the right and the left eigenvectors associated with the zero eigenvalue, may be approximately satisfied in different ways such as

$$(C1) \quad \|g_x\| \text{ is } O(\epsilon) \text{ and } \|f_x^{-1}\| \|f_y\| \cdot \|u_2\| \text{ is } O(1) \text{ near } \mu^*$$

$$(C2) \quad \|f_y\| \text{ is } O(\epsilon) \text{ and } \|f_x^{-1}\| \|g_x\| \cdot \|u_2\| \text{ is } O(1) \text{ near } \mu^*$$

$$(C3) \quad \|f_x^{-1}\| \text{ is } O(\epsilon) \text{ and } \|f_y\| \|g_x\| \cdot \|u_2\| \text{ is } O(1) \text{ near } \mu^*$$

$$(G1) \quad \text{None of the above but near } \mu^*, \text{ the vector } v_2 \text{ is such that } v_2^T \cdot [g_x f_x^{-1} f_y] \approx 0.$$

$$(G2) \quad \text{None of the above but near } \mu^*, \text{ the vector } u_2 \text{ is such that } [g_x f_x^{-1} f_y] \cdot u_2 \approx 0.$$

where $\| \cdot \|$ is an appropriate matrix norm. Conditions C1 and C2 pertain to the case when the coupling matrices g_x and f_y are negligible so that the interaction between generator internal and terminal buses is insignificant to the bifurcation study. Likewise, condition C3 implies that the single machine matrix f_x must be diagonally dominant. The eigenvalues of f_x are in fact proportional to the eigenvalues of the control systems A_{GG} , A_{SS} and A_{EE} , and the system K -matrices (will be derived in Chapter 6). These eigenvalues may be high when the system is operating below its steady state stability limits and with high excitation gain. Despite the implication of these conditions, it is clear that the geometric conditions G1 and G2 not only encompass conditions C1-C3, but also are more likely to occur due to the sparsity and weak coupling property of the Jacobians as noted earlier. G1 and G2 say that near μ^* , $[g_x f_x^{-1} f_y]$ need not be zero, but only that $g_y - J_y$ be nearly singular and that its null space (approximately) overlap the null space of $g_y(\mu^*)$.

Conditions G1 and G2 require examination of the structure and characteristics of the matrix $[g_y - J_y] = g_x f_x^{-1} f_y$ near μ^* and its geometric interaction with the right and left eigenvectors u_2 and v_2 of the null space of $g_y(\mu^*)$.

In order to demonstrate and characterize the validity of the use of the algebraic bifurcation subsystem and subsequently the classical load flow model, analytical expressions of g_y and $[g_y - J_y] = g_x f_x^{-1} f_y$ derived and presented in [52] are

$$g_y = \begin{bmatrix} \frac{\partial P}{\partial \theta} & \frac{\partial P}{\partial V} \\ \frac{\partial Q}{\partial \theta} & \frac{\partial Q}{\partial V} \end{bmatrix} = \begin{bmatrix} g_y^{PT} \\ g_y^{PH} \\ g_y^{PL} \\ g_y^{QT} \\ g_y^{QH} \\ g_y^{QL} \end{bmatrix} = \begin{bmatrix} A_{1K} & B_{1H} & 0 & C_{1K} & D_{1H} & 0 \\ A_{2H} & B_{2HH} & B_{2LH} & C_{2H} & D_{2HH} & D_{2HL} \\ 0 & B_{2LH} & B_{2LL} & 0 & D_{2LH} & D_{2LL} \\ A_{3K} & B_{3H} & 0 & C_{3K} & D_{3H} & 0 \\ A_{4H} & B_{4HH} & B_{4LH} & C_{4H} & D_{4HH} & D_{4HL} \\ 0 & B_{4LH} & B_{4LL} & 0 & D_{4LH} & D_{4LL} \end{bmatrix} \quad (4.20)$$

$$[g_x f_x^{-1} f_y] = g_y - J_y = \begin{bmatrix} K_{P1}^{iq} & 0 & 0 & K_{P7}^{iq} & 0 & 0 \\ 0 & 0 & 0 & 0 & 0 & 0 \\ 0 & 0 & 0 & 0 & 0 & 0 \\ K_{Q1}^{iq} & 0 & 0 & C_{3X} & 0 & 0 \\ 0 & 0 & 0 & 0 & 0 & 0 \\ 0 & 0 & 0 & 0 & 0 & 0 \end{bmatrix} \quad (4.21)$$

Where

$$\begin{aligned} \theta &= [\Delta\theta_T' \ \Delta\theta_H' \ \Delta\theta_L']^t && : \text{angle variables at network buses;} \\ V &= [\Delta V_T' \ \Delta V_H' \ \Delta V_L']^t && : \text{voltage variables at network buses;} \\ P &= [\Delta P_T' \ \Delta P_H' \ \Delta P_L']^t && : \text{voltage-dependent active power load demand;} \\ Q &= [\Delta Q_T' \ \Delta Q_H' \ \Delta Q_L']^t && : \text{voltage-dependent reactive power load demand;} \end{aligned}$$

Note that the submatrices in the fourth row and fourth column blocks of g_y model the reactive power Jacobians associated with the generator terminal buses, while in the classical load flow model (4.18) the fourth row and fourth column blocks are associated with unregulated generator PV-buses which became PQ-buses. Therefore, the difference between the two matrices resides mainly in the fourth row and fourth columns, since the row dimension of submatrices in the fourth row of J_{LF} associated with Q_T^{PQ} and the

column dimension of the submatrices in the fourth column of J_{LF} associated with v_T^{PQ} equal to the number of generators with PV to PQ bus changes, but those in g_y are proportional to the number of generators in the model. These are also differences in the terms A_{1K} , A_{3K} , C_{1K} and C_{3K} of g_y and A_1 , A_3^{PQ} , C_1^{PQ} and C_3^{PQ} of J_{LF} . The relations between these terms as well as their relation to the equivalent algebraic Jacobian matrix J_y is now discussed when the dimension of u_{PQ} and the number of rows associated with v_T^{PQ} and Q_T^{PQ} in (4.18) are zero.

Note that the submatrices A_{1K} and A_{3K} of g_y are given by

$$A_{1K} = K_{P1}^{iq} + A_1 \quad ; \quad A_{3K} = K_{Q1}^{iq} + A_3$$

where A_1 and A_3 do not include the effects of the $K_{P1}^{iq} = \partial P_T / \partial \theta_T$ and $K_{Q1}^{iq} = \partial Q_T / \partial \theta_T$ coupling between generator terminal and internal buses. Thus A_1 and A_3 are identical to the matrices A_1 , A_3^{PQ} of a classical load flow model Jacobian (4.18) since this model includes terminal buses but not internal buses. Also note that

$$C_{1K} = K_{P7}^{iq} + C_1 \quad ; \quad C_{3K} = K_{Q7}^{iq} + C_3$$

where C_1 and C_3 do not include the effects of the $K_{P7}^{iq} = \partial P_T / \partial v_T$ and $K_{Q7}^{iq} = \partial Q_T / \partial v_T$ coupling between generator terminal and internal buses. Therefore C_1 and C_3 are identical except in dimension to the matrices C_1^{PQ} and C_3^{PQ} of a classical load flow model Jacobian (4.18) since this model includes terminal buses but not internal buses. Expressions for K_{P1}^{iq} , K_{Q1}^{iq} , K_{P7}^{iq} and K_{Q7}^{iq} are easily derived [52] and can be found in Appendix A. When adding $[J_y - g_y]$ of (4.21) and g_y of (4.20) to obtain J_y , it turns out that A_{1K} and A_{3K} of g_y are replaced [52] by A_1 and A_3^{PQ} of the classical load flow Jacobian J_{LF} which implies that the exciter and flux decay dynamics have no effect on $\partial P_T / \partial \theta_T$ and $\partial Q_T / \partial \theta_T$ terms of J_y . Furthermore, in J_y the submatrices C_{1K} and C_{3K} of

g_y are replaced by

$$C_{1K}^X = C_{1K} - C_{1X} = C_1 + K_{P7}' - C_{1X}$$

$$C_{3K}^X = C_{3K} - C_{3X} = C_3 + K_{Q7}' - C_{3X}$$

Matrices C_{1X} and C_{3X} are derived in [52] and are dependent on the DC gain of the excitation system K_{EE} which makes diagonal matrices C_{1K}^X and C_{3K}^X have very large negative elements when all exciters are active. However if the armature resistance of the generator $R_a = 0$, then [52]

$$C_{1X} = K_{P7}' \quad \text{thus} \quad C_{1K}^X = C_1.$$

This result implies that when the armature resistance of the generator is neglected, the control systems do not have any effect on the active power-angle Jacobian matrix $C_{1K}^X = C_1$. Since R_a is generally small so that $C_{1K}^X = C_1$ and C_{3K}^X is assumed to be large when exciters are operating at high gain at every generator, the conditions for static bifurcation of J_y

$$0 = J_y \cdot u_2 \tag{4.23(a)}$$

where

$$u_2^T = (u_{PT}^T, u_{PH}^T, u_{PL}^T, u_{QT}^T, u_{QH}^T, u_{QL}^T) \tag{4.23(b)}$$

Equation (4.20), (4.21) and (4.23) imply that

$$A_3 u_{PT} + B_3 u_{PH} + C_{3K}^X u_{QT} + D_{3H} u_{QH} \approx C_{3K}^X \cdot u_{QT} \approx 0 \tag{4.24(a)}$$

since C_{3K}^X is very large due to its being linearly dependent to K_{EE} . From equation 4.24(a) and the fact that C_{3K}^X is diagonally dominant when all generators have excitation control, 4.24(a) suggests that

$$u_{QT} \approx 0 \tag{4.24(b)}$$

Since 4.24(b) is associated with the fourth row of J_y not in J_{LF} when all generators have excitation control and $u_{QT} \approx 0$ eliminates the fourth column of J_y , the remaining

equations of 4.23(a), (which do not include 4.24(a), require that

$$J_{LF} \cdot \begin{bmatrix} u_{PT}^T & u_{PH}^T & u_{PL}^T & u_{PQ} & u_{QH}^T & u_{QL}^T \end{bmatrix}^T \approx 0$$

where u_{PQ} has dimension equal to zero.

Thus Propositions 4.2 implies that the classical load flow model is a bifurcation subsystem of

$$J_y \cdot \Delta y = 0$$

and

$$\begin{bmatrix} \Delta x \\ 0 \end{bmatrix} = J \cdot \begin{bmatrix} \Delta x \\ \Delta y \end{bmatrix}$$

for LF bifurcation for the case where all exciters are active and operating with high gain, R_a on every generator is assumed to be zero, and $\partial f / \partial x$ is invertible.

An option has been added to some load flow algorithms to model the generator flux and exciter loop. In this case, the exciter gain on every generator does not have to be large for the load flow to be a bifurcation subsystem for the differential-algebraic power system model, since in this case $J_{LF} = J_y$ regardless of whether the exciter is present or is disabled by field current limit controllers. The only difference in $J_{LF} = J_y$ when exciters are present or disabled is in the terms C_{1X} and C_{3X} that depend on whether excitation system gain $K_{EE} = K_{SE}^{-1} K_A K_D$ is zero or nonzero, where K_{SE} is the inverse diagonal matrix of the inverse DC gain of the exciter, K_A is a diagonal matrix of the amplifier gain of each excitation system, and K_D is the diagonal matrix of the sensor gain for each generator exciter.

4.5.4 Bifurcation in LF Model or in Generator Dynamics

Recall that the conditions for g_y to be a bifurcation subsystem of J_y and J require that

$$[J_y - g_y] \cdot u_2 = 0 \quad (4.25)$$

when

$$J_y \cdot u_2 = 0 \quad (4.26)$$

From (4.21), condition (4.25) can be written as

$$K_{P1}^{iq} \cdot u_{PT} + C_{1X} \cdot u_{QT} = 0 \quad 4.27(a)$$

$$K_{Q1}^{iq} \cdot u_{PT} + C_{3X} \cdot u_{QT} = 0 \quad 4.27(b)$$

where u_2 is the eigenvector associated with the zero eigenvalue,

$$u_2^T = (u_{PT}^T, u_{PH}^T, u_{PL}^T, u_{QT}^T, u_{QH}^T, u_{QL}^T)$$

The J_y condition in (4.26) for terminal buses can be written

$$A_1 u_{PT} + B_1 u_{PH} + (C_1 + K_{P7}^{iq} - C_{1X}) u_{QT} + D_{3H} u_{QH} = 0 \quad 4.28(a)$$

$$A_3 u_{PT} + B_3 u_{PH} + (C_3 + K_{Q7}^{iq} - C_{3X}) u_{QT} + D_{3H} u_{QH} = 0 \quad 4.28(b)$$

There is very little chance that J_y and J will be singular simultaneously with g_y since the C_{3X} term in equations 4.27(b) and 4.28(b), which is dominant, occurs with different signs. On the other hand, if u_{PT} , u_{PH} , u_{QT} and u_{QH} were zero for a specific bifurcating eigenvalue, then from (4.26) and (4.27) we can see that the bifurcation occurs strictly in the load buses far from the generators in the system, which indicates that J and J_y can reach bifurcation when g_y reaches bifurcation [52]. If u_{PT} , u_{PH} , u_{QT} and u_{QH} are nonzero then g_y is never singular when J and J_y are singular, and singularity in J always occurs due to singularity in J_x . This bifurcation in generator dynamics that occurs whenever u_{PT} , u_{PH} , u_{QT} and u_{QH} are nonzero, will occur when load flow bifurcation occurs if all generator exciters have infinite gain, all generators have zero armature resistance, and f_x is nonsingular, or if the load flow modeling option has been selected that makes $J_y = J_{LF}$.

4.5.5 Conclusion

The bifurcation subsystem method suggests that

- (1) the classical load flow model is a bifurcation subsystem for the differential-algebraic model for all static bifurcations when all exciters are active and high gain at the point of bifurcation; R_a is zero on every generator, and f_x is invertible.
- (2) the classical load flow model with complete DC modeling of generator exciter and flux decay effects is a bifurcation subsystem for LF bifurcations for both

$$J_y \cdot \Delta y = 0$$

and

$$\begin{bmatrix} \Delta \dot{x} \\ 0 \end{bmatrix} = J \cdot \begin{bmatrix} \Delta x \\ \Delta y \end{bmatrix}$$

- (3) the set of algebraic equations for a differential-algebraic model is not likely to be a bifurcation subsystem of all the differential-algebraic model whether exciters are active or disabled, unless u_{PT} , u_{PH} , u_{QT} and u_{QH} are zero. This result implies that bifurcation of these algebraic equations can only occur if it occurs solely in the algebraic equations of load buses in the system, which produce an algebraic bifurcation subsystem.
- (4) as a result of (3), static bifurcations of the differential-algebraic model are either static bifurcations of the reduced differential model with Jacobian J_x when u_{PT} , u_{PH} , u_{QT} and u_{QH} are non zero, or an algebraic bifurcation in the real and reactive power balance equations at load buses when u_{PT} , u_{PH} , u_{QT} and u_{QH} are null. The algebraic bifurcation is referred to as clogging voltage instability in [11] and is due to inability to ship reactive power to load buses. The clogging occurs due to reactive losses that consume the reactive supply. The static bifurcation of the reduced differential model is a saddle node bifurcation because the generic static bifurcation

is a saddle node bifurcation. The static bifurcation is most often a loss of control voltage instability that occurs due to exhaustion of reactive reserves and voltage control at generator buses since the generator terminal bus is affected by the bifurcation. There can be clogging voltage collapse problems [11] that are due to static bifurcation in the reduced differential equation model since clogging voltage collapse can exhaust reactive reserves and cause loss of voltage control, but this is by definition not the cause of the instability. The exhaustion of reactive reserves of these generators could only occur if the generator terminal buses were affected and $u_{QT} \neq 0$.

V

Effect of Hard Limit Discontinuities on Stability Analysis

5.0 Introduction

The Bifurcation Subsystem Method developed in Chapter 4 and the Epoch Based Trajectory Stability Assessment Method developed in Chapter 3 provide a framework for initiating a structural stability analysis on a single-machine-infinite bus (SMIB) model that encompasses local shunt loads, with emphasis on the effects of one type of hard limit discontinuous system transition, the disablement of excitation control. This discontinuous control action is shown to have an effect on the kind, class and the tests for bifurcation occurring on the SMIB model. The goals of this chapter are to:

- (a) Demonstrate two examples of using the bifurcation subsystem method to identify bifurcation subsystems in a model. The generator angle-speed dynamics is the bifurcation subsystem for Hopf bifurcation in the regulated SMIB model, and the angle-speed-flux decay dynamics is the bifurcation subsystems for SN bifurcation, in the unregulated SMIB model, respectively.
- (b) Analyze the effects of hard limit discontinuities by assessing the effect of excitation control or lack of excitation control on the (i) types, (ii) classes of bifurcations produced, and (iii) the stability test needed for detecting the occurrence of bifurcation.

- (c) Derive expressions for the synchronizing and damping torques in a linearized power system model with no exciter, a thyristor exciter, and type 1 exciter models in terms of the model parameter K_1 - K_6 . The damping torques are derived for $f \ll 1$ and for $f \gg 1$.
- (d) Derive conditions on linearized model parameters K_4 and K_5 for the occurrence of Hopf and on parameter K_1 , K_2 , K_3 , K_4 , K_5 and K_6 for Saddle Node bifurcations, and preservation of stability of the equilibrium. Such conditions are derived for the unregulated model and for the regulated model (thyristor and type 1 exciter) SMIB model.

The conditions on model parameters K_4 and K_5 set the stage for establishing diagnostic tests for specific kind and class of Hopf bifurcation in terms of active load, reactive load, shunt capacitive susceptance, and real power transfer levels in Chapter 6.

The stability analysis in this chapter is based on the principle of synchronizing and damping torques or a bifurcation sub-subsystem

$$M\Delta\ddot{\delta} + D\Delta\dot{\delta} = \Delta T_m - \Delta T_e$$

$$\Delta T_e = K_S\Delta\delta + K_D\Delta\dot{\delta} = \Delta T_S + \Delta T_D$$

where

- ΔT_m : incremental change in mechanical power input to the generator
 ΔT_e : incremental change in the electrical power output of the generator
 ΔT_S : incremental change in synchronizing torque
 ΔT_D : incremental change in damping torques of the machine

The use of damping and synchronizing torque model for the model shown in Figure 5.3 was developed in [55] where the generator inertial and exciter dynamics are assumed to produce equivalent damping and synchronizing torques on the inertial dynamics. This type of analysis performed in [55] was later extended in [56], in both classical papers on

power system dynamics. Matrices K_S and K_D were derived in [52] for multi-machine power systems given that the subsystem external to the mechanical dynamics is invertible. The K_S and K_D tests for saddle node and Hopf bifurcations respectively, do not necessarily imply that the bifurcation occurs in the generator mechanical dynamics, nor that the inertial dynamics are a bifurcation subsystem, and neither the test matrices nor the bifurcation subsystem indicates anything about the center manifold for the bifurcation in a non-classical power system model. The system is stable if and only if both the synchronizing and damping torques are positive. If a classical generator model is used, where no flux decay or exciter dynamics are modeled, then the damping and synchronizing torques are namely $\Delta T_S = K_1$, the machine real power coefficient, and $\Delta T_D = D$, the natural damping of the machine. In the case of more complex generator models, ΔT_S and ΔT_D depend on the single machine infinite bus model constants K_1 - K_6 . The form of ΔT_S and ΔT_D in terms of K_1 - K_6 have been derived for nonclassical generator model with different exciter models and for the unregulated model [56]. The system K_1 - K_4 constants (unregulated) and K_1 - K_6 (regulated) are derived as part of this thesis and are expressed as functions of the system operating point, the network parameters, and the infinite bus voltage. Although the parameters or matrices ΔT_S and ΔT_D do not imply that the inertial dynamics contain the center manifold or even a bifurcation subsystem, they are tests for saddle node and Hopf bifurcations in the full system model utilized as effective measures of stability and security, and are for that reason used in this dissertation.

5.1 Linearized Multi-machine Power System Model

The power system model used in this chapter is based on linearizing the differential and algebraic equations of a multi-machine power system model. The modeled system consists of n synchronous generators represented by a two-axis models, m network buses, and an infinite bus for each area in the model. The model takes the multivariable block diagram form shown in Figure 5.1, where the state variables are the electrical angle and rotor speed deviations of the n generators $\Delta\delta$ and $\Delta\omega$, and the q-axis transient EMF deviation $\Delta E'_q$. In this model, T_M is a diagonal matrix of inertial time constants $T_{Mi} = 2H_i$, T'_d is a diagonal matrix of field open circuit time constants T'_{doi} , and D a diagonal matrix of damping coefficients. The inputs to the multi-machine model are the mechanical power deviations ΔP_m and the excitation voltage deviations ΔE_f of the n generators.

The $n \times n$ linearization coefficients matrices K_1 , K_2 , K_3 , K_4 , K_5 and K_6 depend upon the network parameters, the system quiescent operating point, the infinite bus voltage. They change as the system conditions change, and therefore can decouple angle and voltage dynamics or can strongly couple voltage and angle dynamics for other operating conditions. Specific system operating characteristics, such as heavy local loading conditions, large transfer of active power, or a capacitive network can dramatically effect K_1 - K_6 and the kind and class of the bifurcation produced. As the significance of these constants will be revealed throughout this chapter, it is important to explain their definitions. In the next section a linearized SMIB model will be derived, where these constants K_1 - K_6 are scalar.

- (a) $K_1 = \left. \frac{\partial P_{Gi}}{\partial \delta_i} \right|_{|E'_{qi}| = |E'_{qi}|^\circ} : \text{Change in electric power for a small change in rotor angle with constant flux linkage in the direct axis } |E'_{qi}| = |E'_{qi}|^\circ. \text{ The component of torque (or power) } K_1 \Delta \delta_i \text{ is in phase with } \Delta \delta \text{ and hence represents a synchronizing}$

power component. Indeed K_1 is the synchronizing power coefficient in a classical generator model where no exciter or field circuit is present.

- (b) $K_2 = \partial P_{Gi} / (\partial |E'_{qi}|) \big|_{\delta i = \delta i^\circ}$: Change in electric power for a small change in the d-axis flux linkage at constant rotor angle $\delta i = \delta i^\circ$.
- (c) $K_3 = [1 + ((x_{di} - x'_{di})(x_{qi} + x_{ei})) / (Ai)]^{-1}$: K_3 is an impedance factor that takes into account the effect of the external impedance that relates the generator transient closed circuit time constant T'_{do} to the transient open circuit time constant T'_{di} .
- (d) $K_4 = \frac{1}{K_3} (\partial |E'_{qi}|) / (\partial \delta i) \big|_{E_{fdi} = \text{constant}}$: K_4 represents the natural coupling between $\Delta |E'_{qi}|$ and $\Delta \delta i$. It is related to the demagnetizing effect of a change in the rotor angle.
- (e) $K_5 = (\partial |V_{ti}|) / (\partial \delta i) \big|_{|E'_{qi}| = |E'_{qi}|^\circ}$: K_5 is the change in terminal voltage V_{ti} for a small change in rotor angle with constant flux linkage in the direct axis $|E'_{qi}| = |E'_{qi}|^\circ$.
- (f) $K_6 = (\partial |V_{ti}|) / (\partial |E'_{qi}|) \big|_{\delta i = \delta i^\circ}$: Change in terminal voltage V_{ti} for a small change in the d-axis flux linkage at constant rotor angle $\delta i = \delta i^\circ$.

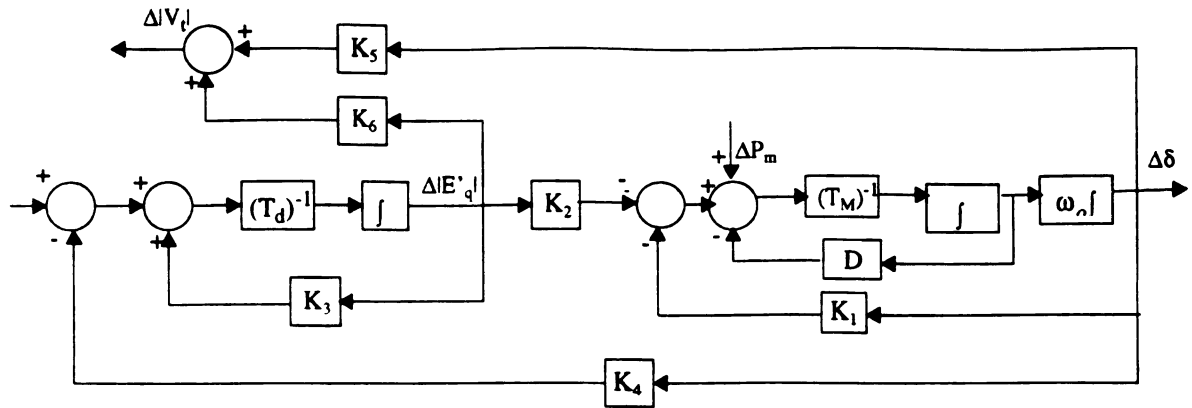


Figure 5.1 Block Diagram of a Power System Model

5.2 Single Machine Infinite Bus Model With Local Load

5.2.1 Model Representation

Considering how large and complex a general power system is, understanding the basic effects and concepts of power system stability phenomena using analytical techniques requires a simple configuration and a reasonably low-order model. A single machine connected to a large system through a transmission network and supplying a local constant impedance load (Z_{sh}) is shown in Figure 5.2 (a). This system may be simplified by using a Thevenin's equivalent of the transmission network external to the machine and its transformer as shown in Figure 5.2(b). Furthermore, because of the relative megawatt (MW) generator capacity and inertia of the machine that represents a generating station compared to the generator MW capacity and inertia of the rest of the large interconnected system, dynamics associated with the single machine will cause virtually no change in the voltage and frequency of a Thevenin equivalent source (V_∞) used to represent the large interconnected system. Such a source of invariable frequency and voltage has been called an infinite

bus [29]. The described single machine infinite bus model has widely been used in the literature as a simple yet powerful tool for understanding of power system stability of far more complex systems under small disturbances [55]. Accordingly, in order to develop an appreciation for the dynamical behavior of the system as it undergoes bifurcations, their causes and effects, it is virtually necessary to investigate such a low-order system before dealing with very large complex systems. The Thevenin electric circuit of a complex transmission network model is shown in Figure 5.2(a) with simplification shown in Figure 5.2(c). This single machine-infinite bus model includes

- (1) A generator and its transformer represented by a voltage source $|E'_q| \angle \delta$ behind a transient reactance $x'_d + x_T$ where x_T is the transformer reactance. This generator and transformer are radially connected to a large interconnected system, via a long transmission corridor with equivalent reactance X_E that is large. The large interconnected system represented by the infinite bus (i) may be a major bus or group of buses that are stiffly interconnected so that they act as a single bus and (ii) contains very large generation capacity and inertia compared to the single machine connected to this bus group via the transmission corridor reactance X_E ;
- (2) A load center at the generator terminal is represented by a constant shunt resistance R_{sh} in parallel with a shunt capacitance or inductance X_{sh} , that can include line charging of the transmission line, local shunt capacitive compensation, or inductive load.
- (3) X_E is the equivalent transmission network inductance shown in Figure 5.2(b);
- (4) The equivalent transmission network resistance R_E shown in Figure 5.2(b) that is neglected in Figure 5.2(c);

- (5) The infinite bus is modeled as a voltage source with voltage $|V_\infty| \angle 0^\circ$.

5.2.2 Model Implications

Despite the simplicity of its configuration, the single-machine infinite bus model can be used to represent

- (a) A generator connected to a large system, via a long equivalent transmission corridor with equivalent reactance x_E that is large. The large system may be a major bus or group of buses of a power system of very large capacity compared to the rating of the machine under consideration, or a large load center. Real power is shipped from the generator to the large load center, whereas reactive power may be shipped in either direction across the transmission network;
- (b) A generator serving a heavy local constant impedance load that can include line charging of the transmission line, local shunt capacitive compensation, or inductance load. With x_E large, the dynamics of the generator serving a local load center can be investigated. Effects of transfer to and from the large remote load center can also be included.

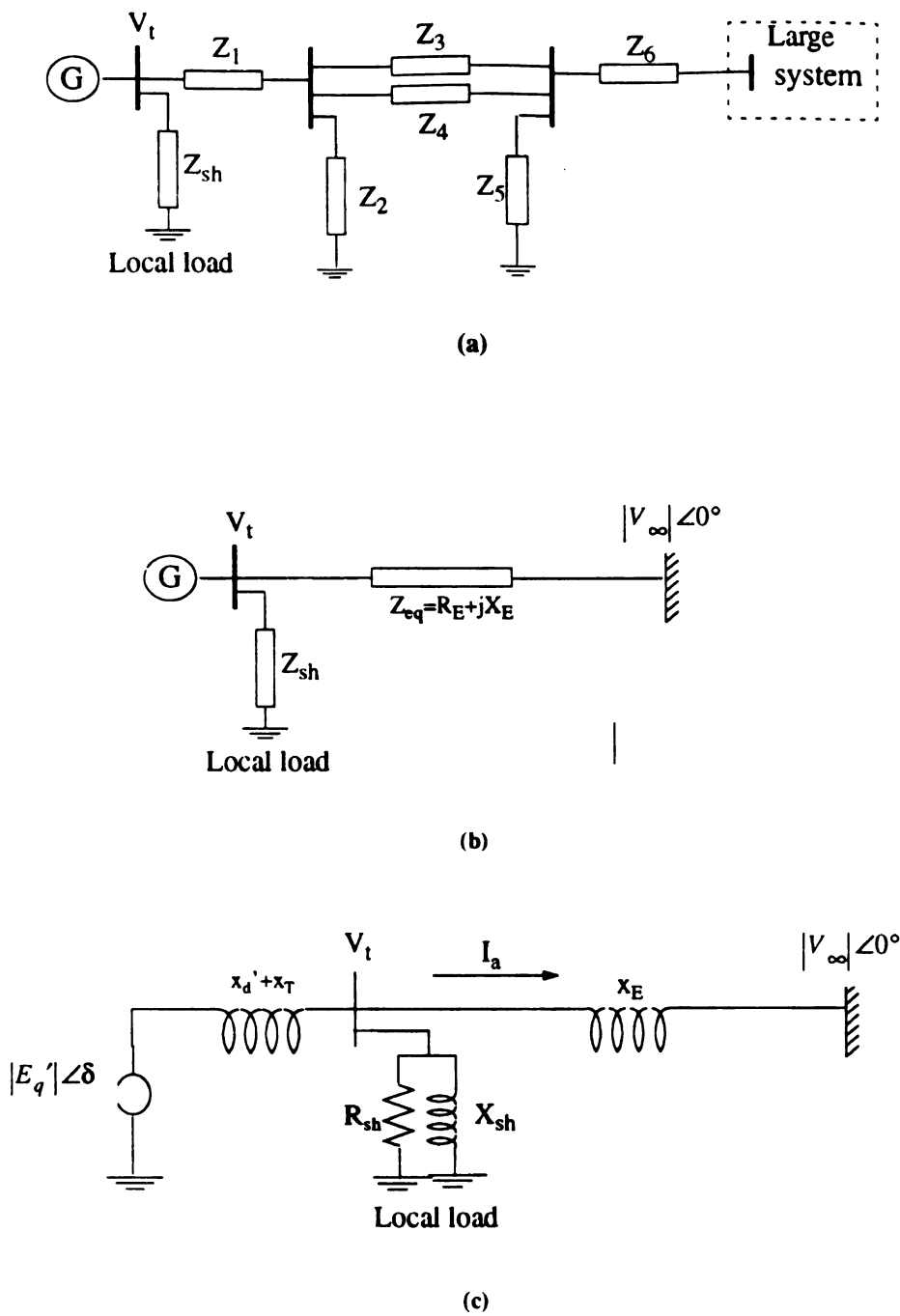
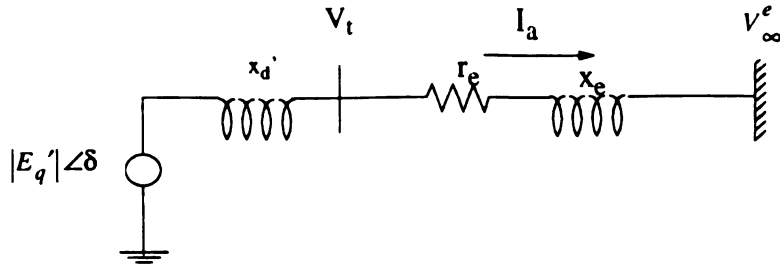
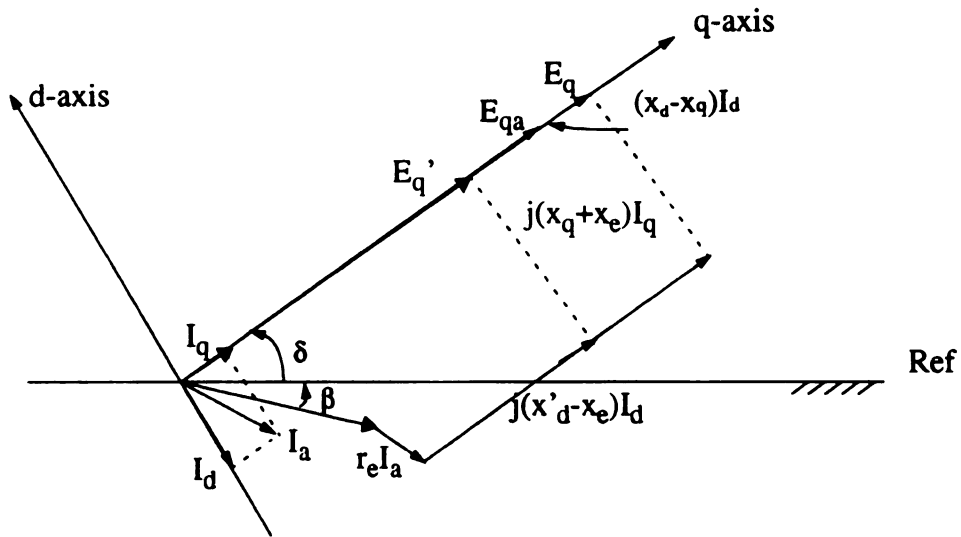


Figure 5.2 Single machine with local load connected to an infinite bus through a transmission network: (a) General configuration of a single machine connected to a large system through transmission lines; (b) Equivalent system where the transmission network is reduced to its Thevenin's equivalent; (c) Circuit model of (b) where the R_E is neglected .



(a)



(b)

Figure 5.3. Simplified single-machine infinite bus model. (a) Equivalent Thevenin model where r_e , x_e and V_∞^e are given by equations (5.1), (5.2) and (5.3) respectively, (b) Phasor diagram for the synchronous machine connected to an infinite bus shown in (a)

5.2.3 Model Equations

The circuit model in Figure 5.3 (a) can be obtained from Figure 5.2 (c) by first transforming the Thevenin's equivalent X_E and $|V_\infty| \angle 0^\circ$ to a Norton's equivalent circuit, aggregating X_E , X_{sh} and R_{sh} , and then transforming the resulting Norton's equivalent to a Thevenin's equivalent. This produces the circuit model shown in Figure 5.3 (a) where r_e and x_e and V_∞^e are the equivalent thevenin's resistance, inductance and infinite bus voltage. The parameter r_e , x_e and V_∞^e are expressed in terms of the original line inductance X_E , and the shunt loads R_{sh} and X_{sh} in equations (5.1), (5.2) and (5.3) respectively.

$$r_e = \frac{R_{sh}}{1 + R_{sh}^2(1/X_{sh} + 1/X_E)^2} \quad (5.1)$$

$$x_e = \frac{R_{sh}^2(1/X_{sh} + 1/X_E)}{1 + R_{sh}^2(1/X_{sh} + 1/X_E)^2} \quad (5.2)$$

$$V_\infty^e = \frac{|V_\infty|}{1 + X_E/X_{sh} + jX_E/R_{sh}} \equiv |V_\infty^e| \angle -\beta \quad (5.3)$$

The differential equations for the single synchronous machine are

$$M\ddot{\delta} + D\dot{\delta} = P_m - P_G(\delta, |E'_q|) \quad (5.4)$$

$$T_{do}(d|E'_q|/dt) + |E_q| = E_{fd} \quad (5.5)$$

Where P_G has the form

$$P_G(\delta, |E'_q|) = \frac{|E'_q||V_\infty^e|}{x'_d + x_e} \sin \delta + \frac{|V_\infty^e|^2}{2} \left(\frac{1}{x_q + x_e} - \frac{1}{x'_d + x_e} \right) \sin 2(\delta - \beta) \quad (5.6)$$

when $r_e = 0$. An equation of P_G is derived when $r_e \neq 0$. The algebraic equations representing the network shown in Figure 5.3 are

$$E_q = V_\infty^e + r_e I_a + j(x_d + x_e)I_d + j(x_q + x_e)I_q \quad (5.7)$$

$$E'_q = V_\infty^e + r_e I_a + j(x'_d + x_e)I_d + j(x_q + x_e)I_q \quad I_d < 0 \quad (5.8)$$

5.2.4 Simplified Linear SMIB Model

A simplified linear model for the synchronous machine connected to an infinite bus through a transmission line with reactance x_e shown in Figure 5.3(a) is derived, based on the phasor diagram in Figure 5.3(b). In the linearized model, the following assumptions have been made:

- (i) The amortisseur effects are neglected;
- (ii) Stator winding resistance is neglected;
- (iii) Balanced conditions are assumed and saturation effects are neglected;
- (iv) The synchronous machine can be represented (electrically) by a constant voltage source behind its direct-axis transient reactance.

Under these assumptions, the linearization of the E'_q equation (5.2), the electric torque/power equation and the terminal voltage equation will be performed in the next subsection.

It should be noted that the equations describing the system are expressed in p.u.

5.2.4.1 The E'_q Equation

From the system algebraic equations (5.7) and (5.8), E_q and E'_q are related by

$$E'_q = E_q + j(x_d - x'_d)I_d \quad (5.9)$$

Using the phasor diagram representation of (5.7)-(5.9), we express I_d (<0) and I_q as functions of $|E'_q|$ and $|V_\infty^e|$. Projecting E'_q and V_∞^e on the q-axis and the d-axis and keeping in mind that I_d is negative yields

$$-(x'_d + x_e)I_d + r_e I_q = |E'_q| - |V_\infty^e| \cos(\delta - \beta) \quad (5.10)$$

$$(x_q + x_e)I_q + r_e I_d = |V_\infty^e| \sin(\delta - \beta) \quad (5.11)$$

$$|E_q| = |E'_q| - (x_d - x'_d)I_d \quad (5.12)$$

Assume steady state operating condition at an operating point such that

$$\delta = \delta^\circ \quad I_q = I_q^\circ \quad |E'_q| = |E'_q|^\circ \quad |V_d| = |V_d|^\circ$$

$$\beta = \beta^\circ \quad I_d = I_d^\circ \quad E_{fd} = E_{fd}^\circ \quad P_G = P_G^\circ = P_G(\delta^\circ, |E'_q|^\circ)$$

Also assume a small perturbation around the operating point, such that

$$\begin{aligned} \delta &= \delta^\circ + \Delta\delta & I_q &= I_q^\circ + \Delta I_q & |V_t| &= |V_t|^\circ + \Delta|V_t| \\ \beta &= \beta^\circ + \Delta\beta & I_d &= I_d^\circ + \Delta I_d & |E'_q| &= |E'_q|^\circ + \Delta|E'_q| \end{aligned}$$

Substituting these into equations (5.10) and (5.11), and using Taylor's expansion method around the nominal solution as the steady operating point yields the following linear equations (5.10')-(5.12')

$$-(x'_d + x_e)\Delta I_d + r_e \Delta I_q = \Delta|E'_q| + |V_\infty^e| \sin(\delta^\circ - \beta^\circ) \cdot \Delta\delta \quad (5.10')$$

$$r_e \Delta I_d + (x_q + x_e)\Delta I_q = |V_t| \cos(\delta^\circ - \beta^\circ) \cdot \Delta\delta \quad (5.11')$$

$$\Delta|E_q| = \Delta|E'_q| - (x_d - x'_d)\Delta I_d \quad (5.12')$$

Solving for ΔI_q and ΔI_d and writing the result in matrix form as

$$\begin{pmatrix} \Delta I_d \\ \Delta I_q \end{pmatrix} = A^{-1} \cdot \begin{pmatrix} -(x_q + x_e) & r_e |V_\infty^e| \cos(\delta^\circ - \beta^\circ) - (x_q + x_e) |V_\infty^e| \sin(\delta^\circ - \beta^\circ) \\ r_e & r_e |V_\infty^e| \sin(\delta^\circ - \beta^\circ) + (x'_d + x_e) |V_\infty^e| \cos(\delta^\circ - \beta^\circ) \end{pmatrix} \begin{pmatrix} \Delta|E'_q| \\ \Delta\delta \end{pmatrix} \quad (5.13)$$

where

$$A^{-1} = r_e^2 + (x_q + x_e)(x'_d + x_e)$$

Replacing ΔI_q from equation (5.13) into equation (5.12'), an expression of the incremental quadrature voltage $\Delta|E_q|$ as solely function of $\Delta|E'_q|$ and $\Delta\delta$ is obtained

$$\begin{aligned} \Delta|E_q| &= [1 + (x_d - x'_d)(x_q + x_e)A^{-1}] \cdot \Delta|E'_q| \\ &+ [(x_d - x'_d)A^{-1}|V_\infty^e| \langle (x_q + x_e) \sin(\delta^\circ - \beta^\circ) - r_e \cos(\delta^\circ - \beta^\circ) \rangle] \cdot \Delta\delta \end{aligned}$$

which can be written as

$$\Delta|E_q| = \frac{1}{K_3} \cdot \Delta|E'_q| + K_4 \cdot \Delta\delta \quad (5.14)$$

Now, substituting into an incremental version of equation (5.12) expressed in the s-domain, the following transfer function is found

$$\Delta|E'_q| = \frac{K_3}{1 + K_3 T'_{do} s} \cdot \Delta|E_{fd}| - \frac{K_3 K_4}{1 + K_3 T'_{do} s} \cdot \Delta\delta \quad (5.15)$$

where

$$K_3 = [1 + A^{-1}(x_d - x'_d)(x_q + x_e)]^{-1} \quad (5.16)$$

$$K_4 = A^{-1}(x_d - x'_d)|V_\infty^e| \cdot [(x_q + x_e)\sin(\delta^\circ - \beta^\circ) - r_e \cos(\delta^\circ - \beta^\circ)] \quad (5.17)$$

5.2.4.2 Electrical Torque Equation

The electric torque T_e is numerically equal to the three-phase generated electric power P_G when expressed in per unit, thus

$$T_e = P_G = \text{Re}(V_t \cdot I_a^*) = V_d I_d + V_q I_q \quad \text{p.u.} \quad (5.18)$$

where V_q and V_d are the projections of the generator terminal voltage V_t on the q-axis and the d-axis, respectively, i.e

$$V_t = V_q + jV_d \quad (5.19)$$

V_q and V_d can be expressed in terms of I_d and I_q by projecting $|V_\infty^e|$ and I_a on the q-axis and the d-axis as shown in the phasor diagram in Figure 5.3, we obtain

$$\begin{aligned} V_t &= V_\infty^e + (r_e + jx_e)I_a \\ &= |V_\infty^e| \cos(\delta^\circ - \beta^\circ) - j|V_\infty^e| \sin(\delta^\circ - \beta^\circ) + (r_e + jx_e)(I_q + jI_d) \\ &= |V_\infty^e| \cos(\delta^\circ - \beta^\circ) + r_e I_q - x_e I_d - j[|V_\infty^e| \sin(\delta^\circ - \beta^\circ) - x_e I_q - r_e I_d] \end{aligned}$$

Which may be expressed using 5.10 and 5.11 simply as

$$V_t = |E'_q| + x'_d I_d - jx_q I_q \quad (5.20)$$

Setting real and imaginary components in these two representations of V_t in equation 5.19 and 5.20 equal, the following is obtained

$$\begin{aligned} V_d &= -x_q I_q \\ V_q &= |E'_q| + x'_d I_d \end{aligned} \quad (5.21)$$

Thus,

$$\begin{aligned} P_G &= x_q I_d I_q + |E'_q| I_q + x'_d I_d I_q \\ &= [|E'_q| - (x_q - x'_d) I_d] I_q \end{aligned} \quad (5.22)$$

Linearizing P_G as expressed in equation (5.22), we get

$$\begin{aligned}\Delta P_G &= \Delta |E'_q| I_q^\circ - (x_q - x'_d) \Delta I_d I_q^\circ + \Delta I_q |E'_q|^\circ - (x_q - x'_d) \Delta I_q I_d^\circ \\ &= \Delta |E'_q| I_q^\circ + |E_{qa}|^\circ \Delta I_q - (x_q - x'_d) \Delta I_d I_q^\circ\end{aligned}$$

where we used the q-axis voltage E_{qa} defined in Figure 5.3 (b) as

$$E_{qa} = E_q + (x_d - x_q) I_d$$

with initial condition values

$$|E_{qa}|^\circ = |E_q|^\circ + (x_d - x_q) I_d^\circ$$

Substituting for $|E_q|^\circ$ from Equation 5.12, one obtains

$$\begin{aligned}|E_{qa}|^\circ &= |E_q|^\circ - (x_d - x'_d) I_d^\circ + (x_d - x_q) I_d^\circ \\ &= |E_q|^\circ - (x_q - x'_d) I_d^\circ\end{aligned}$$

Substituting expressions from equation (5.13) into ΔP_G to finally compute

$$\begin{aligned}\Delta P_G &= [I_q^\circ + A^{-1} |E_{qa}|^\circ r_e + A^{-1} (x_q - x'_d) (x_q + x_e) (I_q^\circ)] \cdot \Delta |E'_q| \\ &\quad + A^{-1} |V_\infty^e| [|E_{qa}|^\circ (r_e \sin(\delta^\circ - \beta^\circ) + (x'_d + x_e) \cos(\delta^\circ - \beta^\circ)) \\ &\quad - (x_q - x'_d) I_q^\circ (r_e \cos(\delta^\circ - \beta^\circ) - (x_q + x_e) \sin(\delta^\circ - \beta^\circ))] \cdot \Delta \delta \\ &\equiv K_1 \cdot \Delta \delta + K_2 \cdot \Delta |E_q|^\circ\end{aligned}\tag{5.23}$$

where

$$\begin{aligned}K_1 &= A^{-1} |V_\infty^e| [|E_{qa}|^\circ (r_e \sin(\delta^\circ - \beta^\circ) + (x'_d + x_e) \cos(\delta^\circ - \beta^\circ))] \\ &\quad + A^{-1} |V_\infty^e| I_q^\circ [(x_q + x_e) (x_q - x'_d) \sin(\delta^\circ - \beta^\circ) - r_e (x_q - x'_d) \cos(\delta^\circ - \beta^\circ)]\end{aligned}\tag{5.24}$$

$$K_2 = r_e |E_{qa}|^\circ A^{-1} + I_q^\circ [1 + A^{-1} (x_q - x'_d) (x_q + x_e)]\tag{5.25}$$

5.2.4.3 Terminal Voltage Equation

The square of the norm of V_t as expressed in equation (5.19) is given by the equation

$$V_t^2 = V_q^2 + V_d^2\tag{5.26}$$

Linearizing equation (5.25) yields

$$\Delta |V_t| = \frac{V_q^\circ}{|V_t|^\circ} \cdot \Delta V_q + \frac{V_d^\circ}{|V_t|^\circ} \cdot \Delta V_d\tag{5.27}$$

ΔV_d and ΔV_q can be obtained from an incremental version of equation (5.21) as

$$\Delta V_d = -x_q \Delta I_q$$

$$\Delta V_q = \Delta |E'_q| + x'_d \Delta I_q$$

Finally, substituting ΔV_d , ΔV_q , and then ΔI_d and ΔI_q from (5.13) with $r_e = 0$ into equation (5.27) we obtain

$$\begin{aligned}
 \Delta |V_t| &= -\frac{V_d^\circ}{|V_t|^\circ} \cdot \frac{x_q}{x_q + x_e} |V_\infty^e| \cos(\delta^\circ - \beta^\circ) \cdot \Delta\delta + \frac{V_q^\circ}{|V_t|^\circ} \cdot \Delta |E'_q| \\
 &\quad - \frac{V_q^\circ}{|V_t|^\circ} \cdot \frac{x'_d}{x'_d + x_e} \cdot \Delta |E'_q| - \frac{V_q^\circ}{|V_t|^\circ} \cdot \frac{x'_d}{x'_d + x_e} \cdot |V_\infty^e| \sin(\delta^\circ - \beta^\circ) \cdot \Delta\delta \\
 &= -\frac{|V_\infty^e|}{|V_t|^\circ} \cdot \left(\frac{x_q}{x_q + x_e} V_d^\circ \cos(\delta^\circ - \beta^\circ) - \frac{x'_d}{x'_d + x_e} V_q^\circ \sin(\delta^\circ - \beta^\circ) \right) \cdot \Delta\delta \\
 &\quad + \frac{V_q^\circ}{|V_t|^\circ} \cdot \frac{x_e}{x'_d + x_e} \cdot \Delta |E'_q| \\
 &= K_5 \cdot \Delta\delta + K_6 \cdot \Delta |E'_q|
 \end{aligned} \tag{5.28}$$

where

$$K_5 = -\frac{|V_\infty^e|}{|V_t|^\circ} \cdot \left(\frac{x_q}{x_q + x_e} V_d^\circ \cos(\delta^\circ - \beta^\circ) - \frac{x'_d}{x'_d + x_e} V_q^\circ \sin(\delta^\circ - \beta^\circ) \right) \tag{5.29}$$

$$K_6 = +\frac{V_q^\circ}{|V_t|^\circ} \cdot \frac{x_e}{x'_d + x_e} \tag{5.30}$$

Equations (5.30), (5.31) and (5.32) below constitute the basic equations for the simplified linear model, which is implemented in the block diagram shown in Figure 5.4 where the dynamic characteristics of the system are expressed in terms of the K constants K_1 - K_6

$$M\ddot{\Delta\delta} + D\Delta\delta = \Delta T_m - \Delta T_e \tag{5.30}$$

$$\Delta |E'_q| = \frac{K_3}{1 + K_3 T_{do} s} \cdot \Delta |E_{fd}| - \frac{K_3 K_4}{1 + K_3 T_{do} s} \cdot \Delta\delta \tag{5.31}$$

$$\Delta P_G = K_1 \cdot \Delta\delta + K_2 \cdot \Delta |E'_q| \tag{5.32}$$

$$\Delta |V_t| = K_5 \cdot \Delta\delta + K_6 \cdot \Delta |E'_q| \tag{5.33}$$

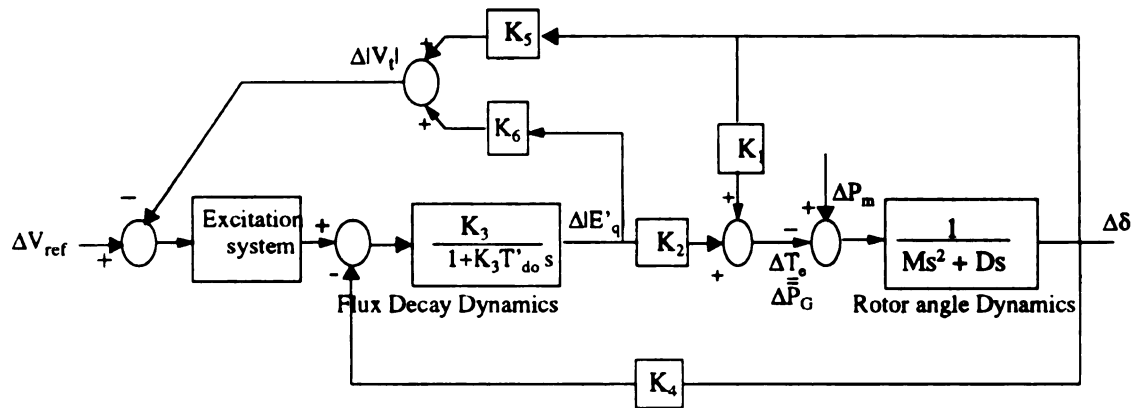


Figure 5.4 Block diagram of the simplified linear model of a synchronous machine connected to an infinite bus, through an external impedance.

5.3 Application Examples of the Bifurcation Subsystems Method on a SMIB Model

Assume that under some system stress, no bifurcation in the model algebraic equations occurs in the SMIB model shown in Figure 5.4. Then, the resulting system bifurcation, if one exist in some subsystem must reside in the model differential equations representing the generator angle, speed, and flux decay dynamics. Using a power system toolbox for Matlab [59] will allow us to demonstrate the existence of bifurcation subsystems in the model differential equations. Example 1 shows that when the system is unregulated, the bifurcation subsystem for SN is the machine angle-speed-flux decay dynamics $(\Delta\delta, \Delta\omega, \Delta E_q')$. In Example 2, the bifurcation subsystem for Hopf is the generator angle-speed dynamics $(\Delta\delta, \Delta\omega)$, called the inertial mode [25,31]. These examples are now presented.

5.3.1 Differential Bifurcation Subsystem for SN (Unregulated Model)

A linearized differential equation model of the unregulated SMIB model is obtained under heavy local loading system stress, i.e. when the shunt inductance G_{sh} is increases as can be seen in Appendix C. The state vector Δx , the A matrix as well as the critical eigenvalue λ^* and its associated eigenvector are given by

$$\Delta x = \begin{bmatrix} \Delta\delta & \Delta\omega & \Delta E_q' & \Delta\psi_{kd} & \Delta E_d' & \Delta\psi_{kq} \end{bmatrix}^T$$

$$A = \begin{bmatrix} 0 & 376.9911 & 0 & 0 & 0 & 0 \\ -0.1980 & -0.0000 & -0.2289 & -0.0000 & -0.0091 & 0.0000 \\ -0.4740 & 0.0000 & -0.5519 & 0.0000 & 0.0000 & -0.0000 \\ -2.1235 & -0.0000 & 30.6816 & -32.2581 & 0.0000 & 0.0000 \\ -0.1333 & -0.0000 & -0.0000 & -0.0000 & -4.0476 & 0.0000 \\ -0.0422 & 0.0000 & 0.0000 & 0.0000 & 15.5923 & -16.3934 \end{bmatrix}$$

$$\begin{aligned}
 \text{eig}(A) &= \begin{bmatrix} -0.2767 \pm j8.6336 \\ -4.0431 \\ -0.0030 \\ -32.2581 \\ -16.3934 \end{bmatrix} & \lambda^* &= -0.0030 & u^* &= \begin{bmatrix} -0.6281 \\ 0.0000 \\ 0.5423 \\ 0.5572 \\ 0.0207 \\ 0.0213 \end{bmatrix}
 \end{aligned}$$

The eigenvalues of A indicate the existence of static bifurcation (SN), provided that transversality and degeneracy conditions for this SN bifurcation [34] hold at this point. Since at this operating point the system differential equations experience bifurcation, the Bifurcation Subsystem Method is used to possibly find a smaller differential bifurcation sub-subsystem for SN. In order to test whether we have a bifurcation subsystem, we need to partition the square matrix A as $A = \begin{bmatrix} A_{11} & A_{12} \\ A_{21} & A_{22} \end{bmatrix}$ where A_{11} is ixi , A_{12} is ixj , A_{21} is jxi , and A_{22} is jxj , $i+j = 6$, $i = 1, \dots, 5$. The Bifurcation Subsystem Method (Proposition 4.1) says that when the full matrix A is near singularity and for all possible subsystems of order $j=2,3,\dots,n$, A_{22} is nonsingular, the term $[A_{12} \cdot A_{22}^{-1} \cdot A_{21}] \cdot u_1^* \approx 0$ as $\mu \rightarrow \mu^*$ for $u_1^* \in \text{Null}(A_{11})$, then the dynamics confined in $\Delta x_1 = A_{11} \cdot \Delta x$ are a bifurcation subsystem for SN. In a practical sense $[A_{11}] \cdot u_1^*$ is never null as μ approaches the bifurcation value μ^* since we never find the exact value of the bifurcation parameter μ^* , and thus

$$N \equiv \|[A_{11}] \cdot u_i^*\|$$

should be a measure of how close the subsystem is experiencing saddle node bifurcation.

The coupling term expressed by

$$C \equiv \|[A_{12}A_{22}^{-1}A_{21}] \cdot u_1^*\|$$

is also never null at μ close but not equal to μ^* , and thus is a good indication of how little the system external to $[A_{11}]$ contributes to producing the saddle node bifurcation in $[A]$.

This is indicated by

$$R \equiv \frac{\| [A_{12} A_{22}^{-1} A_{21}] \cdot u_1^* \|}{\| [A_{11}] \cdot u_1^* \|}$$

When saddle node bifurcation is close to occur in $[A_{11}]$ as measured by N , then if $R \ll 1$, the saddle node bifurcation in $[A_{11}]$ is producing the saddle node bifurcation in $[A]$ with little or no coupling or help from the system external to $[A_{11}]$. Bifurcation subsystems exist if N is small and approximately equals λ^* as $\mu \rightarrow \mu^*$, and C is very small and much less than λ^* for all $\mu \rightarrow \mu^*$. This second condition requires R to be much less than 1.0.

The subsystem used for testing are decided by the ranking of the participation factor or right eigenvector elements except that the dynamics δ and ω are considered together since they are part of the inertial dynamics. Note that both N and C are equal to or less than $\lambda^* = -0.0030$ for all subsystems of order greater or equal to third order, which implies that the bifurcation subsystem is $(\Delta\delta, \Delta\omega, \Delta E_q')$. Note that $N \approx \lambda^*$ and $R = C/N$ is less than one for any subsystem of order equal to or greater than three, indicating that the third order model is the smallest bifurcation subsystem, but that the fourth and fifth order models are all bifurcation subsystems. This third order model is thus the bifurcation subsystem since it is weakly coupled ($R \ll 1$) to the dynamics of $\Delta E_q'$ and $\Delta\psi_{kd}$ from the results in rows 4 and 5 in Table 5.1.

i	subsystem Δx	$[A_{12}A_{22}^{-1}A_{21}] \cdot u_i$	$[A_{11}] \cdot u_i$	N	C	R
1	$[\Delta\delta]$	-4.8397 e+12	0	0	$4.8397e + 12$	inf
2	$\begin{bmatrix} \Delta\delta \\ \Delta\omega \end{bmatrix}$	$\begin{bmatrix} 0 \\ 0.1237 \end{bmatrix}$	$\begin{bmatrix} 0.0019 \\ 0.1243 \end{bmatrix}$	0.1244	0.1237	0.9944
3	$\begin{bmatrix} \Delta\delta \\ \Delta\omega \\ \Delta E_q \end{bmatrix}$	$\begin{bmatrix} 0 \\ -0.1887 \\ -0.0000 \end{bmatrix} 10^{-3}$	$\begin{bmatrix} 0.0019 \\ 0.0002 \\ -0.0016 \end{bmatrix}$	0.0025	$1.8873e - 04$	0.0754
4	$\begin{bmatrix} \Delta\delta \\ \Delta\omega \\ \Delta E_q \\ \Delta\psi_{kd} \end{bmatrix}$	$\begin{bmatrix} 0 \\ -0.1887 \\ 0.0000 \\ 0.0000 \end{bmatrix} 10^{-3}$	$\begin{bmatrix} 0.0019 \\ 0.0002 \\ -0.0016 \\ -0.0017 \end{bmatrix}$	0.003	$1.8873e - 04$	0.0626
5	$\begin{bmatrix} \Delta\delta \\ \Delta\omega \\ \Delta E_q \\ \Delta\psi_{kd} \\ \Delta E_d \end{bmatrix}$	$\begin{bmatrix} 0 \\ -0.0047 \\ 0.0218 \\ -0.2474 \\ -0.3719 \end{bmatrix} 10^{-13}$	$\begin{bmatrix} 0.0019 \\ 0 \\ -0.0016 \\ -0.0017 \\ -0.0001 \end{bmatrix}$	0.003	$4.47e - 14$	$1.49e - 14$

Table 5.1 Computational results for identifying the bifurcation subsystem for SN bifurcation in the SMIB model.

This bifurcation subsystem is quite obvious from Figure 5.5 since three integral blocks have infinite gain when $\lambda = s = 0$ which implies that the states $\Delta\delta, \Delta\omega, \Delta E_q'$ are connected by infinite gain blocks in a loop when saddle node bifurcation occurs. This explains why the flux decay and mechanical dynamics have both been argued to be associated with saddle node bifurcation when in fact both are part of the bifurcation subsystem. It should be noted that the saddle node bifurcation could be due to inertial dynamics or the flux decay dynamics experiencing bifurcation and yet the bifurcation subsystem $(\Delta\delta, \Delta\omega, \Delta E_q')$ would still be from Figure 5.5 because there is a loop with infinite gains relating $(\Delta\delta, \Delta\omega, \Delta E_q')$.

In order to see whether the information obtained from the participation matrix indicates similar conclusions, the participation factor have been computed for this case and summarized in Table 5.2. This information indicates the only state with significant participation in this SN bifurcation is the $\Delta E_q'$, which is one of the states in the bifurcation subsystem. The eigenvector u^* is also a poor prediction of the bifurcation subsystem since $(\Delta\delta, \Delta\omega, \Delta E_q')$ are predicted to be associated with the dynamics experiencing bifurcation.

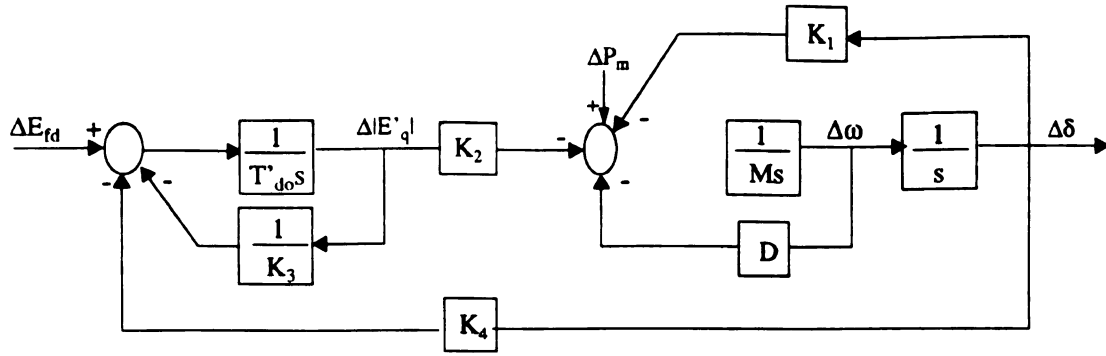
It should be noted that the bifurcation subsystem does not necessarily contain the center manifold dynamics since no formal theory has been presented that suggests so for this saddle node bifurcation. The fact that $R \ll 1$ as $\mu \rightarrow \mu^*$ so that the coupling of the external system is not affecting the conditions for bifurcation $[A_{11} - A_{12} \cdot A_{22}^{-1} \cdot A_{21}] \cdot u_1^* \approx [A_{11}] \cdot u_1^*$ long before bifurcation occurs in the full model matrix $[A]$ and in the bifurcation subsystem matrix $[A_{11}]$ at the value of μ^* , suggests but does not prove that (i) the center manifold of the full system is contained in the bifurcation subsystem, or (ii) that the bifurcation subsystem necessarily contains any portion of the center manifold dynamics. The proof is beyond the scope of this thesis.

Several factors suggest the bifurcation subsystem contains the center manifold beyond the discussion above are:

- (i) a root locus of the unregulated SMIB model shows that the eigenvalue associated with $\Delta E_q'$ is the one approaching zero;
- (ii) the participation factor indicates $\Delta E_q'$ is by far the largest element;
- (iii) the test matrix [52] K_S for saddle node bifurcation in the full system to be derived for the unregulated model is $K_1 - K_2 K_3 K_4 < 0$ and thus depends on the parameters of the bifurcating subsystem;
- (iv) a test matrix T developed by [51] for an equivalent flux decay model $\Delta \dot{E}'_q = T \Delta E'_q$ is $T = (-1/T'_{do})[1/K_3 - K_2 K_4/K_1]$ for the SMIB model shown in Figure 5.5, is singular when the full system is experiencing saddle model bifurcation. This test matrix also depends on all the parameters of the bifurcating subsystem. This test matrix if it exists assures that loss of causality has not occurred and that saddle node bifurcation has not occurred [51] in mechanical dynamics $K_1 \neq 0$;
- (v) the test matrices T and K_S for saddle node bifurcation in the full system, do not theoretically guarantee that bifurcation occurs in flux decay or inertial dynamics respectively as their derivations might suggest, but solely that a saddle node bifurcation in the full system exists. This confirms the above result that as long as $K_1 \neq 0$, both T and K_S and are singular at the same point, i.e. the point of bifurcation. This would suggest that the bifurcation subsystem $(\Delta \delta, \Delta \omega, \Delta E_q')$ containing all the parameters in both T and K_S and no others, contain the center manifold of the full system model;
- (vi) the fact that the flux decay eigenvalue in a root locus is the one approaching zero [59] as the term $K_2 K_4$ increases and that the participation factor so heavily weighs $\Delta E_q'$

might suggest the center manifold is just the $\Delta E_q'$ dynamics, but the fact that both T and K_S are both singular at saddle node bifurcation, and both depend on all the parameters of the bifurcation subsystem and no others, the center manifold would appear to lie within the bifurcation subsystem.

Without determining the center manifold, it is impossible to say whether it is tangent to the eigenvector of $\Delta E_q'$ in the $(\Delta\delta, \Delta\omega, \Delta E_q')$ bifurcation subsystem subspace, or even whether it lies outside the bifurcation subsystem. It is clear that the test matrices T and K_S are diagnostic in saying the center manifold lies solely in the inertial or flux decay dynamics since both are zero at the bifurcation. The above results (i-vi) suggest that the bifurcation subsystem may well contain the center manifold but no proof exists that it does.



(a)

Figure 5.5 Block diagram of the a linearized machine model showing the bifurcation subsystem and the test matrix T.

State	$\Delta \delta$	$\Delta \omega$	$\Delta E'_q$	$\Delta \psi_{kd}$	$\Delta E'_d$	$\Delta \psi_{kq}$
Participation factor	0.0000	0.0000	0.2088	0.0000	0.0000	0.0000

Table 5.2 Participation factor results for the SN bifurcation in the SMIB model

5.3.2 Differential Bifurcation subsystem for Hopf (Regulated Model)

A linearized differential model of a regulated SMIB model is obtained when the transmission network inductance x_e or the power transfer to the infinite bus has been gradually increased. The input parameters for this bifurcations are given in Appendix E. The state vector Δx , the A matrix as well as its eigenvalues and the critical one λ^* , are given by

$$\Delta x = [\Delta\delta \ \Delta\omega \ \Delta E_q' \ \Delta\psi_{kd} \ \Delta E_d' \ \Delta\psi_{kq} \ \Delta V_{As} \ \Delta V_R]^T$$

$$A = \begin{bmatrix} 0 & 376.9911 & 0 & 0 & 0 & 0 & 0 & 0 \\ -0.1395 & 0 & -0.0868 & -0.0781 & -0.0072 & -0.0318 & 0 & 0 \\ -0.0542 & 0.0000 & -2.0818 & 2.0781 & -0.0240 & -0.1056 & 0.0000 & 1.9373 \\ -2.9066 & 0.0000 & 30.7985 & -33.5716 & 0.0000 & 0.0000 & 0.0000 & 0.0000 \\ -0.0934 & 0.0000 & 0.0000 & 0.0000 & -8.3982 & 6.5047 & 0.0000 & 0.0000 \\ -0.9893 & 0.0000 & 0.0000 & 0.0000 & 15.6517 & -19.6571 & 0.0000 & 0.0000 \\ 3.2771 & 0.0000 & -9.5117 & -8.5604 & 3.0798 & 1.5531 & -0.1499 & 0.0000 \\ 47.0239 & 0.0000 & -163.5591 & -186.1236 & 56.3153 & 247.8250 & 14.9613 & -172.9860 \end{bmatrix}$$

$$eig(A) = \begin{bmatrix} -171.59 \\ -32.99 \\ -25.59 \\ 0.09 \pm j7.16 \\ -3.94 \\ -1.46 \pm j0.41 \end{bmatrix} \quad \lambda^* = 0.09 \pm j7.16$$

The eigenvalues of A indicate the existence of a swing mode of frequency

$$\omega = 7.16 \text{ rad/s}$$

Since at this operating point the system differential equations are at bifurcation, it is possible to find a differential bifurcation sub-subsystem for Hopf. Proposition 4.3 implies formulating the matrix

$$B = A - j\omega I_{8 \times 8}$$

$$\begin{aligned}
 eig(B) = & \begin{bmatrix} -171.59 - j7.16 \\ -32.99 - j7.16 \\ -25.59 - j7.16 \\ 0.09 \\ 0.09 - j14.32 \\ -3.94 - j7.16 \\ -1.46 + j6.75 \\ -1.46 - j6.57 \end{bmatrix} & \lambda^* = 0.09 & \mu^* = \begin{bmatrix} 0.3285 + j0.8108 \\ -0.0153 + j0.0064 \\ 0.0424 + j0.0114 \\ -0.0022 - j0.0591 \\ -0.0349 + j0.0082 \\ -0.0499 - j0.0160 \\ 0.3991 + j0.0264 \\ 0.3991 + j0.0264 \end{bmatrix}
 \end{aligned}$$

In order to test whether a bifurcation subsystem exists, the B matrix is partitioned as

$B = \begin{bmatrix} B_{11} & B_{12} \\ B_{21} & B_{22} \end{bmatrix}$ where B_{11} is ixi , B_{12} is ixj , B_{21} is jxi , and B_{22} is jxj , $i+j=8$, $i=1, \dots, 7$, and form column vectors $u_i = [u_1 \dots u_i]$, $i=1, \dots, 7$. Note that

$$N = \|[B_{11}] \cdot u_1^*\| \quad ; \quad C \equiv \|[B_{12}B_{22}^{-1}B_{21}] \cdot u_1^*\| \quad \text{and} \quad R = C/N$$

are defined as for saddle node bifurcation for all subsystems where B_{22} is nonsingular. N must be less than λ^* and C must be $\ll \lambda^*$ as $\mu \rightarrow \mu^*$ for a bifurcation to exist. The values of N and C are less than $\lambda^* = 0.09$ and $R \ll 1$ only for the second order subsystem, indicating that $(\Delta\delta, \Delta\omega)$ is the bifurcation subsystem for this mode of oscillation. Since for this subsystem $R = 0.0551$ the bifurcation subsystem $(\Delta\delta, \Delta\omega)$ produces the bifurcation in the full subsystem without coupling to the external system.

The participation factor information for this bifurcation is presented in Table 5.4. These results indicate that the generator inertial dynamics $\{\Delta\delta, \Delta\omega\}$ have higher participation in the occurrence of the bifurcation than the rest of the states. It is worth noting that these two states form the bifurcation subsystem obtained using the bifurcation subsystem method, and thus the participation factor can indeed sometimes agree with bifurcation subsystem method results. Although participation factors can sometimes indicate the states in a bifurcation subsystem, there is no theoretical assurance the bifurcation subsystem is correct in assessing the center manifold dynamics. The large drop off in participation factor

elements for states other than $(\Delta\delta, \Delta\omega)$ may indeed contain the center manifold. However the fact that K_D will be shown in Section 5.4 to depend on parameters outside $(\Delta\delta, \Delta\omega)$ suggests that the bifurcation subsystem may only contain a portion of the center manifold dynamics. Since may only be true since $D = 0$ and the bifurcation subsystem must be $(\Delta\delta, \Delta\omega)$. If $D \neq 0$ then the bifurcation subsystem may be larger if one exists.

i	subsystem Δx	$[B_{12}B_{22}^{-1}B_{21}] \cdot u_i$	$B_{11} \cdot u_i$	N	C	R
1	$[\Delta\delta]$	5.7393 - j2.5040	5.7393 - j2.5040	6.2636	6.2617	0.9997
2	$\begin{bmatrix} \Delta\delta \\ \Delta\omega \end{bmatrix}$	$\begin{bmatrix} 0 \\ 0.0017 - j0.0041 \end{bmatrix}$	$\begin{bmatrix} 0.0313 + j0.0748 \\ 0.0003 - j0.00351 \end{bmatrix}$	0.0812	0.0045	0.0551
3	$\begin{bmatrix} \Delta\delta \\ \Delta\omega \\ \Delta E_q \end{bmatrix}$	$\begin{bmatrix} 0 \\ -0.0020 - j0.0051 \\ -0.0280 - j0.3729 \end{bmatrix}$	$\begin{bmatrix} 0.0313 + j0.0748 \\ -0.0034 - j0.0045 \\ -0.0243 - j0.3729 \end{bmatrix}$	0.3807	0.3740	0.9824
4	$\begin{bmatrix} \Delta\delta \\ \Delta\omega \\ \Delta E_q \\ \Delta\psi_{kd} \end{bmatrix}$	$\begin{bmatrix} 0 \\ -0.0018 - j0.0004 \\ -0.0164 - j0.4964 \\ 0.0000 \end{bmatrix}$	$\begin{bmatrix} 0.0313 + j0.0748 \\ -0.0032 - j0.0002 \\ -0.0288 - j0.4937 \\ -0.0003 - j0.0055 \end{bmatrix}$	0.5011	0.4967	0.9911
5	$\begin{bmatrix} \Delta\delta \\ \Delta\omega \\ \Delta E_q \\ \Delta\psi_{kd} \\ \Delta E_d \end{bmatrix}$	$\begin{bmatrix} 0 \\ -0.0016 - j0.0005 \\ -0.0153 - j0.4953 \\ 0.0000 \\ 0.3261 + j0.1039 \end{bmatrix}$	$\begin{bmatrix} 0.0313 + j0.0748 \\ -0.0030 - j0.0001 \\ -0.0280 - j0.4939 \\ -0.0003 - j0.0055 \\ 0.3214 + j0.1048 \end{bmatrix}$	0.6046	0.6023	0.9961
6	$\begin{bmatrix} \Delta\delta \\ \Delta\omega \\ \Delta E_q \\ \Delta\psi_{kd} \\ \Delta E_d \\ \Delta\psi_{kq} \end{bmatrix}$	$\begin{bmatrix} 0 \\ 0 \\ -0.0106 - j0.4953 \\ 0.0000 \\ 0.0000 \\ 0.0000 \end{bmatrix}$	$\begin{bmatrix} 0.0313 + j0.0748 \\ -0.0014 + 0.0006 \\ -0.0227 - j0.4922 \\ -0.0003 - j0.0055 \\ -0.0032 + j0.0008 \\ -0.0046 - j0.0014 \end{bmatrix}$	0.4994	0.4936	0.9884
7	$\begin{bmatrix} \Delta\delta \\ \Delta\omega \\ \Delta E_q \\ \Delta\psi_{kd} \\ \Delta E_d \\ \Delta\psi_{kq} \\ \Delta V_{As} \end{bmatrix}$	$\begin{bmatrix} 0 \\ 0 \\ -0.0267 - j0.4934 \\ 0.0000 \\ 0.0000 \\ 0.0000 \\ 0.0000 \end{bmatrix}$	$\begin{bmatrix} 0.0313 + j0.0048 \\ -0.0014 + j0.0006 \\ -0.0227 - j0.4922 \\ -0.0003 - j0.0055 \\ -0.0032 + j0.0008 \\ -0.0046 - j0.0014 \\ 0.0370 + j0.0020 \end{bmatrix}$	0.5008	0.4942	0.9868

Table 5.3 Computational results for identifying the bifurcation subsystem for Hopf bifurcation in the SMIB model: Inertial mode.

state	Participation factor
$\Delta\delta$	0.0132-j0.0101
$\Delta\omega$	-0.0129+j0.0105
$\Delta E_q'$	0.0004-j0.0008
$\Delta\psi_{kd}$	j0.0001
$\Delta E_d'$	j0.0002
$\Delta\psi_{kq}$	j0.0002
ΔV_{As}	-j0.0001
ΔV_R	0

Table 5.4 Participation factor results for the inertial Hopf bifurcation in the SMIB model

5.4 Effect of Hard Limit Discontinuities on Stability Analysis

Diagnosing and assessing stability problems in the SMIB model is dependent on whether the system is regulated by an active excitation control or whether it is unregulated. The effect of the hard limit discontinuity on stability analysis can then be viewed by means of the damping and synchronizing torque coefficients K_D and K_S since both K_D and K_S are determined in terms of K_1 - K_6 constants when the system is regulated and unregulated. Conditions for system stability in terms of constraints on the K-constants are derived and summarized in proposition 5.1-3 for before and after the hard limit discontinuity that disables the generator exciter occurs.

The damping and synchronizing torque coefficients K_D and K_S are derived for the case when (a) the generator terminal voltage is unregulated, (b) when a thyristor type excitation system is used, and (c) when an IEEE dc Type 1 excitation system is used. The

effects of measurement or sensor dynamics are included in this analysis. Finally important conclusions are determined on how the variation of the system K-constants affect the damping and synchronizing torques to cause a Hopf or SN bifurcation in the SMIB dynamics. First, a general formula for ΔT_D , ΔT_S , K_D and K_S will be derived in the next section.

5.4.1 Synchronizing and Damping Torques

Consider a change in electrical torque following a disturbance at an arbitrary frequency. The restoring forces that act to this change are in form of braking torques that develop in phase with machine rotor angle and in phase with machine rotor speed [55]. Indeed, the change in electrical torque of a synchronous machine can be resolved into two main components

$$\Delta T_e = K_S \Delta \delta + K_D \Delta \dot{\delta} \equiv \Delta T_S + \Delta T_D \quad (5.34)$$

where ΔT_S is the component of torque change in phase with rotor angle perturbation $\Delta \delta$ and thus referred to as the synchronizing torque, and ΔT_D is the component of torque in phase with the speed deviation $\Delta \omega$ and thus referred to as the damping torque. K_D and K_S are called the damping and the synchronizing torque coefficients, respectively. System stability depends on the existence of both components of torques for each machine. Positive synchronizing torques assure restoring of the rotor angle after a small incremental change of this angle, whereas positive damping torque is necessary to damp out any oscillation following a disturbance. A necessary and sufficient condition for the system to be stable is that both damping and synchronizing torque coefficients K_D and K_S be positive [51]. A decrease in either coefficient implies a destabilizing effect and therefore, evaluation of these coefficients can be used as a proximity measure to oscillatory instability or to an

increasing change in the machine rotor angle. First, ΔT_D , ΔT_S , K_D and K_S are defined as:

$$\Delta T_S \equiv \operatorname{Re} \left(\frac{\Delta T_e}{\Delta \delta} \right)_{s=j\omega} \quad \text{and} \quad \Delta T_D \equiv \operatorname{Im} \left(\frac{\Delta T_e}{\Delta \delta} \right)_{s=j\omega} \quad (5.35)$$

$$K_S = \frac{\Delta T_S}{\Delta \delta} \quad \text{and} \quad K_D = \frac{\Delta T_D}{\omega \Delta \delta} \quad (5.36)$$

A transfer function $\Delta T_e / \Delta \delta$ that is independent of the type of excitation system used, may be derived from the block diagram in Figure 5.4, in which $G_e(s)$ refers to the transfer function representation of the AVR and the exciter, and $G_3(s)$ represents the transfer function of the field circuit. From the block diagram we see that

$$\Delta |E'_q| = G_3(s) \cdot \{ \Delta E_{fd} - K_4 \Delta \delta \}$$

$$\Delta E_{fd} = -G_e(s) \cdot \{ K_5 \Delta \delta + K_6 \Delta |E'_q| \}$$

$$\Delta |E'_q| = -K_4 G_3(s) \cdot \Delta \delta - K_5 G_e(s) G_3(s) \cdot \Delta \delta - K_6 G_e(s) G_3(s) \cdot \Delta |E'_q|$$

By grouping terms involving $\Delta |E'_q|$ and rearranging,

$$\Delta |E'_q| = \frac{-K_4 G_3(s) - K_5 G_e(s) G_3(s)}{1 + K_6 G_e(s) G_3(s)} \cdot \Delta \delta \quad (5.37)$$

Replacing (5.35) in the expression of ΔT_e given in equation (5.31),

$$\Delta T_e = K_1 \Delta \delta + K_2 \Delta |E'_q| = K_1 \cdot \Delta \delta - K_2 \cdot \frac{K_4 G_3(s) + K_5 G_e(s) G_3(s)}{1 + K_6 G_e(s) G_3(s)} \cdot \Delta \delta$$

Finally the general transfer function $\Delta T_S / \Delta \delta$ is given by equation (5.38).

$$\therefore \frac{\Delta T_e}{\Delta \delta} = K_1 - \frac{K_2 G_3(s) (K_4 + K_5 G_e(s))}{1 + K_6 G_e(s) G_3(s)} \quad (5.38)$$

5.4.1.1. Unregulated system ($G_e(s) = 0$)

A system that is not under an active excitation control is called unregulated. In such condition, K_5 , K_6 and $G_e(s)$ in the block diagram in Figure 5.4 can be set to zero. The transfer function $\Delta T_S / \Delta \delta$ is then equals to

$$\frac{\Delta T_e}{\Delta \delta} = K_1 - K_2 K_4 G_3(s)$$

$$\frac{\Delta T_e}{\Delta \delta} = K_1 - \frac{K_2 K_3 K_4}{1 + K_3 T'_{do} s}$$

$$\left. \frac{\Delta T_e}{\Delta \delta} \right|_{s=j\omega} = K_1 - \frac{K_2 K_3 K_4 \cdot (1 - j\omega K_3 T'_{do})}{1 + \omega^2 (K_3 T'_{do})^2} \quad (5.39)$$

The damping and synchronizing torques ΔT_S and ΔT_D are the real and imaginary parts of $\Delta T_e / \Delta \delta$ in (5.39) respectively and are equal to

$$\Delta T_S = K_1 \cdot \Delta \delta - \frac{K_2 K_3 K_4}{1 + \omega^2 T'^2_d} \cdot \Delta \delta \quad (5.40a)$$

$$\Delta T_D = K_2 K_4 \cdot \frac{K_3 \cdot T'_d}{1 + \omega^2 T'^2_d} \cdot \omega \cdot \Delta \delta \quad (5.40b)$$

where $T'_d = K_3 T'_{do}$

From Equation 5.34, K_S and K_D are given by

$$K_D = K_2 K_4 \cdot \frac{K_3 \cdot T'_d}{1 + \omega^2 T'^2_d} \quad (5.41a)$$

$$K_S = K_1 - \frac{K_2 K_3 K_4}{1 + \omega^2 T'^2_d} \quad (5.41b)$$

From these two expressions, we can see that the damping and synchronizing coefficients are positive if they satisfy the conditions:

$$\begin{array}{lll} K_D > 0 & \text{if and only if} & K_4 K_2 > 0 \\ K_S > 0 & \text{if and only if} & K_1 > \frac{K_2 K_3 K_4}{1 + \omega^2 T'^2_d} \end{array}$$

5.4.1.2 Thyristor-Type Excitation system

This is a simplified thyristor type excitation system that includes only the elements that are considered necessary for representing a specific excitation system, namely the terminal voltage transducer time constant T_R with gain K_R , the exciter with gain K_E and time constant T_E . The transfer function is given by

$$G_e(s) = \frac{|\Delta E_{fd}|}{\Delta |V_t|} = \frac{-K_E K_R}{(1 + sT_E)(1 + sT_R)} \quad (5.42)$$

For typical values for the terminal voltage transducer time constant T_R and for the gains and time constants in fast exciters, acceptable bounds for T_R , the exciter gain T_E and exciter time constant T_R satisfy

$$K_E \gg 1 ; \quad T_E \ll 1 \quad \text{and} \quad T_R \ll 1$$

Substituting $G_e(s)$ in (5.42) into the general transfer function in equation (5.38), and collecting the powers of s in the numerator and the denominator, we obtain

$$\frac{\Delta T_e}{\Delta \delta} = K_1 - \frac{a_o + a_1 s + a_2 s^2}{b_o + b_1 s + b_2 s^2 + b_3 s^3} \quad (5.43)$$

Where

$$a_o = K_2 K_3 K_4 + K_2 K_3 K_5 K_E K_R$$

$$a_1 = K_2 K_3 K_4 (T_E + T_R)$$

$$a_2 = K_2 K_3 K_4 T_E T_R$$

$$b_o = 1 + K_3 K_6 K_E K_R \quad \equiv K_3 K_6 K_E K_R$$

$$b_1 = T'_d + T_E + T_R$$

$$b_2 = T_E T_R + T'_d [T_E + T_R]$$

$$b_3 = T'_d T_E T_R$$

Evaluating $\Delta T_s / \Delta \delta$ at $s = j\omega$, we get

$$\left. \frac{\Delta T_e}{\Delta \delta} \right|_{s=j\omega} = K_1 - \frac{a_o - a_2 \omega^2 + j a_1 \omega}{b_o - b_2 \omega^2 + j(b_1 \omega - b_3 \omega^2)} \quad (5.44)$$

Therefore ΔT_s and ΔT_D are given by:

$$\Delta T_s = K_1 \cdot \Delta \delta - \frac{[a_o - a_2 \omega^2][b_o - b_2 \omega^2] + a_1 \omega [b_1 \omega - b_3 \omega^3]}{[b_o - b_2 \omega^2]^2 + [b_1 \omega - b_3 \omega^3]^2} \cdot \Delta \delta \quad (5.45a)$$

$$\Delta T_D = \frac{[a_o - a_2 \omega^2][b_1 \omega - b_3 \omega^3] - a_1 [b_o - b_2 \omega^2]}{[b_o - b_2 \omega^2]^2 + [b_1 \omega - b_3 \omega^3]^2} \cdot (\omega \Delta \delta) \quad (5.45b)$$

(a) Frequency Range ($\omega \ll 1$)

Setting the ω^0 terms to zero in the numerator and the denominator of K_D and K_S yields,

$$K_D = \left. \frac{\Delta T_D}{\omega \Delta \delta} \right|_{\omega=0} = \frac{a_o b_1 - a_1 b_o}{b_o^2}$$

$$= \frac{(K_2 K_3 K_4 + K_E K_R K_2 K_3 K_5)(T'_d + T_E + T_R) - K_2 K_3 K_4 (T_E + T_R)(1 + K_3 K_6 K_E K_R)}{(1 + K_3 K_6 K_E K_R)^2}$$

or approximately

$$K_D \cong K_5 K_2 \frac{(T'_d + T_E + T_R)}{K_3 K_6^2 K_E K_R} - K_4 K_2 \frac{(T_E + T_R)}{K_6 K_E K_R} \quad (5.46a)$$

by assuming $K_E \gg 1$

Similarly, the synchronizing torque coefficient is

$$K_S = K_1 - \frac{a_o b_o}{b_o^2} = K_1 - \frac{K_2 K_3 K_4 + K_E K_R K_2 K_3 K_5}{1 + K_3 K_6 K_E K_R}$$

or,

$$K_S \cong K_1 - K_4 \cdot \frac{K_2}{K_6 K_E K_R} - K_5 \cdot \frac{K_2}{K_6} \quad (5.46b)$$

Therefore positive damping and synchronizing torques are obtained for the following conditions:

$$K_D > 0 \quad \text{if we have} \quad K_5 > K_4 K_3 K_6 \cdot \frac{T_E + T_R}{T'_d + T_E + T_R}$$

$$K_S > 0 \quad \text{if we have} \quad K_1 > K_5 \cdot \frac{K_2}{K_6} + \frac{K_4}{K_E K_R} \cdot \frac{K_2}{K_6}$$

(b) Frequency Range ($\omega \gg 1$)

In this range, the terms involving the highest power of ω dominate. Hence, keeping only these terms from equations 5.45(a-b), approximate expressions for K_D and K_S may be obtained as,

$$K_D = \frac{a_2 b_3}{b_3^2 \omega^2} = K_2 K_4 \cdot \frac{1}{\omega^2 T'_d} \quad (5.47a)$$

Similarly, the synchronizing torque coefficient may be obtained by retaining only the highest powers of ω in the numerator and the denominator

$$K_S = K_1 - \frac{(a_2 b_2 - a_1 b_3) \omega^4}{b_3^2 \omega^6} = K_1 - \frac{a_2 b_2 - a_1 b_3}{b_3^2 \omega^2}$$

or,

$$K_S \equiv K_1 - \frac{K_2 K_3 K_4}{\omega^2 \langle T'_{do} \rangle^2} \quad (5.47b)$$

5.4.1.3 IEEE dc Type1 Excitation System

The gain of the voltage transducer block is usually close to unity, its time constant is small, in the 0.2 to 0.4 range. The amplifier gain K_A is typically on the range 25 to 400, its time constant T_A is typically in the range 0.02 to 0.4 sec. The power system stabilizer parameter values are K_F in the range 0.02 to 0.1, and T_F in the range 0.35 to 2.2 sec. The block diagram of this system has been shown in Figure 2.2, from which the transfer function is given by

$$\begin{array}{lll} 25 \leq K_A \leq 400 & 0.02 \leq T_A \leq 0.1 & 0 \leq S_E \leq 1.3 \\ 0.02 \leq K_F \leq 0.1 & 0.35 \leq T_F \leq 2.2 & K_R \equiv 1 \\ -1.0 \leq K_E \leq 1.0 & 0.5 \leq T_E \leq 1.0 & T_R \equiv 0.05 \end{array}$$

The transfer function for this excitation system is given by

$$G_e(s) = \frac{-K_A K_R (1 + sT_F)}{[(1 + sT_A)(1 + sT_F)(S_E + K_E + sT_E) + sK_A K_F] \cdot (1 + sT_R)} \quad (5.50)$$

Substituting $G_e(s)$ into the transfer function in equation (5.38) and collecting terms of powers of “s” in the numerator and denominator we obtain

$$\frac{\Delta T_e}{\Delta \delta} = K_1 - \frac{a_0 + a_1 s + a_2 s^2 + a_3 s^3 + a_4 s^4}{b_0 + b_1 s + b_2 s^2 + b_3 s^3 + b_4 s^4 + b_5 s^5} \quad (5.51)$$

Where

$$\begin{aligned} a_0 &= MK_2 K_3 K_4 + K_2 K_3 K_5 K_A K_R \\ &\equiv K_2 K_3 K_5 K_A K_R && \text{since } K_A \equiv M \\ a_1 &= K_2 K_3 K_4 T_{a1} + K_2 K_3 K_5 K_A K_R T_R \\ a_2 &= K_2 K_3 K_4 T_{a2} \\ a_3 &= K_2 K_3 K_4 T_{a3} \end{aligned}$$

$$a_4 = K_2 K_3 K_4 T_A T_E T_F T_R \equiv T_{a_4}$$

$$b_o = M + K_3 K_6 K_A K_R$$

$$\equiv K_3 K_6 K_A K_R \text{ since } K_3 K_6 K_A K_R \gg M$$

$$b_1 = K_3 K_6 K_A K_R T_F + T_{b_1}$$

$$\equiv K_3 K_6 K_A K_R T_F + T_{b_1}$$

$$b_2 = [T'_d + T_R] K_A K_F + T_{b_2}$$

$$b_3 = K_A K_F \cdot T'_d T_R + T_{b_3}$$

$$b_4 = T_{b_4}$$

$$b_5 = T'_d T_A T_E T_F T_R = T_{b_5}$$

$$M = S_E + K_E$$

$$T = K_3 T'_{do}$$

$$T_{a_1} = K_A K_F + T_E + M(T_A + T_F + T_R)$$

$$T_{a_2} = K_A K_F T_R + (T_E + M T_R)(T_A + T_F) + M T_A T_F + T_E T_R$$

$$T_{a_3} = T_A T_E T_F + T_E T_R (T_A + T_F) + M T_A T_F T_R$$

$$T_{b_1} = K_A K_F + K_3 K_6 K_A K_R T_F + M[T'_d + T_A + T_F + T_R] + T_E$$

$$T_{b_2} = T_E [T + T_R] + M[T_A T_F + T'_d T_R] + [T_E + M T + M T_R][T_A + T_F]$$

$$T_{b_3} = [T'_d T_E + M T'_d T_R + T_E T_R][T_A + T_F] + T_A T_F [T_E + M T'_d + M T_R] + T'_d T_R T_E$$

$$T_{b_4} = T_A T_E T_F (T'_d + T_R) + T'_d T_E T_R [T_A + T_F] + M T'_d T_A T_F T_R$$

Now, evaluating $\Delta T / \Delta \delta$ at $s = j\omega$, we get

$$\left. \frac{\Delta T_c}{\Delta \delta} \right|_{s=j\omega} = K_1 - \frac{A_o + jA_1}{B_o + jB_1} \quad (5.52)$$

Where

$$A_o = a_o - a_2 \omega^2 + a_4 \omega^4$$

$$A_1 = a_1 \omega - a_3 \omega^3$$

$$B_o = b_o - b_2 \omega^2 + b_4 \omega^4$$

$$B_1 = b_1 \omega - b_3 \omega^3 + b_5 \omega^5$$

The synchronizing and the damping torques can finally be deduced.

$$\Delta T_S = \left(K_1 - \frac{A_o B_o + A_1 B_1}{B_o^2 + B_1^2} \right) \cdot \Delta \delta \quad (5.53a)$$

$$\Delta T_D = \frac{A_o B_1 - A_1 B_o}{B_o^2 + B_1^2} \cdot (\omega \Delta \delta) \quad (5.53b)$$

(a) Lower Frequency Range ($\omega \ll 1$)

In this range of frequency, we can neglect the terms in ΔT_S and ΔT_D of higher exponents.

$$K_D \equiv \frac{a_o b_1 - a_1 b_o}{b_o^2} \quad (5.54)$$

Evaluating the numerator yields to

$$\begin{aligned} a_o b_1 - a_1 b_o &= [K_A K_R K_2 K_3 K_5] \cdot [K_A K_R K_3 K_6 T_F + T_{b_1}] \\ &- [K_2 K_3 K_4 T_{a_1} + K_A K_R K_2 K_3 K_5 T_R] \cdot K_A K_R K_3 K_6 \end{aligned}$$

Replacing in equation (5.54) gives an approximate expression for K_D , for $\omega \ll 1$.

$$K_D \equiv K_5 \cdot \frac{K_2}{K_6} \left(T_F - T_R + \frac{T_{b_1}}{K_A K_R K_3 K_6} \right) - K_4 \cdot \frac{K_2}{K_6} \frac{T_{a_1}}{K_A K_R} \quad (5.55a)$$

Similarly,

$$K_S \equiv K_1 - \frac{a_o b_o}{b_o^2} \equiv K_1 - \frac{K_2 K_3 K_5 K_A K_R}{K_3 K_6 K_A K_R}$$

or,

$$K_S \equiv K_1 - K_5 \cdot \frac{K_2}{K_6} \quad (5.55b)$$

Therefore,

$$\begin{aligned} K_D > 0 \quad \text{if we have} \quad K_5 &> K_4 K_3 K_6 \cdot \frac{T_{a_1}}{T_{b_1} + K_A K_R K_3 K_6 (T_F - T_R)} \\ K_S > 0 \quad \text{if we have} \quad K_1 &> K_5 \cdot \frac{K_2}{K_6} \end{aligned}$$

(b) Frequency Range ($\omega \gg 1$)

$$K_D = \frac{T_{a_4} T_{b_5}}{T_{b_5}^2 \omega^2} = \frac{T_{a_4}}{T_{b_5} \omega^2} = \frac{K_2 K_3 K_4}{\omega^2 T_d'^2} \quad (5.56a)$$

Similarly, the synchronizing coefficient may obtained by retaining only the highest powers of ω in the numerator and the denominator

$$K_S = K_1 - \frac{(a_2 b_2 - a_1 b_3) \omega^4}{b_3^2 \omega^6} = K_1 - \frac{(a_2 b_2 - a_1 b_3)}{b_3^2 \omega^2} \equiv K_1 - \frac{K_2 K_3 K_4}{\omega^2 T_d'^2} \quad (5.56b)$$

5.4.2 Bifurcation Tests for the SMIB

Given that the system K-constants K_2 , K_3 and K_6 are positive, bifurcation tests for SN and Hopf Bifurcations in both the regulated and unregulated SMIB models have been derived in the previous section and are stated in the form of two propositions and two corollaries, followed by their proofs.

Proposition 5.1 (Unregulated system)

- (i) A sufficient (and necessary) condition for a Hopf bifurcation to occur in the unregulated SMIB model is that $K_4 < 0$.
- (ii) A sufficient (and necessary condition) for a saddle node bifurcation to occur prior to Hopf bifurcation in the unregulated SMIB model is that $K_1 - K_2 K_3 K_4 < 0$ when $K_4 > 0$

Proof:

- (i) *Since all the terms in the expression of the damping coefficient for the unregulated SMIB given in equation (5.41a) are positive except K_4 , then its sign depends on the sign of the parameter K_4 , i.e. $K_D < 0$ when $K_4 < 0$.*
- (ii) *Similarly, the expression for the synchronizing torque coefficient K_S in equation (5.41b) indicates that it is negative if and only if $K_1 - K_2 K_3 K_4 < 0$ when $m_w = 0$ as is the case for saddle node bifurcation. The condition $K_4 > 0$ assures that Hopf bifurcation has not occurred.*

Corollary 5.1 (Unregulated System)

The unregulated system is stable if (and only if) the constant K_4 lies in the range

$$0 < K_4 < \frac{K_1}{K_2 K_3} (1 + \omega^2 T_d'^2)$$

Proof:

Equations 5.41 (a) and (b) indicate that sufficient synchronizing forces exist in the system

$$\text{iff } K_S = K_1 - \frac{K_2 K_3 K_4}{1 + \omega^2 T_d'^2} > 0, \text{ which can be rewritten as}$$

$$K_4 < \frac{K_1}{K_2 K_3} (1 + \omega^2 T_d'^2)$$

Since stability is assured only when both synchronizing and damping torque coefficients are positive, this condition combined with $K_4 > 0$ prove the claim of the corollary.

Proposition 5.2 (Regulated system, Inter-area mode)

When $f < 1$ and $K_4 > 0$ under voltage regulation, (i) A necessary condition for a Hopf bifurcation to occur in the SMIB model is that $K_5 < 0$ and (ii) A sufficient condition for a saddle node bifurcation to occur in the SMIB model is that K_1, K_2, K_5 and K_6 satisfy

$$K_1 - \frac{K_5 K_2}{K_6} < 0 \quad \text{for Type I exciter}$$

$$K_1 - \frac{K_5 K_2}{K_6} - \frac{K_4 K_2}{K_3 K_6 K_R} < 0 \quad \text{for Thyristor exciter}$$

Proof:

(i) Equation 5.46(a) and 5.55(a) indicated that sufficient damping forces exist in the SMIB system if

$$K_D \equiv K_5 K_2 \frac{(T_d' + T_E + T_R)}{K_3 K_6^2 K_E K_R} - K_4 K_2 \frac{(T_E + T_R)}{K_6 K_E K_R} > 0 \quad \text{for Thyristor type}$$

$$K_D \equiv K_5 \cdot \frac{K_2}{K_6} \left[T_F - T_R + \frac{T_{b1}}{K_A K_R K_3 K_6} \right] - K_4 \cdot \frac{K_2 T_{a1}}{K_6 K_A K_R} > 0 \quad \text{for Type I exciter}$$

which can be rewritten as

$$K_5 > \frac{K_3 K_4 K_6 (T_E + T_R)}{(T_d' + T_E + T_R)} \quad \text{and} \quad K_5 > K_4 \cdot \frac{T_{a1}}{K_A K_R} \left(T_F - T_R + \frac{T_{b1}}{K_A K_R K_3 K_6} \right)^{-1}$$

for a thyristor type exciter and type I exciter, respectively. By observing the terms on the right hand side of both inequalities of K_5 , we can conclude that they are generally small and either positive or negative depending on the sign of K_4 . Thus, K_5 is sufficiently positive, no Hopf bifurcation occur; and when K_5 is sufficiently negative Hopf

bifurcation occurs.

- (ii) Similarly, equation 5.46(b) and 5.55(b) indicated that sufficient synchronizing forces are positive in the SMIB system if

$$K_S \equiv K_1 - K_4 \cdot \frac{K_2}{K_6 K_E K_R} - K_5 \cdot \frac{K_2}{K_6} > 0 \quad \text{and} \quad K_S \equiv K_1 - K_5 \cdot \frac{K_2}{K_6} > 0$$

for a thyristor type exciter and type I exciter, respectively. If K_5 is sufficiently positive, large and increasing, saddle node bifurcation occurs.

Corollary 5.2 (Regulated System)

The SMIB model is stable for $f < 1$ if the constant K_5 lies in the range

$$K_4 K_3 K_6 \cdot \frac{T_{a1}}{T_{b1} + K_A K_R K_3 K_6 (T_F - T_R)} < K_5 < \frac{K_1 K_6}{K_2} \quad \text{Type I exciter}$$

$$K_4 K_3 K_6 \cdot \frac{T_E + T_R}{T + T_E + T_R} < K_5 < \frac{K_1 K_6}{K_2} - \frac{K_4}{K_E K_R} \quad \text{Thyristor exciter}$$

Proof:

- (i) For thyristor exciter, equations 5.46(a) and (b) indicate that sufficient damping and synchronizing forces exist in the system if

$$K_D \equiv K_5 K_2 \frac{(T'_d + T_E + T_R)}{K_3 K_6 K_E K_R} - K_4 K_2 \frac{(T_E + T_R)}{K_6 K_E K_R} > 0$$

$$K_S \equiv K_1 - K_4 \cdot \frac{K_2}{K_6 K_E K_R} - K_5 \cdot \frac{K_2}{K_6} > 0$$

These two conditions may be rewritten respectively as

$$K_5 > K_4 K_3 K_6 \cdot \frac{T_E + T_R}{T'_d + T_E + T_R} \quad \text{and} \quad K_5 < \frac{K_1 K_6}{K_2} - \frac{K_4}{K_E K_R}$$

- (ii) For a Type I exciter, equations 5.55(a) and (b) indicate that sufficient damping and synchronizing forces exist in the system if

$$K_D \equiv K_5 \cdot \frac{K_2}{K_6} \left(T_F - T_R + \frac{T_{b1}}{K_A K_R K_3 K_6} \right) - K_4 \cdot \frac{K_2}{K_6} \frac{T_{a1}}{K_A K_R} > 0$$

$$K_S \equiv K_1 - K_5 \cdot \frac{K_2}{K_6} > 0$$

These conditions may be rewritten respectively as

$$K_5 > K_4 K_3 K_6 \cdot \frac{T_{a1}}{T_{b1} + K_A K_R K_3 K_6 (T_F - T_R)} \quad \text{and} \quad K_5 < \frac{K_1 K_6}{K_2}$$

Since stability is assured only when both synchronizing and damping torque coefficients are positive, conditions for positive damping are combined with conditions for positive synchronizing for the thyristor type exciter and for the Type 1 exciter, which leads to the desired result of the corollary. If K_5 is below the lower limit or K_5 exceeds the upper limit Hopf bifurcation occurs.

5.4.3 Conclusions

It is our desire to hopefully find a subsystem of the full model which experiences, produces, and causes the same bifurcation in the full system model. Determining the center manifold dynamics requires finding a nonlinear transformation that is often given in terms of a Taylor series and may be infinitesimally linked to all the states of the model even if it virtually lies in a subsystem of the full model which experiences, produces, and causes the bifurcation. Determining such a subsystem if one exists is essential to diagnosing the location, class, cause, and cure for a bifurcation, and that is important from an engineering sense. Determining the center manifold is thus not what is desired, but a subsystem of the full model which experiences, produces, and causes the bifurcation, and which is normally of larger dimension than that of the center manifold. One may be able to diagnose the location, class, cause and cure without resorting to finding the center manifold transformation, or its approximation.

The subsystem which experiences bifurcation may or may not produce bifurcation in the full system since the structure or parameters external to the subsystem may help pro-

duce the bifurcation both in the full system and subsystem. This is especially true if the geometric coupling of the bifurcating subsystem and the external system in the direction of the bifurcating eigenvector is not zero but approaches zero. Thus the subsystem that produces the bifurcation experienced by the subsystem and the full system may be of larger dimension than the subsystem experiencing bifurcation. The subsystem causing bifurcation may be still larger than the subsystem experiencing or producing the bifurcation in the full system model and the subsystem. The subsystem that causes bifurcation must include all model parameters, controls, and discontinuous changes that cause the bifurcation to develop. The discontinuous changes include under-load tap changes, switchable shunt capacitors switching changes, equipment outages, over-excitation limit relays,...etc. The controls include maximum excitation limiter controls, under-load tap changer controls, switchable shunt capacitor controls, and excitation system controls.

The results of this chapter along with chapter 4 imply the bifurcation subsystem method may provide such a tool for identifying the subsystem that experiences, produces, and causes a specific kind and class of bifurcation, since

- (a) the theoretical conditions for existence of bifurcation subsystem was applied to show that they exist and can be determined. The bifurcation subsystem showed some promising results in identifying the subsystem that experiences the bifurcation in the full model;
- (b) the sensitivity matrices K_S , K_D and T were derived in two recent Ph.D dissertations with the purpose of identifying the subsystem that causes and produces the bifurcations, and which may also contain the center manifold. It has been shown that the test matrices K_S , and T are not necessarily associated with the subsystem that experi-

ences, produces, or causes the bifurcation, but the parameters of the system they depend on can help identifying the bifurcation subsystem;

- (c) The results on Hopf bifurcation indicate that the bifurcation subsystem obtained (Example 2) which experiences the bifurcation of the full system model may be too small to track what produces and even less capable of tracking what causes and cures that bifurcation, since the test matrices suggest that K_D depends on K_4 and K_5 which lie outside the bifurcation subsystem $(\Delta\delta, \Delta\omega)$. This result may be true since the $(\Delta\delta, \Delta\omega)$ dynamics are experiencing bifurcation for all μ , and this may imply that the bifurcation subsystem producing and causing the bifurcation should be identified as $\mu \rightarrow \mu^*$, and not at the point of bifurcation, so that the subsystem captures the causes and cure for that bifurcation;
- (d) the determination of what K_S , K_D and T depend on for a generator with exciter, a thyristor based exciter, and a dc1 model exciter, gives implicit information for determining the subsystem which experiences the bifurcation in each case.

VI

A Diagnosis for SN and Hopf Bifurcations in a Discontinuous SMIB Model

6.0 Introduction

The goal of this chapter is to perform a diagnostic study to assess the structural causes, operational stresses, and stabilizing requirements for the occurrence of SN and inter-area modes of oscillations that occur in the generator inertial and flux decay dynamics of a single-machine-infinite-bus model (SMIB). The tool for this study is based on the bifurcation tests derived and concluded in propositions 5.1-2 and corollaries 5.1-2 of Chapter 5.

The diagnostic study is performed by formulating three study models: (1) a power transfer model where the effects of both the network inductance x_e and real and reactive power transfer are investigated; (2) a local loading model where the effect of local loading on system stability may be investigated; (3) a power transfer-local loading model where the effect of local load model and transfer can be investigated. The SMIB local load may be capacitive, inductive or some combination. The generator exciter may be enabled (regulated case) or disabled (unregulated case).

The objective of the analysis in this chapter is to establish that (i) increased local load causes quite different bifurcation phenomena in the regulated and unregulated load center models and (ii) that increased power transfer causes quite different bifurcations in

the regulated and unregulated power transfer model: When the exciter is enabled, the regulated model is vulnerable to Hopf bifurcation for increased power transfer, whereas when the exciter is disabled, the system is vulnerable to saddle node bifurcation in the flux decay dynamics as power transfers increase. The analysis also shows that when the local loading in light-real, heavy-capacitive, the regulated local load center model is vulnerable to Hopf bifurcation, and the unregulated local load center model is vulnerable to saddle node bifurcation. The combination local load center/transfer model is then used to validate, extend, or possibly disagree with the diagnostic conclusions obtained from the local load center or the transfer models.

6.1 Diagnostic Models Formulation

Based on operational and structural parameter variations of the SMIB, three operationally and structurally different models may be obtained. This kind of diagnostic modeling is permissible by the SMIB model since this model represents a generator connected to a large system, via a long equivalent transmission corridor with equivalent reactance x_e . The large system may be (a) a major bus or group of buses of a power system of very large capacity compared to the rating of the machine under consideration, or (b) a large load center. Such a structure allows formulating three study models as follows.

6.1.1 Power Transfer Model ($R_a = X_a = \text{infinity}$)

In a power transfer model, no local load or equivalent line shunts are modeled, so that the generated real and reactive power are solely used to satisfy the power transfer requirements to the 'large' system at the side of the infinite bus. Real power is shipped from the generator to the infinite bus, whereas reactive power may be shipped in either direction across the

transmission network. The effects of the power transfer as well as the network inductance may then be investigated. In the power transfer model shown in Figure 6.1, the system steady state conditions are computed for given values of P_∞ , Q_∞ and $V_\infty = 1.0\angle 0$ p.u.

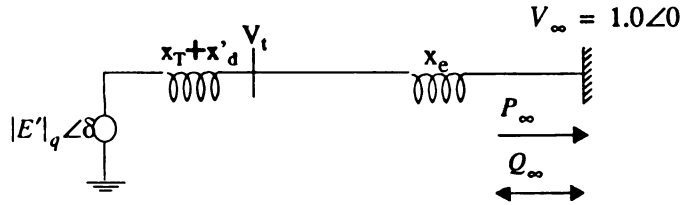


Figure 6.1 Power transfer model

6.1.2 Local Load Model

A local loading model is obtained when a shunt constant load is connected to the generator terminals while the power transfer requirements to the infinite bus are negligible. The local constant impedance load can include line charging of the transmission line, local shunt capacitive compensation, or inductance load. With x_e large, the dynamics of the generator serving a local load center can be investigated. This results in a model where stability problems are solely associated with the local load center. Note that since the power absorbed by the local load is proportional to V^2/Z_{sh} , the local load is capacitive when $X_{sh} < 0$ and the reactive absorbed is proportional to $1/X_{sh}$, it is inductive when $X_{sh} > 0$ and the load is proportional to $1/X_{sh}$. Similarly, the real shunt load is proportional to $1/R_{sh}$. The local load is shown in Figure 6.2

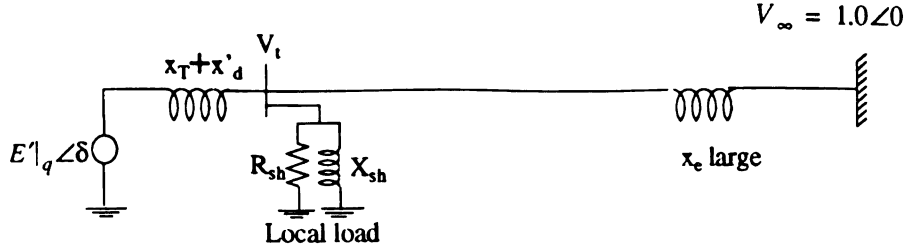


Figure 6.2 Local loading model

6.1.3 Combination Local Load/Power Transfer Model

Under normal operation, power system models serve both local loading and power transfer requirement patterns, and therefore a diagnostic study of this model is necessary. The more realistic SMIB model consists of real local loading in combination with power transfer model.

6.2 Diagnostic Study

From Propositions 5.1 and 5.2, it is clear that since the system constants K_2 , K_3 and K_6 are positive for a generator mode of operation of the machine, the occurrence of Hopf bifurcation in the unregulated and regulated SMIB model depends on the parameters K_4 and K_5 which approximate the sign change behavior of the test matrix K_D , respectively. The operating conditions where $K_5 < 0$ cause undamped oscillations in the generator inertial dynamics when the exciter is active. The operating conditions where $K_4 < 0$ cause negative damping in the SMIB model with a local load when the exciter is disabled. Similarly, the terms $K_1 - K_2 K_5 / K_6$ and $K_1 - K_2 K_3 K_4$ which approximate the sign change behavior of the test matrix K_S are indication to the occurrence of SN bifurcation for the regulated and the unregulated systems, respectively. These conclusions are based on results in Chapter 5.

The scope of this section is to investigate the change in the parameters K_4 , K_5 as well as $K_1 - K_2 K_3 K_4$ and $K_1 - K_2 K_5 / K_6$, for the purpose of establishing a diagnosis for the occurrence of Hopf and saddle node bifurcations in systems subject to relay-type discontinuous hard limit action. It should be noted that these K_1 - K_6 parameters are associated with the bifurcation subsystems that experience saddle node and Hopf bifurcations in a single-machine-infinite-bus model. The bifurcation subsystem would approximately indicate the generator and dynamics (bifurcation class) experiencing bifurcation. Investigating how the key indices for sign changes in test matrices (K_S, K_D) for occurrence of Hopf (K_4, K_5) and saddle node ($K_1 - K_2 K_3 K_4, K_1 - K_2 K_5 / K_6$) change with load parameters provides important diagnosis of why the bifurcation occurs and what can be done to prevent it. The parameter and stress tests that will be investigated are:

- (a) Power transfer to or from the infinite bus ($P_\infty > 0$ and $Q_\infty \geq 0$ or $Q_\infty \leq 0$)
- (b) Local loading: inductive or capacitive shunt $X_{sh} > 0$ or $X_{sh} < 0$ in parallel with a real load (R_{sh})
- (c) Network inductance (x_e).

In this diagnostic study, the real power transfer P_∞ is varied between 0.1 and 1.0 p.u., ($P_\infty = 0.1, 0.2, \dots, 1$ p.u.), and the reactive power transfer to the infinite bus Q_∞ is either positive ($Q_\infty = 0, 0.1, 0.2, \dots, 1$ p.u.) indicating reactive power absorption by the infinite bus, or negative ($Q_\infty = -1.0, -0.9, -0.8, \dots, 0$ p.u.), indicating reactive power supply by the infinite bus. Power transfer levels of ± 1.0 indicate maximum system rating since for $|V_\infty| = 1$ and $x_e = 0.4$,

$$P_\infty = 1.0 = \frac{|V_t||V_\infty|}{x_e} \sin(\angle V_t - \angle V_\infty) = 2.5|V_t| \sin(\angle V_t - \angle V_\infty)$$

$$Q_\infty = 1.0 = \frac{-|V_\infty|^2 + |V_\infty||V_t| \cos(\angle V_t - \angle V_\infty)}{x_e} = 2.5(-|V_\infty|^2 + |V_\infty||V_t| \cos(\angle V_t - \angle V_\infty))$$

so that the system is operating at

$$\angle V_t - \angle V_\infty = 15.1^\circ$$

$$|V_t| = 1.45 \text{ p.u.}$$

This level of terminal voltage indicates heavy reactive supply to the infinite bus with large reactive losses sufficient to bring on instability in the network equations let alone the SMIB dynamics. Similarly, when $P_\infty = 1.0$ and $Q_\infty = -1.0$ the system operates at:

$$\angle V_t - \angle V_\infty = 33.5^\circ$$

$$|V_t| = 0.72 \text{ p.u.}$$

and this level of angle difference indicates heavy real and reactive power loads at the infinite bus and very large I^2X losses sufficient to bring on instability in the SMIB dynamics. Thus $P_\infty = 1.0$ and $Q_\infty = \pm 1.0$ indicate the system is heavily stressed and it is operating at marginal values of voltages and angle differences.

Similarly, The chosen ranges of the local load R_{sh} , X_{sh} , and x_e are such that $1 \leq 1/R_{sh} \leq 6$, and $1 \leq 1/X_{sh} \leq 6$ result in acceptable system operating conditions and viable system voltages and angles required for normal operation: When $X_{sh} = 0.17$, the resulting voltage at the terminal bus shown in Figure 6.1 is approximately $V_t = 0.45$, since $x'_d + x_T = 0.2 \text{ p.u.}$. Operating below this voltage level, is considered outside the system capabilities [59]. However parameter studies in literature [55,56] usually consider the entire range of $R_{sh}, X_{sh} = 0.1, \dots, 1.0 \text{ p.u.}$ i.e, $1 \leq 1/R_{sh} \leq 10$, and $1 \leq 1/X_{sh} \leq 10$, as it is the approach in this study. For this kind of study, when solvability was not possible, the cases were skipped as will be observed in the tabulated results and the associated figures.

The results of this diagnostic study are summarized in tables for operating conditions resulting in bifurcations, and tables for operating conditions where no bifurcations occurred. The tables indicate the test parameter, the kind of bifurcation tested, the network

and the power transfer operating conditions used. The arrows in the tables point to the range where the test parameter was more sensitive, i.e. was more negative.

6.2.1 Power Transfer Model

6.2.1.1 Effect of P_{inf} and Q_{inf}

The effect of P_{∞} and Q_{∞} on the parameters K_4 , K_5 as well as $K_1 - K_2K_3K_4$ and $K_1 - K_2K_5/K_6$ is simulated in Figures E1.1-E1.4 in Appendix E1, while the bifurcation results and the associated figures are summarized in Table 5.1. In these figures, the parameters K_4 , K_5 as well as $K_1 - K_2K_5/K_6$ and $K_1 - K_2K_3K_4$ are plotted versus sequential 0.1 p.u. step increases in real power transfer P_{∞} , and for increases in levels of reactive power transfer $Q_{\infty} = 0, 0.1, 0.2, \dots, 1$ p.u. or $Q_{\infty} = -1, -0.9, -0.8, \dots, 0$ p.u.. The simulation results on bifurcations of this study are summarized in Table 6.1(a) for cases resulting in bifurcations, and in Table 6.1(b) for non-bifurcation cases. A careful review of these tables indicates ranges of P_{∞} , $Q_{\infty} \geq 0$, $Q_{\infty} \leq 0$ when oscillatory and non-oscillatory instability occurs, the points (pointed by arrows) where the measure of instability of a particular kind (K_4 , K_5 , $K_1 - K_2K_5/K_6$, $K_1 - K_2K_3K_4$) is most negative over the range of P_{∞} and Q_{∞} , the kind of bifurcation (SN or Hopf) that occurs, the values of (P_{∞}, Q_{∞}) where the bifurcation occurs (in general at points opposite to where the arrows point to) and whether the instability occurs in the regulated or unregulated model. The tables are so complete so that the discussion that follows may be superfluous. The results indicate that Hopf bifurcation occurs in the regulated model but not in the unregulated model, and saddle node occurs in the unregulated model but not in the regulated model.

Namely, when the model is regulated, Figure E1.1(a) shows that (i) as the real power

transfer P_∞ increases and the reactive power is such that $0 \leq Q_\infty < 0.3$, K_5 is positive and decreasing; (ii) for $3 \leq Q_\infty < 0.7$, $K_5 = \partial|V_t|/\partial\delta$ decreases and becomes negative as P_∞ increases; and (iii) for higher levels of reactive power transfer, i.e. when $Q_\infty > 0.7$ pu, $K_5 < 0$. This implies that the regulated SMIB model is subject to undamped oscillations in the inertial dynamics when the generator terminal voltage begins to decrease for increases in δ and occurs for the range of values (P_∞, Q_∞) shown in Table 6.1. The fact that Hopf bifurcation occurs when $K_5 = \partial|V_t|/\partial\delta$ is negative for a regulated system due to large P_∞ and Q_∞ indicates that Hopf bifurcation in the inertial dynamics is due to voltage if not voltage instability.

Diagnosis for the causes of undamped oscillations in the system is also performed when the reactive power is withdrawn from the infinite bus, i.e. real and reactive power transfer are in opposite directions. From Figure E1.1(b), we see that (i) when $Q_\infty = -0.3, \dots, 0$ p.u. $K_5 > 0$ and (ii) when $Q_\infty = -1.0, \dots, -0.5$ p.u. $K_5 < 0$. An oscillatory mode in the regulated SMIB model may then be brought on by negative reactive power transfer, i.e. generator reactive absorption.

Power transfer also affected the synchronizing term $K_1 - K_2K_3K_4$ for the unregulated machine, where it became negative for heavy-real and heavy-reactive power transfer to the infinite bus, as indicated by Table 6.1(a).

Note that the non-bifurcation cases are summarized in Table 6.1(b). Real and reactive power transfer to the infinite bus has no effect on the parameter K_4 , since K_4 is positive and increasing for the whole range of (P_∞, Q_∞) . If no local load is present at the generator side, K_4 -associated oscillatory stability problems in the unregulated model do not seem to appear. The synchronizing torques for the regulated model are not affected by the transfer

of real/reactive power, whereas when the system is heavily stressed by real/reactive power supply to the infinite bus, the synchronizing coefficient in the unregulated model is driven to zero, indicating the occurrence of saddle bifurcation. The bifurcation subsystem of $(\Delta\delta, \Delta\omega, \Delta E_q')$ explains why heavy real and reactive power transfer cause saddle node bifurcation because K_1 decreases with real power transfer and K_2 and K_4 coupling between inertial (real power) and flux decay (reactive power) increases with real and reactive power transfer causing $K_1 - K_2K_3K_4$ to approach zero.

The diagnosis study will now focus on the effect of the transmission network inductance.

6.2.1.2 Effect of transmission network inductance x_e

The effect of the transmission network inductance is simulated when $P_\infty = 0.8$ p.u. and $Q_\infty = 0.5$ p.u. in Figure 6.3. As the network inductance increases, the constant K_s decreases, and finally changes sign at $x_e \approx 0.4$ p.u. The system damping coefficient also decreases and changes sign, indicating that the system damping forces are insufficient to damp the ongoing oscillatory modes. This implies that long transmission corridors, cause undamped oscillation in the regulated SMIB model. The inter-area oscillations often occur in a multi-machine model between two groups of machines connected by a long line carrying significant transfer.

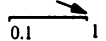
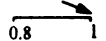
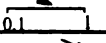
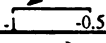
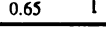
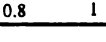
Excitation System	Bifurcation		Network			Power Transfer		Figure
	Kind	Test	x_e	$1/R_{sh}$	$1/X_{sh}$	P_{inf}	Q_{inf}	
R	H	$K_s < 0$	0.4	0	0			E1.1(a)
R	H	$K_s < 0$	0.4	0	0			E1.1(b)
U	SN	$K_1 - K_2K_3K_4 < 0$	0.4	0	0			E1.4(a)

Table 6.1 (a) Results on the power transfer model bifurcation diagnosis

Excitation System	Bifurcation		Network			Power Transfer		Figure
	Kind	Test	x_e	$1/R_{sh}$	$1/X_{sh}$	P_{Inf}	Q_{Inf}	#
U	H	$K_4 > 0$	0.4	0	0	$\sqrt{0.1} \quad 1$	$\sqrt{-1 \quad 0} \quad 1$	E1.2
U	SN	$K_1 - K_2 K_3 K_4 > 0$	0.4	0	0	$\sqrt{0.1} \quad 1$	$\sqrt{-1} \quad 0$	E1.4
R	SN	$K_1 - K_2 K_3 / K_4 > 0$	0.4	0	0	$\sqrt{0.1} \quad 1$	$\sqrt{-1 \quad 0} \quad 1$	E1.3

Table 6.1(b) Power transfer model non-bifurcation results

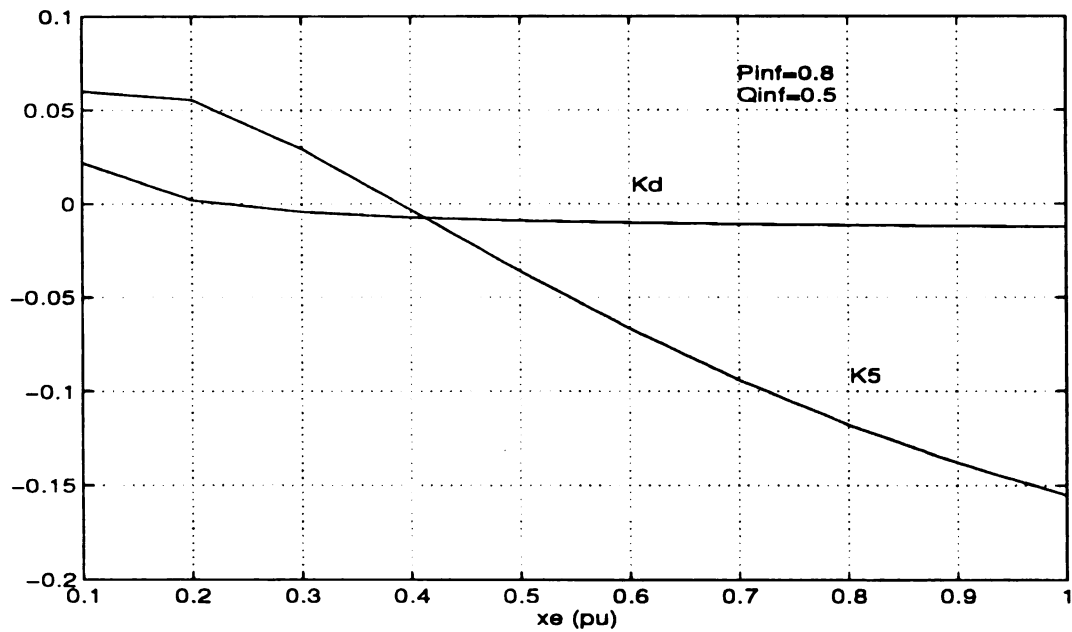


Figure 6.3 Power Transfer Model: Effect of transmission inductance on the parameter K_5 and the damping torque K_d .

6.2.2 Local Load Model

The effect of the local constant impedance load parameters X_{sh} and R_{sh} on the occurrence of system bifurcations is simulated in Figures E2.1-E2.4. The bifurcation results, the associated operating conditions and figures are summarized in Tables 6.2(a-b). In the local load model, R_{sh} is a positive parameter between $0.1 \leq R_{sh} \leq 1$ and X_{sh} may be negative or positive, depending on whether it is capacitive or inductive, respectively. Note that $x_e = 0.9$ which effectively isolates the local load bus from the infinite bus. In this case, no transfer of power to or from the infinite bus is permitted. Therefore, three cases are considered: the effect of (i) real-inductive load and (ii) real-capacitive load. The simulation results on bifurcations of this study are summarized in Table 6.2(a) for cases resulting in bifurcations, and in Table 6.2(b) for non-bifurcation cases. A careful review of these tables indicated ranges of $(1/R_{sh}, 1/X_{sh})$, when oscillatory and non-oscillatory instability occurs, the points (pointed by arrows) where the measure of instability of a particular kind (K_4 , K_5 , $K_1 - K_2K_5/K_6$, $K_1 - K_2K_3K_4$) is most negative over the range of $(1/R_{sh}, 1/X_{sh})$, the kind of bifurcation (SN or Hopf) that occur, the values of $(1/R_{sh}, 1/X_{sh})$ where the bifurcation occurs (in general at points opposite to where the arrows point to) and whether the instability occurs in the regulated or unregulated model. The tables are so complete so that the discussion that follows may be superfluous.

6.2.2.1 Effect of real-inductive local loading

When the shunt local load was real-inductive, the parameter K_4 was negative for the entire R_{sh} - X_{sh} range. Furthermore, K_4 was most negative at $1/R_{sh} = 2.5$ and decreased as $1/X_{sh}$ was decreasing. This implies that the unregulated SMIB model was subject to undamped oscillations in the inertial dynamics, as summarized in Table 6.2(a).

6.2.2.2 Effect of real-capacitive local loading

When the shunt local load is real-capacitive load, Table 6.2(b) shows that the parameter K_4 is negative and decreasing for the entire R_{sh} - X_{sh} range from Figures E2.1(a-b) results. Furthermore, K_4 is decreasing when the inductance $1/X_{sh}$ is negative and $|1/X_{sh}|$ increasing. This implies that the unregulated SMIB model is subject to undamped oscillations in the inertial dynamics. Table 6.2(a) also indicates that the synchronizing term $K_1 - K_2 K_5 / K_6$ became negative for light-real, heavy capacitive local loading, implying that the regulated model is vulnerable to SN bifurcation. The capacitive shunt is larger than $x'_d + x_T = 0.2$ p.u. when $|X_{sh}| = 1$ and becomes the same size as $x'_d + x_T$ as $|X_{sh}|$ becomes smaller, causing heavier capacitive loading. This appears to cause the network to induce the saddle node bifurcation.

6.2.2.3 Effect of the transmission network

We notice that K_4 is negative if no power transfer to the infinite bus occurs, regardless of the local real power load (R_{sh}), or the shunt capacitance/reactance (X_{sh}) at the generator side, which indicates that undamped oscillations in the unregulated SMIB model are associated with (i) heavily loaded load centers; (ii) local shunt capacitive system compensation; (iii) transmission lines with high capacitive/inductive charging; and (iv) when power transfer from or to the infinite bus is not possible.

On the other hand, under the real-inductive and real-capacitive local loading operating conditions, Table 6.2(b) summarizes the non-bifurcations cases. Both K_5 and the synchronizing term $K_1 - K_2 K_3 K_4$ are positive for the local load variations. This diagnostic study implies that in a local model, it is unlikely to experience (i) Hopf in the regulated model; or (ii) SN in the unregulated model.


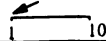
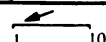
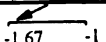
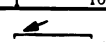
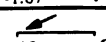
Excitation System	Bifurcation		Network			Power Transfer		Figure
Reg/Un	Kind	Test	x_o	$1/R_{sh}$	$1/X_{sh}$	P_{inf}	Q_{inf}	#
U	H	$K_4 < 0$	0.9			0	0	E2.1(a)
U	H	$K_4 < 0$	0.9			0	0	E2.1(b)
R	SN	$K_1 - K_2 K_3 / K_6 < 0$	0.9			0	0	E2.4(b)

Table 6.2(a) Results on the local loading model bifurcation diagnosis

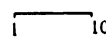
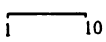
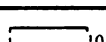
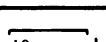
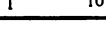
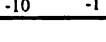
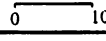
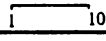

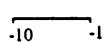
Excitation System	Bifurcation		Network			Power Transfer		Figure
Reg/Un	Kind	Test	x_o	$1/R_{sh}$	$1/X_{sh}$	P_{inf}	Q_{inf}	#
R	H	$K_5 > 0$	0.9			0	0	E2.2(a)
R	H	$K_5 > 0$	0.9			0	0	E2.2(b)
U	SN	$K_1 - K_2 K_3 K_4 > 0$	0.9			0	0	E2.3(a)
U	SN	$K_1 - K_2 K_3 K_4 > 0$	0.9			0	0	E2.3(b)
R	SN	$K_1 - K_2 K_3 / K_6 > 0$	0.9			0	0	E2.4(a)

Table 6.2(b) Non-bifurcation results on the local loading model diagnosis

6.2.3 Conclusion of the Power Transfer and Local Load Models

From the diagnostic stress tests results of the power transfer and local loading models, we deduce the following three conclusions: (i) undamped oscillations in the regulated SMIB model are highly associated with the transfer of active and reactive power (supply or absorption) along transmission corridors; (ii) undamped oscillations in the unregulated SMIB model are associated with heavy capacitive local loading; and (iii) power transfer causes different kinds of bifurcations in the SMIB depending on whether the generator is

regulated or unregulated: the effect of relay-type control action.

The regulated SMIB model is vulnerable to Hopf bifurcation when considerable reactive power transfer is absorbed by the generator $-1 \leq Q_{\infty} \ll 0$. The unregulated model is vulnerable to Hopf bifurcation in the generator inertial dynamics under local capacitive and local real loading operating conditions. Therefore, shunt capacitive load (generator absorption) causes Hopf in the unregulated model, and transfer of reactive power to the generator (generator absorption) causes Hopf in the regulated model. The same conclusions hold in the regulated model for $(Q_{\infty} > 0)$ and in the unregulated model for $(1/X_{sh} > 0)$.

Hopf bifurcation occurs both in the regulated and unregulated models for heavy absorption of reactive power. This is not surprising due to armature reaction that reduces the rotor field flux for reactive absorption and is shown to cause instability due to insufficient synchronizing torque between rotating rotor stator flux waves.

The unregulated SMIB model is vulnerable to SN bifurcation when considerable real and reactive power is supplied by the generator $0.4 \leq P_{\infty} \leq 1$, $0 \ll Q_{\infty} \leq 1$. The regulated model is vulnerable to SN bifurcation in the generator inertial dynamics under heavy-local capacitive, and heavy-real local loading. Therefore, transfer of reactive power to the infinite bus causes SN in the regulated model, and shunt capacitive load (generator absorption) causes SN in the unregulated model.

Finally, no saddle node bifurcation occurs in the regulated power transfer model, and no saddle node in the unregulated local loading model. In correlation, no Hopf bifurcation occurs in the unregulated power transfer model, and no Hopf in the regulated local loading model $(1/R_{sb}, 1/X_{sb})$.

6.2.4 Combination Local Load-Power Transfer Model

The diagnostic study now focuses on the more realistic model consisting of a local load in combination with power transfer requirement patterns. The variation of the machine damping and synchronizing torques under the effect of the various local loading patterns, and power transfer patterns is investigated for both the case where the generator is regulated ($K_5, K_1 - K_2 K_5 / K_6$) and the case where the generator is unregulated ($K_4, K_1 - K_2 K_3 K_4$). Various transfer and loading patterns are considered: (i) the effect of power transfer for a local loading pattern, (ii) the effect of local loading for a power transfer pattern, and (iii) the effect of the transmission network. Simulation for the combination model bifurcation diagnosis are shown in the figures in Appendix E3, and the bifurcation results are summarized in Tables 6.3(a-c).

6.2.4.1 Effect of Power Transfer

First, the local shunt load and the transmission network inductance are fixed respectively at $R_{sh} = 0.65$ p.u., $X_{sh} = \pm 0.17$ p.u. and $x_e = 0.4$ p.u., while the power transfer to the infinite bus (P_∞, Q_∞) is varied. Note that $x_e = 0.4$ p.u. rather than 0.9 p.u. as in the local load center model. The bifurcation results for the effect of P_∞ and Q_∞ on the parameters K_4 and K_5 as well as $K_1 - K_2 K_5 / K_6$ and $K_1 - K_2 K_3 K_4$ are summarized in Table 6.3(a). The occurrence of bifurcation as shown in the table indicates that (i) when the load X_{sh} is inductive, $K_5 < 0$ for both the case when $Q_\infty \geq 0$ and the case when $Q_\infty \leq 0$; (ii) when X_{sh} is capacitive, $K_5 < 0$ for both when $Q_\infty \geq 0$ and $Q_\infty \leq 0$; and (iii) the parameter $K_4 > 0$ for the power transfer stress tests except when the local load is capacitive and reactive power is being supplied by the infinite bus ($X_{sh} = -0.17, Q_\infty \leq 0$). Note that while (i) and (ii) confirm the power transfer model diagnosis results, (iii) occurred only in the combination model,

and thus extends the diagnostic conclusions. This result (iii) may be due to the effect of the large shunt capacitive load which caused Hopf bifurcation in the unregulated model for shunt capacitive load and no power transfer.

Power transfer stress on the system seem to also ultimately cause (i) SN bifurcation in the regulated model when the local load is real-capacitive $X_{sh} = -0.17$ and P_∞ increasing, Q_∞ decreasing; and (ii) SN in the unregulated model when the local load is inductive $X_{sh} = 0.17$ and P_∞ and $Q_\infty \geq 0$ are increasing. These results in (ii) above extend the SN bifurcation results obtained from the power transfer model.

6.2.4.2 Effect of Local Loading

The power transfer to the infinite bus, the local shunt load and the transmission network inductance are fixed respectively at $P_\infty = 0.8$ p.u., $Q_\infty = 0.5$ p.u. and $x_e = 0.4$ p.u., while the local shunt load at R_{sh} and X_{sh} are varied. The bifurcation results for the effect of R_{sh} and X_{sh} on the parameters K_4 and K_5 as well as $K_1 - K_2K_3K_4$ and $K_1 - K_2K_5/K_6$, are summarized in Tables 6.3(b-c). The occurrence of bifurcation as shown in the table indicate that when the model is regulated, (i) the parameter K_5 changed sign for the light- real, heavy-inductive local loading conditions (approximately $1/R_{sh} \leq 1.67$, $1/X_{sh} \geq 2.0$), and is decreasing for lighter $1/R_{sh}$ loading conditions as can be seen from Figure E3.9(a); and (ii) the parameter K_5 is positive with no change in sign when the local load is real-capacitive from Figure 3.9(b) results.

Given the system is unregulated, (i) when the shunt load is real-capacitive, the parameter K_4 changes sign under the heavy-capacitive loading conditions ($1/X_{sh} \leq -1.67$, generator reactive absorption); and (ii) when the shunt load is real-inductive, the parameter K_4 is positive which implies that shunt real-inductive real loading patterns are unlikely to

cause undamped oscillatory behavior in the unregulated machine dynamics in the SMIB.

Figures E3.11 and E3.12 in Appendix E3, show the variation of the machine synchronizing torques under the effect of the machines local loading patterns, for both when the system is regulated ($K_1 - K_2 K_5 / K_6$) and unregulated ($K_1 - K_2 K_3 K_4$). For the regulated system, the summarized figures in Table 6.3(b) indicate that (i) the synchronizing torque coefficient is positive for real-inductive loading conditions; and (ii) negative for light-real, heavy-capacitive loading ($1/R_{sh}$ small, $|1/X_{sh}| \geq 1.67$). When the generator exciter is disabled, the synchronizing torque is positive for the entire R_{sh} - X_{sh} range. This implies that the system is unlikely to experience static kind of instability when the generator is unregulated.

6.2.4.3 Effect of transmission network

The effect of the system's transmission network inductance x_e on the system synchronizing and damping forces is simulated in Figure 6.4. The system operating conditions were at $P_\infty = 0.8$ p.u., $Q_\infty = 0.5$ p.u., $X_{sh} = 0.4$ p.u., and two real loading levels were tested, $R_{sh} = 0.17$ and $R_{sh} = 0.87$. For this case, the damping torques are plotted versus x_e . We see that (i) both K_s and K_d both decrease as x_e increases, and (ii) K_D is very much more negative for heavy loading conditions, but K_s is slightly more negative for light loading conditions. This behavior confirms the results obtained from the power transfer model.

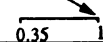



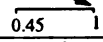

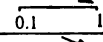
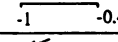
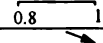
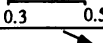
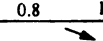
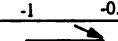
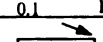
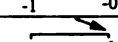
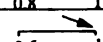
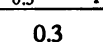
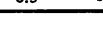
Excitation System	Bifurcation		Network			Power Transfer		Figure
Reg/Un	Kind	Test	x_e	R_{sh}	X_{sh}	P_{inf}	Q_{inf}	#
R	H	$K_5 < 0$	0.4	0.65	+0.17			E3.1(a)
R	H	$K_5 < 0$	0.4	0.65	+0.17			E3.1(b)
R	H	$K_5 < 0$	0.4	0.65	-0.17			E3.2(a)
R	H	$K_5 < 0$	0.4	0.65	-0.17			E3.2(b)
R	SN	$K_1 - K_2 K_3 / K_6 < 0$	0.4	0.65	-0.17			E3.6(a)
R	SN	$K_1 - K_2 K_3 / K_6 < 0$	0.4	0.65	-0.17			E3.6(b)
U	H	$K_4 < 0$	0.4	0.65	-0.17			E3.4(b)
U	SN	$K_1 - K_2 K_3 K_4 < 0$	0.4	0.65	+0.17			E3.7(a)
U	SN	$K_1 - K_2 K_3 K_4 < 0$	0.4	0.65	-0.17		0.3	E3.8(a)

Table 6.3 (a) Results on the combination model bifurcation diagnosis

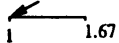
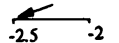
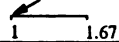

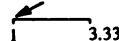
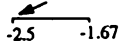
Excitation System	Bifurcation		Network			Power Transfer		Figure
Reg/Un	Kind	Test	x_e	$1/R_{sh}$	$1/X_{sh}$	P_{inf}	Q_{inf}	#
U	H	$K_4 < 0$	0.4			0.8	0.5	E3.10(b)
R	H	$K_5 < 0$	0.4			0.8	0.5	E3.9(a)
R	SN	$K_1 - K_2 K_3 / K_6 < 0$	0.4			0.8	0.5	E3.12(b)

Table 6.3 (b) Combination model: Effect of Local loading

Excitation System	Bifurcation		Network			Power Transfer		Figure
Reg/Un	Kind	Test	x_e	R_{sh}	X_{sh}	P_{inf}	Q_{inf}	#
U	H	$K_4 > 0$	0.4	0.65	+0.17	$\overline{0.1} \quad 1$	$\overline{0} \quad 1$	E3.3(a)
U	H	$K_4 > 0$	0.4	0.65	+0.17	$\overline{0.1} \quad 1$	$\overline{-0.8} \quad 0$	E3.3(b)
U	H	$K_4 > 0$	0.4	0.65	-0.17	$\overline{0.1} \quad 1$	$\overline{0.3} \quad 1$	E3.4(a)
U	SN	$K_1 - K_2 K_3 K_4 > 0$	0.4	0.65	+0.17	$\overline{0.1} \quad 1$	$\overline{-0.8} \quad 0$	E3.7(b)
U	SN	$K_1 - K_2 K_3 K_4 > 0$	0.4	0.65	-0.17	$\overline{0.1} \quad 1$	$\overline{-1} \quad -0.1$	E3.8(b)
R	SN	$K_1 - K_2 K_3 / K_6 > 0$	0.4	0.65	+0.17	$\overline{0.1} \quad 1$	$\overline{0.1} \quad 1$	E3.5(a)
R	SN	$K_1 - K_2 K_3 / K_6 > 0$	0.4	0.65	+0.17	$\overline{0.1} \quad 1$	$\overline{0.1} \quad 1$	E3.5(b)
R	H	$K_5 > 0$	0.4	$\overline{1} \quad 10$	$\overline{-2.5} \quad -1$	0.8	0.5	E3.9(b)
R	H	$K_4 > 0$	0.4	$\overline{1} \quad 10$	$\overline{1} \quad 10$	0.8	0.5	E3.10(a)
R	SN	$K_1 - K_2 K_3 / K_6 > 0$	0.4	$\overline{1} \quad 10$	$\overline{1} \quad 10$	0.8	0.5	E3.12(b)
U	SN	$K_1 - K_2 K_3 K_4 > 0$	0.4	$\overline{1} \quad 10$	$\overline{1} \quad 10$	0.8	0.5	E3.11(a)
U	SN	$K_1 - K_2 K_3 K_4 > 0$	0.4	$\overline{1} \quad 10$	$\overline{-2.5} \quad -1$	0.8	0.5	E3.11(b)

Table 6.3 (c) Combination model: Non-bifurcation cases

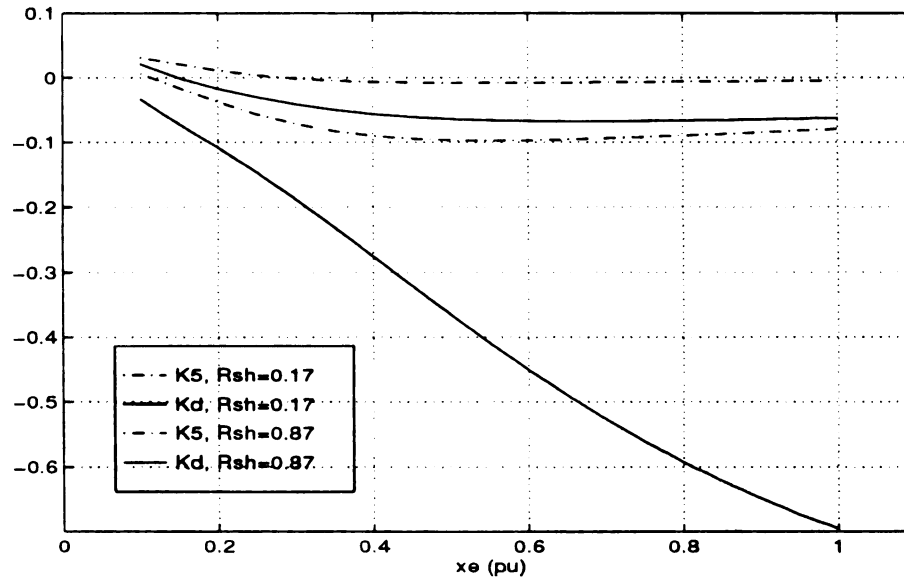


Figure 6.4 Combination Model: Damping torque coefficient K_d and parameter K_5 for different levels of real local loading

6.2.5 Discussion of the Combination Model Results

How do the power transfer and local loading models predict, disagree, or possibly extend the results obtained from the combination model?. The combination model diagnostic study shows that combining both models may extend or confirm the results from each individual model, depending on operating conditions or stress is dominating. The following conclusions are drawn:

- a) Although local capacitive or inductive local loading ($X_{sh} < 0$ or $X_{sh} > 0, P_{\infty} = Q_{\infty} = 0$) did not cause Hopf bifurcation in the regulated model in the local load diagnostic study for reactive supply ($Q_{\infty} \geq 0$) to the infinite bus, local inductive or capacitive loading in combination with reactive power supply to the infinite bus ($X_{sh} = \pm 0.17, Q_{\infty} \geq 0$) appears to drive the system to oscillatory instability (Figures E3.1(a) and E3.2(a)). This extends the local loading model results and allows the diagnostic conclusion that the regulated model Hopf bifurcation can occur when the reactive power is supplied to the infinite bus. The problem is aggravated when real power supply P_{∞} increases and real loading ($1/R_{sh}$) decreases. This result may be due to the transfer of power to the infinite bus over a weak but extremely weak line.
- b) Although local capacitive loading ($X_{sh} < 0$ or $X_{sh} > 0, P_{\infty} = Q_{\infty} = 0$) did not cause Hopf in the regulated model, for reactive power supply from the infinite bus ($Q_{\infty} \leq 0$) local capacitive or inductive loading (Figure E3.1(b), E3.2(b)) in combination with reactive power supply from the infinite bus ($X_{sh} = \pm 0.17, Q_{\infty} \leq 0$) seem to drive the system to oscillatory instability. This extends the local loading model results and allows the diagnostic conclusion that the regulated model Hopf can occur when reactive power is supplied from the infinite bus. The problem is aggravated when real

power supply P_∞ increases and real loading ($1/R_{sh}$) decreases. This result may be due to the large active power transfer to the infinite bus, and reactive power transfer from the infinite bus.

- c) For saddle node bifurcation, although power transfer stress seems to affect the unregulated model synchronizing torque, and not the regulated model, in the combination model the following bifurcation occurred:
 - (i) SN bifurcation in the regulated model occurs when the local load is real-capacitive ($X_{sh} = -0.17$), active power transfer to the infinite bus is increased and reactive power from the infinite bus is increased (Figures E3.6(a-b)). This bifurcation was not observed in the power transfer model diagnosis, but appears to be caused by the presence of the heavy capacitive local load $|1/X_{sh}| \approx 6$, as diagnosed by the local loading model.
 - (ii) SN in the unregulated model for power transfer ($P_\infty \geq 0, Q_\infty \geq 0$) to the infinite bus and either $X_{sh} > 0$, or $X_{sh} < 0$). These results (Figures E3.7(a), E3.8(a)) are consistent with the SN bifurcation results obtained from the power transfer model.
- (d) The effect of local loading stress seems to be less severe in the presence of real and reactive power transfer to the infinite bus. The local loading model diagnosis showed that $K_4 \leq 0$ for the entire range of R_{sh} - X_{sh} . In the combination model, Figure E3.10 (a) shows that the parameter $K_4 > 0$ for a significant portion of the operating range of R_{sh} - X_{sh} .

6.3 Diagnostic Summary

The diagnostic study demonstrated that the cause and effect of a specific kind of bifurcation in the SMIB model are dependent on (1) the effect of the relay-type control action, i.e. whether the system is regulated or unregulated; (2) local loading-power transfer operating requirement patterns; and (3) transmission network inductance. The comprehensive power transfer and local loading pattern variations in the three study models, has been the mean for drawing (if possible) conclusions for diagnosing the causes of SN and Hopf bifurcations in the SMIB. Furthermore, the results establish the classes of saddle node and Hopf bifurcations that were observed in the SMIB model.

6.3.1 Classes of Hopf Bifurcation in a SMIB Model

H1: Power Swing Mode (Regulated)

This oscillation mode occurs when K_f is negative in the single machine infinite bus model, when the voltage regulator is still operating within its fields current limits. This oscillation is observed in the generator angle/speed/flux decay dynamics, and is associated with low frequency inter-area oscillations. It is a supercritical (stable) Hopf bifurcation since these oscillations are stable inter-area oscillations. It is often referred to as a power swing mode, since it is brought on by considerable power transfer between two areas. The power swing mode can be associated with a single generator, two generators or with groups of generators. There are two subclasses:

1. Reactive Power Supply Swing Mode (regulated)
2. Reactive Power Absorption Swing Model (regulated)

H.2: Voltage Collapse Mode (Unregulated)

Occurs in the inertial and flux decay dynamics of the generator in a single machine infinite bus model, when the exciter is completely disabled, and the single machine parameter K_4 is negative. These classes of Hopf bifurcations are likely to be the limit cycles that develop as a precursor to voltage collapse and thus are called voltage collapse modes. It is not clear whether voltage collapse oscillatory modes are supercritical or subcritical Hopf bifurcations. The diagnostic study showed that these undamped oscillations in the unregulated SMIB model are associated with (i) heavy loaded local load centers; (ii) local shunt capacitive system compensation; (iii) transmission lines with high capacitive line charging; and (iv) when power transfer from or to the infinite bus is not possible. There are two subclasses:

- 1- Reactive Power Supply Voltage Collapse Mode (unregulated)
- 2- Reactive absorption Voltage Collapse Mode (unregulated)

It should be noted that there is a Voltage Mode that is subcritical Hopf bifurcation that depends solely on the exciter and flux decay dynamics.

6.3.2 Classes of Static Bifurcation in a SMIB Model (SN)

Similarly, two classes of static bifurcation may occur on a Type 2 power system model:

SN.1 Static Bifurcation in generator inertial dynamics (Regulated)

Static bifurcation in generator inertial dynamics may be associated with the loss of transient stability [36] such as the voltage instability that occurred in the Czechoslovakian system after tripping lines in a major interface [30]. This class of static bifurcation is likely to occur when the disturbances are very large and the

transmission interfaces or boundaries are weak, so that loss of stability occurs soon after the contingency before the field current level/duration limits are reached. It would appear from the results in this chapter that the static bifurcation in generator inertial dynamics occurs the local network is capacitive near a local generator, real power is shipped away from that generator, and reactive power is shipped to that generator.

SN.2 Static Bifurcation in generator inertial dynamics(Unregulated)

This bifurcation has been called classic voltage instability and is due to insufficient reactive supply in the EHV system, an example of which is the blackout that occurred in the French system [37]. This class of stability has been analyzed with the use of a sensitivity matrix T between reactive generation and voltage at generator internal buses [51] that is diagonally dominant for inductive networks (networks that absorb reactive power), and not diagonally dominant for capacitive network (network with long high voltage transmission lines). Classic voltage instability has been described as occurring when generators reach their field current limits and the field current limit controllers disable the exciters. An important implication to this result is that studying this saddle node bifurcation must include the field current limit controllers action in the model.

VII

Thesis Summary and Future Research

7.1 Dissertation summary

This thesis addressed three major difficulties in diagnosing the cause of a specific stability problem in a power system. These difficulties are (a) the size and complexity of the model, (b) the various kinds and classes of bifurcation that can occur in the model, and (c) the lack of smoothness in the dynamic behavior after a disturbance or during operation, (d) the inability to determine a subsystem of the full model that experiences the same bifurcation as the full system for each kind and class of bifurcation. These different problems in a power system have been and still are in need of better methods for stability analysis, developing application software, and problem diagnosis in a large power system. This thesis will address all four problems and hopefully provide the basis for methods that can be utilized to establish where, why, and what can be done to prevent loss of stability for three kinds (kinds) of bifurcation: Hopf, saddle node, and Load Flow bifurcations observed on a specific power system model as well as all of the specific subsystems of the model affected by each particular kind of bifurcation (classes). The contributions of this work can be summarized in the following four sections:

A) Diagnostic Classification

First, the diagnostic study started by classifying (a) the model types used in power system studies, (b) the kind and (c) class of bifurcations. This classification is performed in Chapter 2 of the thesis. The kind and class of a bifurcation observed depends on the model used. Four model types are classified: Type1 model is the simplest model where both generator and loads are modeled by algebraic equations and under load tap changers (ULTCs) and switchable shunt capacitors controls are modeled. Type 4 model represents both generators and loads by differential equations and yet all the ULTCs controls dynamics and switching capacitor inductors, etc. are included. Type2 and Type 3 models are simplified Type 4 models that eliminate the load dynamics and generator dynamics respectively. The complete Type 4 dynamic model has been developed only for small test systems.

B) Epoch Bases Trajectory Stability Assessment Method

Virtually every local bifurcation is brought on by a sequence of equipment outages and hard-limit discontinuities enabling or disabling various controls. Although dynamic system theory is fairly well developed for smooth systems, it is currently being developed for nonsmooth systems. These hard limit discontinuities do not cause immediate enablement or disablement of a particular control. The dynamical system theory for nonsmooth systems [27] is not sufficiently well developed to be able to determine the sequence of hard limit discontinuities when each discontinuity has a different length time delay. Current dynamical system theory for smooth system can be applied to intervals (t_i^*, t_{i+1}^-) called epochs where discontinuities occur only at $[t_i]$, the discontinuous change

at $[t_i]$ can be computed; and the time $T_i = t_{i+1}^* - t_i^*$ is long compared to the settling time of the dynamics. Therefore, a method aimed at assessing asymptotic stability of the transient during (t_i^*, t_{i+1}^*) and the stability of quasi equilibria or limit cycles in each epoch is proposed. This method called the Epoch Based Trajectory Stability Assessment, is based on a trajectory simulation method implemented by [28] that does not require time simulation in (t_i^*, t_{i+1}^*) , but only computes the quasi equilibria (\bar{x}_i, \bar{y}_i) for each epoch for $i = 1, \dots, N$. This method allows the assessment of the stability of individual trajectories for a power system by assessing stability for every epoch through (a) assessing stability of the sequence of quasi equilibria or the limit cycles, and (b) the asymptotic stability to each quasi equilibrium or limit cycle.

C) Bifurcation Subsystem Method:

A third a major contribution in this diagnostic framework is the establishment of the Bifurcation Subsystem Method, This method attempts to identify the smallest subsystem, a subset of the equations of the full system model that experiences and causes the same bifurcation that occurs in the full system model. A bifurcation subsystem can loosely be defined as a truncated portion of the actual power system model that experiences the same bifurcation in the full system model. The Bifurcation Subsystem Method utilizes the geometry associated with the various submatrices of the full system differential-algebraic

Jacobian $J = \begin{bmatrix} f_x & f_y \\ g_x & g_y \end{bmatrix}$ since

$$\text{Det}(J) = \text{Det}(g_y) \cdot \text{Det}(f_x - f_y g_y^{-1} g_x) \text{ when } g_y \text{ is nonsingular;}$$

$$\text{Det}(J) = \text{Det}(f_x) \cdot \text{Det}(g_y - g_x f_x^{-1} f_y) \text{ when } f_x \text{ is nonsingular;}$$

and with the eigenvectors associated with the bifurcating eigenvalue to establish

conditions for existence of such systems. The fact that the Jacobian of the truncated portion of the system (g_y) must be singular somewhat restricts the set of possible subsystems that one is using to find the bifurcation subsystem. The bifurcation subsystem must satisfy both the linear and the transversality test conditions for bifurcation that is used to test for bifurcation in the full system model. The null space of the effects of the truncated system ($f_y g_y^{-1} g_x$) must be common with the null space of the bifurcation subsystem (f_x) in which the right or left eigenvector of the bifurcating eigenvalue resides. The portion of the full system external to this bifurcation subsystem has no effect on the linear conditions for bifurcation to be satisfied in the full system model only at bifurcation (asymptotic), or as bifurcation develops for $\mu \neq \mu^*$ (structural), and yet the equilibrium point is dependent on the variations in the full system equations which results in bifurcation in both the full system and the bifurcation subsystem. Propositions for the existence of bifurcation subsystems for a particular kind of bifurcation were derived and proved. Possible bifurcation subsystems in a power system Type 2 model are:

- (a) Differential Bifurcation Subsystem Experiencing SN;
- (b) Differential Bifurcation Subsystem Experiencing Hopf;
- (c) Algebraic Bifurcation Subsystem for LF;
- (d) Differential Bifurcation Sub-subsystem Experiencing SN;
- (e) Differential Bifurcation Sub-subsystem Experiencing Hopf;
- (g) Differential-algebraic Bifurcation Subsystem.

It should be noted that the bifurcation subsystem is not the center manifold of a specific bifurcation since the same bifurcation subsystem could exist for saddle node bifurcation in the flux decay dynamics, and for saddle node bifurcation in the inertial dynamics. The

sensitivity matrices K_S , K_D and T also do not necessarily identify the center manifold dynamics, and thus do not necessarily identify the exact class and location of a specific bifurcation. The research has shown that what is desired is not to determine the center manifold dynamics, but rather a subsystem of the original model that experiences the same bifurcation as the full system. The bifurcation subsystem may in most cases be an excellent approximation of the possibly larger subsystem that causes and produces the bifurcation in the full model, as it is the desired result. The root locus of the bifurcating eigenvalue and the participation factor information provides additional diagnostic information on such a subsystem.

Determining sensitivity matrices K_S , K_D or T as a function of the model parameters K_1 - K_6 and then studying how K_S , K_D or T vary with changes in operating conditions and hard limit discontinuities also can assist in indicating the subsystem that produces, causes and cures a specific bifurcation, in special cases.

D) Stability Conditions and Diagnosis:

Lastly, the Epoch Based Trajectory Stability Assessment Method and the Bifurcation Subsystem Method are the framework for initiating a diagnostic study for Hopf and saddle node bifurcations on a single-machine-infinite bus (SMIB) model to (a) computationally demonstrate and validate the use of the bifurcation subsystem method to identify bifurcation subsystems in the SMIB; (b) identify the classes of saddle node and Hopf bifurcations that may occur in the SMIB model: the generator angle/speed dynamics and angle/speed/flux decay dynamics are bifurcation subsystems for Hopf and SN bifurcations in both the regulated and unregulated SMIB models, respectively; (c) gain better

understanding on the effects of hard limits by assessing the effect of excitation control on the types and classes of bifurcations produced; and (d) establish an understanding to the causes, operational and structural stresses, and stabilizing requirements for SN, local and inter-area modes of oscillations that occur in generator inertial, flux decay and exciter dynamics of the SMIB model. This study was performed by formulating three study model: (1) a power transfer model; (2) a local loading model; and (3) a combination power-transfer/local loading model. The diagnostic study demonstrated that the cause and effect of a specific kind of bifurcation in the SMIB model are dependent on (1) the effect of the relay-type control action, i.e whether the system is regulated or unregulated; (2) Local loading or power transfer operating patterns; and (3) transmission network inductance across interfaces.

7.2 Future Research

The following topics are subjects for further investigation:

1. Develop a load flow program based on the Bifurcation Subsystem Method to obtain load flow bifurcation subsystems that experience the same bifurcation as the full system, but also include what produces and causes the bifurcation. Evaluate how load flow subsystems change with (a) decoupling of P-V and Q- Θ Jacobian submatrices; (b) generator reaching field current limits; (c) under-load tap changers reaching tap limits; (d) switchable shunt capacitors reaching shunt susceptance limits; and (e) the effects of multiple contingencies. This knowledge allows the prediction of the most critical bifurcation subsystem in the system for a load flow model, given any equipment outage or operating condition combination using proximity measures and diag-

nostic tools. A heuristic method has been developed for identifying bifurcation subsystems that experience the bifurcation of the full system, given certain assumptions are true. The work would establish the bifurcation subsystems when the assumptions are not made and when they are true.

2. Develop a dynamic stability program based on the Bifurcation Subsystem Method to obtain dynamic bifurcation subsystems that not only experience the bifurcation of the full model, but also produce and cause the bifurcation. Evaluate these subsystems change with (a) decoupling the generator/load dynamics of the system; (b) hard limit discontinuities in generator and network controls; and with (c) the effects of multiple contingencies. This knowledge allows the prediction of the most critical bifurcation subsystem in the system for a differential-algebraic model for any equipment outage or operating condition combination using proximity measures and diagnostic tools.
3. Develop proximity measures for each class of bifurcation subsystem found in a load flow or a differential algebraic model. These proximity measures can be (a) reactive reserves on a particular group of generators; (b) measures of properties of sensitivity matrices like K_S , K_D or T ; (c) measures of properties of the system matrices K_1 - K_6 ; or (d) measures of properties of the Jacobian of the bifurcation subsystem that produced the bifurcation.
4. Develop diagnostic procedures for identifying the kind, class, location, cause, and remedial action needed for each bifurcation subsystem or class of bifurcation identi-

fied in a load flow or differential algebraic model. The diagnosis should be based on identifying how the system matrix A ; sensitivity matrices like K_s , K_D or T ; sensitivity matrices K_1 - K_6 ; or Jacobian matrix J are affected by load, transfer, reactive reserve exhaustion, etc. that produce each bifurcation class.

APPENDICES

APPENDIX A
POWER SYSTEM DYNAMIC MODEL

Appendix A

Power System Dynamic Model

A.1 Nonlinear Model

The dynamic model of the full power system [52] is described in this section. Without loss of generality, we assume that the connection between each generator and its high-side bus is equivalently one-to-one, and that the power system has n buses total buses including m machines with m high-side buses and $(n-m)$ other (load) buses. The subscripts used in the various variables used in the model equations, are described here:

Subscript t : represents the generator terminal PV-buses (including switchable shunt capacitor buses. Eg: P_{Gt} , P_{Ct} , V_t ... etc, $t = 2, \dots, m$.

Subscript H : represents the generator-transformer high-side PQ-buses. Eg: P_{Gt} , P_{Ct} .

Subscript L : represents the rest of the P-Q buses. Eg: P_{Cl}

Subscript G : represents the active or reactive power generations

Subscript C : represents the non-voltage (i.e constant) active or reactive power load or injection

A.1.1 Swing Equation

For each synchronous machine,

$$\dot{\delta} = \omega - \omega_o$$

$$M \dot{\omega} = -D(\omega - \omega_o) + P_m - P_e$$

Where

δ : angular rotor position, measures in electrical radians of the relative to a synchronous rotating frame

ω : angular speed

ω_0 : nominal angular speed

D : approximate damping constant due to damper winding effects(pu/(rad/s))

$M = 2H/\omega_0$: moment of inertia (sec/(rad/sec))

H : moment of inertia constant (MW - sec/MVA)

P_m : mechanical input power to the machine

P_e : electric power output of each generator

A.1.2 Flux Decay Equation

For each synchronous machine,

$$T'_{do}\dot{E}'_q = E_{fd} - K_{E3}E'_q + (x_d - x'_d) \cdot U_{qt} \cdot V_t$$

$$K_{E3} = 1 - (x_d - x'_d) \cdot B_q > 1$$

$$U_{qt} = G_a \sin(\delta - \theta_t) - B_q \cos(\delta - \theta_t)$$

$$G_a = \frac{R_a}{R_a^2 + x'_d x_q} \quad ; \quad B_q = \frac{-x_q}{R_a^2 + x'_d x_q}$$

Where

T'_{do} : d-axis open-circuit transient time constant

E_{fd} : field winding voltage

E'_q : induced stator voltage due to the flux linkage of the filed winding

A.1.3 Excitation system

A typical excitation system in shown in Figure A1, is responsible for controlling the terminal voltage. Using the following notation:

V_C : output of load (or line drop) compensator

V_S : output of power system stabilizer (PSS)

V_{ref} : reference (set point) voltage

V_D : voltage detector output

K_D : dc (direct current) gain of voltage detector

- T_D : time constant of voltage detector
 T_{GR} : transient gain reduction
 T_B : lagging time constant of TGR
 T_C : leading time constant of TGR
 V_A : output of automatic voltage regulator (AVR)
 K_A : dc gain of AVR
 T_A : time constant of AVR
 E_{fd} : output of exciter (field voltage of synchronous machine)
 $1/K_{SE}$: dc gain of exciter. Note that K_{SE} is function of the saturation effect of the exciter.
 T_E/K_{SE} : time constant of exciter
 K_F : washout gain of stabilizing feedback of excitation system
 T_F : washout time constant of stabilizing feedback of excitation system

The state space model of the IEEE-DC1 excitation system is given by

$$\begin{bmatrix} T_D \dot{V}_D \\ T_F \dot{V}_F \\ T_A \dot{V}_A \\ T_B \dot{V}_B \\ T_E \dot{E}_{fd} \end{bmatrix} = \begin{bmatrix} -1 & 0 & 0 & 0 & 0 \\ 0 & -1 & 0 & 0 & -K_F/T_F \\ -K_A \frac{T_C}{T_B} & -K_A \frac{T_C}{T_B} & -1 & K_A & -K_A \left(\frac{T_C}{T_B} \right) \left(\frac{K_F}{T_F} \right) \\ -\left(1 - \frac{T_C}{T_B} \right) & -\left(1 - \frac{T_C}{T_B} \right) & 0 & -1 & -\left(1 - \frac{T_C}{T_B} \right) \left(\frac{K_F}{T_F} \right) \\ 0 & 0 & 1 & 0 & -K_{SE} \end{bmatrix} \begin{bmatrix} V_D \\ V_F \\ V_A \\ V_B \\ E_{fd} \end{bmatrix} + \begin{bmatrix} K_D V_C \\ 0 \\ K_A \left(\frac{T_C}{T_B} \right) (V_{ref} + V_S) \\ \left(1 - \frac{T_C}{T_B} \right) (V_{ref} + V_S) \\ 0 \end{bmatrix}$$

A.1.4 Power System Stabilizer

A power system stabilizer improves the dynamic stability of a synchronous machine and/or a power system, using other regulator input signals in addition to terminal voltage through its excitation system. Some common stabilizer input signals are accelerating power, machine speed, frequency and terminal voltage. A state space model for the PSS model shown in Figure A2 may be written using V_{S0} , V_{S2} and V_{S4} shown in the block diagram.

$$\begin{bmatrix} T_S \dot{V}_{S0} \\ T_{S2} \dot{V}_{S2} \\ T_{S4} \dot{V}_{S4} \end{bmatrix} = \begin{bmatrix} -1 & 0 & 0 \\ 1 - \frac{T_{S1}}{T_{S2}} & -1 & 0 \\ \left(1 - \frac{T_{S3}}{T_{S4}}\right) \frac{T_{S1}}{T_{S2}} & 1 - \frac{T_{S3}}{T_{S4}} & -1 \end{bmatrix} \begin{bmatrix} V_{S0} \\ V_{S2} \\ V_{S4} \end{bmatrix} + \begin{bmatrix} -K_S \\ \left(1 - \frac{T_{S1}}{T_{S2}}\right) K_S \\ \left(1 - \frac{T_{S3}}{T_{S4}}\right) \left(\frac{T_{S1}}{T_{S2}}\right) K_S \end{bmatrix} V_{SI}$$

$$V_S = \frac{T_{S3} T_{S1}}{T_{S4} T_{S2}} K_S V_{SI} + \frac{T_{S3} T_{S1}}{T_{S4} T_{S2}} V_{S0} + \frac{T_{S3}}{T_{S4}} V_{S2} + V_{S4}$$

A.1.5 Speed-Governing-Turbine System Model

The speed-governing system controls the mechanical input power, using a turbine system and rotor speed as an input signal. Figure A3 present the general model of speed governing system, for steam-turbine and hydro-turbine. In the figure, P_{GV} is the power at the gate or valve and represents the input of the turbine system. The state space model of the speed-governing-turbine system may be obtained by combining both models.

a. Speed Governing-Turbine

$$\begin{bmatrix} T_1 \dot{P}_1 \\ T_3 \dot{P}_{GV} \\ T_{CH} \dot{P}_{VHP} \\ T_{RH1} \dot{P}_{HP} \\ T_{RH2} \dot{P}_{IP} \\ T_{CO} \dot{P}_{LP} \end{bmatrix} = \begin{bmatrix} -1 & 0 & 0 & 0 & 0 & 0 \\ -1 & -1 & 0 & 0 & 0 & 0 \\ 0 & 1 & -1 & 0 & 0 & 0 \\ 0 & 0 & 1 & -1 & 0 & 0 \\ 0 & 0 & 0 & 1 & -1 & 0 \\ 0 & 0 & 0 & 0 & 1 & -1 \end{bmatrix} \begin{bmatrix} P_1 \\ P_{GV} \\ P_{VHP} \\ P_{HP} \\ P_{IP} \\ P_{LP} \end{bmatrix} + \begin{bmatrix} K_G \left(1 - \frac{T_2}{T_1}\right) (\omega - \omega_o) \\ -K_G \left(1 - \frac{T_2}{T_1}\right) (\omega - \omega_o) + P_o \\ 0 \\ 0 \\ 0 \\ 0 \end{bmatrix}$$

$$P_M = F_{VHP} P_{VHP} + F_{HP} P_{HP} + F_{IP} P_{IP} + F_{LP} P_{LP}$$

b. Hydraulic Governing-Turbine

$$\begin{bmatrix} T_1 \dot{P}_1 \\ T_3 \dot{P}_{GV} \\ T_W \dot{P}_W \end{bmatrix} = \begin{bmatrix} -1 & 0 & 0 \\ -1 & -1 & 0 \\ 0 & a_{WG} & -a_{WW} \end{bmatrix} \begin{bmatrix} P_1 \\ P_{GV} \\ P_{VHP} \end{bmatrix} + \begin{bmatrix} K_G \left(1 - \frac{T_2}{T_1}\right) (\omega - \omega_o) \\ -K_G \left(1 - \frac{T_2}{T_1}\right) (\omega - \omega_o) + P_o \\ 0 \end{bmatrix}$$

$$P_M = F_{GV} P_{GV} + P_W \quad ; \quad a_{WG} = \frac{a_{13} a_{21}}{a_{11}^2} \quad ; \quad a_{WW} = \frac{1}{a_{11}} \quad ; \quad F_{GV} = a_{23} - \frac{a_{13} a_{21}}{a_{11}}$$

A.1.7 Load Compensator Model

The load compensator uses the terminal voltage and current as feedback measurement of the excitation system model. A state space representation of this model is given by:

$$V_C = V_t + (R_C + jX_C)I_t = V_{Cd} + jV_{Cq}$$

$$V_{Cd} = K_{d2} \dot{E}_q' + K_{d7} V_t$$

$$V_{Cq} = K_{q2} \dot{E}_q' + K_{q7} V_t$$

Where,

$$K_{d2} = -(X_C G_a + R_C B_q)$$

$$K_{q2} = R_C G_a - X_C B_q$$

$$K_{d7} = (1 + X_C B_d' - R_C G_a) \sin(\delta - \theta_t) - K_{d2} \cos(\delta - \theta_t)$$

$$K_{q7} = (1 - K_{q2}) \cos(\delta - \theta_t) - (X_C G_a + R_C B_d') \sin(\delta - \theta_t)$$

A.1.6 Algebraic Load Flow equation

(i) *At Internal Bus:* for each synchronous machine

$$P_e = E'^2 G_{EE} - E'_q V_t T_{PE} + V_t^2 G_{Et}$$

$$Q_e = E'^2 B_{EE} + -E'_q V_t U_{QE} - V_t^2 B_{Et}$$

(ii) *At terminal Bus: for $t = n+1, \dots, n+m; h = 1, \dots, m$*

$$-P_{Dt} = V_t^2 G_{tq} - V_t E'_q T_{tq} + V_t^2 (G_{Cth} + G_{th}) - V_t V_h T_{th}$$

$$-Q_{Dt} = -V_t^2 B_{tq} + -V_t E'_q U_{tq} - V_t^2 (B_{Cth} + B_{th}) - V_t V_h U_{th}$$

(iii) *At high-side bus: for $h = 1, \dots, m; t = n+h$, we have*

$$-P_{Dh} = V_h^2 (G_{Cht} + G_{ht}) - V_h V_t T_{ht} + V_h^2 \sum_{j=1}^n (G_{Chj} + G_{hj}) - \sum_{j=1}^n V_t V_j T_{tj} \quad i \neq j$$

$$-Q_{Dh} = -V_h^2 (B_{Cht} + B_{ht}) - V_h V_t U_{ht} - V_h^2 \sum_{j=1}^n (H_{Chj} + H_{hj}) - \sum_{j=1}^n V_t V_j U_{tj} \quad i \neq j$$

(iv) *At load bus: for $i = m+1, \dots, n$, we have*

$$-P_{Di} = V_i^2 \sum_{j=1}^n (G_{Cij} + G_{ij}) - \sum_{j=1}^n V_i V_j T_{ij} \quad i \neq j$$

$$-Q_{Di} = -V_i^2 \sum_{j=1}^n (B_{Cij} + B_{ij}) - \sum_{j=1}^n V_i V_j U_{ij} \quad i \neq j$$

$$T_{ij} = G_{ij} \cos(\theta_i - \theta_j) + B_{ij} \sin(\theta_i - \theta_j) \quad i \neq j$$

$$U_{ij} = G_{ij} \sin(\theta_i - \theta_j) - B_{ij} \cos(\theta_i - \theta_j) \quad i \neq j$$

$$G_{ij} = G_{ij} \sin(\theta_i - \theta_j) + B_{ij} \sin(\theta_i - \theta_j)$$

$$U_{ij} = G_{ij} \sin(\theta_i - \theta_j) - B_{ij} \cos(\theta_i - \theta_j)$$

A.2 Linearized Power System Model

Taylor series expansion is used to obtain a linear model about a nominal isolated equilibrium point. Linearization is necessary for the load demand model, power balance equations, swing equation, flux decay equation and load compensator. The jacobian matrix full linear model is expressed in terms of submatrices that are explicitly given below.

$$\begin{bmatrix} T_{XX}\Delta\dot{X}_X \\ T_{EE}\Delta\dot{X}_E \\ T_{GG}\Delta\dot{X}_G \\ T_{SS}\Delta\dot{X}_S \\ -\Delta P_C \\ -\Delta Q_C \end{bmatrix} = \begin{bmatrix} A_{XX} & A_{XE} & A_{XG} & 0 & A_{X\theta} & A_{XV} \\ A_{EX} & A_{EE} & 0 & A_{ES} & A_{E\theta} & A_{EV} \\ A_{GX} & 0 & A_{GG} & 0 & 0 & 0 \\ A_{SX} & 0 & 0 & A_{SX} & 0 & 0 \\ A_{PX} & 0 & 0 & 0 & A_{P\theta} & A_{PV} \\ A_{QX} & 0 & 0 & 0 & A_{Q\theta} & A_{QV} \end{bmatrix} \begin{bmatrix} \Delta X_X \\ \Delta X_E \\ \Delta X_G \\ \Delta X_S \\ \Delta\theta \\ \Delta V \end{bmatrix} + B_o \Delta U_o$$

Where,

$$f_x = \begin{bmatrix} T_{XX} & 0 & 0 & 0 \\ 0 & T_{EE} & 0 & 0 \\ 0 & 0 & T_{GG} & 0 \\ 0 & 0 & 0 & T_{SS} \end{bmatrix}^{-1} \begin{bmatrix} A_{XX} & A_{XE} & A_{XG} & 0 \\ A_{EX} & A_{EE} & 0 & A_{ES} \\ A_{GX} & 0 & A_{GG} & 0 \\ A_{SX} & 0 & 0 & A_{SX} \end{bmatrix} ; f_y = \begin{bmatrix} T_{XX} & 0 & 0 & 0 \\ 0 & T_{EE} & 0 & 0 \\ 0 & 0 & T_{GG} & 0 \\ 0 & 0 & 0 & T_{SS} \end{bmatrix}^{-1} \begin{bmatrix} A_{X\theta} & A_{XV} \\ A_{E\theta} & A_{EV} \\ 0 & 0 \\ 0 & 0 \end{bmatrix}$$

$$\Delta X_X = [\Delta\omega^t \ \Delta\delta^t \ \Delta E_F^t]^t : \text{states of mechanical and flux decay dynamics;}$$

$$\Delta E_F = [\Delta E_q'^t \ \Delta E_d'^t \ \Delta\Psi_{ld}^t \ \Delta\Psi_{lq}^t]^t : \text{states of flux decay dynamics}$$

$$\Delta X_E = [\Delta V_D^t \ \Delta V_F^t \ \Delta V_A^t \ \Delta V_B^t \ \Delta E_{fd}^t]^t : \text{states of excitation system}$$

$$\Delta X_G = [\Delta P_1^t \ \Delta P_{GV}^t \ \Delta P_{VHP}^t \ \Delta P_{HP}^t \ \Delta P_{IP}^t \ \Delta P_{LP}^t]^t$$

:states of speed-governing-turbine systems;

$$\Delta X_S = [\Delta V_{S0}^t \ \Delta V_{S2}^t \ \Delta V_{S4}^t]^t : \text{states of power system stabilizer;}$$

$$\Delta\theta = [\Delta\theta_T^t \ \Delta\theta_H^t \ \Delta\theta_L^t]^t : \text{angle variables at network buses;}$$

$$\Delta V = [\Delta V_T^t \ \Delta V_H^t \ \Delta V_L^t]^t : \text{voltage variables at network buses;}$$

$$\Delta P_C = [\Delta P_{CT}^t \ \Delta P_{CH}^t \ \Delta P_{CL}^t]^t$$

: coefficients of non-voltage-dependent active power load demand model;

$$\Delta Q_C = [\Delta Q_{CT}^t \ \Delta Q_{CH}^t \ \Delta Q_{CL}^t]^t$$

: coefficients of non-voltage-dependent reactive power load demand model;

$T_{XX} = \text{diag}[M \ I \ T'_{do}]$: diagonal matrix composed of inertia constants of synchronous machines, identity matrix, and time constants of flux decay dynamics;

$T_{EE} = \text{diag}[T_D \ T_F \ T_A \ T_B \ T_E]$: time constants of the excitation systems dynamics;

$T_{GG} = \text{diag}[T_1 \ T_3 \ T_{CH} \ T_{RH1} \ T_{RH1} \ T_{CO}]$

: time constants of speed-governing-turbine systems;

$T_{SS} = \text{diag}[T_S \ T_{S2} \ T_{S4}]$: time constants of power system stabilizers;

$M = \text{diag}[M_1 \ M_2, \dots, M_m]$: inertia constants for m synchronous machines

I : $m \times m$ identity matrix

T'_{do} : $m \times m$ diagonal matrix of time constants of flux decay dynamics

$$A_{XX} = \begin{bmatrix} -D & -K_{P1}^{qt} & -K_{P2}^{qt} \\ I & 0 & 0 \\ 0 & -K_{E4} & -K_{E3} \end{bmatrix} \quad A_{XE} = \begin{bmatrix} 0 & 0 & 0 & 0 & 0 \\ 0 & 0 & 0 & 0 & 0 \\ 0 & 0 & 0 & 0 & I \end{bmatrix} \quad A_{XG} = \begin{bmatrix} 0 & 0 & F_{VHP} & F_{HP} & F_{IP} & F_{LP} \\ 0 & 0 & 0 & 0 & 0 & 0 \\ 0 & 0 & 0 & 0 & 0 & 0 \end{bmatrix}$$

$$A_{SX} = \begin{bmatrix} -K_S & 0 & 0 \\ I_{21}K_S & 0 & 0 \\ I_{43}T_{21}K_S & 0 & 0 \end{bmatrix} \quad A_{SS} = \begin{bmatrix} -I & 0 & 0 \\ I_{21} & -I & 0 \\ I_{43}T_{21} & I_{43} & -I \end{bmatrix} \quad A_{X\theta} = \begin{bmatrix} K_{P1}^{qt} & 0 & 0 \\ 0 & 0 & 0 \\ K_{E4} & 0 & 0 \end{bmatrix}$$

$$A_{PX} = \begin{bmatrix} 0 & -K_{P1}^{iq} & -K_{P2}^{iq} \\ 0 & 0 & 0 \\ 0 & 0 & 0 \end{bmatrix} \quad A_{QX} = \begin{bmatrix} 0 & -K_{Q1}^{iq} & K_{Q2}^{iq} \\ 0 & 0 & 0 \\ 0 & 0 & 0 \end{bmatrix} \quad A_{P\theta} = \begin{bmatrix} A_{1K} & B_{1H} & 0 \\ A_{2H} & B_{2HH} & B_{2HL} \\ 0 & B_{2LH} & B_{2LL} \end{bmatrix}$$

$$A_{PV} = \begin{bmatrix} C_{1K} & D_{1H} & 0 \\ C_{2H} & D_{2HH} & D_{2HL} \\ 0 & D_{2LH} & D_{2LL} \end{bmatrix} \quad A_{Q\theta} = \begin{bmatrix} A_{3K} & B_{3H} & 0 \\ A_{4H} & B_{4HH} & B_{4HL} \\ 0 & B_{4LH} & B_{4LL} \end{bmatrix} \quad A_{QV} = \begin{bmatrix} C_{3K} & D_{3H} & 0 \\ C_{4H} & D_{4HH} & D_{4HL} \\ 0 & D_{4LH} & D_{4LL} \end{bmatrix}$$

$$A_{ES} = \begin{bmatrix} 0 & 0 & 0 \\ 0 & 0 & 0 \\ K_A^T B C^T T_{43} T_{21} & K_A^T B C^T T_{43} & K_A^T B C \\ I_{BC}^T T_{43} T_{21} & I_{BC}^T T_{43} & I_{BC} \\ 0 & 0 & 0 \end{bmatrix} \quad A_{EE} = \begin{bmatrix} -I & 0 & 0 & 0 & 0 \\ 0 & -I & 0 & 0 & -T_F^{-1} K_F \\ -K_A^T B C & -K_A^T B C & -I & K_A & -K_A^T B C^T T_F^{-1} K_F \\ -I_{BC} & -I_{BC} & 0 & -I & -I_{BC}^T T_F^{-1} K_F \\ 0 & 0 & I & 0 & -K_{SE} \end{bmatrix}$$

$$A_{EX} = \begin{bmatrix} 0 & K_D K_{C1} & K_D K_{C2} \\ 0 & 0 & 0 \\ A_{Aw} & 0 & 0 \\ A_{Bw} & 0 & 0 \\ 0 & 0 & 0 \end{bmatrix} \quad A_{X\theta} = \begin{bmatrix} -K_D K_{C1} & 0 & 0 \\ 0 & 0 & 0 \\ 0 & 0 & 0 \\ 0 & 0 & 0 \\ 0 & 0 & 0 \end{bmatrix} \quad A_{EV} = \begin{bmatrix} -K_D K_{C7} & 0 & 0 \\ 0 & 0 & 0 \\ 0 & 0 & 0 \\ 0 & 0 & 0 \\ 0 & 0 & 0 \end{bmatrix}$$

$$A_{GX} = \begin{bmatrix} [I - T_1^{-1} T_2] K_G & 0 & 0 \\ -T_1^{-1} T_2 K_G & 0 & 0 \\ 0 & 0 & 0 \\ 0 & 0 & 0 \\ 0 & 0 & 0 \\ 0 & 0 & 0 \end{bmatrix} \quad A_{GG} = \begin{bmatrix} -I & 0 & 0 & 0 & 0 & 0 \\ -I & -I & 0 & 0 & 0 & 0 \\ 0 & I & -I & 0 & 0 & 0 \\ 0 & 0 & I & -I & 0 & 0 \\ 0 & 0 & 0 & I & -I & 0 \\ 0 & 0 & 0 & 0 & I & -I \end{bmatrix} \quad B_{E0} = \begin{bmatrix} 0 & 0 \\ 0 & 0 \\ K_A^T B C & 0 \\ I - T_{BC} & 0 \\ 0 & 0 \end{bmatrix} \quad B_{G0} = \begin{bmatrix} 0 & 0 \\ 0 & I \\ 0 & 0 \\ 0 & 0 \\ 0 & 0 \\ 0 & 0 \end{bmatrix}$$

$$A_{XV} = \begin{bmatrix} -K_{P1}^{qt} & 0 & 0 \\ 0 & 0 & 0 \\ K_{E7} & 0 & 0 \end{bmatrix}$$

$$A_{1K} = K_{P1}^{iq} + A_1 ; \quad A_{1K} = K_{P7}^{iq} + C_1 ; \quad A_{3K} = K_{Q1}^{iq} + A_3 ; \quad C_{3K} = K_{Q7}^{iq} + C_3$$

$$I_{43} = I + T_{43} ; \quad I_{21} = I + T_{21} ; \quad T_{43} = T^{-1} s_4 T_{S3} ; \quad T_{21} = T^{-1} s_2 T_{S1} ; \quad T_{BC} = T_B^{-1} T_C$$

$$I_{BC} = I - T_{BC} ; \quad A_{Aw} = K_A^T B C^T T_{43} T_{21} K_S ; \quad B_{Bw} = I_{BC} T_{43} T_{21} K_S$$

$$K_{E4} = -(x_d - x'_d) \cdot T_{qt} V_t$$

$$K_{E7} = -(x_d - x'_d) \cdot U_{qt}$$

$$U_{PE} = k_1 U_{dt} - G_a (x_q - x'_d) T_{qt}$$

$$T_{PE} = k_1 T_{dt} - G_a (x_q - x'_d) U_{qt}$$

$$U_{QE} = k_2 U_{dt}$$

$$T_{QE} = k_2 T_{dt}$$

$$K_{P1}^{qt} = E'_q V_t U_{PE} + V_t^2 (x_q - x'_d) (T_{dt} T_{qt} - U_{dt} U_{qt})$$

$$K_{P2}^{qt} = 2E'_q G_{EE} - V_t T_{PE}$$

$$K_{Q1}^{qt} = -E'_q V_t T_{QE} + 2V_t^2 (x_q - x'_d) U_{qt} T_{qt}$$

$$K_{Q2}^{qt} = -2E'_q B_{EE} - V_t U_{QE}$$

$$K_{P7}^{qt} = 2V_t G_{Et} - E'_q T_{PE}$$

$$K_{Q7}^{qt} = -2V_t B_{Et} - E'_q U_{QE}$$

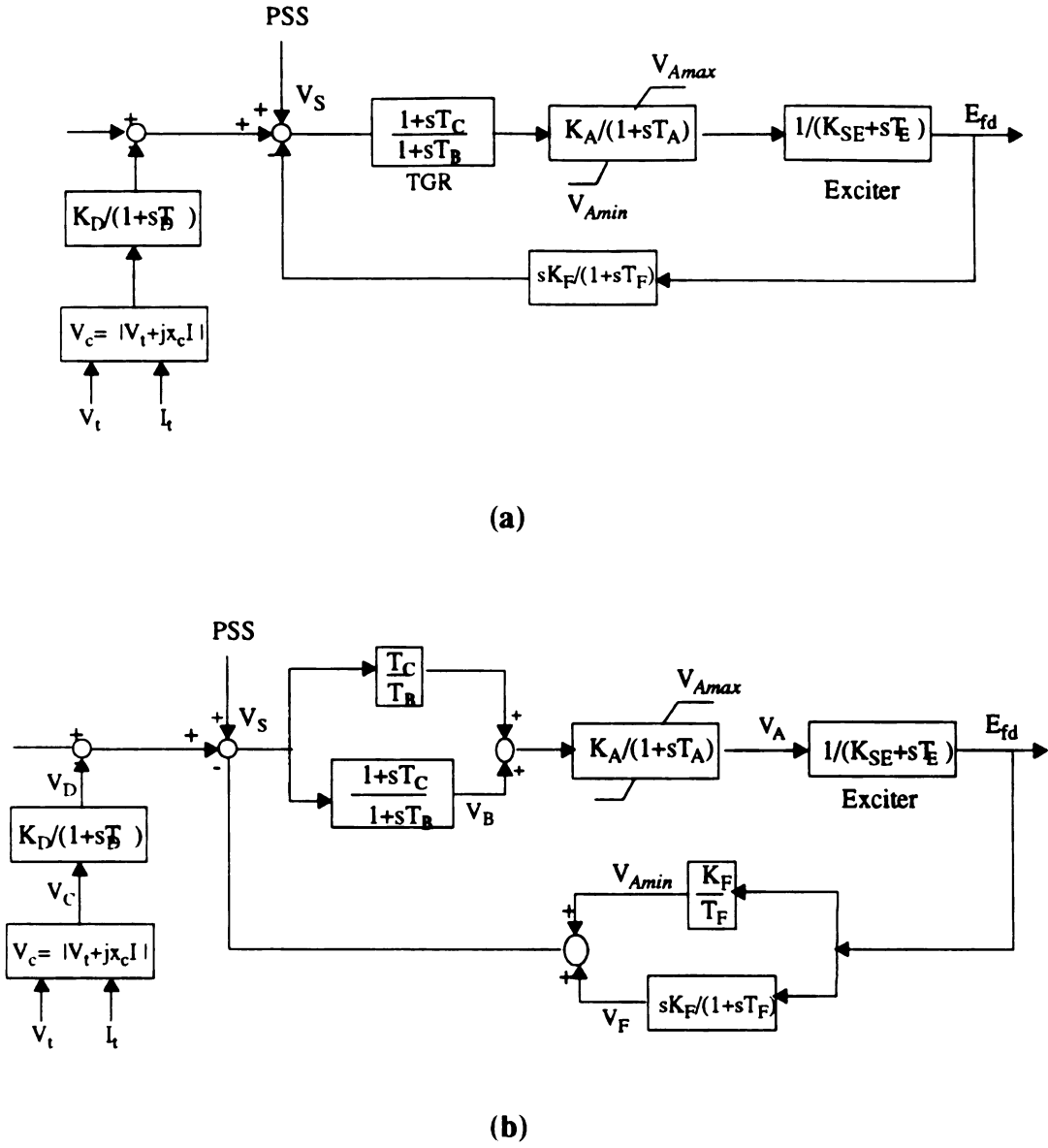


Figure A1. IEEE-DC1 Excitation System Model

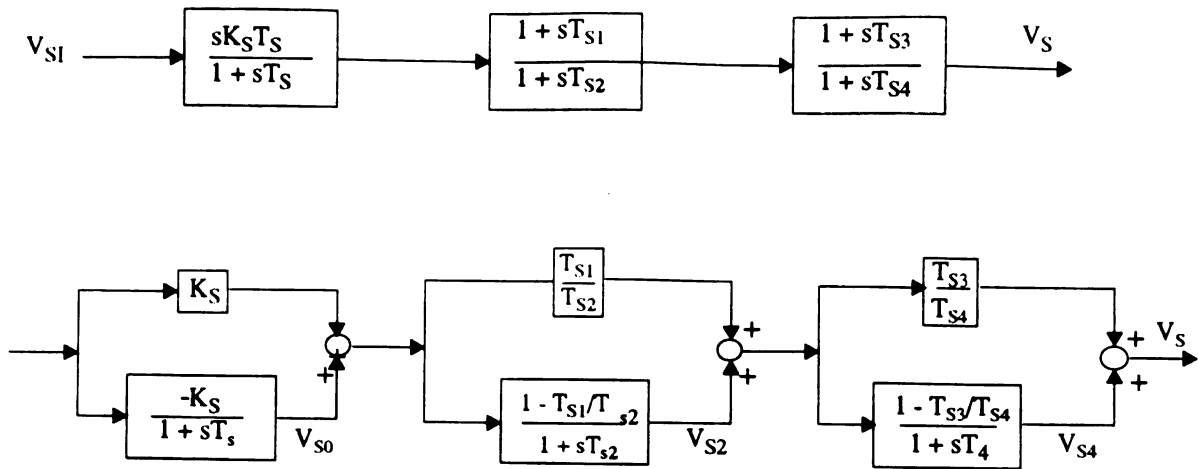


Figure A2. Power system stabilizer model

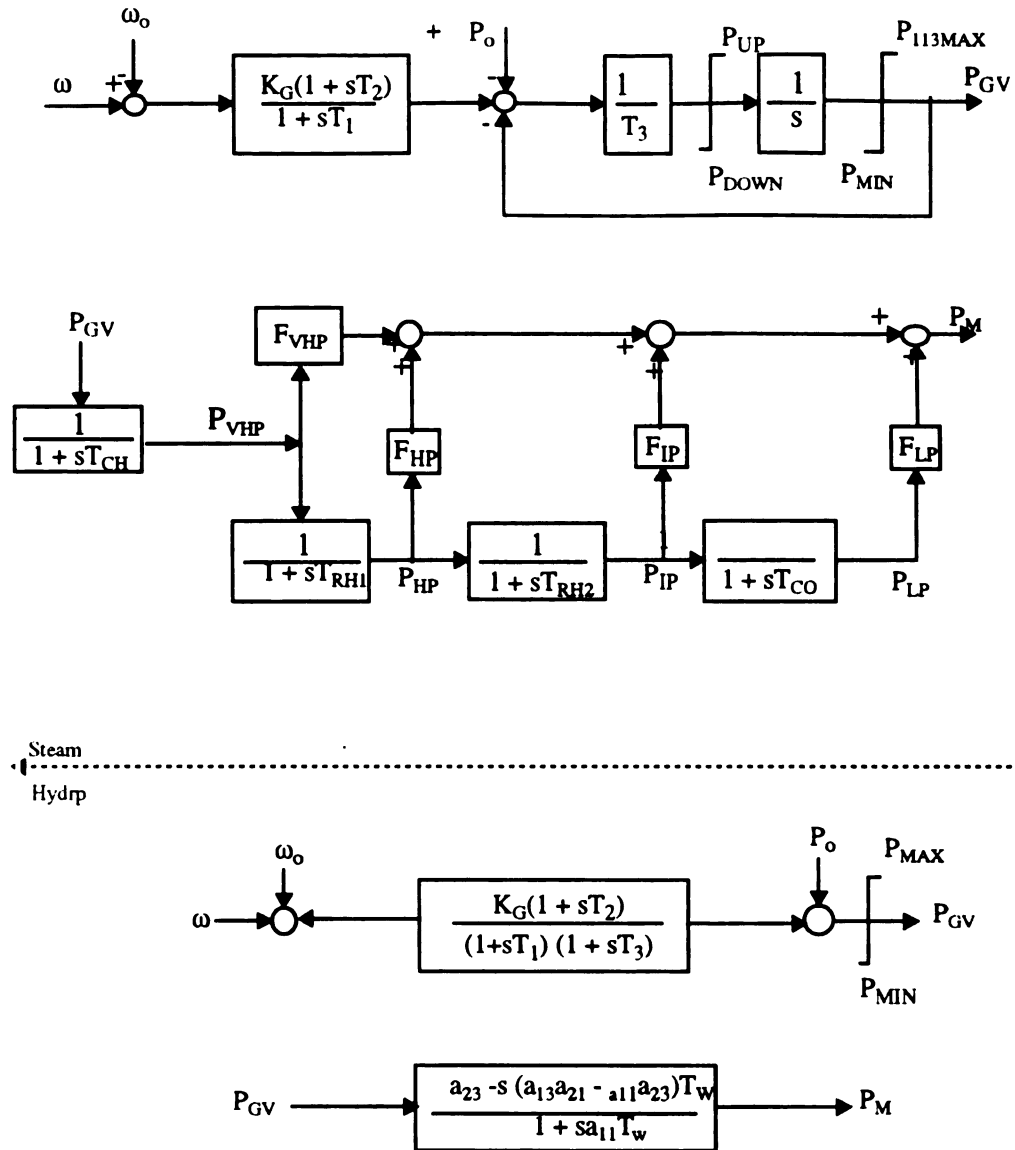


Figure A3. Speed-Governing-Turbine System Model

APPENDIX B

COMMON DEFINITIONS FOR POWER SYSTEM STABILITY

APPENDIX B

COMMON DEFINITIONS FOR POWER SYSTEM STABILITY

In order to facilitate analysis of stability problems, identify the essential associated factors and to formulate methods of assessing and improving stable operation, stability problems have been classified into appropriate categories. A classification recently presented in [29], summarizes the most widely used stability definitions, the associated concepts, and the related terms. The classification is based on the following considerations: (a) the physical nature of the resulting instability, (b) The size of the disturbance considered, (c) the devices, processes and time span required to determine stability.

B.1 Rotor angle stability

Any unbalance between the generation and load results in a net accelerating (or decelerating) torque exerted on the rotors. From the swing equation, we see that this transient causes the rotors of the synchronous machines to “swing”. If the net torque is sufficiently large to cause the rotor to swing far enough so that one or more machines “slip a pole”, synchronism is lost. However an appreciable increase in the machine’s rotor angular velocities does not necessarily mean that synchronism will be lost. The important factor is the angle difference between machines, where the rotor angle is measured with respect to a synchronously rotating reference. Rotor angle stability is the ability of interconnected synchronous machines of a power system to remain in synchronism after

being subject to a transient disturbance.

B.2 Small signal (or small-disturbance) stability

It is the ability of the power system to maintain synchronism when subject to small disturbances. The disturbances are considered small enough to cause a small change from the operating equilibrium point, so that linearization of system equations is permissible. The powerful tool of linear system theory may therefore be explored for purpose of analysis.

B.3 Transient stability

Transient stability is the ability of a system to maintain synchronism when subjected to a severe disturbance. The system response involves large excursion of the generator rotor angle. Stability depends on both the initial state and the severity of the disturbance. Usually the system is altered so that the post-disturbance steady state operating point differs from that prior to the disturbance.

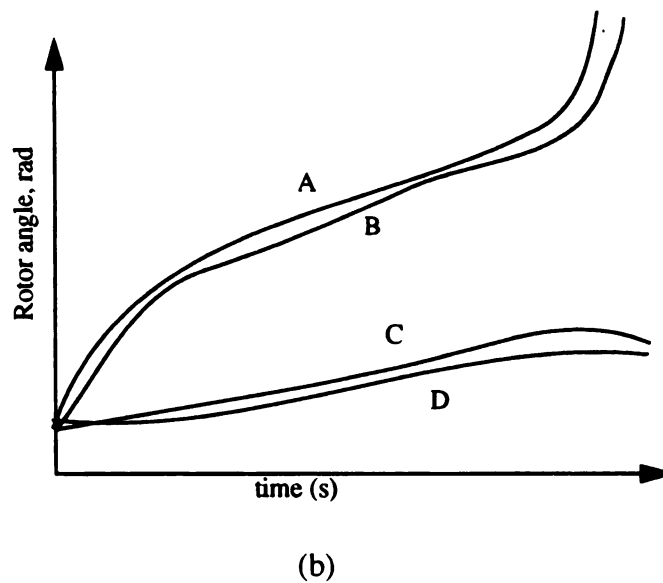
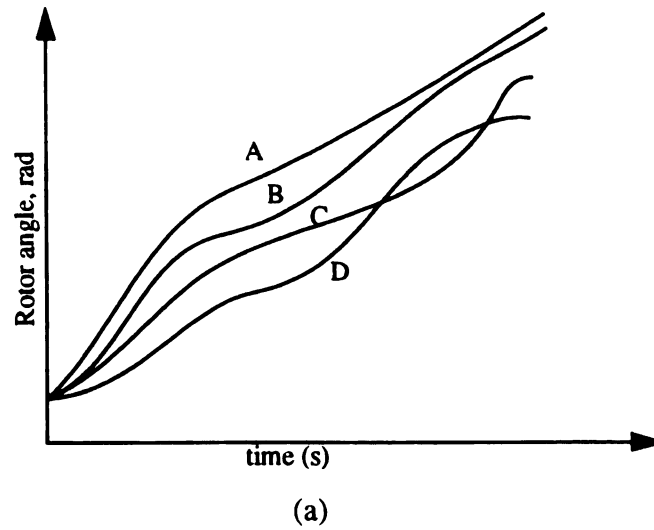


Figure B1. Response of a four-machine system during a transient [57]
(a) stable system; (b) unstable system

B.4 Voltage stability and voltage collapse

A power system at a given operating state is voltage stable, if an injection of reactive power causes the voltage magnitude at this node increases and all other voltages also increase or at least do not decrease. A system enters a state of voltage instability if a

disturbance, increase in load demand, or a change in system condition causes a progressive and uncontrollable drop in voltage.

APPENDIX C

DEFINITION OF HOPF AND SADDLE NODE BIFURCATIONS WITH TRANSVERSALITY CONDITIONS

Appendix C

Definition of Hopf and Saddle Node Bifurcations with Transversality Conditions

Hopf and Saddle node bifurcations have been recognized as the two generic bifurcations in variety of power system models, and are generally detected by monitoring the eigenvalues at a certain operating point, as a particular parameter of interest is varied slowly. Saddle node involves the coalescence and disappearance of two neighboring equilibrium points, while Hopf involves the emergence of a small amplitude periodic orbit from an equilibrium as the parameter is varied

(a1) Saddle Node Bifurcation

Let $\dot{x} = f(x, \mu)$ be a system of differential equations in R^n depending on the single parameter μ . At $\mu = \mu^*$, assume that there is an equilibrium point $\bar{X} = (\bar{x}(\mu^*), \mu^*)$ for which the following hypotheses are satisfied

(SN1) $f_x = \partial f / \partial x(\bar{x}(\mu^*), \mu^*)$ has one simple eigenvalue $\lambda(\mu^*) = 0$ with right eigenvector v and left eigenvector w . f_x all other $(n-1)$ eigenvalues with negative real part

(SN2) $w \cdot [\partial f / \partial \mu(\bar{x}(\mu^*), \mu^*)] \neq 0$

(SN3) $w \cdot [(\partial f / \partial \mu(\bar{x}(\mu^*), \mu^*))(v, v)] \neq 0$

Then the system undergoes a saddle node bifurcation from $\bar{X} = (\bar{x}(\mu^*), \mu^*)$

(a2) Hopf-Andronov Bifurcation

Let $\dot{x} = f(x, \mu)$ be a system of differential equations in R^n depending on the single parameter μ . At $\mu = \mu^*$, assume that there is an equilibrium point $\bar{X} = (\bar{x}(\mu^*), \mu^*)$ for which the following hypotheses are satisfied

(H1) $f_x = \partial f / \partial x(\bar{x}(\mu^*), \mu^*)$ has a simple zero eigenvalue $\lambda(\mu^*) = 0$ and no other eigenvalues with zero real part.

(H2) $\frac{d}{d\mu}(Re\lambda(\mu))|_{\mu=\mu^*} \neq 0$ (Transversality condition)

Then a small amplitude non-constant periodic orbit of $\dot{x} = f(x, \mu)$ emerges from

$\bar{X} = (\bar{x}(\mu^*), \mu^*)$ at $\mu = \mu^*$

APPENDIX D

**INPUT DATA FILES FOR THE BIFURCATION
SUBSYSTEM EXAMPLES**

APPENDIX D

INPUT DATA FOR BIFURCATION SUBSYSTEM EXAMPLES

EXAMPLE 1 (SN)

```
% The single machine infinite bus system for power system
% stabilizer design
% datasmib.m

% bus data format
% bus: number, voltage(pu), angle(degree), p_gen(pu),
%      q_gen(pu), p_load(pu), q_load(pu), gshunt, bshunt,
%      bus_type
%      bus_type - 1, swing bus
%                 - 2, generator bus (PV bus)
%                 - 3, load bus (PQ bus)
% the voltage on bus 2 is adjusted for zero Q at machine 1
bus = [ 1 1.05      0.0   0.7   0.4  0.0  0.0  0.00  0.300  2;
        2 1.08103  0.0   0.0   0.0  0.0  0.0  0.0  0.0  1;
        3 1.0      0     0     0    0    0    0.0  0.0  3];

% line data format
% line: from bus, to bus, resistance(pu), reactance(pu),
%       line charging(pu), tap ratio, phase shifter angle

line = [1 3 0.0 0.61 0. 1. 0.;
        2 3 0.0 0.1000 0. 1. 0.;
        2 3 0.0 0.1000 0. 1. 0.];

% Machine data format
% machine: 1. machine number
%          2. bus number
%          3. base mva
%          4. leakage reactance x_l(pu)
%          5. resistance r_a(pu)
%          6. d-axis synchronous reactance x_d(pu)
%          7. d-axis transient reactance x'_d(pu)
%          8. d-axis subtransient reactance x''_d(pu)
%          9. d-axis open-circuit time constant T'_do(sec)
%          10. d-axis open-circuit subtransient time
%              constant T''_do(sec)
%          11. q-axis synchronous reactance x_q(pu)
```

```

%      12. q-axis transient reactance x'_q(pu)
%      13. q-axis subtransient reactance x''_q(pu)
%      14. q-axis open-circuit time constant T'_qo(sec)
%      15. q-axis open circuit subtransient time
%           constant T''_qo(sec)
%      16. inertia constant H(sec)
%      17. damping coefficient d_o(pu)
%      18. dampling coefficient d_l(pu)
%      19. bus number
%      20. S(1.0) - saturation factor
%      21. S(1.2) - saturation factor
% note: machine 1 uses mac_sub model, machine 2 uses mac_em
%      model
mac_con = [
1 1 991    0.15 0    2.0 0.2    0.2 5.0 0.031 1.91 0.2 0.2 ...
0.66 0.061 2.8756    0.0 0    1 0 0;
2 2 100000 0.00 0    0.  0.01 0    0    0    0    0    ...
0    0    3.0    2.0 0    2 0 0];
% Exciter data format
% exciter:  1. exciter type - 3 for ST3
%           2. machine number
%           3. input filter time constant T_R
%           4. voltage regulator gain K_A
%           5. voltage regulator time constant T_A
%           6. voltage regulator time constant T_B
%           7. voltage regulator time constant T_C
%           8. maximum voltage regulator output V_Rmax
%           9. minimum voltage regulator output V_Rmin
%          10. maximum internal signal V_Imax
%          11. minimum internal signal V_Imin
%          12. first stage regulator gain K_J
%          13. potential circuit gain coefficient K_p
%          14. potential circuit phase angle theta_p
%          15. current circuit gain coefficient K_I
%          16. potential source reactance X_L
%          17. rectifier loading factor K_C
%          18. maximum field voltage E_fdmax
%          19. inner loop feedback constant K_G
%          20. maximum inner loop voltage feedback V_Gmax
% exc_con = [
% 3 1 0 7.04 0.4 0.00 1.0 7.57 0 0.2 -0.2 200 4.365 20 ...
% 4.83 0.091 1.096 6.53 1 6.53];

```

EXAMPLE 2 (Hopf)

```

% The singl machine infinite bus system for power system
% stabilizer design
% datasmib.m

% bus data format
% bus: number, voltage(pu), angle(degree), p_gen(pu),
%      q_gen(pu), p_load(pu), q_load(pu), gshunt, bshunt,
%      bus_type

```

```

%      bus_type - 1, swing bus
%              - 2, generator bus (PV bus)
%              - 3, load bus (PQ bus)
% the voltage on bus 2 is 90 degrees adjusted for zero Q at machine 1
%      #   V      ang   Pg    Qg    Pl    Ql    Gsh  Bsh  type
bus = [ 1 1.05      0.0   0.90   0.80  0.0   0.0   0.0   0.0   2;
        2 1.08103  0.0   0.0    0.0  0.0   0.0   0.0   0.0   1;
        3 1.0      0     0     0    0.7  0.4   0.0   0.0   3];

% line data format
% line: from bus, to bus, resistance(pu), reactance(pu),
%       line charging(pu), tap ratio, phase shifter angle
%       fr to r    x    chg  tap pshft
line = [1 3 0.0 0.6      0.    1.  0.;
        2 3 0.0 0.01     0.    1.  0.;
        2 3 0.0 0.01     0.    1.  0.];

% Machine data format
% machine:  1. machine number
%           2. bus number
%           3. base mva
%           4. leakage reactance x_l(pu)
%           5. resistance r_a(pu)
%           6. d-axis synchronous reactance x_d(pu)
%           7. d-axis transient reactance x'_d(pu)
%           8. d-axis subtransient reactance x''_d(pu)
%           9. d-axis open-circuit time constant T'_do(sec)
%          10. d-axis open-circuit subtransient time
%              constant T''_do(sec)
%          11. q-axis synchronous reactance x_q(pu)
%          12. q-axis transient reactance x'_q(pu)
%          13. q-axis subtransient reactance x''_q(pu)
%          14. q-axis open-circuit time constant T'_qo(sec)
%          15. q-axis open circuit subtransient time
%              constant T''_qo(sec)
%          16. inertia constant H(sec)
%          17. damping coefficient d_o(pu)
%          18. damping coefficient d_l(pu)
%          19. bus number
%          20. S(1.0) - saturation factor
%          21. S(1.2) - saturation factor
% note: machine 1 uses mac_sub model, machine 2 uses mac_em
%       model
mac_con = [
1 1 991      0.15 0   2.0 0.245 0.2 5.0 0.031 1.91 0.42 0.2 ...
0.66 0.061  2.8756  0.0 0   1 0 0;
2 2 100000 0.00 0   0. 0.01 0   0   0   0   0   0 ...
0   0       3.0     2.0 0  2 0 0];

% Exciter data format
% exciter:  1. exciter type - 3 for ST3
%           2. machine number
%           3. input filter time constant T_R

```

```

%      4. voltage regulator gain K_A
%      5. voltage regulator time constant T_A
%      6. voltage regulator time constant T_B
%      7. voltage regulator time constant T_C
%      8. maximum voltage regulator output V_Rmax
%      9. minimum voltage regulator output V_Rmin
%     10. maximum internal signal V_Imax
%     11. minimum internal signal V_Imin
%     12. first stage regulator gain K_J
%     13. potential circuit gain coefficient K_p
%     14. potential circuit phase angle theta_p
%     15. current circuit gain coefficient K_I
%     16. potential source reactance X_L
%     17. rectifier loading factor K_C
%     18. maximum field voltage E_fdmax
%     19. inner loop feedback constant K_G
%     20. maximum inner loop voltage feedback V_Gmax
exc_con = [
3 1 0.00 1.9 0.19 3.7 0.08 7.57 0 0.2 -0.2 400 4.365 23 ...
4.83 1.0 1.096 6.53 2.949 6.53];

```

APPENDIX E1

FIGURES FOR DIAGNOSTIC ANALYSIS POWER TRANSFER MODEL

APPENDIX E1

FIGURES FOR DIAGNOSTIC ANALYSIS POWER TRANSFER MODEL

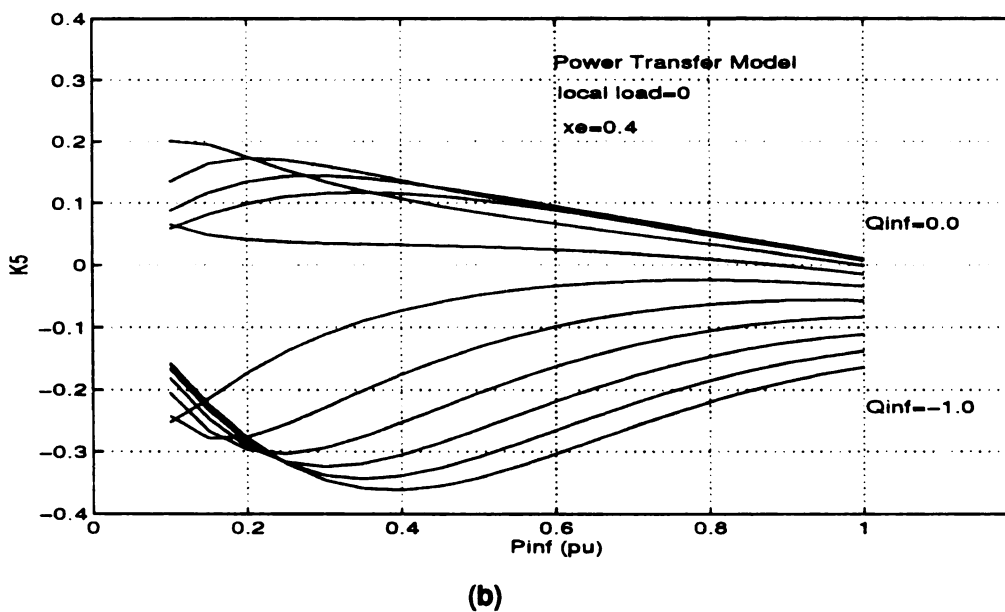
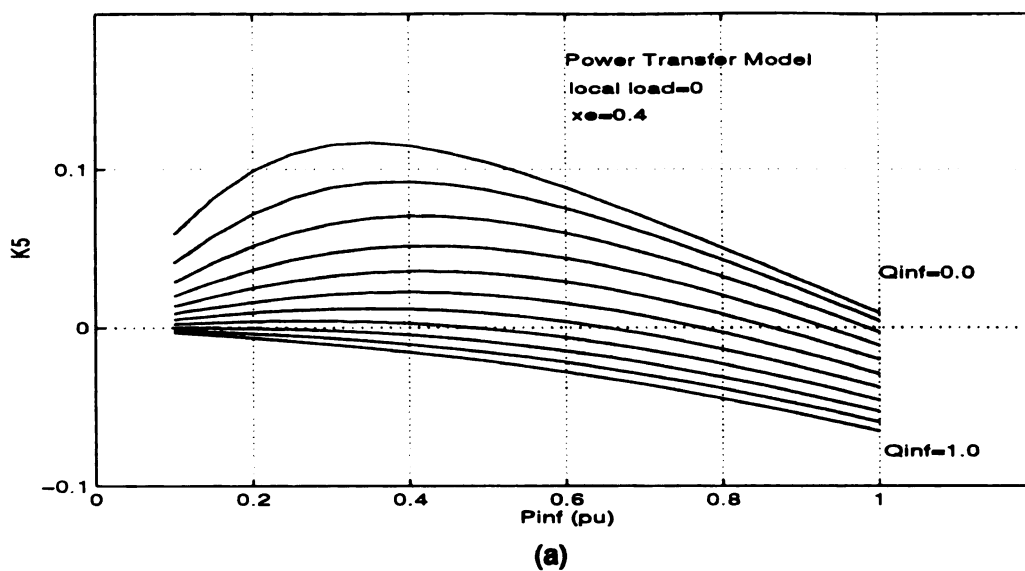


Figure E1.1 Power Transfer Model: Effect of real and reactive power transfer to the infinite bus on the parameter K_5 . (a) Real and reactive power flow in the same direction, (b) Real and reactive power flow in opposite directions.

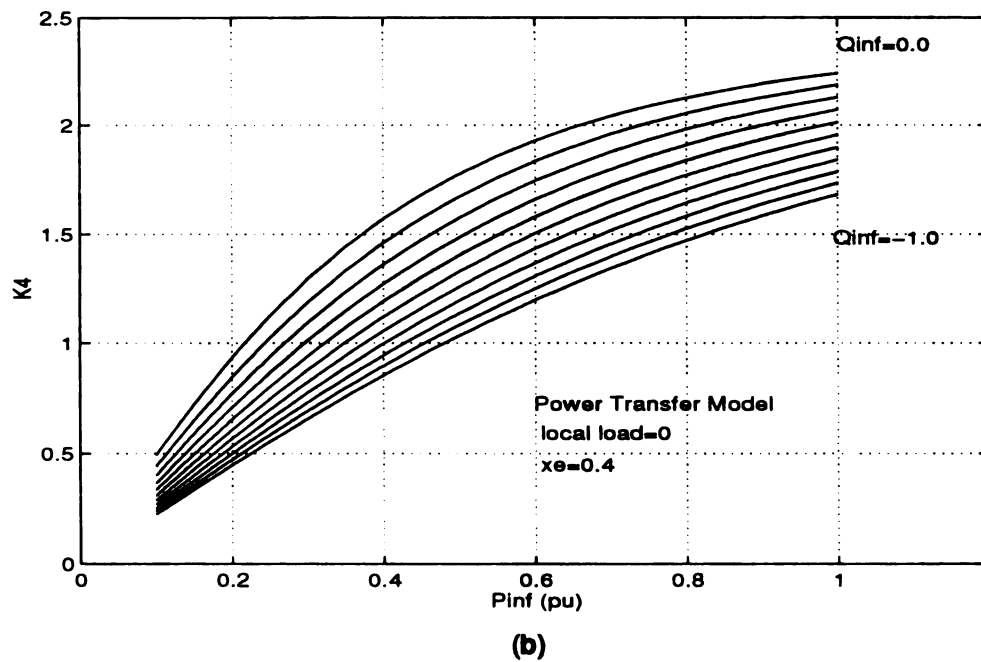
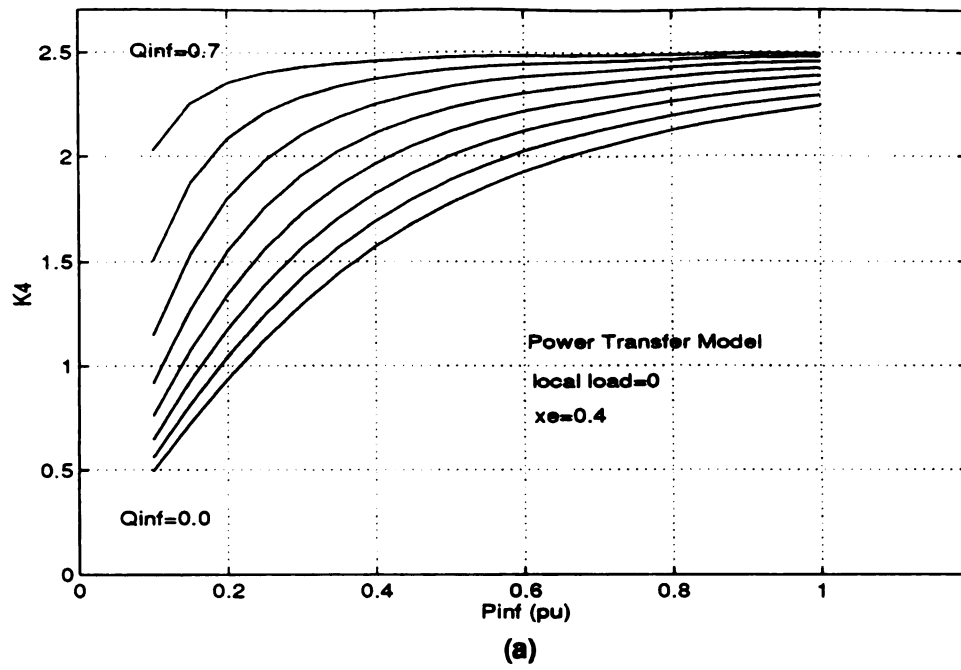
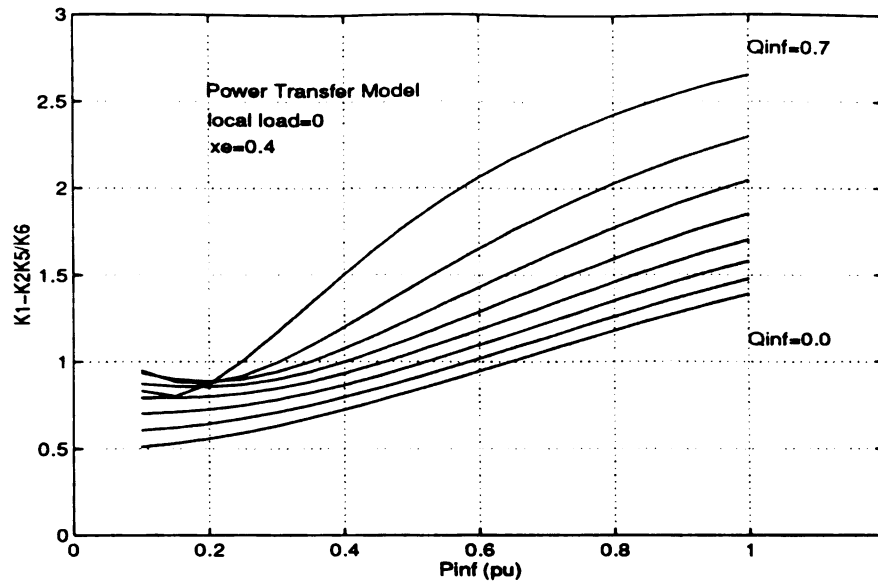
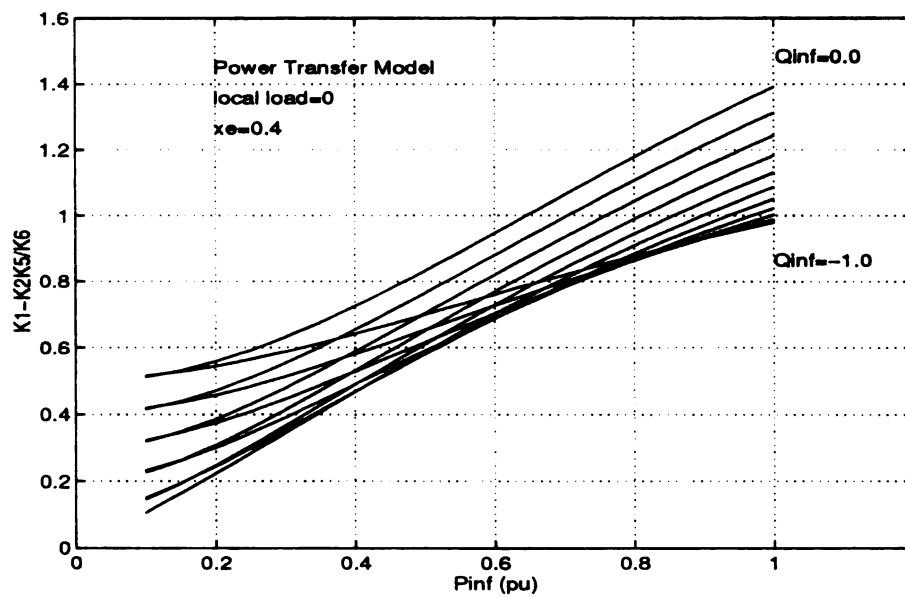


Figure E1.2 Power Transfer Model: Effect of real and reactive power transfer to the infinite bus on the parameter K_4 . (a) Real and reactive power flow in the same direction, (b) Real and reactive power flow in opposite directions.

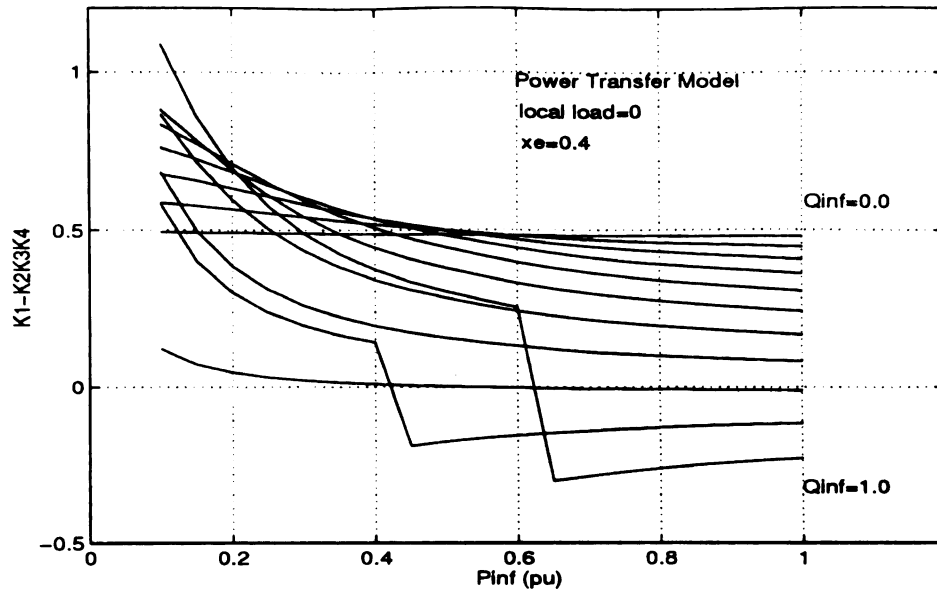


(a)

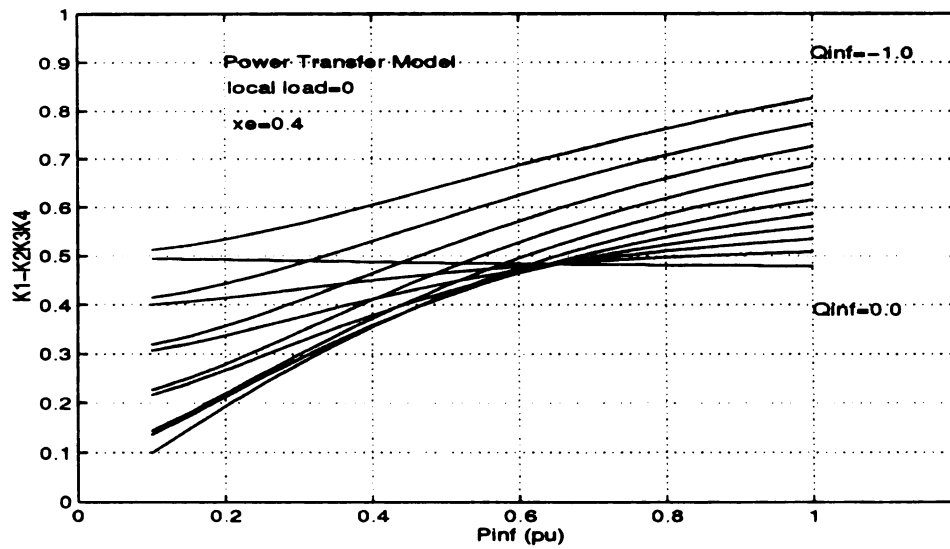


(b)

Figure E1.3 Power Transfer Model: Effect of real and reactive power transfer to the infinite bus on the parameter $K_1 - K_2K_5/K_6$. (a) Real and reactive power flow in the same direction, (b) Real and reactive power flow in opposite directions.



(a)



(b)

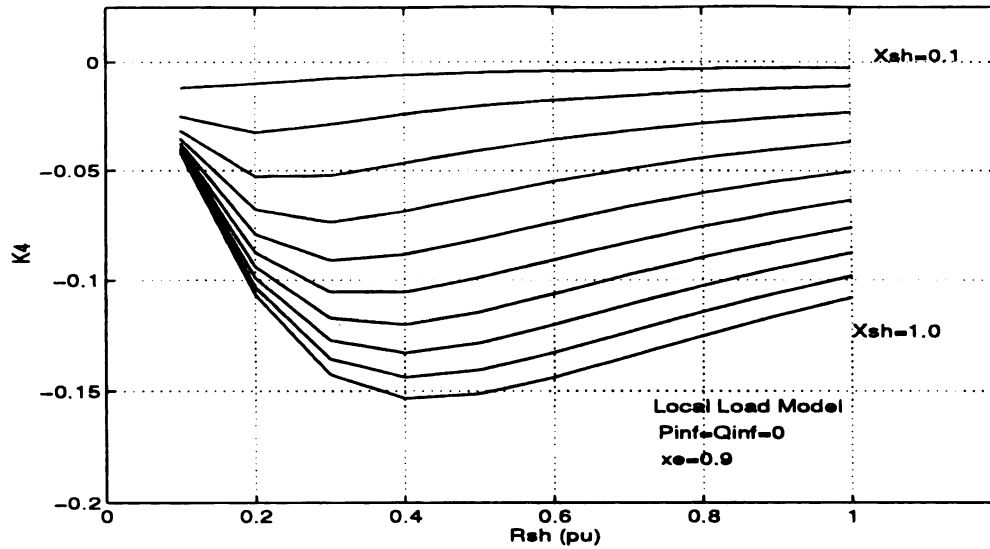
Figure E1.4 Power Transfer Model: Effect of real and reactive power transfer to the infinite bus on the parameter $K_1 - K_2K_3K_4$. (a) Real and reactive power flow in the same direction, (b) Real and reactive power flow in opposite directions.

APPENDIX E2

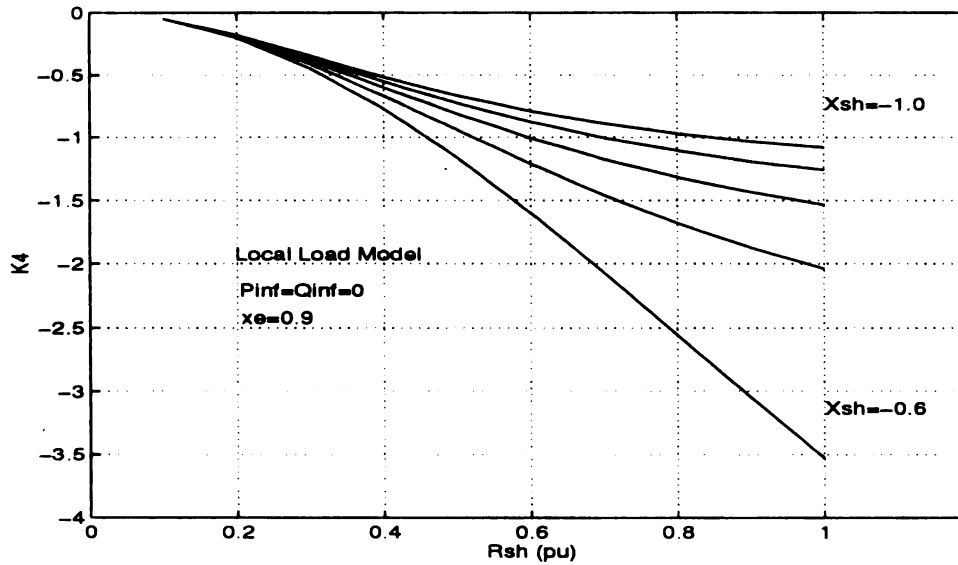
FIGURES FOR DIAGNOSTIC ANALYSIS LOCAL LOADING MODEL

APPENDIX E2

FIGURES FOR DIAGNOSTIC ANALYSIS LOCAL LOADING MODEL

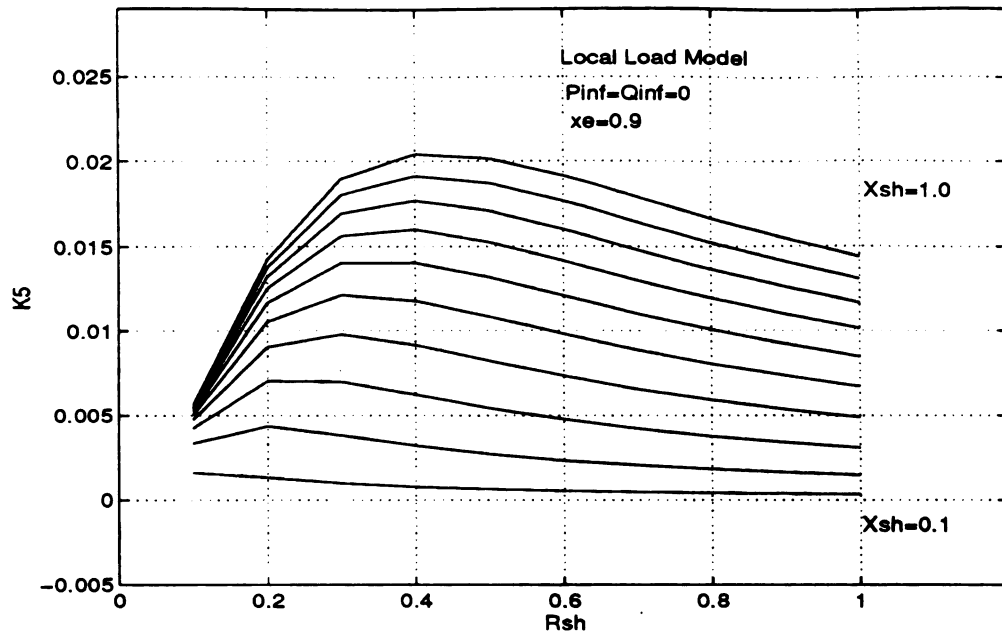


(a)

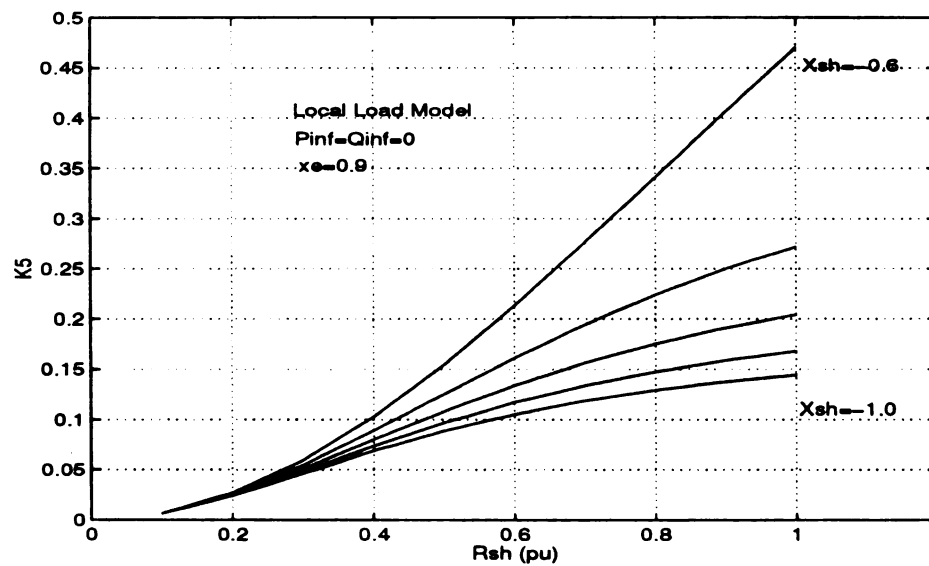


(b)

Figure E2.1 Local Loading Model: Effect of the shunt local load on the parameters K_4 , (a) Inductive loading, (b) Capacitive loading



(a)



(b)

Figure E2.2 Local Loading Model: Effect of the shunt local load on the parameter K_5 , (a) Inductive loading, (b) Capacitive loading

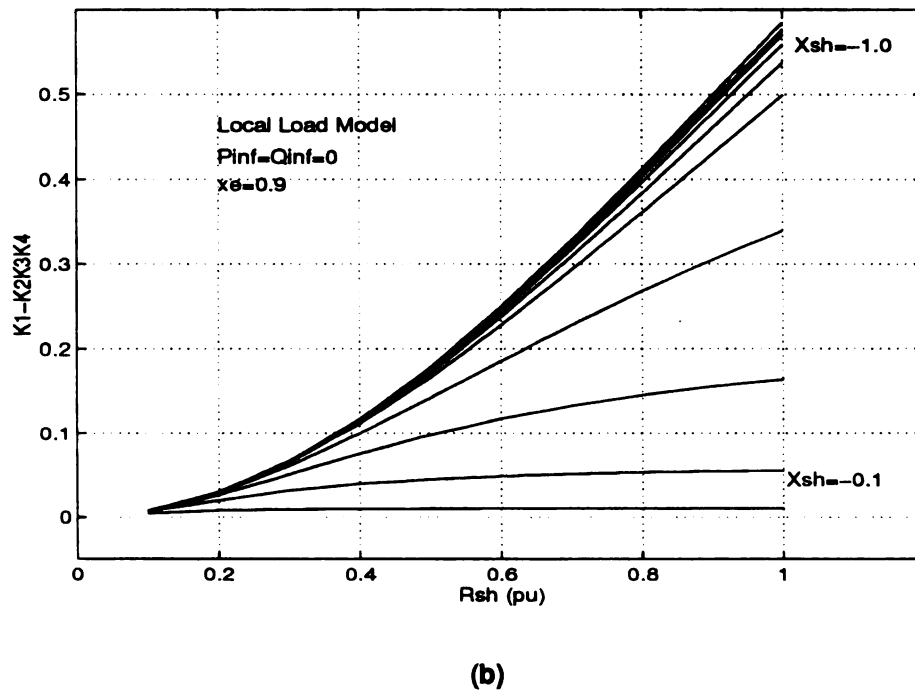
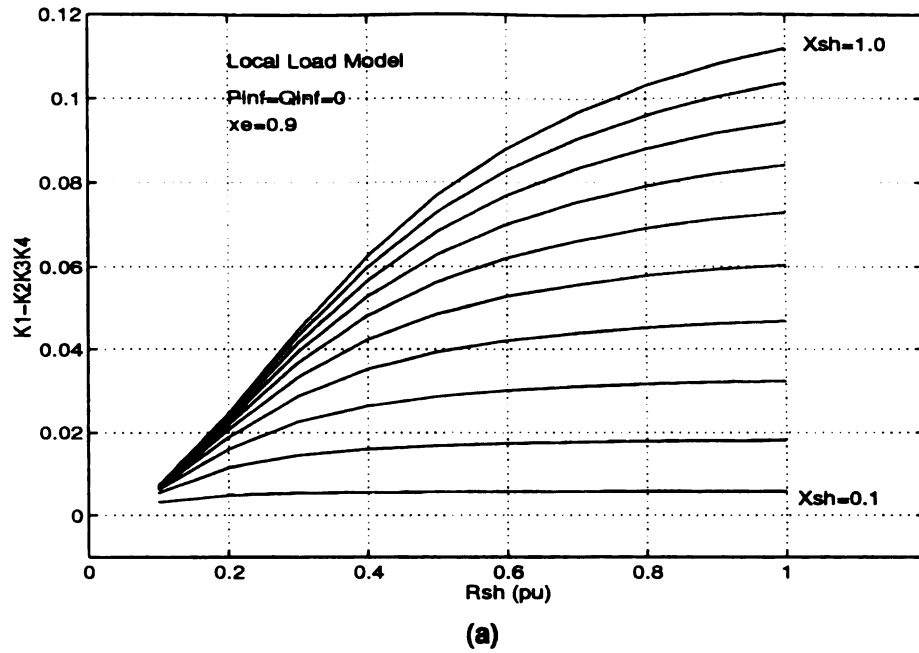
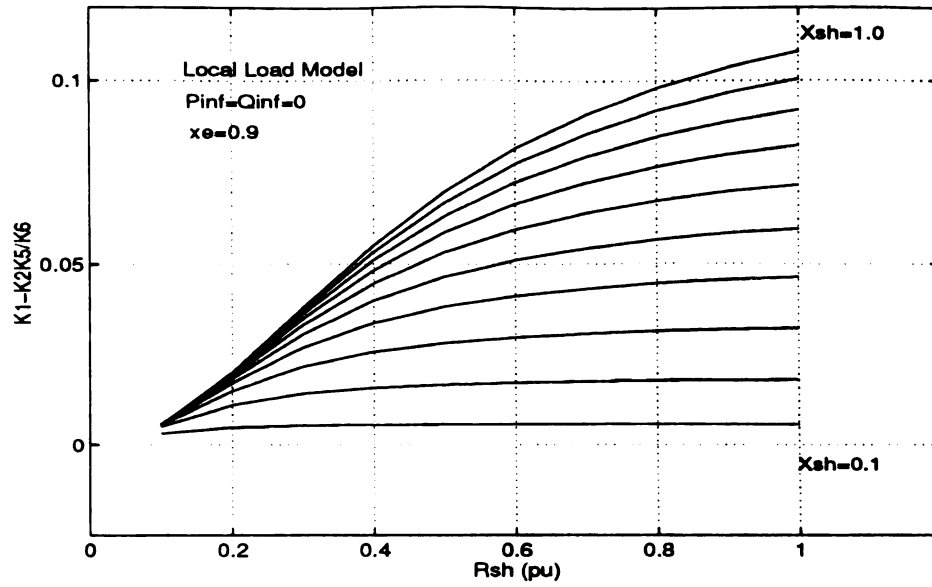
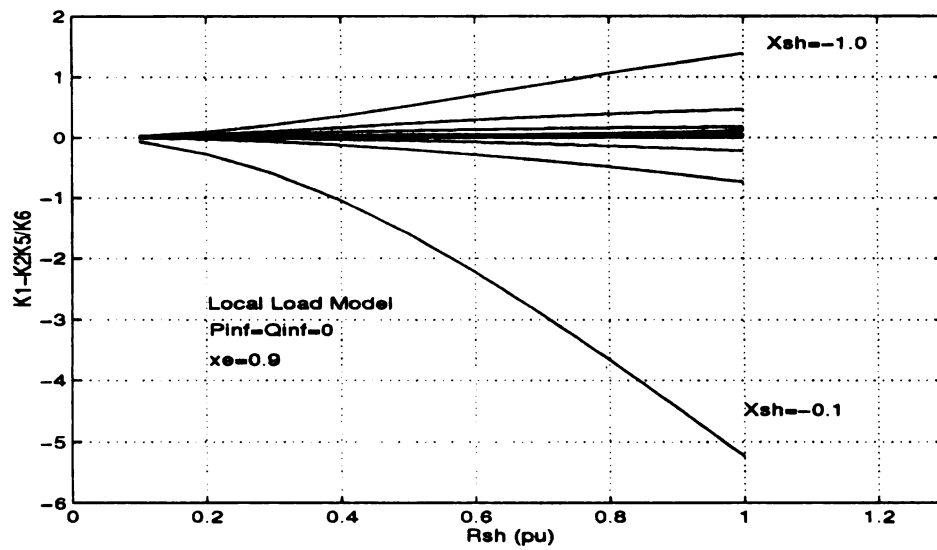


Figure E2.3 Local Loading Model: Effect of the local load on the parameters $K_1-K_2K_3K_4$, (a) Inductive loading, (b) Capacitive loading



(a)



(b)

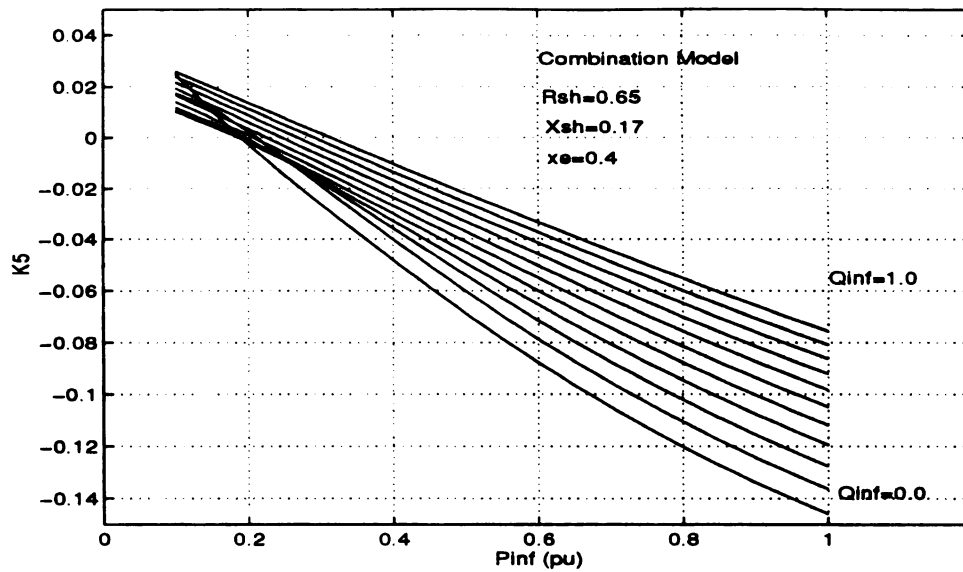
Figure E2.4 Local Loading Model: Effect of real-inductive loading on the parameters $K_1 - K_2K_5/K_6$ (a) Inductive loading, (b) Capacitive loading

APPENDIX E3

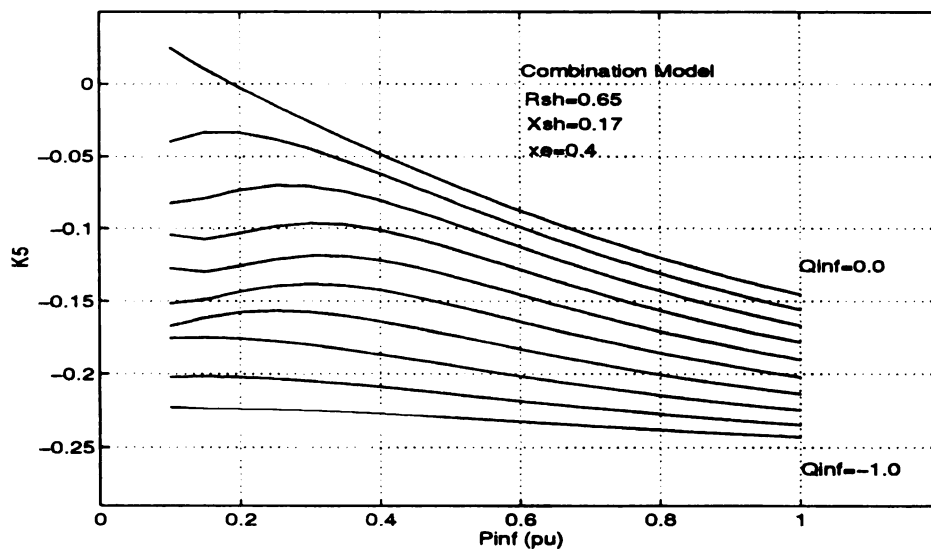
FIGURES FOR DIAGNOSTIC ANALYSIS COMBINATION MODEL

APPENDIX E3

FIGURES FOR DIAGNOSTIC ANALYSIS LOCAL LOADING MODEL

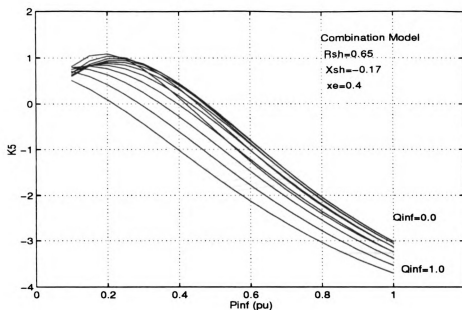


(a)

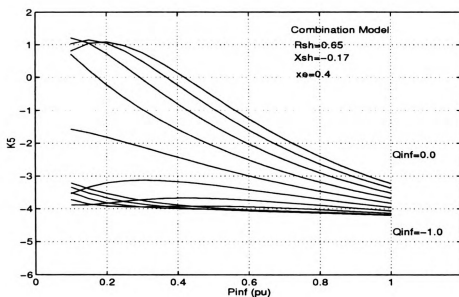


(b)

Figure E3.1 Combination Model: Effect of power transfer on the parameter K_5 when the local load is real-inductive. (a) Power flow in the same direction, (b) Real and reactive power flow in opposite directions.

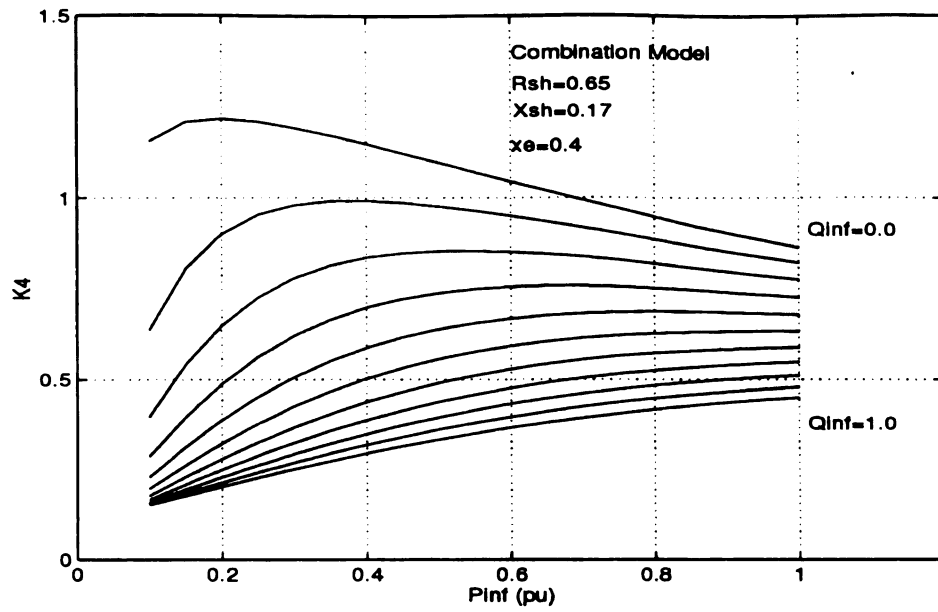


(a)

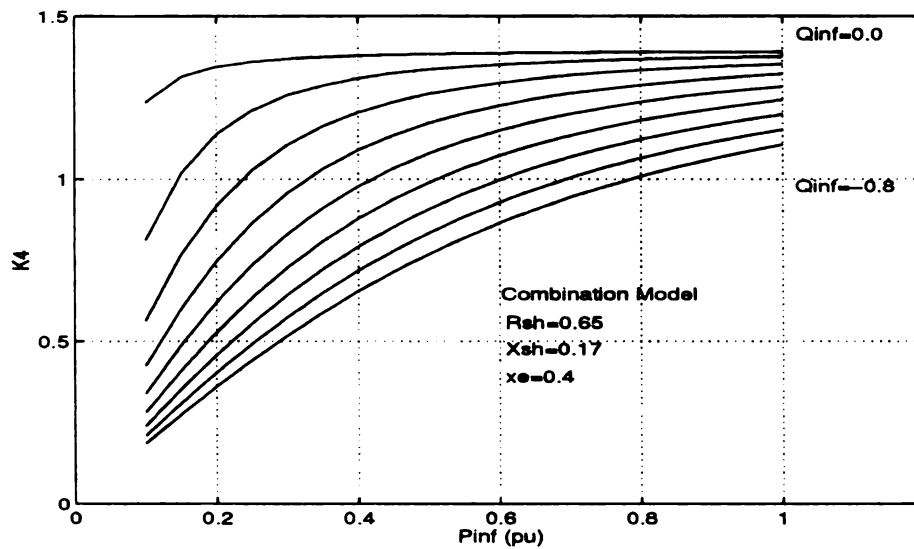


(b)

Figure E3.2 Combination Model: Effect of power transfer on the parameter K_s when the local load is real-capacitive. (a) Power flow in the same direction, (b) Real and reactive power flow in opposite directions.

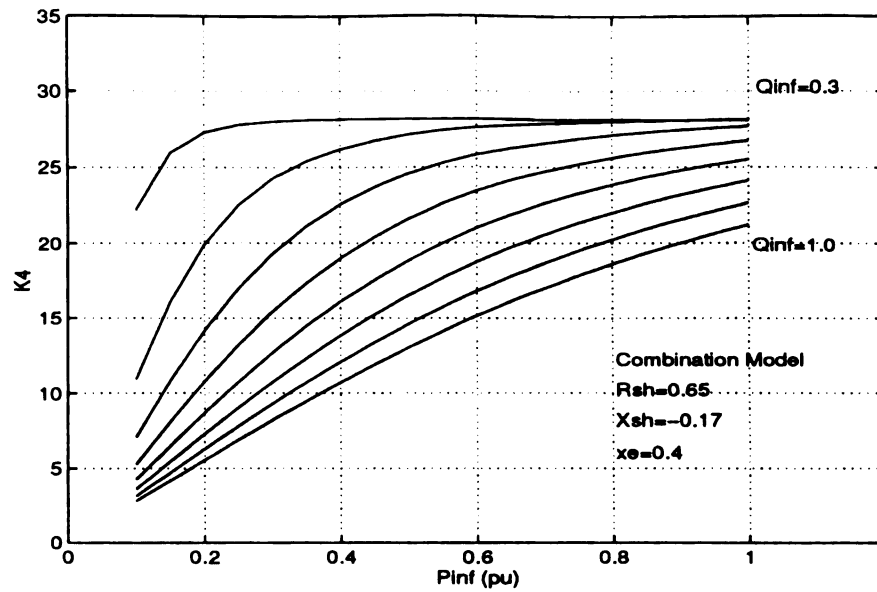


(a)

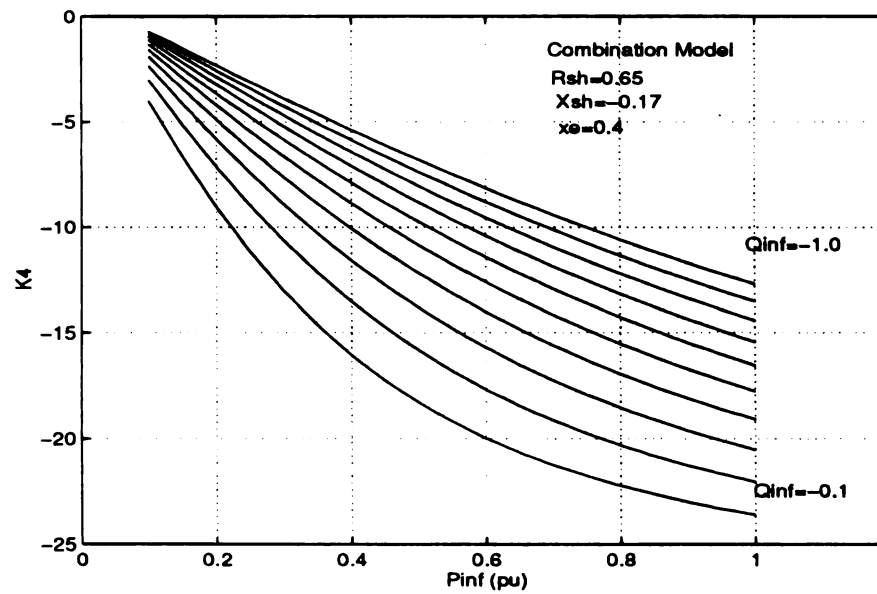


(b)

Figure E3.3 Combination Model: Effect of power transfer on the parameter K_4 when the local load is real-inductive. (a) Power flow in the same direction, (b) Real and reactive power flow in opposite directions.

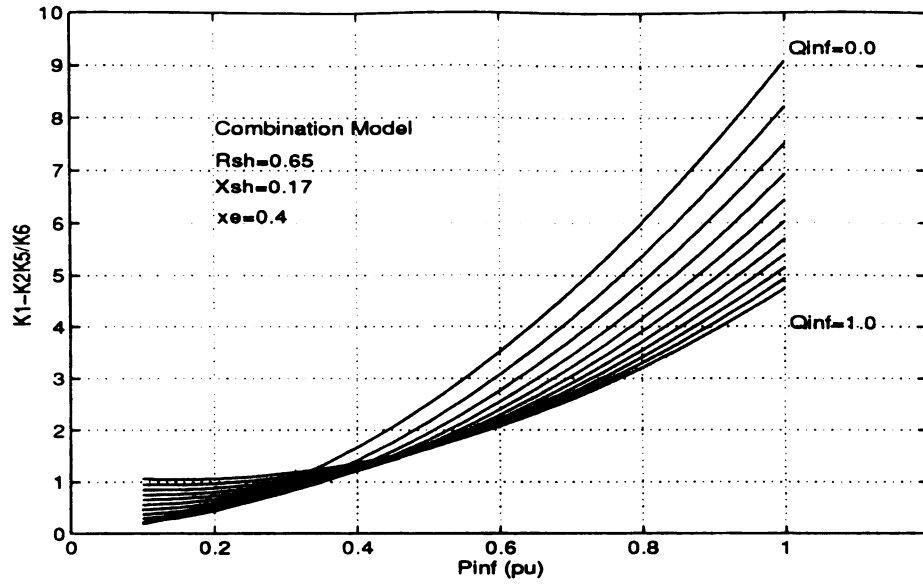


(a)

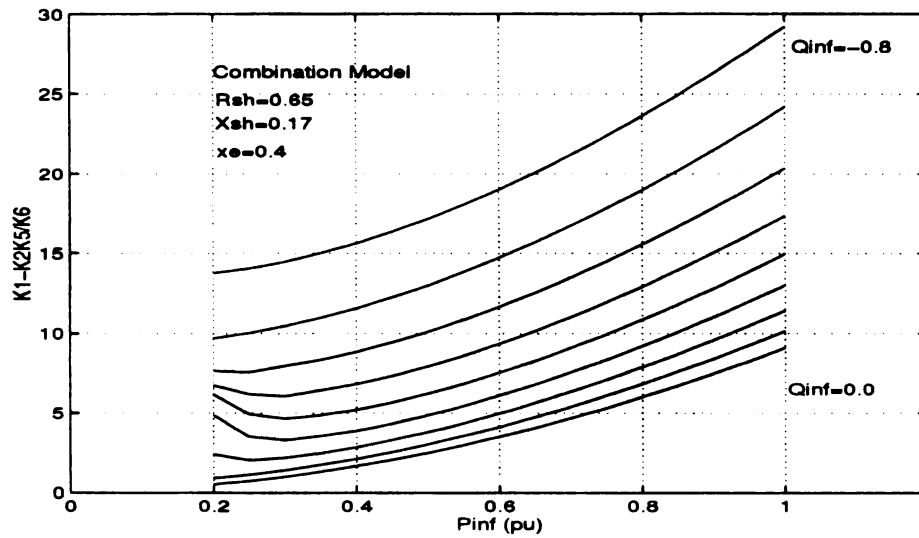


(b)

Figure E3.4 Combination Model: Effect of power transfer on the parameter K_4 when the local load is real-capacitive. (a) Power flow in the same direction, (b) Real and reactive power flow in opposite directions.

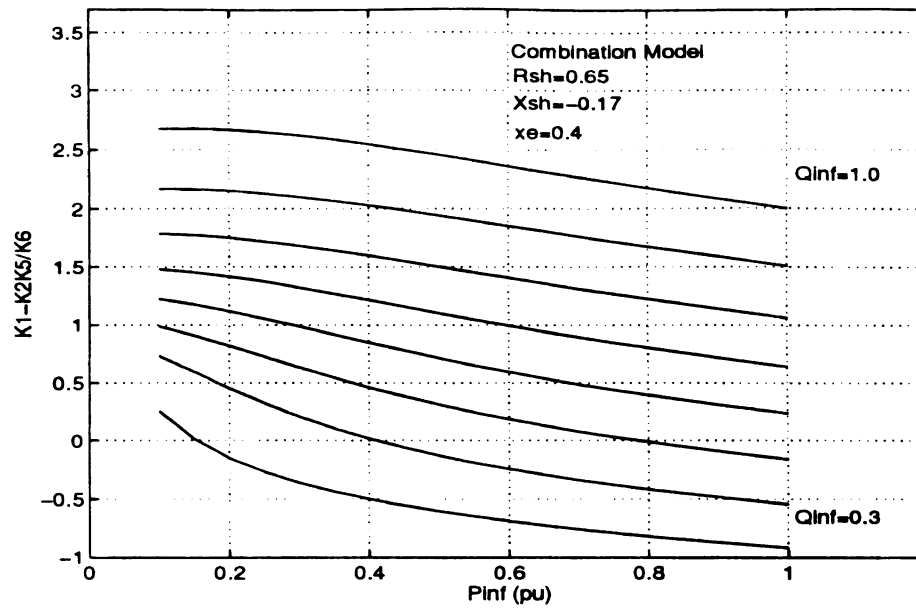


(a)

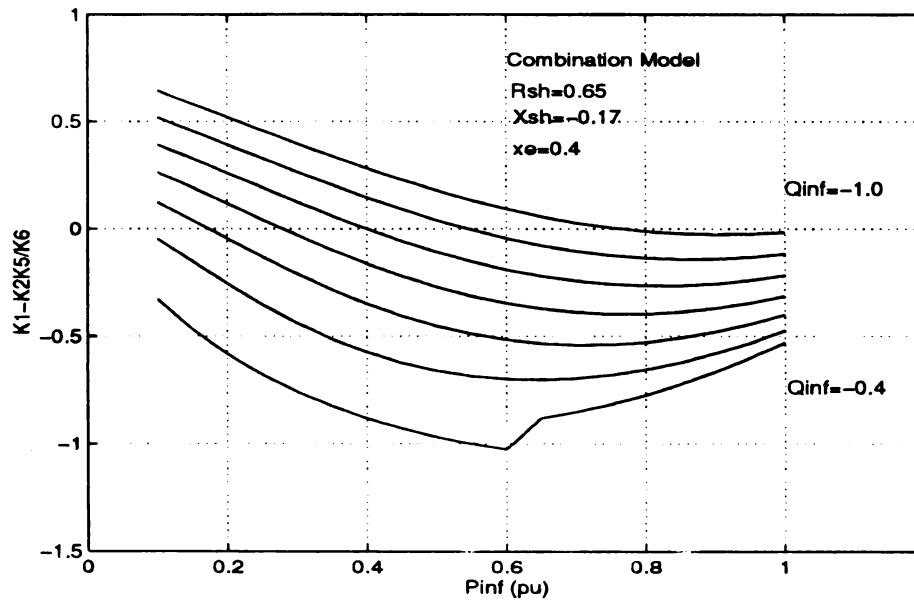


(b)

Figure E3.5 Combination Model: Effect of power transfers to the infinite bus on the synchronizing term $K_1 - K_2 K_5 / K_6$ (regulated) when the local load is real-inductive. (a) Real and reactive power flow in the same direction, (b) Real and reactive power flow in opposite directions.

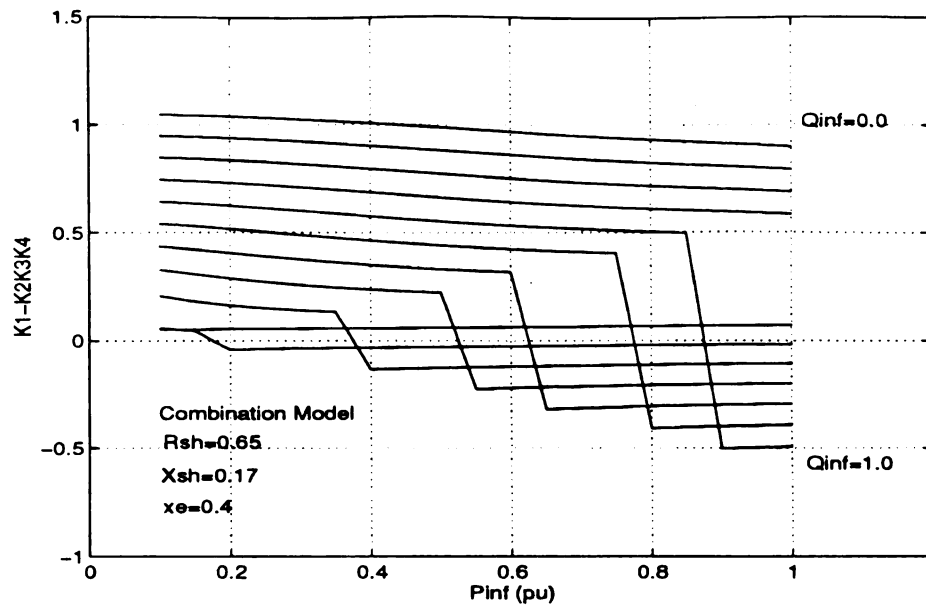


(a)

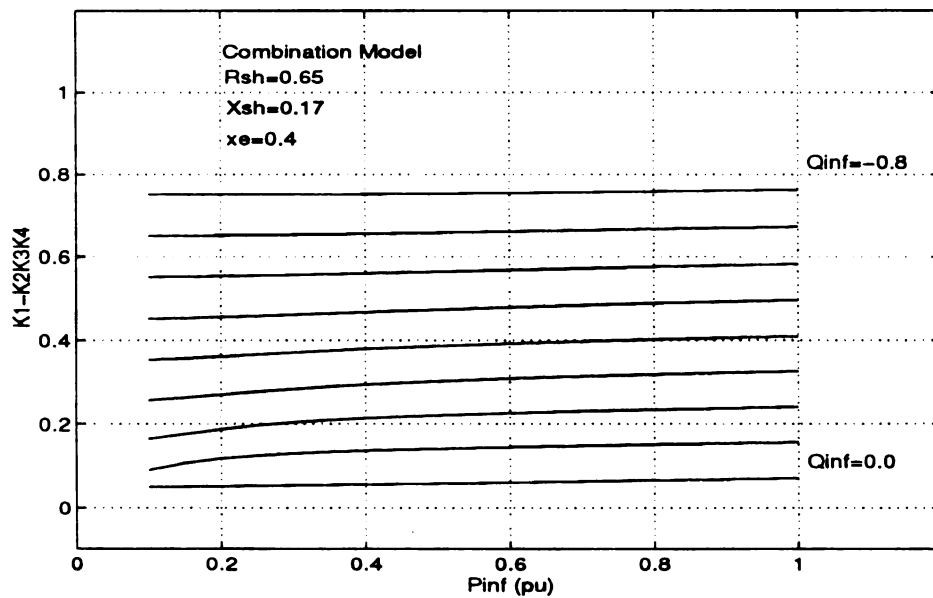


(b)

Figure E3.6 Combination Model: Effect of power transfers to the infinite bus on the synchronizing term $K_1 - K_2K_5/K_6$ (regulated) when the local load is real-capacitive. (a) Real and reactive power flow in the same direction, (b) Real and reactive power flow in opposite directions.

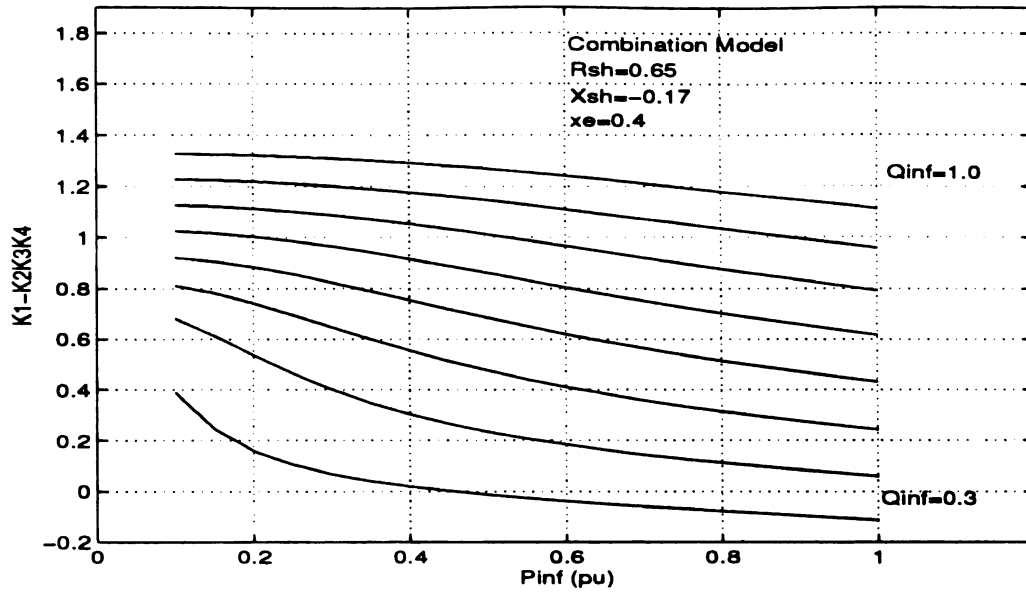


(a)

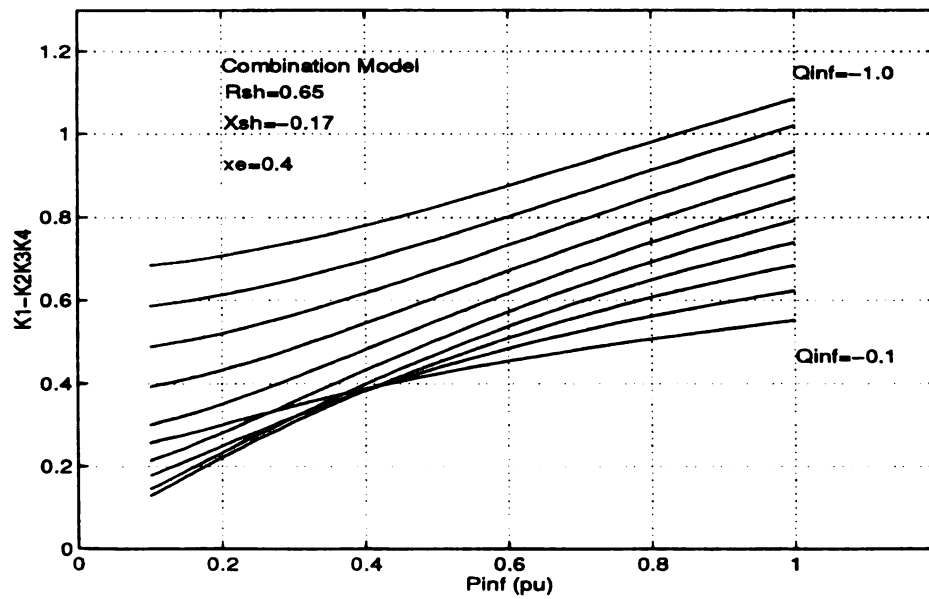


(b)

Figure E3.7 Combination Model: Effect of power transfers to the infinite bus on the synchronizing term $K_1 - K_2 K_3 K_4$ (unregulated) when the local load is real-inductive. (a) Real and reactive power flow in the same direction, (b) Real and reactive power flow in opposite directions.

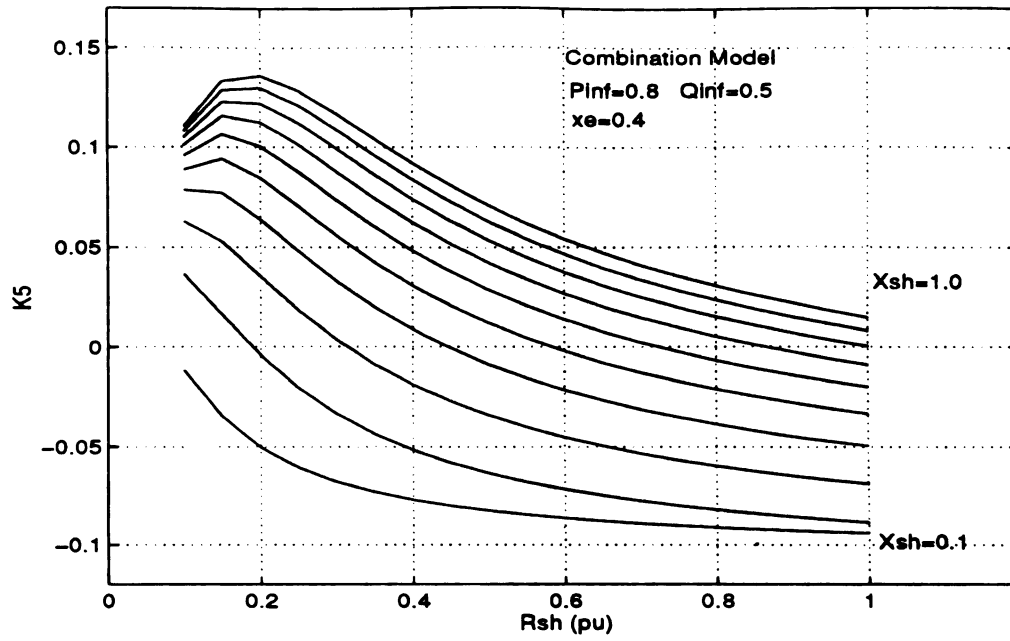


(a)

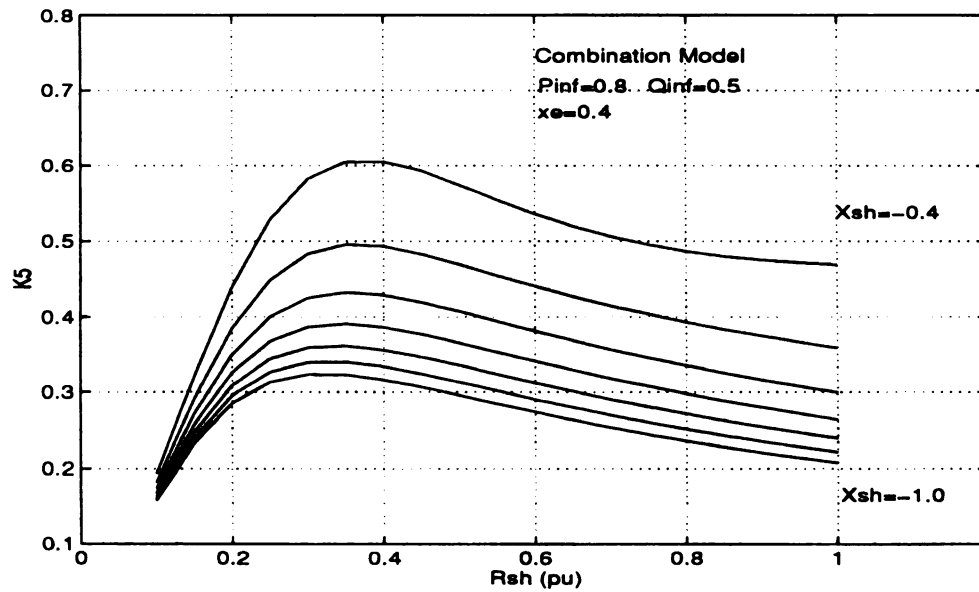


(b)

Figure E3.8 Combination Model: Effect of power transfers to the infinite bus on the synchronizing term $K_1 - K_2 K_3 K_4$ (unregulated) when the local load is real-capacitive. (a) Real and reactive power flow in the same direction, (b) Real and reactive power flow in opposite directions.



(a)



(b)

Figure E3.9 Combination Model: Effect of local loading on the parameter K_5 (regulated) when the transfer to the infinite bus is at $P_{inf}=0.8$, $Q_{inf}=0.5$.
 (a) real-inductive loading; (b) real-capacitive loading.

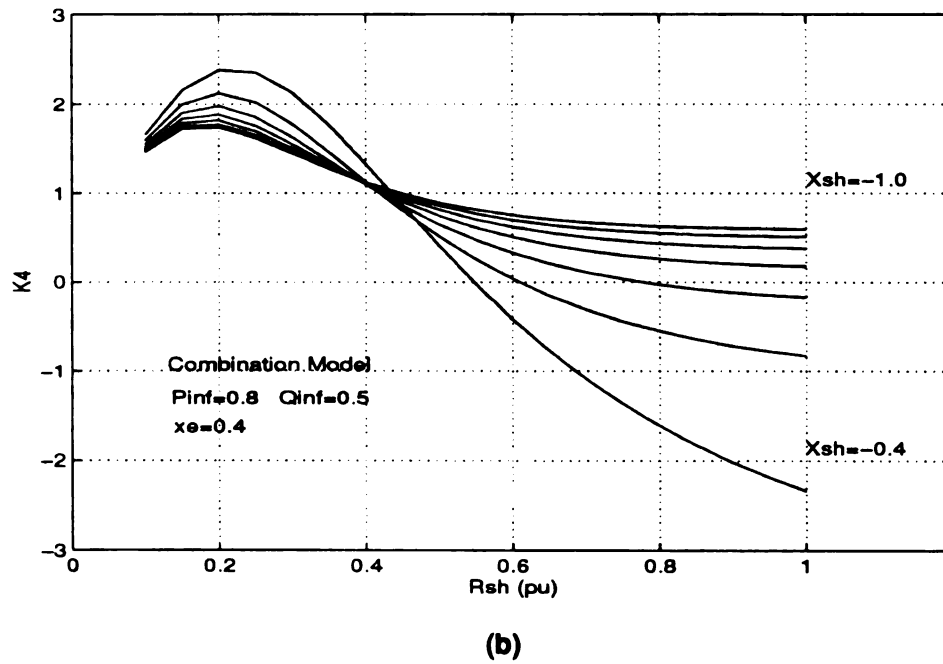
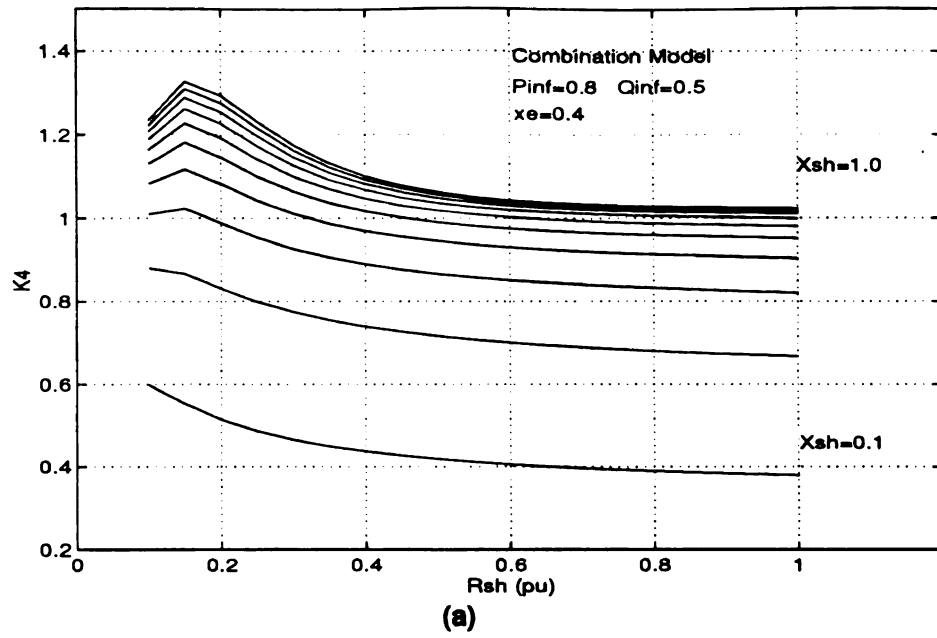
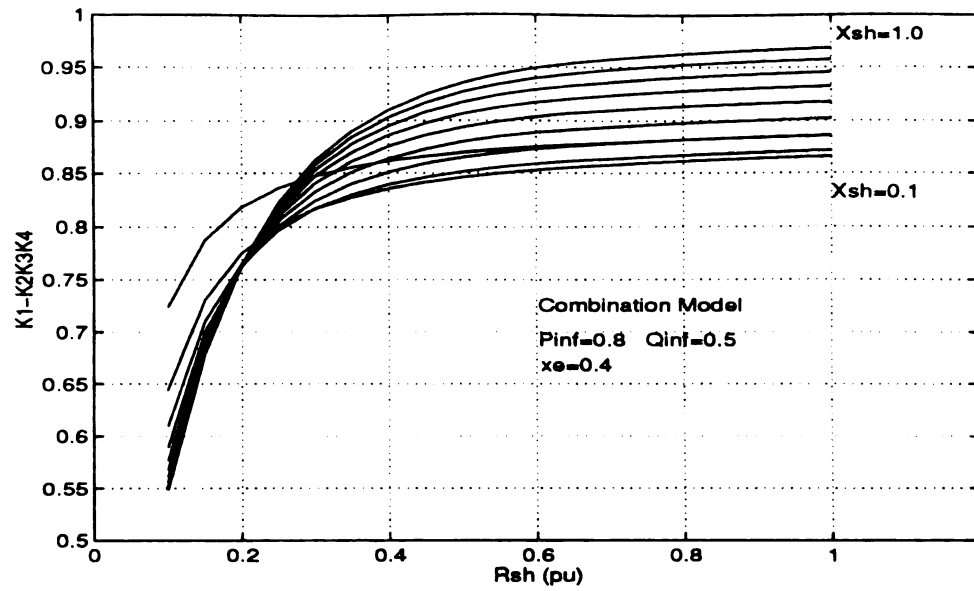
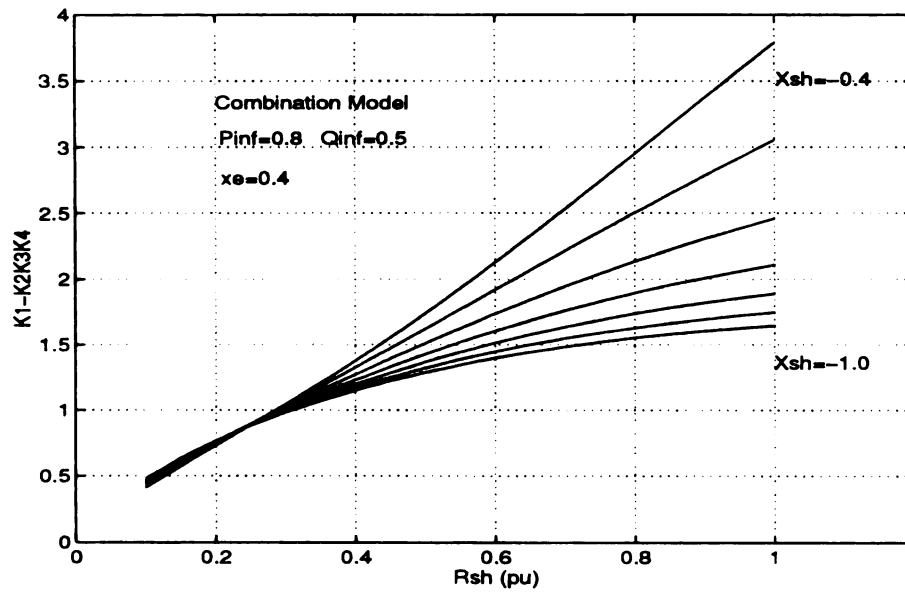


Figure E3.10 Combination Model: Effect of local loading on the parameter K_4 (unregulated) when the transfer to the infinite bus is at $P_{inf}=0.8$, $Q_{inf}=0.5$. (a) real-inductive loading; (b) real-capacitive loading.

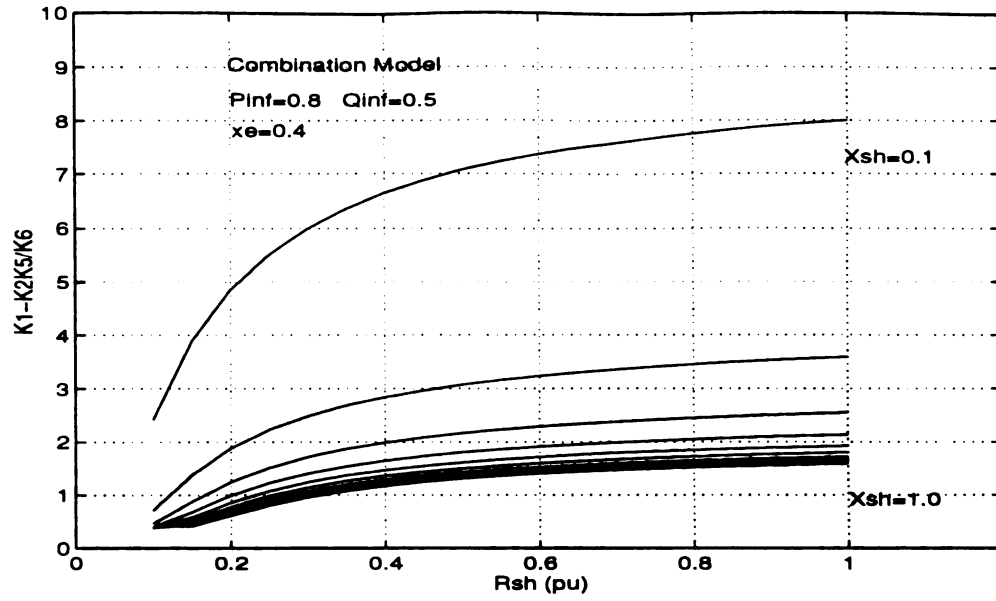


(a)



(b)

Figure E3.11 Combination Model: Effect of local loading on the parameter $K_1-K_2K_3K_4$ (unregulated) when the transfer to the infinite bus is at $P_{inf}=0.8$, $Q_{inf}=0.5$. (a) real-inductive loading; (b) real-capacitive loading.



(a)

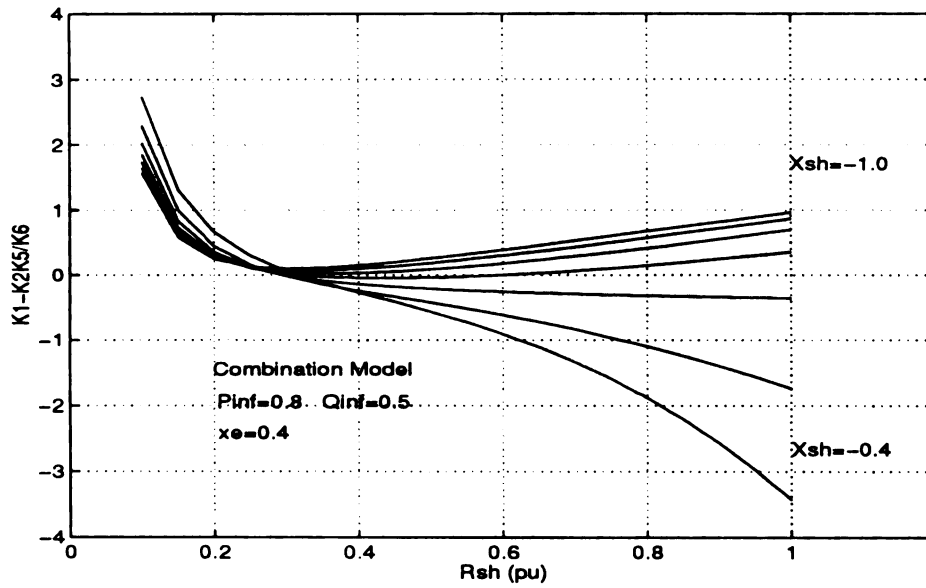
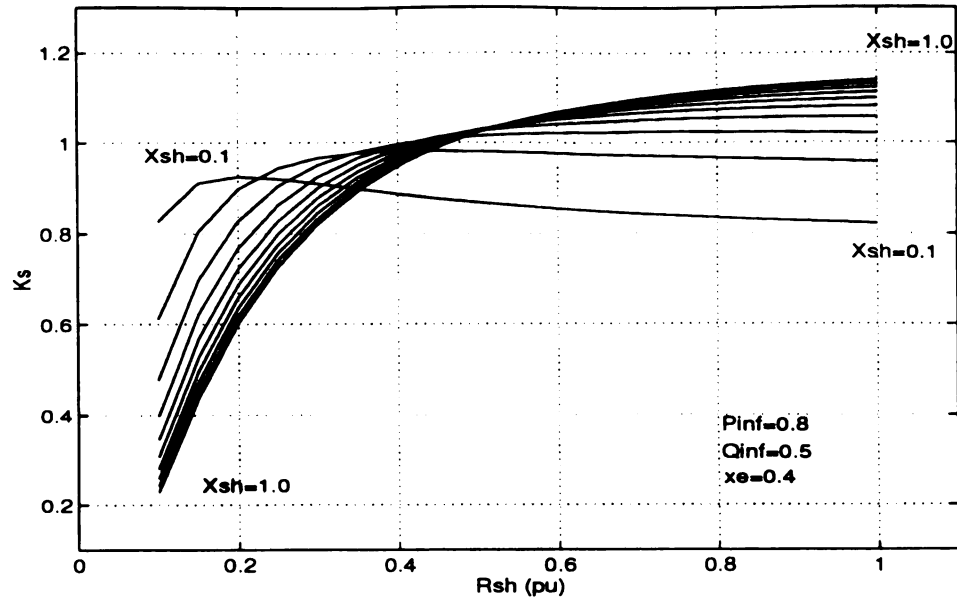
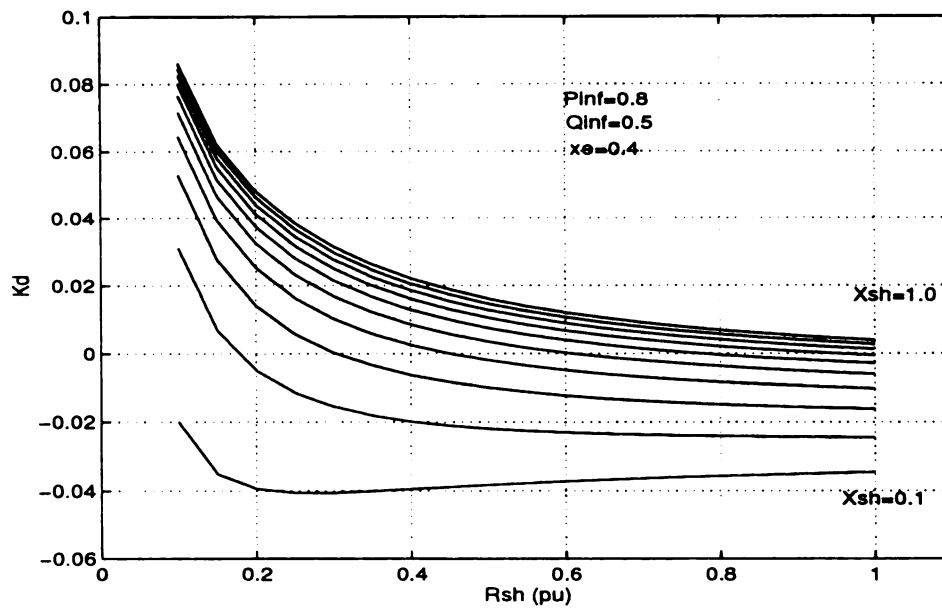


Figure E3.12 Combination Model: Effect of local loading on the parameter $K_1 - K_2 K_5 / K_6$ (regulated) when the transfer to the infinite bus is at $P_{inf}=0.8$, $Q_{inf}=0.5$.
 (a) real-inductive loading; (b) real-capacitive loading.



(a)



(b)

Figure E3.13 Combination Model: Effect inductive-real local load on the system synchronizing and damping torque coefficients when $P_{inf}=0.8$, $Q_{inf}=0.5$
 (a) synchronizing torque coefficient K_s , (b) damping torque coefficient K_d .

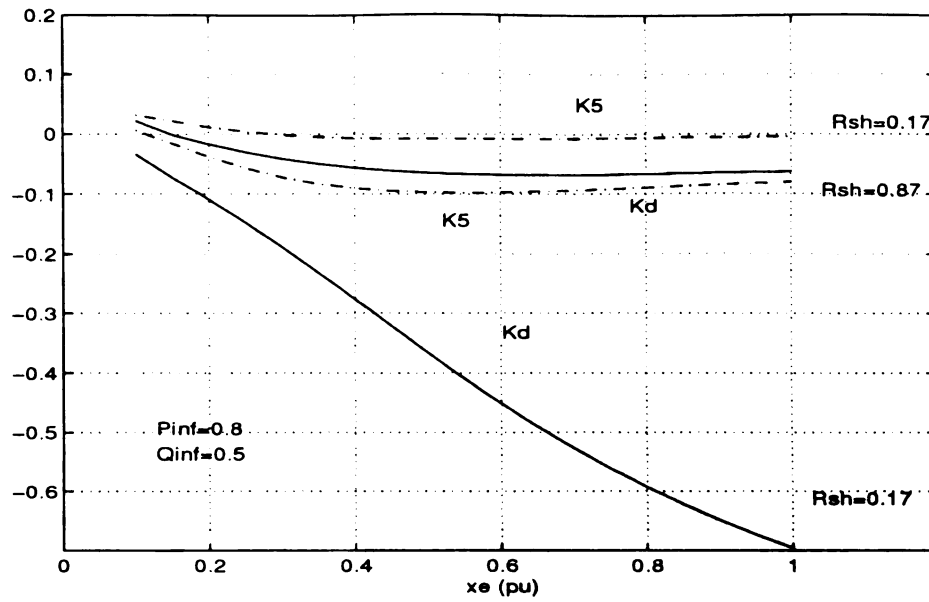


Figure E3.14 Combination Model: Damping torque coefficient K_d and parameter K_5 for different levels of real local loading

BIBLIOGRAPHY

REFERENCES

- [1] P. Kundur, G. J. Rogers, D. Y. Wong, L. Wang, and M.G. Lauby, "A Comprehensive Computer Program Package for Small Signal Stability Analysis of Power Systems", *IEEE Transactions on Power Systems*, Vol. 5, No. 4, pp. 1076-1083, Nov 1990
- [2] B. Gao, G. K. Morison, and P. Kundur, "Voltage Stability Evaluation Using Modal Analysis", *IEEE Transactions on Power Systems*, Vol. 7, No. 4, pp. 1529-1542, Nov 1992
- [3] Bruce C. Moore, "Principle Component Analysis in Linear Systems: Controllability, Observability, and Model Reduction", *IEEE Transactions on Automatic Control*, Vol. AC-26, No. 1, Feb 1981
- [4] Kokotovic, P.V., Allemong, J. J., Winkelman, J. R., and Chow, J. H., "Singular Perturbation and Iterative Separation of Time Scales", *Automatica*, Vol. 16: pp. 23-33, Jan 1980
- [5] I. Dobson, "Observations on the Geometry of Saddle Node Bifurcation and Voltage Collapse in Electric Power Systems", *IEEE Transactions on Circuits and Systems, Part 1*, 39(3):pp. 240-243, March 1992
- [6] Chhewang Rinzin, Fernando L. Alvarado, and Rambanu Adapa, "Formulas for Geographic Differentiation of Security Limits", *24th American Power Symposium*, Oct 1992
- [7] Yakout Mansour, Wilsun Xu, Fernando Alvarado, Chhewang Rinzin, "SVC Placement Using Critical Modes of Voltage Instability", *IEEE Transactions on Power Systems*, Vol. 9, No. 2, May 1994
- [8] "MSU Voltage Stability Security Assessment and Planning Methodology Programs", *Department of Computing and Technology, Michigan State Univ., East Lansing*, 1994
- [9] R. A. Schlueter, T. Y. Guo, T. Lie, F. Li, J. Ashley, "Voltage Collapse Security Assessment on the B. C. Hydro System", *Division of Engineering Research, Report PSL-BC1 to B. C. Hydro*, March 1991
- [10] "SVC for Dynamic Voltage Stabilization of 132 kV System in Western Canada", *ABB Advertising Application Note A02-0144 E*, ABB Power Systems, 1994
- [11] R. A. Schlueter, K. B. Kilani, S. Liu, "A Voltage Stability Security Assessment Method", *submitted to IEEE Working Group on Voltage Collapse for IEEE Tutorial*, Jan 1996
- [12] Perez-Arriaga, G.C Verghese, F.C. Schweppe, "Selective Modal Analysis With Applications to Power Systems, Part I: Heuristic Introduction", *IEEE PES 1982 Winter Meeting*,

New York

- [13] Vittal, V., N. Bhatia, and A. A. Fouad, "Analysis of the Inter-area Mode Phenomena in Power Systems Following Large Disturbance", *IEEE Transactions on Power Systems*, (6):pp. 1515-1521, 1991
- [14] E. H. Abed and P. P. Varaiya, "Nonlinear Oscillations in Power Systems", *Electric Power and Energy Systems*, Vol. 6:pp. 37-43, No. 1, January 1984
- [15] C. Rajagopalan, P.W. Sauer and M.A. Pai, " Analysis of Voltage Control Systems exhibiting Hopf Bifurcations," *Proceedings 28th Decision and Control Conf.*, Tampa, FL, pp. 332-335, December 1989.
- [16] J.H. Chow, A. Gebreselassie, "Dynamic Voltage Stability Analysis of a Single Machine Constraint Power Load System", *Proceedings of the 29th Conference on Decision and Control*, Honolulu, Hawaii, Dec 1990
- [17] Venkatasubramanian, V., H. Schattler and J. Zaborsky, "A taxonomy of the Dynamics of a Large Power System with Emphasis on its Voltage Stability", *Proc. Bulk Voltage Stability and Security*, Deep Creek Lake, Aug, 1991
- [18] C. Rajagopalan, B. Lesieutre, P. W. Sauer, M. A. Pai, "Dynamic Aspects of Voltage / Power Characteristics", *IEEE Transactions on Power Systems*, Vol. 7, No. 13:pp. 990-1000, Aug 1992
- [19] F. Alvarado, M.Gu, Y. Hu, "Direct Detection of Instability Points Using an Augmented Formulation", *Proceedings of the 24th North American Power Symposium*, Reno, Nevada, Oct, 1992
- [20] Lee, B. and V. Ajarapu, "Observation of Chaos in an Electrical Power System Via Period Doubling", *IEE Proceedings of Part C*. Vol. 140, No. 6, pp. 490-496, Nov, 1993
- [21] Ajarapu, V. and B. Lee, "The application of Bifurcation Theory to Study the Nonlinear Dynamical Phenomena in an Electric Power System", *IEEE Transactions on Power Systems*, Vol. 7, No. 1, pp. 424-432, Feb 1992
- [22] Abed, E. H., J. C. Alexander, H. Wang, A. M. A. Hamdan, and H. C. Lee, "Dynamic Bifurcation in a Power System Model Exhibiting Voltage Collapse", *Technical Research Report, System Research Center*, U. Maryland, College Park, MD, U.S.A., Feb 1992
- [23] Chiang, H. D., C. W. Liu, P. P. Varaiya, F. F. Wu, and M. G. Lauby, "Chaos in a Simple Power System", *IEEE PES Winter Meeting Paper 92WM151-1PWRS*
- [24] Chiang, H-D, I. Dobson, R.J. Thomas, J.S. Thorp, F.A. Lazhar, "On the Voltage Collapse in Power Systems", *IEEE Trans. on Power Systems*, 5:pp. 601-611, May 1990
- [25] Robert A. Schlueter, Khadija B. Kilani, and Uhi Ahn, "Impact of Modeling Accuracy on Type, Kind, and Class of Stability Problems in a Power System Model". *Proceedings of the ECC & NSF International Workshop on Bulk Power System Voltage Stability, Security and Control, Phenomena - III*, pp. 117-156, Aug 1994

- [26] V. Venkatasubramanian, X. Jiang, H. Schttler, and J. Zaborszky, "A Taxonomy of the Dynamics of the Large Electric Power System with Emphasis on Its Voltage Stability", *Proceedings of the NSF International Workshop on Bulk Power System Voltage Phenomena - II*, pp. 9-52, 1991
- [27] V. Venkatasubramanian, X. Jiang, H. Schttler, and J. Zaborszky, "Current Status of the Taxonomy Theory of Large Power System Dynamics, DAE Systems with Hard Limits" *Proceedings of the ECC & NSF International Workshop on Bulk Power System Voltage Stability, Security and Control, Phenomena - III*, pp. 15-103, Aug, 1994
- [28] T. Van Cutsem, Y. Jaquemart, J.-N. Marquet, P. Pruvot., "A Comprehensive Analysis of Mid-term Voltage Stability", *IEEE Transactions on Power Systems*, Vol. 10, No. 3:pp. 1173-1182, August 1995
- [29] P. Kundur, *Power System Stability and Control*, Vol 1 of the EPRI Power System Engineering Series, McGraw Hill, New York 1994
- [30] W.R. Lashs. "Control of voltage stability on EHV power systems", *Ph.D. Dissertation*, University of South Wales, Australia, May 1992
- [31] B.C. Lesieutre, P.W. Sauer, M.A. Pai, "Development and comparative study of P, Q load models", *IEEE Winter Power Meeting*, Paper 94 WM 166-9 PWRs.
- [33] Hassan K. Khalil, "Nonlinear Systems", *Macmillan Publishing Company*, New York, 1992
- [34] J. Guckenheimer and P. Holmes, "Nonlinear Oscillations, Dynamical Systems and Bifurcations of Vector Fields," *Applied Mathematical Sciences*, Springer, New York, 1986
- [35] R.A Schlueter, "Unification and Classification of Algebraic Tests for Voltage Stability," *Electric Mach. Power Systems.*, 12, pp. 557-590, 1993
- [36] G. Taylor, Voltage Stability, Part 1, Survey of Voltage Collapse Phenomena, *NERC Rep.*, National Electric Reliability Council, Princeton, NJ, Aug, 1991
- [37] IEEE Systems Dynamic Performance Report, "Voltage Stability of Power Systems: Concepts, analytical tools, and industry Experience", *IEEE Document No. 90 TH 0358-3 PWR*, 1990
- [38] IEEE Systems Dynamic Performance Report, "Suggested Techniques for voltage stability analysis", *IEEE Document No. 93 TH 0620-5PWR*, 1994
- [40] N.W. Miller, W.W.Price, "Influence of Load Modeling Assumptions on the Dynamics of the Large System Voltage Collapse Simulations", *Proceedings of the ECC & NSF International Workshop on Bulk Power System Voltage Stability, Security and Control, Phenomena - III*, pp. 635-641, Aug 1994
- [41] M. Amorouayeche, M. Brown, R. Craven, J.L. Jardim, A. Johannesen. P. Kundur, R. Marconato, K. Maslo, F. Mc Namara, B. Meyer, J.V. Mitsche, Y. Nakanishi, W.W. Price, J.L.

- Sancha, K. Walve, D. Xia, R. Yokoyama, "Tools for Simulating Long Term Dynamics", *Electra* No. 163, pp. 151-165, December 1995
- [42] R. A. Schlueter, I-P. Hu and T-Y. Huo, "Dynamic/Static Voltage Stability Security Criteria", *Proceedings of the NSF International Workshop on Bulk Power System Voltage Phenomena - Voltage Stability and Security*, pp. 265-303, 1991
- [43] *Modeling of Voltage Collapse Including Dynamic Phenomena*, Final Report, CIGRE Task Force 38-02-10, December 1992
- [44] M. Amorouayeche, M. Brown, R. Craven, J.L. Jardim, A. Johannesen, P. Kundur, R. Marconato, K. Maslo, F. Mc Namara, B. Meyer, J.V. Mitsche, Y. Nakanishi, W.W. Price, J.L. Sancha, K. Walve, D. Xia, R. Yokoyama, "Tools for Simulating Long Term Dynamics", *Electra* No. 163, pp. 151-165, December 1995
- [45] I. Dobson, L. Lu, "Immediate Change in Stability and Voltage Collapse When Generator Power Limits are Reached", *Proceedings of the NSF International Workshop on Bulk Power System Voltage Phenomena - Voltage Stability and Security*, pp. 65-73, 1991.
- [47] V. Venkatasubramanian, X. Jiang, H. Schattler, and J. Zaborszky, "Discussion of Impact of Modeling Accuracy on Type, Kind, and Class of Stability Problems in a Power System Model", *Proceedings of the ECC & NSF International Workshop on Bulk Power System Voltage Stability, Security and Control, Phenomena - III*, pp. 171-172, Aug 1994
- [48] R. A. Schlueter, "Closure of Discussion of Impact of Modeling Accuracy on Type, Kind, and Class of Stability Problems in a Power System Model", *Proceedings of the ECC & NSF International Workshop on Bulk Power System Voltage Stability, Security and Control, Phenomena - III*, pp. 172-173, Aug 1994
- [49] Lee, B. and V. Ajjarapu, "A Unified Frame Work to Study Voltage Stability of Structure Preserving Power System Model", Submitted for Publication in *IEEE Trans. on Power Systems*
- [50] S. Wiggins, "Introduction of Applied Nonlinear Dynamical Systems and Chaos", *Springer-Verlag*, New York, 1990
- [51] I. Hu, "Voltage Collapse Bifurcation on a Power System Transient Stability Model", *P.h.D. Dissertation*, Michigan State University, July 1990
- [52] T.Y. Guo, "Structural bifurcation tests for voltage collapse and low frequency oscillations in power systems", *P.h.D. Dissertation*, Michigan State University, March 1992
- [53] F.R. Gantmacher " *The Theory of Matrices*", vol 1(2), Chelsea Publishing Company, New York, 1977.
- [54] Y. Tamura, H. Mori, and S. Iwamoto, "Relashionship between Voltage Instability and Multiple Load Flow Solutions in Electric Power Systems", *IEEE Transactions on Power Apparatus and Systems*, Vol. PAS-102, pp. 1115-1123, May 1983
- [55] Francisco P. Demello and Charles Concordia, "Concept of Synchronous Machine Stability

- as Affected by Excitation Control", *IEEE Transactions on Power Apparatus and Systems*, Vol. PAS-88, No. 4, pp. 316-329, April 1969
- [56] F. P. deMello, T. F. Laskowsky, "Concept of Power System Dynamic Stability", *IEEE Transactions on Power Apparatus and Systems*, Vol. PAS-94, No. 3, pp. 827-833, May-June 1975
- [57] A.A. Fouad and P. M. Anderson, "Power System Control and Stability", *Iowa State University Press*, Ames, IA, 1977
- [58] Sotomayor, J., "Generic Bifurcations of Dynamical Systems", *Edited by P.M. Peixoto, Academic Press*, NY, 1973
- [59] "Power System Toolbox", *Cherry Tree Scientific Software, RR#5 Calborne, Ontario K0K 1S0, Canada.*
- [59] Arthur R. Burgen, "Power System Analysis", *Prentice Hall, Inc., Englewood Cliffs, New Jersey 07632*, 1986

MICHIGAN STATE UNIV. LIBRARIES



31293015700853